


2016

The Relationship Between Magmatism and Deformation During the Acadian Orogeny: A Case Study from Eastern-Central Vermont

Samuel William Lagor
University of Vermont

Follow this and additional works at: <http://scholarworks.uvm.edu/graddis>

 Part of the [Geology Commons](#), and the [Tectonics and Structure Commons](#)

Recommended Citation

Lagor, Samuel William, "The Relationship Between Magmatism and Deformation During the Acadian Orogeny: A Case Study from Eastern-Central Vermont" (2016). *Graduate College Dissertations and Theses*. Paper 566.

This Thesis is brought to you for free and open access by the Dissertations and Theses at ScholarWorks @ UVM. It has been accepted for inclusion in Graduate College Dissertations and Theses by an authorized administrator of ScholarWorks @ UVM. For more information, please contact donna.omalley@uvm.edu.

THE RELATIONSHIP BETWEEN MAGMATISM AND DEFORMATION
DURING THE ACADIAN OROGENY: A CASE STUDY
FROM EASTERN-CENTRAL VERMONT

A Thesis Presented

by

Samuel William Lagor

to

The Faculty of the Graduate College

of

The University of Vermont

In Partial Fulfillment of the Requirements
for the Degree of Master of Science
Specializing in Geology

May, 2016

Defense Date: January 22, 2016
Thesis Examination Committee:

Laura E. Webb, Ph.D., Advisor
Donald S. Ross, Ph.D., Chairperson
Keith A. Klepeis, Ph.D.
Jon Kim, Ph.D.
Cynthia J. Forehand, Ph.D., Dean of the Graduate College

ABSTRACT

The Silurian–Devonian metasedimentary rocks of the Connecticut Valley–Gaspé trough (CVGT) were subjected to multiple deformational and metamorphic events during the Acadian orogeny in the Middle–Late Devonian. Plutons intruding the Devonian Waits River and Gile Mountain Formations have been considered post-tectonic, but microstructural studies of the intrusions and their metamorphic aureoles indicate some of these plutons intruded syntectonically. This study investigates the relationship between Acadian deformation and intrusion of the Knox Mountain pluton (KMP) of central Vermont. Structural and geochronological data were collected along a c. 15 km transect from the western limit of the CVGT, where the unconformable Richardson Memorial Contact coincides with the Dog River Fault Zone, into the margin of the KMP in the east. Field and microstructural observations indicate the KMP intruded syntectonically. Evidence for Acadian deformation post-dating intrusion includes folded and boudinaged granitic dikes at the margin of the KMP, and microstructures such as flame perthite, myrmekite, deformation twins, and textures associated with grain-boundary migration recrystallization in the granite. In the metamorphic aureole, biotite porphyroblasts overgrow S_3 , the earliest Acadian secondary foliation, and were deformed during S_4 crenulation cleavage development. The KMP intruded at 377 ± 5.2 Ma based on a U-Th-total Pb monazite crystallization age, which is concordant with the published age of the nearby Barre granite. The timing of S_4 foliation development in the CVGT is constrained locally by $^{40}\text{Ar}/^{39}\text{Ar}$ geochronology at ~ 365 Ma, consistent with the microstructurally-inferred relative-age relationships. Plateau/weighted mean $^{40}\text{Ar}/^{39}\text{Ar}$ ages from across the transect and minimum ages from argon-loss profiles show a general trend of younging towards the east, suggesting these rocks have been affected by Alleghanian and Mesozoic deformation and exhumation.

ACKNOWLEDGEMENTS

I regard the completion of this thesis document and master's program as one of the most significant mental and physical accomplishments of my life. However, seeing this document to completion was certainly not the result of my actions alone, and I remain indebted to countless individuals (most of whom will not be named here). To my adviser, Dr. Laura Webb, as I have said before, the patience, guidance, and understanding you have shown me throughout this process will take me a lifetime to pay forward. I cannot thank you enough for sharing your wisdom, encouragement, and a laugh with me, and always I needed them most. It has been a pleasure working in the department as a teacher's assistant under a number of other geology faculty, and I thank you all for the advice, anecdotes, and kindness you have shared with me throughout these three years. I am incredibly grateful for the guidance and passion of Dr. Jeff Chiarenzelli and Dr. Sean Regan since my time working alongside them at St. Lawrence. You gentlemen helped instill my passion for geology, and I look forward to continued collaborations. I need to thank Matt Van Brocklin, who always ensured I had a place to stay, and that the machines were running smooth any time I made it back to Canton.

The results of this project would be nowhere-to-be-found were it not for Dan Jones. Thanks for everything from the good beer to the unsolicited advice. Big shout-out to all the assistants I had in the field. Jacob Vincent, Ifan Hywel, Drew Groth, Beth Pidgeon, Hannah Blatchford, and John Gilbert, your second opinions became my preliminary interpretations! Finally, I could not have done this without my friends and family backing me. Hannah, Tess, Elle, Gabe, and Ida, I love you more than words can tell.

TABLE OF CONTENTS

ACKNOWLEDGEMENTS.....	ii
LIST OF FIGURES.....	v
LIST OF TABLES.....	vi
LIST OF APPENDICES.....	vii
CHAPTER 1: COMPREHENSIVE LITERATURE REVIEW.....	1
1.1. Introduction.....	1
1.2. The Emplacement of Granite During Collisional Orogenies.....	2
1.2.1. Introduction.....	2
1.2.2. Generating Melt—Crustal Anatexis, Migmatites, and the Effect of Strain	4
1.2.3. Melt Focus and Extraction.....	6
1.2.4. Magma Ascent and Emplacement.....	8
1.2.5. Emplacement in the Ductile Regime.....	9
1.2.6. Emplacement in the Brittle Regime.....	10
1.2.7. Construction of Plutons.....	10
1.2.8. Dikes.....	11
1.2.9. Geochronology.....	12
1.2.10. Relevance to this Study.....	14
1.3. Geologic Setting of the Connecticut Valley-Gaspé Trough.....	15
1.3.1. Regional Geology.....	15
1.3.2. Magmatism in the CVGT.....	19
1.3.3. Structural Geology.....	21
1.4. Geochronology of the Connecticut Valley-Gaspé Trough.....	23
1.4.1. Formation of Grenvillian Basement.....	24
1.4.2. Tectonic Model for the Taconic Orogeny.....	24
1.4.3. Summary of the Taconic Orogeny in Western Vermont.	25
1.4.4. Tectonic Model for the Acadian Orogeny.....	26
1.4.5. Acadian Overprinting on Taconian Rocks.....	27
1.4.6. Deposition and Deformation of Devonian Rocks of the CVGT.....	28
1.4.7. Timing of Magmatism in the CVGT.....	30
1.4.8. Summary.....	31
CHAPTER 2: ARTICLE FOR SUBMISSION.....	53
Abstract.....	53
1. Introduction.....	54
2. Geologic Background.....	55
2.1. Geologic Setting of the Connecticut Valley-Gaspé Trough.....	55
2.1.1. Regional Geology.....	55
2.1.2. Magmatism in the CVGT.....	59
2.1.3. Structural Geology.....	61
2.2. Constraints on the Timing of Tectonic Events.....	63
2.2.1. Formation of Grenvillian Basement.....	64

2.2.2. Tectonic Model for the Taconic Orogeny.....	64
2.2.3. Tectonic Model for the Acadian Orogeny.....	65
2.2.4. Acadian Overprinting on Taconian Rocks.....	66
2.2.5. Deposition and Deformation of Devonian Rocks of the CVGT.....	68
2.2.6. Timing of Magmatism in the CVGT.....	69
3. Methods.....	70
3.1. Microstructural Analysis.....	71
3.2. Ca and K Mapping of Biotite Grains under a Scanning Electron Microscope.....	72
3.3. ⁴⁰ Ar/ ³⁹ Ar Dating of Biotite, Muscovite, and Potassium Feldspar.....	74
3.4. U-Th Total Pb Monazite Dating.....	73
4. Results.....	75
4.1. 13SL02A.....	76
4.2. 13SL05A.....	77
4.3. 13SL05B.....	78
4.4. 13SL19A.....	79
4.5. 14SL03A.....	80
4.6. 13SL12A.....	80
4.7. 14SL02A.....	81
4.8. 13SL20B.....	81
4.9. 13SL20C.....	82
4.10. 13SL20D.....	83
4.11. 13SL21A.....	84
5. Discussion.....	85
5.1. Timing of Intrusion of the Knox Mountain Pluton.....	88
5.2. Timing of Cooling for the Knox Mountain Pluton’s Metamorphic Aureole...	90
5.3. Timing of Foliation Development in the CVGT.....	92
5.4. Observations Across the Transect and Region.....	93
5.5. Future Investigations.....	95
6. Conclusions.....	96

LIST OF FIGURES

Chapter 1: Comprehensive Literature Review

Figure 1: Geologic provinces of New England and eastern Canada, with field area.....	32
Figure 2: Field area and sample locations.....	34

Chapter 2: Article for Submission

Figure 1: Geologic provinces of New England and eastern Canada, with field area.....	99
Figure 2: Field area and sample locations.....	101
Figure 3: Cross section of transect, with plateau (or weighted mean) and minimum ages plotted versus location along transect.....	102
Figure 4: Select photomicrographs.....	104
Figure 5: $^{40}\text{Ar}/^{39}\text{Ar}$ age spectra.....	106–7
Figure 6: Evidence for solid-state deformation of granite.....	108
Figure 7: Gaussian histogram of monazite compositional domains.....	110
Figure 8: Cooling history of the Knox Mountain Pluton.....	111
Figure 9: Structural data.....	112

LIST OF TABLES

Table 1: Regional correlation of Taconian and Acadian Fabrics, central Vermont.....	113
Table 2: $^{40}\text{Ar}/^{39}\text{Ar}$ results summary.....	114–115
Table 3: Modal mineralogy based on petrographic observations of samples prepared in thin section.....	116–117

LIST OF APPENDICES

Appendix A: Photomicrographs.....	137
Appendix B: $^{40}\text{Ar}/^{39}\text{Ar}$ Analytical Results (for all samples).....	149

CHAPTER 1: COMPREHENSIVE LITERATURE REVIEW

1.1. Introduction

The relative timing and relationship between deformation and magmatic intrusion during orogenesis is often controversial, especially in polyphase orogens (Castonguay *et al.*, 2011). Polyphase deformation structures are pervasive in the metamorphic cores of orogenic belts that have been affected by multiple deformational events. Structural and metamorphic studies have been integrated with $^{40}\text{Ar}/^{39}\text{Ar}$ geochronologic data to understand the evolution of deformation during the Acadian orogeny (e.g. Castonguay *et al.*, 2007; 2011; Tremblay *et al.*, 2000), but limited work has been done to investigate the timing of deformation with respect to the intrusion of Acadian plutons (e.g. Hannula *et al.*, 1999).

$^{40}\text{Ar}/^{39}\text{Ar}$ data from mineral grains that formed during deformation can provide age constraints on specific structural and metamorphic events. Solar *et al.* (1998; and references therein) have proposed that testing whether granite genesis, extraction, ascent and emplacement was synchronous with metamorphism and deformation can be achieved by: 1) precisely dating regional deformation with thermochronology, 2) precisely determining the timing of crystallization of a pluton with crystallization ages of U-Pb minerals like zircon or monazite, and 3) comparison of cooling histories of rocks within and outside the pluton's metamorphic aureole.

Determining the nature, absolute timing, and duration of both deformation and intrusion are essential for understanding the dynamics of Acadian orogenic events in Vermont. Most of the plutonic bodies of the Connecticut Valley-Gaspé Trough (CVGT;

Figure 1; Figure 2) in eastern Vermont lack foliations and have long been thought to be post-tectonic intrusions due to their circular map patterns (e.g. Paterson *et al.*, 1991; Hannula *et al.*, 1999). In addition to the Victory Pluton (discussed below), the Barre pluton of central Vermont (Figure 2) is a notable exception, and is interpreted to be a syn-tectonic intrusion based on semi-concordant foliations of the pluton and country rock, as well as deformation in quartz grains from pluton margins to core (Richter, 1987).

This study addresses the question of whether the nearby Knox Mountain pluton, one of the largest Acadian plutons in New England (at +400km²), is a syn-tectonic or post-tectonic intrusion with respect to the regional deformation events of the Acadian Orogeny that resulted in and multiple generations of folds and foliations (F₃, F₄, and F₅; S₃, S₄, and S₅). Arguments are based on U/Th total Pb and ⁴⁰Ar/³⁹Ar geochronology of the pluton, its metamorphic aureole, and folded metasediments of the CVGT unaffected by contact metamorphism, with geochronologic results supported by regional field evidence and microstructural observations. This literature review will introduce three general topics related to this endeavor, including discussions on 1) the emplacement of granite generally derived from the melting of sedimentary rocks (S-type granite) associated with collisional orogenesis; 2) the tectonic setting of the central CVGT; and, 3) previous geochronologic investigations on rocks affected by the Acadian orogeny.

1.2. The Emplacement of Granite During Collisional Orogenesis

1.2.1. Introduction

Granitic rocks are one of the most fundamental components of Earth's continental crust, but constraints on mechanisms and timing of granite emplacement remain

controversial (Brown, 2013, and references therein). Studies on rare earth element anomalies from various crustal levels indicate that anatexis of the lower crust and migration of partial melt to the upper crust are a primary reason for intracrustal differentiation (Brown, 2013). Experimental studies have greatly advanced understanding on how melt is extracted during anatexis in pelites, amphibolites, and other mica-bearing protoliths. However, there is a strong need to have better constraints on the rates of crustal melting, time scales of melt segregation, focusing, and extraction, rates of magma ascent and emplacement, and time scales of pluton construction from multiple pulses of magma (Brown, 2013). Because the Knox Mountain pluton is a granodioritic rock derived from the anatexis of Al-rich metasedimentary units during a collisional orogeny (with minor contribution from the Grenville basement; Arth and Ayuso, 1997; Coish, 2010), S-type granites are the focus of this literature review, and granite that is a product of fractional crystallization of mantle-derived magma will not be discussed.

Many studies have shown that plutons are constructed incrementally from multiple batches of magma (e.g. Deniel *et al.*, 1987; Brown and Solar, 1999; Miller, 2008; Pressley and Brown, 1999; Clemens and Benn, 2010), and there is evidence of multiple diking events at the margins of the Knox Mountain pluton (Westerman and Coish, 2009). Experimental studies show that when a body of rock follows a prograde P-T evolution, many cycles of melt buildup and extraction are predicted to occur along the suprasolidus in P-T space (Handy *et al.*, 2001; Brown, 2007, 2010; Hobbs and Ord, 2010). Though large plutons can have cryptic internal structures and contacts that are difficult to recognize in the field, high-precision zircon geochronology and isotopic investigations have confirmed that plutons grow by addition of discrete batches of

magma (Deniel *et al.*, 1987; Hogan and Sinha, 1991; Brown and Pressley, 1999; Pressley and Brown, 1999; Coleman *et al.*, 2004; Matzel *et al.*, 2005, 2006; Schaltegger *et al.*, 2009; Miller *et al.*, 2007; Miller, 2008; Clemens and Benn, 2010; Acosta-Vigil *et al.*, 2012). Connolly and Podladchikov (2012) claim that even with an idealized homogeneous crust perturbed by an idealized melting reaction, melt flow is episodic with oscillations in fluid pressure. Bartley *et al.* (2008) proposed that plutons experience incremental growth by diking, with emplacement either between earlier sheets of granite and wall rocks (antitaxial growth), or within earlier sheets of granite (syntaxial growth) via a crack-seal mechanism. At the margins of the Knox Mountain pluton, thick granitoid sills are interlayered with the country rock, the Waits River Formation (Westerman and Coish, 2009). Before pluton construction can be discussed further, the mechanisms and time scales of melt generation, focusing, extraction, ascent, and emplacement must be summarized.

1.2.2. Generating Melt—Crustal Anatexis, Migmatites, and the Effect of Strain

Water plays a major role in initiating the partial melting of continental crust. In the presence of aqueous fluids under standard crustal pressures, pelites, greywackes, and silicious igneous rocks can begin to melt around 650–700°C (Brown and Korhonen, 2009; Sawyer, 2010). Studies from Reichardt and Weinberg (2012a, 2012b) show that mafic magma tends to be absent in zones of crustal thickening from collisional orogenies. Brown (2013) assumes that heat in orogenic crust is due to a combination of radioactive, mechanical (e.g., shear heating), and chemical (e.g., latent heat) processes, and that some heat can be redistributed by conduction and advection via intracrustal melt migration. During a prograde metamorphic cycle, melting can take millions to tens of millions of

years (10^6 – 10^7 yr) to occur along grain boundaries (Hermann and Rubatto, 2003; Reno *et al.*, 2009, 2012; Korhonen *et al.*, 2012). Melting and melt segregation are associated with deformation, and anatectic melts are thought to experience fast rates of segregation assisted by deformation, perhaps on the order of 10 – 10^4 yr for a single batch of melt (Sawyer, 1991; Harris *et al.*, 2000).

Migmatite terranes represent locations where melting has occurred, melt has accumulated, melt has transferred, and from which melt has drained (e.g., Brown, 2001b, 2008). In collisional orogenies, the amount of vertical displacement of melt from the anatectic zone to the level of emplacement varies according to several factors, including the tectonic setting, the degree of orogenic thickening, and the amount of post-orogenic extension and collapse, in addition to other variables (Brown and Solar, 1999). While we lack a full explanation as to how segregated melt in veins links to ascent of magma in conduits, we know that during deformation, melt can migrate perpendicular to the maximum principal stress when melt pressure overcomes the principal stresses and the tensile strength of the host rock (Wickham, 1987; Lucas and St. Onge, 1995; Brown and Solar, 1998a; Vernon and Paterson, 2001). Melt migration that is synchronous with folding can lead to the formation of disaggregated layers in diatexite migmatites, where the transport of melt was integral to the accommodation of strain (Weinberg and Mark, 2008). After studying leucosomes in migmatites, Weinberg *et al.* (2013) suggested melt migrates towards the hinge zone of antiformal folds. The amount and distribution of melt, the grain size of developing minerals, and the strain rate control the overall effect of melt on deformation, and whether or not strain will be localized in the concentrations of melt (Dell'Angelo and Tullis, 1988).

1.2.3. Melt Focusing and Extraction

The rate of heat flow in the crust is the determining factor for the rate of crustal melt production, and this is a function of the mechanism of heating and the thermal diffusivities of magma protoliths (Brown, 2013). Early melt segregation via diffusive mass transfer operates on a time scale approaching millions of years (10^6 yr) because there are many factors that affect rates and efficiencies of diffusion (Costa *et al.*, 2003; Dohmen and Chakraborty, 2003). Melt extraction aided by shear has been calculated at much faster rates (10^4 yr) based on deformation experiments on suprasolidus granite (e.g., Rutter and Mecklenburgh, 2006), and numerical modeling yields faster extraction times of a few thousand years (10^3 yr; e.g., Rabinowicz and Vigneresse, 2004). Inverse modeling of geochemical data by Harris *et al.* (2000) has yielded rates of extraction, ascent, and emplacement that are faster still for Himalayan granites (10^2 – 10^3 yr).

The mass transfer of melt involves a multitude of physical and chemical processes that operate at various time scales and are linked by the feedback relations between melting and deformation (Brown, 2010). The production of substantial quantities of melt requires the breakdown of hydrate minerals in a quartz and feldspar-bearing protolith at temperatures of at least 750 °C for mica-bearing rocks (Clemens, 2006). The timescale required to achieve temperatures exceeding 900 °C in the continental crust might be tens of millions of years (10^7 yr; Thompson and Connolly, 1995; Clark *et al.*, 2011). Even without fluids present, at 1000 °C pelites, graywackes, granites, andesites, and amphibolites may yield 20–70 vol % of H₂O-undersaturated melt (Clemens, 2006), of which 80–95 vol % could be extracted (Sawyer, 2001). However, it is important to highlight the differences in the time scales of melt generation and extraction. Anatexis in

the lower crust driven by heat supply is a continuous process, while melt extraction is a cyclically occurring discontinuous process (e.g., Brown and Solar, 1998a; Handy *et al.*, 2001; Vigneresse, 2004).

Modeling by several authors (e.g., Petford and Koenders, 1998; Bons and van Milligen, 2001; Ablay *et al.*, 2008; Hobbs and Ord, 2010) suggests that extraction of melt may be a self-organized critical phenomenon, and field studies on the size frequency distribution and spacing of plutons show that magmatic systems are self-organized from the bottom up (e.g., Bons and Elburg, 2001; Cruden and McCaffrey, 2001; Cruden, 2006; Koukouvelas *et al.*, 2006). Rosenberg and Handy (2005) suggest that ~7 volume % melt is the “melt connectivity transition” necessary to facilitate episodic extraction. The melt connectivity transition is dependent on some combination of melt fraction and distribution, but once it has been reached, a melt-bearing network of deformation bands will likely form as well (Brown, 2004, 2010). Systems can converge during episodic extraction on an optimal structure to maximize melt extraction (Brown, 2010; Hobbs and Ord, 2010), and a network of veins eventually drain melt from the source (e.g. Sawyer, 1991, 1994, 1998, 2001; Brown 1994, 2010; Brown *et al.* 1995). The rate of melt production and deformation-induced pressure gradients drive the system to continue moving melt from grain boundaries and pore spaces to vein networks. Focused melt flow requires dilatant shear failure at low melt fractions, consistent with the melt connectivity transition mentioned above (Rosenberg and Handy 2005; Brown, 2013). Deformation and pressure help the melt to drain from the source via a limited number of discrete tabular or cylindrical conduits to eventually feed upper-crustal plutons (Vigneresse, 1988; Brown and Solar, 1998b; Vigneresse *et al.*, 1999; Cruden, 2006). Magma ascent conduits

will mimic apparent finite strain of deformation where tectonic fabrics are steep because fabric anisotropies control the directionality of melt extraction (Brown and Solar, 1998a, 1998b, 1999; Weinberg *et al.*, 2009; Marcotte *et al.*, 2005). Processes involving pervasive migration facilitate the emplacement of melt sheets parallel to fabrics and other zones of high-permeability (Weinberg, 1999).

1.2.4. Magma Ascent and Emplacement

During collision, accumulated melt is able to migrate laterally and upwards between reservoirs because of a feedback relation that enhances melt flow. A higher melt percentage leads to increased porosity after melt migration, melt drainage to instabilities created by this porosity, and coupling between flow and melt fraction (Connolly, 2010; Connolly and Podladchikov, 1998, 2007, 2012). At first approximation, the volume of magma emplaced in the middle to upper crust seems to be equivalent to the volume of melt extracted from the middle to lower crust (Brown, 2013). The spacing of plutons exposed in collisional terranes in formerly active continental margins suggests that ascent is spatially focused, and the spacing of plutons likely reflects the size of the footprint of the source that was drained to feed them (Bons and Elburg, 2001; Cruden, 2006). The vertical distance between the site of melt accumulation and its source rarely exceeds 30 km (Brown, 2013). Crystallization and liquid fractionation occur continuously during melt extraction until the melt crosses the anatectic front. If a sufficient volume of melt has been produced before crustal-melting is no longer viable, the evolved melt can migrate to an upper-crustal level pluton via either fractures (e.g. Clemens and Mawer, 1992; Brown, 2004; Weinberg and Regenauer-Lieb, 2010), shear zones (e.g. Strong and Hanmer, 1981; D'Lemos *et al.*, 1992; Hutton and Reavy, 1992; Brown, 1994; Rosenberg,

2004), or conduits controlled by strain (e.g. Brown and Solar, 1998a, 1998b, 1999; Weinberg, 1999).

The means by which granite magma is emplaced in the upper crust to form kilometer-scale plutons remains controversial, and many mechanisms of accommodation have been argued to control the relationship between deformation and emplacement. Authors have demonstrated numerous mechanisms of intrusion, including emplacement via diking, diapirism, and intrusion into various shear regimes (Brown, 2013, and references therein). Determining and describing all of the various styles of emplacement is difficult because of the cryptic nature of internal contacts within large plutonic bodies, and because successively younger batches of magma likely intrude next to rock that is not fully crystalline (Brown, 2013). Additionally, emplacement styles will vary depending on whether magma ascent ceases in the ductile continental crust, the brittle continental crust, or in the ductile-to-brittle transition zone.

1.2.5. Emplacement in the Ductile Regime

In regions of the continental crust where conditions favor ductile deformation, emplacement can occur simply by a decrease in the rate of magma ascent approaching the ductile-to-brittle transition zone. Many authors have noted that this phenomenon may lead to the construction of sheeted plutons (e.g., Brown and Solar, 1998a; Miller and Paterson, 2001; Mahan *et al.*, 2003; Bartley *et al.*, 2008). Instabilities (internal and external to the conduit) in the magma wall-rock system can cause lateral expansion of an ascent conduit, and this lateral magma movement slows its ascent (Brown, 2001a, 2001b). External instabilities include variations in the strength of the wall rock and the stress field around the ascent column. Lagarde *et al.*, (1990) have proposed that blob-like

plutons are able to form because of the exploitation of lower stress sectors leading to the expansion of the ascent column. Instabilities internal to the ascent column include variations in the flow rate, surpassing the critical column width for flow without freezing, and changes in the cross-sectional shape above the anatectic zone (Brown, 2013).

Factors internal and external to the conduit affect one another. For example, advective heating of the country rock can lead to weakening of the wall rock and swelling of the conduit, a slowing of magma ascent, and perhaps crystallization.

1.2.6. Emplacement in the Brittle Regime

Brittle modes of emplacement are favored when vertical flow switches to predominantly horizontal flow and vertical inflation. Inflation is accommodated by depressing the floor and/or lifting of the roof (Cruden, 1998, 2006), sometimes aided by a component of ductile strain in the aureole (e.g., Wagner *et al.*, 2006) can be associated with faulting (Benn *et al.*, 1997; Clemens and Benn, 2010). The vertical growth of plutons is limited by the host-rock's mechanical properties, as well as the depth of emplacement. The thickness of the source and volume of anatexis there control how much vertical growth can be accommodated by floor depression, and this mechanism of accommodation seems to become more important with increasing depth (Cruden, 1998, 2006; Cruden and McCaffrey, 2001, 2002). Gravity modeling of plutons (e.g., Vigneresse, 1995) suggests that magma ascent commonly ends at the ductile-to-brittle transition zone.

1.2.7. Construction of Plutons

As suggested above, plutons undergo a preliminary birth stage of lateral spreading, followed by an inflation stage dominated by vertical thickening (Petford *et al.*,

2000). Tabular granites are often oriented parallel to other orogenic features in zones of apparent flattening strain, demonstrating that magma is emplaced in structures at high angles to the far-field maximum principal stress (Brown and Solar, 1998b; Solar and Brown, 2001). In the brittle-to-ductile transition zone, magma ascent velocity is either controlled by host rock viscosity, or magma viscosity when intruding an elastic, narrow fracture (Sumita and Ota, 2011). However, magma ascent through the crust can change as the wall-rock rheology evolves from ductile to brittle; it becomes possible for a buoyancy-driven liquid filled crack to migrate as a diapir-like hybrid (Brown, 2013). It is important to remember that these diapirs are actively emplaced during regional contractional deformation, so they are much different than diapirs that form during regional extension (i.e., salt diapirs; Jackson and Vendeville, 1994). In terms of how they are fed, elongate wedge-shaped plutons tend to be thick and have only a few root zones, while thin, equidimensional laccoliths tend to have many root zones (Brown and Solar, 1998b; Vigneresse *et al.*, 1999; Clemens and Benn, 2010).

1.2.8. Dikes

Dikes are defined by Brown (2013) as bodies of granite with high aspect ratios that are discordant to country rock foliations. Their formation is thought to initiate via hydrofractures (Bons *et al.*, 2001, 2004), or via ductile fracture (Brown, 2004, 2010; Weinberg and Regenauer-Leib, 2010). From there they propagate through the solid crust by brittle-elastic fracture until a decrease in transport rate causes freezing of the melt (Hobbs and Ord, 2010). Hydrofractures are thought to drain the anatectic zone of melt and transport melt through subsolidus crust via self-organized dikes (Bons *et al.*, 2004). This hydrofracturing is aided by diking *sensu-stricto*, or brittle fracture and elastic

deformation of the host rock at the tip of a fracture (Brown, 2013). Cracks propagate from dilation and shear bands which allows melt to flow through the deformation band network, down hydraulic potential gradients (Brown 2004, 2005). During ascent, an increase in viscosity of the subsolidus crust may change the fracture propagation mechanism from a ductile fracture process to a brittle-elastic fracture process (Brown 2008, 2010; Weinberg and Rengener-Lieb, 2010; Brown *et al.*, 2011; Sumita and Ota, 2011). Dikes in close proximity to one another can coalesce to focus melt ascent into a smaller number of larger-volume dikes (Brown, 2013). Ascent times for melt in a dike are likely less than one year (10^{-2} – 10^{-1} yr), yielding ascent rates of 10^{-2} – 10^{-1} m/s (Petford *et al.*, 1993; Clemens, 1998). If this is true, a small dike 1 km in length that is 3 m wide could transfer 10^3 km³ of melt from source to sink in ~1000 years (10^3 yr).

1.2.9. Geochronology

Accessory minerals such as zircon, monazite, and apatite have importance that far outweighs their modal abundance. They represent a significant reservoir for a number of petrogenetically important trace elements including zirconium, yttrium, heavy rare earth elements, hafnium and uranium in zircon, and phosphorus, thorium, and the light rare earth elements in monazite. Zircon and monazite can be used to date the crystallization of igneous intrusions because of their high closure temperatures, and can also be used to estimate the temperatures of crystallization of granitic hosts (e.g., Watson and Harrison, 1983; Montel, 1993). The initial lead isotope composition of a melt is sensitive to the age(s) and abundance of zircon in the source the melt derives from, and the amount of radiogenic lead that is incorporated into the melt via the dissolution of zircon during anatexis (Hogan and Sinha, 1991). Though zircon is heralded as a precise

geochronometer, unique crystallization ages of granites based on the U-Pb dating of zircon is complicated by zircon's ability to survive emplacement of multiple pulses of magma that eventually crystallize to a large pluton (Miller *et al.*, 2007). Nevertheless, zircon and monazite remain some of the only precise tools geologists have to date the emplacement of granite, and estimate the time scales required for the processes of melting, segregation, and emplacement described above. Chemical modeling is another means of estimating time scales it takes processes to occur. Ayres and Harris (1997) observed a major undersaturation of light rare earth elements in a granitoid, and concluded that its emplacement occurred in less than 10,000 years (10^4 yr). Experimental studies on melts undersaturated in zirconium indicate that emplacement of that magma could have occurred in as little as 100 years (10^2 yr; Patino Douce and Harris, 1998). Crystallization of melts can take between 500 to 30,000 years, where longer crystallization times are from granite laccoliths that were constructed from multiple batches of melt (Harris *et al.*, 2000). Many questions about the time scales of granite emplacement still remain. We are unsure if U-Pb ages retrieved from accessory minerals record the duration of a process such as crustal melting, or register the time taken for the magma to crystallize. It is unclear if the timing of anatexis initiation and melt connectivity can be dated using accessory minerals (Brown, 2013). It is clear that more experimental and geochronological investigations will be necessary to fully understand the rates of crustal melting, melt extraction, and magma emplacement involved in the construction of granitic plutons in collisional orogens.

1.2.10. Relevance to this Study

It is clear that all of the mechanisms involved in the generation and emplacement of magma during collision orogenies is not completely understood. However, the abundance of granitoid rocks in orogenic belts suggests anatexis of sedimentary rocks is a common phenomenon during orogenesis, and that emplacement of granite via this mechanism is a substantial way to generate continental crust (Brown, 2013).

The granodiorite that comprises the Knox Mountain pluton is believed to have been generated during the Acadian orogeny by the partial melting of the metasedimentary units into which the pluton intrudes (Arth and Ayuso, 1997; Coish, 2010). Regional geology suggests the plutons of the New Hampshire Plutonic Series were emplaced within the crustal column at a depth of roughly 15 kilometers (Westerman and Coish, 2009), under roughly greenschist-facies pressure-temperature conditions (230–480 °C, ≤ 0.4 GPa; Laird and Albee, 1981; Castonguay *et al.*, 2007; McWilliams *et al.* 2013).

The Knox Mountain pluton is a biotite-rich two-mica granodiorite, with evidence that some sections were constructed via multiple diking events, including late stage leucocratic and pegmatitic dikes (Westerman and Coish, 2009). At the Knox Mountain pluton margin, granitoid dikes surrounding xenoliths of hornfels-facies Waits River Formation are folded coherently, suggesting the pluton intruded around the ductile-to-brittle transition zone, and the Waits River Formation, Gile Mountain Formation, and Knox Mountain granite of central Vermont have all experienced both brittle and ductile deformation.

1.3. Geologic Setting of the Connecticut Valley-Gaspé Trough

1.3.1. Regional Geology

The rocks of New England preserve a record of the Paleozoic accretionary history of the margin of Laurentia (Figure 1). The Paleozoic geology of central Vermont records the closure of the Iapetus Ocean during collision and accretion of arcs and terranes with the Laurentian margin (Stanley and Ratcliffe, 1985; Pinet and Tremblay, 1995). The Middle to Late Ordovician Taconic orogeny is associated with east-dipping subduction of the Laurentian margin and eventual closure of the westernmost Neo-Iapetus ocean due to collision with the Shelburne Falls island arc (Karabinos *et al.*, 1998). The termination of Taconic orogenesis is marked by the development of a west-dipping subduction zone east of and beneath the Bronson Hill arc to the east of Laurentia within the Iapetus Ocean. During the Silurian, post-Taconian convergence occurred in conjunction with extension due to slab break-off of the west-subducting Gondwanan crust. Rising asthenosphere in the Québec embayment resulted in continuous extension that yielded Paleozoic basins, including the Connecticut Valley-Gaspé trough (CVGT) and Central Maine trough (Karabinos *et al.*, 1998; Rankin *et al.*, 2007).

During the Silurian and Early Devonian, the Taconic orogen was eroded significantly, and the resulting shales, limestones, and sandstones were deposited in the elongate series of marginal basins to the east of the mountains (namely, the CVGT), extending from southern New England to the Gaspé Peninsula (Tremblay and Pinet, 2005). The west-directed contractional events of the ensuing Acadian orogeny folded most of the sediments in the trough into recumbent, isoclinal kilometer-scale nappes that locally verge towards the southwest. Metamorphism due to burial, regional deformation,

and contact heat from magmatic intrusion metamorphosed them to schists, phyllites, marbles and quartzites (Hannula *et al.*, 1999; Robinson *et al.*, 1991).

In the Northern Appalachian Belt, up to 50% of the surface exposure consists of the Silurian and Devonian metasedimentary and igneous rocks described above (Figure 1; Tremblay and Pinet, 2005). Contrasting interpretations of these sedimentary basins has yielded the proposal of several possible tectonic scenarios for how Avalonia terranes accreted onto the Laurentian margin (Nance *et al.*, 2002). Robinson *et al.* (1998) suggested these rocks formed from backarc extension in foreland basins with lithosphere delamination along a SE-dipping subduction zone, while other authors believe the delamination occurred along a NW-dipping subduction zone (e.g. van Staal and de Roo, 1995; Moench and Aleinikoff, 2002). Bradley (1983) suggested foreland basins were overlying two subduction zones plunging opposite directions. Finally, multiple authors have proposed these rocks formed in transpressive or transtensional rift basins (e.g. Keppie and Dostal, 1994; Bourque, *et al.*, 1995). Rankin *et al.* (2007) state that delamination of the lithosphere in an east-dipping subduction zone caused asthenospheric upwelling. This upwelling led to basement uplift, partial melting of the crust, and inter-plate magmatism, all of which contributed to the regional extension that resulted in the formation of the CVGT.

In Vermont, the Connecticut Valley-Gaspé trough is bound unconformably to the west by the “Richardson Memorial contact” (RMC), which locally coincides with the Dog River Fault Zone (DRFZ), and to the east by faults of the Bronson Hill anticlinorium (Westerman, 1987; McWilliams *et al.*, 2010). The debate surrounding the tectonic versus stratigraphic origin of the RMC has historically been controversial, and the contact has

been interpreted as a fault related to Acadian deformation (e.g. Hatch *et al.*, 1988), a Silurian erosional unconformity (e.g. Hatch, 1982), or a syn-depositional fault and unconformity (Karabinos, 1998). Although Westerman (1987) suggested that the RMC corresponds to the DRFZ in central Vermont, Walsh *et al.* (2010) note that in central Vermont, the RMC and DRFZ are not always coincident. Because RMC most appropriately refers to a stratigraphic contact, the faulted boundary at the westernmost limit of the CVGT shall be referred to as the DRFZ herein. The DRFZ has been correlated to two décollements based on regional folds, stratigraphic position, and surface trace: the Surface of Acadian Structural Disharmony to the south in Massachusetts, and the La Guadeloupe fault to the north in Québec (Hatch and Stanley, 1988; Kim and Klepeis, 2015).

The metasedimentary rocks of the CVGT include, from oldest to youngest, the Silurian Shaw Mountain Formation, the Silurian and Devonian Northfield Formation, the Silurian and Devonian Waits River Formation, and the Devonian Gile Mountain Formation (Figure 2; Walsh *et al.*, 2010). The Shaw Mountain Formation was first described by Currier and Jahns (1941), and is a predominantly a graded quartz-pebble conglomerate that unconformably overlies the RMC (and all pre-Silurian rocks in the valley). Work by several authors (e.g. Boucot and Thompson, 1963; Doll, 1984; Westerman, 1987) says that the bryozoans, brachiopod, coral and echinoderm fossil content of the Shaw Mountain Formation indicate a Middle Silurian age. The Northfield Formation is predominantly a dark grey phyllite with thin (<20 cm) layers of micaceous quartzite, matrix-supported conglomerate, and impure limestone, formally named by Doll *et al.* (1961), but also recognized by Currier and Jahns (1941) and Cady (1956) as

the Northfield slate. To the east, the Northfield Formation grades into the Waits River Formation (Walsh *et al.*, 2010).

The Waits River Formation was first described by Currier and Jahns (1941) as all rocks stratigraphically above the Northfield Slate, and stratigraphically below the Gile Mountain Formation. The Waits River Formation consists of interbedded phyllites and impure marbles of varying thicknesses, often referred to as crystalline limestones “because of their poor commercial qualities compared to the marbles of western Vermont,” (Cady, 1956). Regional fossil evidence from Hueber *et al.*, (1990) and Lavoie and Asselin (2004), combined with regional structural studies (e.g. Fisher and Karabinos, 1980; Hatch, 1988) suggest the Waits River and Northfield formations both lie stratigraphically beneath the Gile Mountain Formation. The Gile Mountain Formation is dominated by interbedded phyllite and quartzite, with minor calcareous phyllite and impure limestone (Walsh *et al.*, 2010). The segment of Gile Mountain Formation exposed to the west of the Knox Mountain pluton was initially interpreted to be a distinct unit named the Westmore Formation (e.g. Murthy, 1957), but alternate interpretations and revisions to the structure and stratigraphy of eastern Vermont indicate that the Westmore and Gile Mountain formations are one in the same, and are repeated due to the occurrence of the Brownington syncline (whose significance will be discussed below; Konig, 1961). The Gile Mountain and Waits River formations are cut by numerous granitic dikes and plutons associated with the Devonian New Hampshire plutonic suite, some of which (including the Knox Mountain pluton) have exposed areas of greater than 400 m² (Billings, 1956; Hannula *et al.*, 1999; Westerman and Coish, 2009). Both

sedimentary units have experienced significant metamorphism associated with both the orogenic events of the Acadian, as well as the intrusion of this plutonic series.

The Acadian orogeny has been divided into two separate metamorphic realms, the eastern and western belts, based on distinct styles of metamorphism (Armstrong *et al.*, 1992). The western Acadian belt was subjected to Barrovian-type metamorphism and is characterized by high-temperature and high-pressure conditions, and in central Vermont, the metamorphic grade generally increases towards the east (Armstrong *et al.*, 1992; Tremblay *et al.*, 2000; Walsh *et al.*, 2010). McWilliams *et al.* (2013) suggests the rocks of the CVGT were deformed at greenschist-facies conditions in southeastern Vermont. Greenschist-facies conditions in the range of 230–480 °C, ≤ 0.4 GPa have been cited in northern Vermont east of the Green-Mountain anticlinorium (Laird and Albee, 1981; Castonguay *et al.*, 2007). In terms of index mineralogical zones in central Vermont, the DRFZ is located in the biotite-grade zone, and the biotite–garnet isograd occurs roughly two kilometers east of Montpelier and maintains the same strike as the metasedimentary units in the region (see Figure 2). The garnet–staurolite isograd commences roughly five kilometers west of the Knox Mountain pluton near Plainfield, Vermont, and locally envelopes the Knox Mountain and the Barre plutons, suggesting magmatic intrusion post-dates the peak of regional metamorphism (Richter, 1987).

1.3.2. Magmatism in the CVGT

Significant intrusive magmatism occurred in conjunction with the transpressive orogenic events of the Acadian, yielding 14 distinct plutons within the CVGT as part of the New Hampshire plutonic series (Arth and Ayuso, 1997; Westerman and Coish, 2009). Many of the plutonic bodies often referred to as “granite” technically have the

composition of adamellite, and are most appropriately classified as granodiorites (Konig, 1961). Solar *et al.* (1998) have suggested that there is a general feedback relationship between contractional deformation and crustal anatexis that helps focus granite extraction and ascent through the crust during orogenies that explains how magma emplacement occurs in conjunction with compression. Westerman and Coish (2009) note that plutons in the CVGT with high aspect ratios (length divided by width) typically have a high alignment with regional foliations in the host country rock. Konig (1961) found flow structures in mica-rich sections of the Knox Mountain pluton near its eastern margin that are subparallel to the pluton margin itself. The map-view structures and corresponding shapes of metamorphic aureoles have been cited to suggest that of many Acadian intrusive bodies intruded after peak Acadian deformation and metamorphism (Richter *et al.*, 1997). Hannula *et al.* (1999) demonstrated that it is possible to correlate microstructures found in an intrusive body with microstructures in a pluton's metamorphic aureole. Their microstructural analysis of the Acadian Victory pluton in northeast Vermont correlated microstructures from the intrusion with the Monroe Fault and the pluton's metamorphic aureole to demonstrate syntectonic intrusion, with an intrusion depth of 14–20 kilometers. Numerous lines of evidence have been cited to indicate that the Knox Mountain pluton was injected forcefully, perhaps with the aid of mechanical stoping. Evidence includes unaltered and (mostly) unrotated xenoliths of country rock within the pluton, drag folds and fractures in the country rock migrating away from the Knox Mountain pluton, and country rock that conforms to the shape of the pluton (i.e. the strike of the country rock changes and remains parallel with the pluton margin near West Dover, Vermont; Hall, 1959; Konig, 1961).

1.3.3. Structural Geology

Five generations of folding from ductile deformation with associated structures are recognized in the field area (See Table 1). The five generations are designated from oldest to youngest D_1 – D_5 , where D_1 and D_2 fabrics are interpreted to be a product of the Taconian orogeny, and D_3 , D_4 , and D_5 are interpreted to be a product of the Acadian orogeny. Locally, Taconian deformation yielded tight to isoclinal folds with penetrative, coplanar fabrics in the pre-Silurian rocks stratigraphically below the RMC. S_1 is a relict layer-parallel foliation in the Cambrian/Ordovician Moretown and Cram Hill Formations. S_2 sometimes appears as the dominant schistosity in the Moretown Formation as a pinstripe texture, though it is often a relict texture where overprinted by S_3 . D_3 – D_5 are the three youngest events in the CVGT, and associated fabrics from these three deforming events are present on both sides of the DRFZ. Locally, the third generation foliation (S_3) strikes northeast, dips steeply to the northwest, and is the most penetrative and dominant deformational fabric in the CVGT, especially in close proximity to and on both sides of the DRFZ (Walsh *et al.*, 2010; Westerman, 1987).

D_3 is the first event associated with the Acadian orogeny, and it resulted in the folding of the Silurian–Devonian Northfield, Waits River, and Gile Mountain Formations into a major regional syncline, where F_3 folds plunge 10° – 25° to the north, strike to the north-north-east, and dip 40° – 75° to the west. The field area of interest falls on the western limb of this major synclinal structure. The axial region of the fold consists of Gile Mountain Formation, and the Waits River Formation is found on both limbs (Konig, 1961; Figure 2; Figure 3). Richardson (1906) first recognized the Brownington syncline in the St. Johnsbury quadrangle. It was officially named by Doll (1951), and then traced

southward into the Lynodnville quadrangle by Denis (1956), and eventually the Plainfield quadrangle by Konig (1961), where its axial trace runs parallel to the contact between the Waits River and Gile Mountain formations, and subparallel to the pluton margin (Figure 2). In the western end of the Plainfield quadrangle, Konig (1961) also recognized bedding-cleavage relationships and drag-fold relationships, and proposed the existence of the Woodbury syncline in the western limits of the CVGT, and Nichols anticline between the two synclinal structures (Figure 2).

D₄ resulted in minor folds that are left-stepping in the west and right-stepping in the east, with strikes to the northwest and dips 30°–35° to the northeast (Walsh *et al.*, 2010). In addition to the development of these minor folds, this deformational event essentially resulted in the tightened the pre-existing F₃ folds. S₄ foliations often display box-fold geometries with crenulation lineations in the eastern segment of the Connecticut Valley Sequence in Vermont (Walsh *et al.*, 2010). Crenulation fabrics are generally visible in the local metapelitic rocks, but are often absent in the massive impure limestone beds (i.e. the thicker calcareous units of the Waits River Formation). S₅ is weakly developed and only locally pervasive in this section of the CVGT, although further south, in the Strafford and Barre East quadrangles, D₅ is responsible for the dome structures, such as the Strafford Dome, from which F₃ folds plunge gently away (Murthy, 1957). The tightness of F₄ minor folds also tend to decrease away from F₅ domes (Murthy, 1957). Bean (1953) suggests there may be a low-density granitic intrusion beneath the domal structures, citing residual negative gravity anomalies as evidence.

Work by Hannula *et al.* (1990) on the Victory Pluton in the north eastern Vermont segment of the CVGT determined that pluton was emplaced 14–20 kilometers deep after

the development of the dominant foliation (S_3), but probably in some conjunction with S_4 or S_5 development, citing brittle and ductile structures within the pluton as evidence.

Anderson and Coish (1999) used hornblende geobarometry to determine that three of the plutons in northeastern Vermont and the CVGT intruded at depths ranging from 8–14 km.

There is a general increase in metamorphic grade with associated changes in deformation, and a corresponding decrease in age as one progresses south in the CVGT. There exists a need to correlate the timing of pre-Acadian fabric development in southern Québec and northern Vermont (Castonguay *et al.*, 2011). Workers are still trying to determine the relationship between the D_1 and D_2 pre-Acadian fabrics observed in Vermont and the D_1 , D_2 , and D_3 pre-Acadian fabrics observed in Québec. The timing of these deformational events and the timing of formation of the CVGT has been constrained (and can be better constrained) using a number of dating techniques, including $^{40}\text{Ar}/^{39}\text{Ar}$ and U/Pb geochronology.

1.4. Geochronology of the Connecticut Valley-Gaspé Trough

This section summarizes previous geochronologic investigations within the Connecticut Valley-Gaspé trough, and summarizes a suite of articles that span the regional extent of the trough. Much of the known timing of Acadian deformation has been observed as an overprint on age on Neoproterozoic to Middle Ordovician Taconian structures (west of the CVGT). Therefore, cooling ages attributed to both Taconic and Acadian orogenic events will be presented herein. Because of the extent of work that has been done throughout the region affected by Acadian deformation, this analysis

introduces the formation of the Grenvillian basement rocks of Vermont, provides tectonic models for the Taconic and Acadian orogenies, and includes a final note on the timing of intrusion of some members of the New Hampshire Plutonic series within the CVGT.

1.4.1. Formation of Grenvillian Basement

Doolan (2007) suggests the rocks exposed at the surface of the Earth today in Vermont were deposited upon or transported onto an ancient “basement” of rocks, which themselves were accreted onto the Laurentian margin during the Grenville orogeny. Today, rocks of Grenvillian age are exposed in the Adirondack Mountains of New York, and McLelland *et al.* (1988) reported several U-Pb zircon studies from the magmatic Adirondack highlands with ages ranging from 1321 ± 60 Ma– 1009 ± 10 Ma, with errors at 2σ . Exposures of allochthonous Grenvillian basement in southern Vermont yield similar ages, and the trondhjemitic gneisses of the Mount Holly Complex yield ages of volcanism and plutonism that range from 1.35–1.31 Ga (Ratcliffe *et al.*, 1991).

1.4.2. Tectonic Model for the Taconic Orogeny

The Taconic orogenic cycle was a complex orogeny that lasted from Late Cambrian and Late Ordovician time (~500–450 Ma; Stanley and Ratcliffe, 1985; van Staal and Barr, 2012). The orogeny was due to the closure of the Neo-Iapetus Ocean, a basin that originally opened due to rifting of the Rodinian continent and Laurentian continental margin during the Latest Proterozoic to Early Cambrian. Nb/Y and HREE concentrations suggest the associated basaltic and gabbroic magmas that intruded during rifting are similar to rift basalts from Iceland and the East African Rift, and indicate these magmas were tapping an undepleted mantle source. Cawood *et al.* (2001) has suggested that rifting may have occurred over multiple episodes between 570–543 Ma. The ensuing

westward-imbrication of these rift-transition-rift rocks during the Taconic orogeny has metamorphosed them to the greenstone and amphibolite members of Rowe-Hawley slice of northern Vermont (Coish *et al.*, 2011).

The Taconic Orogeny resulted in contrasting geometries in the Canadian Appalachians and Vermont due to the irregular nature of the Laurentian margin and linear nature of the accreted volcanic arc (Stanley and Ratcliffe, 1985). In Québec and western Massachusetts, a western-directed “piggyback” sequence of thrust slices is observed, with early-emplaced, thrust-bounded allochthonous slices in the east and ophiolite-capped thrust slices in the west. At least three distinct tectonic events are recognized in the Canadian Appalachians, and van Staal *et al.* (2009, and references therein) suggests arc-continent collision was occurring with little diachroneity by 480–470 Ma. The conclusion of the Taconic orogeny is marked by the subsidence of plate convergence between Laurentia and the Shelburne Falls arc, due to the development of the west-dipping subduction zone and the subsequent development of the Bronson Hill arc, ca. 454 Ma (Karabinos *et al.*, 1998).

1.4.3. Summary of the Taconic Orogeny in Western Vermont

In western Vermont, only two Taconic tectonic events are recognized, and there remains some difficulty correlating these two events with the three events recognized in Canada (Castonguay *et al.*, 2011). Stanley and Ratcliffe (1985) used stratigraphic and structural correlations to determine a relative chronological sequence of events that depict the evolution of the Taconic orogeny. They conclude that the metasedimentary rocks of the Champlain Valley Sequence and Taconic Allochthons were deposited in the westernmost Neo-Iapetus Ocean on either Grenvillian basement or the aforementioned

rift-transitional-rift rocks during the Cambrian and Early Ordovician (~541 Ma–470 Ma). Coarse-grained clastic rocks like the Cheshire and Monkton formations were the product of weathering the Himalaya-scale Grenvillian Mountains, and were being deposited in a near-shore environment on the Laurentian margin. These and other sedimentary units were accreted on the Laurentian margin as the Neo-Iapetus closed during the Taconic orogeny in the Middle to Late Ordovician. Stanley and Ratcliffe (1985) suggest that nearly 1,000 km of shortening was accommodated by secondary cleavage development and low-angle thrust faulting. In northern Vermont, a trend in younging is observed from west to east towards the hinterland of the orogeny, where significant folding, refolding, and fault activation occurred. It is also worth noting that the Taconic rocks of New England have been significantly more affected by Acadian deformation in the form of minor folds compared to the rocks of the Canadian Appalachians (Stanley and Ratcliffe, 1985; van Staal and Barr, 2012).

1.4.4. Tectonic Model for the Acadian Orogeny

Tremblay and Pinet (2005) suggested east-dipping slab break-off ca. 435 Ma was responsible for asthenospheric upwelling that led to the opening of the CVGT. Westward-migrating extension followed upwelling ca. 420–415 Ma, and Rankin *et al.* (2007) demonstrated that magmatism ca. 428–416 Ma was coeval with the extension that formed the CVGT based on $^{207}\text{Pb}/^{206}\text{Pb}$ dating of mafic dikes in northern Vermont. The Acadian orogeny is thought to be a product of closing both the Iapetus ocean between Laurentia and Avalonia, and a narrow Acadian Seaway that separated Avalonia from the Ganderia terrane further east via northwest-dipping subduction zones (present-day coordinates; van Staal and Barr, 2012). The suturing of Avalonia and Ganderia occurred

during the Silurian in association with the closure of the Acadian Seaway from 442–421 Ma, and was followed by subsequent collision between Laurentia and Avalonia from 421–390 Ma (van Staal and Barr, 2012, and references therein).

Dextral-oblique collision between the Meguma terrane and composite Laurentia occurred from ca. 395–340 Ma (van Staal, 2007; van Staal *et al.*, 2009). This oblique, protracted collision was mainly accommodated by the Cobequid-Chedabucto fault system on land in Nova Scotia, and included a component of northwest-directed thrusting (Piper and Piper, 2002; van Staal and Barr, 2012). Orogen-normal structures from Acadian crustal shortening include upright and steeply inclined folds, and high-angle reverse faults, and dextral shear zones are the main orogen-parallel structures (e.g. van Staal and de Roo, 1995).

1.4.5. Acadian Overprinting of Taconian Rocks

Laird *et al.* (1984) were interested in determining the timing of Acadian deformation in rocks east of the Green Mountain anticlinorium (Green Mountain/Rowe-Hawley Slices). The $^{40}\text{Ar}/^{39}\text{Ar}$ data they generated from biotite, muscovite, actinolite, hornblende, and glaucophane indicate high-to-medium-pressure metamorphism during the Taconic orogeny from ca. 471–439 Ma is overprinted by a medium pressure retrograde Acadian metamorphism from ca. 386–355 Ma. They found that Cambrian and Ordovician metamorphism occurred at ca. 460 ± 10 Ma in northeastern Vermont, with a Devonian overprint around ca. 360 ± 5 Ma just east of the Green Mountain anticlinorium (1σ errors). Whitehead *et al.* (1996) performed $^{40}\text{Ar}/^{39}\text{Ar}$ dating on muscovite and orthoclase from southeastern Québec and observed a clear Taconic age around 460 Ma, with one sample displaying the Acadian overprint at 377 Ma. $^{40}\text{Ar}/^{39}\text{Ar}$ age spectra from

within the footwall of La Guadeloupe fault, a fault that correlates with the DRFZ, are in agreement with these Acadian overprint ages (Tremblay *et al.* 2000; Walsh *et al.*, 2010). They report a peak in deformation and metamorphism around 380 Ma, a D₂ recrystallization around 375 Ma, and a D₃ thermal event ca 365 Ma (2σ errors), based on ⁴⁰Ar/³⁹Ar dating of biotite and muscovite in southern Québec.

Chan *et al.* (2000) were working in the Taconic Allochthon of southwestern Vermont, and report that Acadian S₁ and S₂ overprinting and foliation development occurred respectively at 370.7 ± 1.0 Ma and 345.5 ± 1.7 Ma (2σ errors) based on ⁴⁰Ar/³⁹Ar dating of cleavage domains. Also working in southwestern Vermont, Spear and Harrison (1989) used ⁴⁰Ar/³⁹Ar geochronology to constrain the timing of the Acadian metamorphic overprint in the Green Mountain anticlinorium and CVGT. They concluded that the Acadian overprint is not remarkably pervasive in some sections of southern Vermont, and it is sometimes easiest to observe within the axis of domes exposing Grenvillian basement in the CVGT. Sutter *et al.* (1985) were interested in constraining the Acadian overprint and Taconic peak in the Green Mountain anticlinorium as well, and by doing K/Ar dating on whole rock samples they found that peak metamorphic conditions were reached around 465 ± 5 Ma with the retrograde Acadian event occurring at 376 ± 5 Ma in southwestern Vermont (1σ errors).

1.4.6. Deposition and Deformation of Devonian Rocks of the CVGT

McWilliams *et al.* (2010) reports that in central Vermont, the deposition of the Waits River formation lasted from ~423 Ma–415 ± 2 Ma, and the age of deposition of the Gile Formation is at 411 ± 1 Ma, and these ages were generated via U/Pb dating of detrital zircons (1σ errors). Thompson *et al.* (1997) dated a dike crosscutting

amphibolites from the Standing Pond Volcanics member of the Waits River Formation to ca. 423 ± 4 Ma (1σ error), providing a minimum age constraint on the eruption age. Spear and Harrison (1989) performed $^{40}\text{Ar}/^{39}\text{Ar}$ dating on metamorphic hornblendes from the Standing Pond Volcanics, yielding ages ranging from 397 ± 10 Ma– 350 ± 7 Ma (1σ errors).

In southeastern Vermont on the eastern margin of the CVGT, McWilliams *et al.* (2013) dated the timing of deformation along the Westminster West Fault zone via $^{40}\text{Ar}/^{39}\text{Ar}$ step heating. They found that the Waits River formation records cooling ages that correspond to a peak of Acadian deformation at 365 Ma, and have evidence this region was subjected to deformation during the Alleghanian orogeny (c. 300 Ma). Though this late Paleozoic deformation has not been reported in Vermont before, Moecher *et al.* (1997) have reported evidence of static reheating without deformation with a similar age (300–295 Ma) further south in the CVGT within the Waterbury dome. Dietsch (2015) was able to constrain the timing of crystallization of a felsic orthogneiss of the Waterbury gneiss in the Waterbury dome via SHRIMP U-Pb ages of zoned zircons, yielding two populations with ages of 437 ± 4 Ma and 387 ± 5 Ma (2σ errors). Moecher *et al.* (1997) attempted to constrain the cooling ages of the Waterbury dome and CVGT in southern Connecticut via $^{40}\text{Ar}/^{39}\text{Ar}$ total fusion and $^{40}\text{Ar}/^{39}\text{Ar}$ step heating of hornblende and muscovite. They note that ages get notably younger progressively further south, with their southernmost samples yielding cooling ages 50–100 Myr younger than their samples from the Waterbury dome. Their calculated ages range from 374 ± 3 Ma in close proximity to the dome, to 254 ± 1 Ma tens of kilometers south of the dome (2σ errors). This is strong evidence this section of the CVGT was affected by an Alleghanian

thermal event.

1.4.7. Timing of Magmatism in the CVGT

Simonetti and Doig (1990) dated several granitic plutons along the La Guadeloupe fault in southern Québec with $^{87}\text{Rb}/^{86}\text{Sr}$ whole-rock and U/Pb zircon dating, yielding a range of ages from 384 ± 3 Ma– 374 ± 1 Ma (2σ errors). Naylor (1971) used Rb/Sr dating techniques to constrain the cooling ages of a number of New Hampshire Plutonic series granitic plutons in the CVGT in northeast and east-central Vermont. Observed ages generated from individual mica grains ranged from 380–316 Ma, but they feared a few of their samples were subjected to some kind of isotopic disturbance. Arth and Ayuso (1997) also performed Rb-Sr dating on multiple plutons from northeast Vermont, yielding the ages of 390 ± 14 Ma, 376 ± 9 Ma, and 370 ± 17 Ma for the Nulhegan, Willoughby, and Derby plutons, respectively. Aleinikoff *et al.* (2011) dated a few Vermont/New Hampshire granite bodies, but they opted to date zircon and monazite grains via the U-Pb method. They claim these bodies intruded at a temperature lower than zircon's closure temperature, so their calculated age dates represent an age of crystallization. They found a granite body in Gassetts, NH crystallized at 392 ± 6 Ma, the Barre granite crystallized at 368 ± 4 Ma, and the Guilford Dome crystallized as late as 366 ± 1 Ma (2σ errors). As noted earlier, work by Hannula *et al.* (1990) in the north eastern Vermont segment of the CVGT has helped constrain the timing of intrusion relative to regional fabric development for the Victory Pluton, stating it was emplaced after the development of the dominant foliation (S_4), but probably in some conjunction with S_5 development.

1.4.8. Summary

The culmination of these findings poses some very interesting conclusions and questions to guide future studies in the Connecticut Valley-Gaspé trough. In addition to a fuller understanding of the timing of deformation and its relationship to magmatism in the CVGT, it would be desirable to constrain the spatial extent and timing of the Alleghanian deformation within the trough. If the motion along the Westminster West fault zone is indeed due to this late Paleozoic deformation, how far north and how far west was this Alleghanian deformation able to propagate? Are there possibly other structures that have been historically attributed to the Taconic or Acadian that may have been reactivated or have actually developed during the Alleghanian? Though this study cannot address all of the above questions, the information presented here suggests there is much work to be done correlating the timing of pluton intrusion relative to deformation in surrounding country rock (specifically, the Knox Mountain pluton for this study). Because these plutons were presumed to have intruded after the major tectonic activity of the Acadian, they have not been extensively studied for geochronology.

Figures

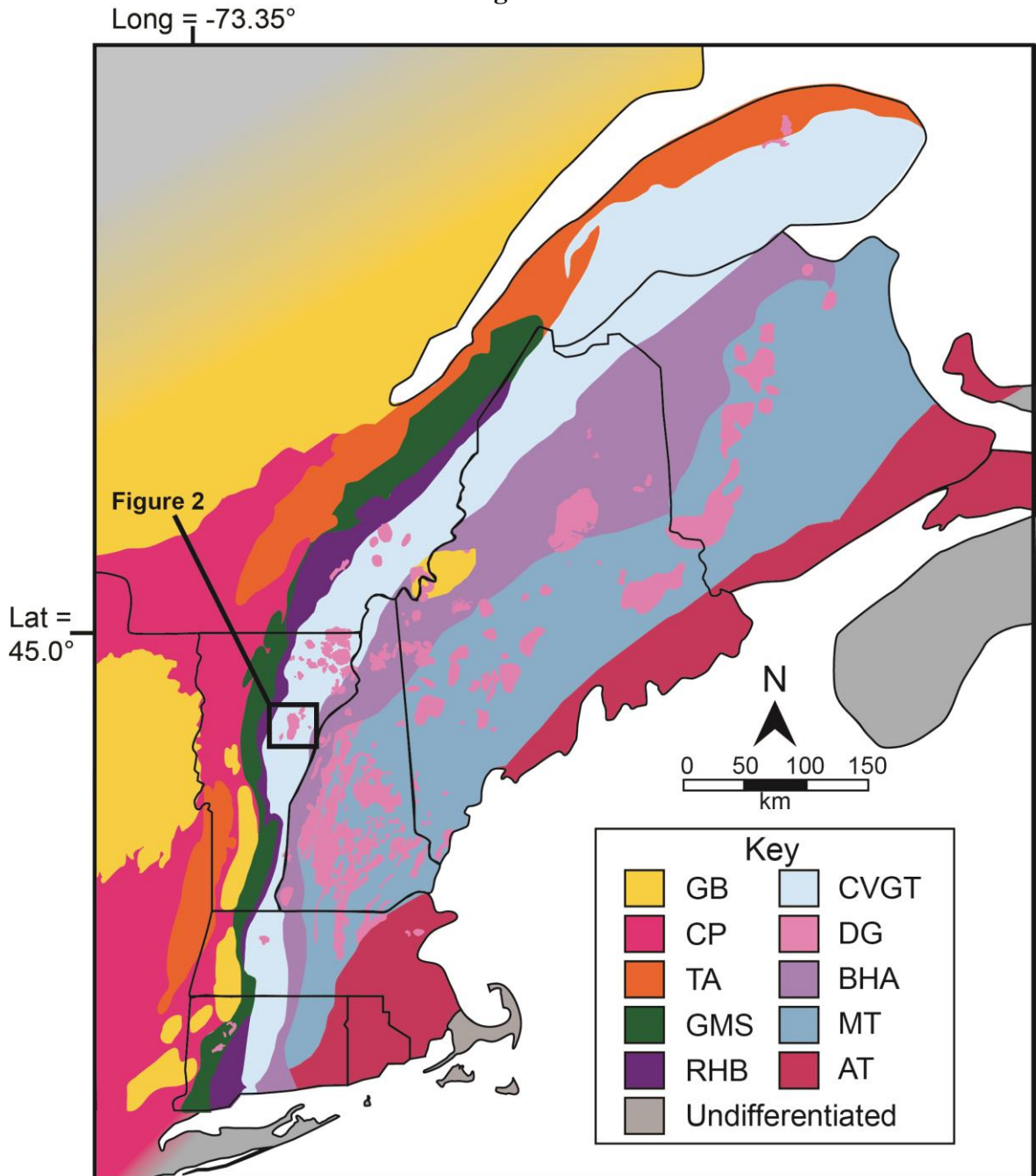


Figure 1: The geologic provinces of New England and maritime Canada record the Paleozoic accretionary history of North America. The following abbreviations have been assigned to the region's tectonic elements: GB- Grenvillian Basement; CP- Carbonate Platform; TA- Taconic Allochthon; GMS- Green Mountain Slice; RHB- Rowe-Hawley Belt; CVGT- Connecticut Valley Gaspé Trough; BHA: Bronson Hill Anticlinorium; MT- Merrimack Trough; AT- Avalon Terrane. Devonian-aged granitic plutons associated with the Acadian orogeny have been highlighted in pink, and the field area shown in

Figure 2 is highlighted in the thick black box. The following state and provincial bedrock maps were used in compilation of this figure: Canada: Weeler *et al.* (1996); Québec: Thériault *et al.* (2012); New Brunswick: Mersereau *et al.* (2008); Nova Scotia: Keppie *et al.* (2000); Maine: Osberg *et al.* (1985); New Hampshire: Lyons *et al.* (1997); Massachusetts: Zen *et al.* (1983); Rhode Island: Hermes *et al.* (1994); Connecticut: Rodgers, (1985); New York: Fisher *et al.* (1970); Vermont: Ratcliffe *et al.* (2011).

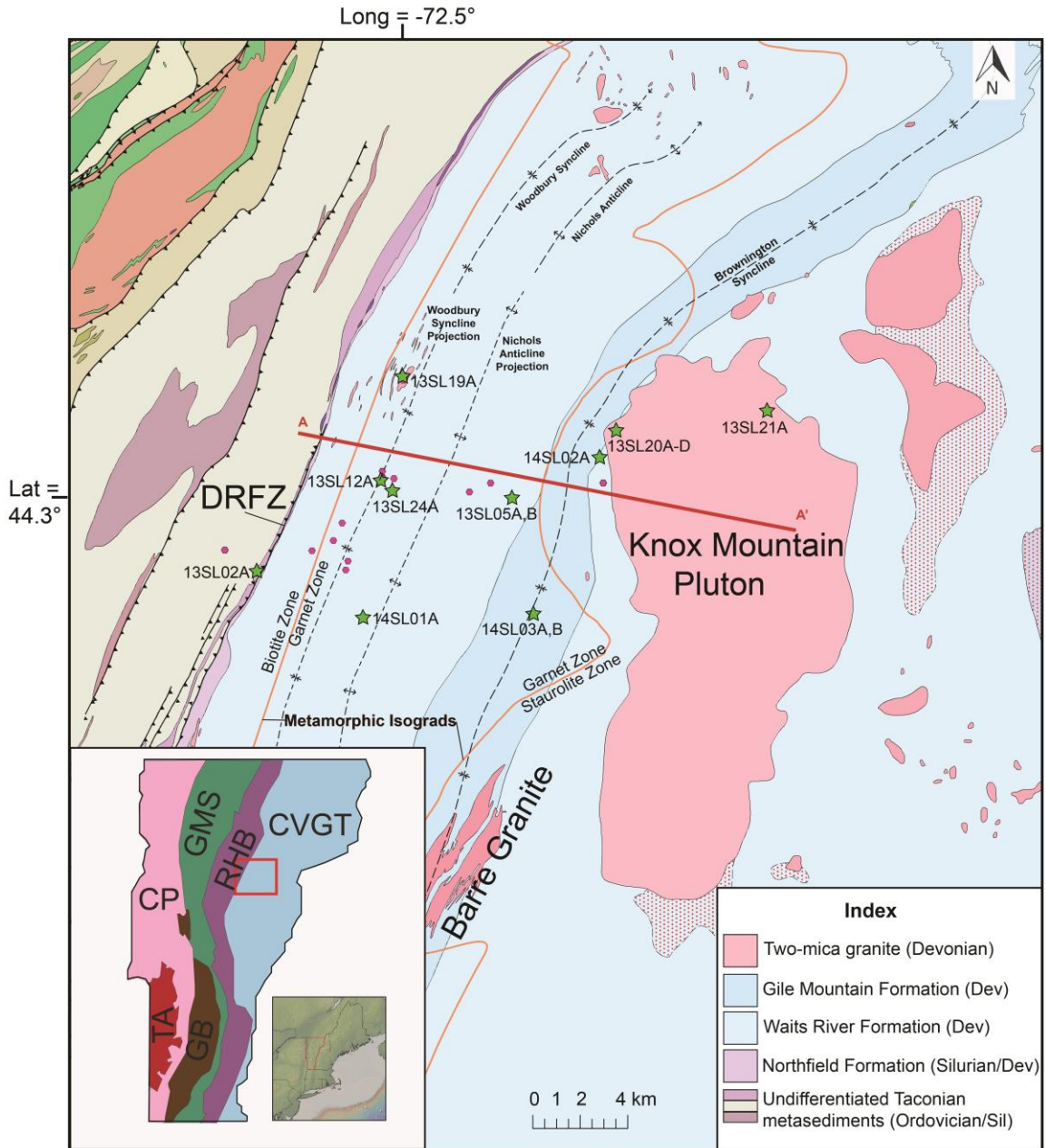


Figure 2: Geologic bedrock map of field locality, modified from the USGS Vermont state bedrock map by Ratcliffe *et al.* (2011). The red line A–A' designates the transect of interest (shown in cross section in Figure 3), extending from the Dog River fault zone (DRFZ) in the west to the margins of the Knox Mountain Pluton in the east. Oriented hand samples have been obtained from localities designated with a green star. Additional structural data was collected at localities marked with a pink hexagon (may appear as a dot). The red stipple pattern is defined by Ratcliffe *et al.* (2011) as a granite overprint. Inset shows map area within the geologic provinces of Vermont.

BIBLIOGRAPHY

- Ablay, G.J., Clemens, J.D., & Petford, N., 2008, Large-scale mechanics of fracture-mediated felsic magma intrusion driven by hydraulic inflation and buoyancy pumping, *in* Thompson, K., and Petford, N., eds., *Structure and Emplacement of High-Level Magmatic Systems: Geological Society of London Special Publication 302*, p. 3–29.
- Acosta-Vigil, A., Buick, I., Cesare, B., London, D., & Morgan VI, G.B., 2012, The extent of equilibration between melt and residuum during regional anatexis and its implications for differentiation of the continental crust: A study of partially melted metapelitic enclaves: *Journal of Petrology*, v. 53, p. 1319–1356, doi: 10.1093/ptrology/egs018.
- Aleinikoff, J. N., Ratcliffe, N. M., & Walsh, G. J., 2011, Provisional zircon and monazite Uranium-Lead geochronology for selected rocks from Vermont: U.S. Geological Survey Open-File Report 2011–1309, p. 1–46, available only online at <http://pubs.usgs.gov/of/2011/1309/>.
- Anderson, M. T., & Coish, R. A., 1999, Depth constraints on the origin of Northeast Kingdom granites: *Geological Society of America, Abstracts with Programs*, v. 31, no. 2, p. A-1.
- Armstrong, T. R., Tracy, R. J. & Hames, W. E., 1992. Contrasting styles of Taconian, eastern Acadian, and Western Acadian metamorphism, central and western New England. *In* *Journal of Metamorphic Geology*. v. 10, p. 415–426.
- Arth, J. G., & Ayuso, R. A., 1997, The Northeast Kingdom batholiths, Vermont: Geochronology and Nd, O, Pb, and Sr isotopic constraints on the origin of Acadian granitic rocks: *In* *The Nature of Magmatism in the Appalachian Orogen*, Geological Society of America Memoir 191. p. 1–18.
- Ayres, M., & Harris, N., 1997, REE fractionation and Nd isotope disequilibrium during crustal anatexis: Constraints from Himalayan leucogranites: *Lithos*, v. 139, p. 249–269.
- Bartley, J.M., Coleman, D.S., & Glazner, A.F., 2008, Incremental pluton emplacement by magmatic crack-seal: *Transactions of the Royal Society of Edinburgh–Earth Sciences*, v. 97, p. 383–396.
- Bean, R. J., 1953, Relation of Gravity anomalies to the geology of Central Vermont and New Hampshire: *Geological Society of America Bulletin*, v. 64, p. 509–538.
- Benn, K., Horne, R.J., Kontak, D.J., Pignotta, G.S., & Evans, N.G., 1997, Syn-Acadian emplacement model for the South Mountain batholith, Meguma terrane, Nova Scotia: Magnetic fabric and structural analyses: *Geological Society of America Bulletin*, v. 109, p. 1279–1293, doi:10.1130/0016-7606(1997)109<1279:SAEMFT>2.3.CO;2.

Billings, M. P., 1956, The geology of New Hampshire, Part II, Bedrock geology, Concord, New Hampshire. State Planning and Development Commission: Mineral Resources Survey, p. 203.

Bons, P.D., & Elburg, M.A., 2001, Fractal size distribution of plutons: An example from the Lachlan fold belt, Australia, *in* Chappell, B.W., and Fleming, P.D., eds., S-Type Granites and Related Rocks: Australian Geological Survey Organisation Record 2001/2, p. 21–22.

Bons, P.D., & van Milligen, B.P., 2001, New experiment to model self-organized critical transport and accumulation of melt and hydrocarbons from their source rocks: *Geology*, v. 29, p. 919–922, doi:10.1130/0091-7613(2001)029<0919:NETMSO>2.0.CO;2.

Bons, P.D., Dougherty-Page, J., & Elburg, M.A., 2001, Stepwise accumulation and ascent of magmas: *Journal of Metamorphic Geology*, v. 19, p. 627–633, doi:10.1046/j.0263-4929.2001.00334.x.

Bons, P.D., Arnold, J., Elburg, M.A., Kalda, J., Soesoo, A., & van Milligen, B.P., 2004, Melt extraction and accumulation from partially molten rocks: *Lithos*, v. 78, p. 25–42, doi:10.1016/j.lithos.2004.04.041.

Bourque, P.-A., Brisebois, D., & Malo, M., 1995, Gaspé Belt, *In* Williams, H., (ed.), *Geology of the Appalachian-Caledonian Orogen in Canada and Greenland: Geological Survey of Canada, Geology of Canada*, v. 6, p. 316–351.

Bradley, D. C., 1983, Tectonics of the Acadian orogeny in New England and adjacent Canada. *Journal of Geology*. v. 91, p. 381–400.

Brown, M., 1994, The generation, segregation, ascent and emplacement of granite magma: The migmatite-to crustally- derived granite connection in thickened orogens: *Earth-Science Reviews*, v. 36, p. 83–130, doi: 10.1016/0012-8252(94)90009-4.

Brown, M., 2001a, Crustal melting and granite magmatism: Key issues: *Physics and Chemistry of the Earth*, v. 26, p. 201–212, doi:10.1016/S1464-1895(01)00047-3.

Brown, M., 2001b, Orogeny, migmatites and leucogranites: A review: *Proceedings of the Indiana Academy of Sciences*, v. 110, p. 313–336.

Brown, M., 2004, Melt extraction from lower continental crust: *Transactions of the Royal Society of Edinburgh—Earth Sciences*, v. 95, p. 35–48, doi:10.1017/S0263593300000900.

Brown, M., 2005, Synergistic effects of melting and deformation: An example from the Variscan belt, western France, *In* Gapais, D., Brun, J.-P., and Cobbold, P.R., (eds.), *Deformation Mechanism, Rheology and Tectonics: From Minerals to the Lithosphere: Geological Society of London Special Publication 243*, p. 205–226.

Brown, M., 2006, Melt extraction from the lower continental crust of orogens: The field evidence, *In* Brown, M., and Rushmer, T., (eds.), *Evolution and Differentiation of the Continental Crust*: Cambridge, UK, Cambridge University Press, p. 332–384.

Brown, M., 2007, Crustal melting and melt extraction, ascent and emplacement in orogens: Mechanisms and consequences: *Journal of the Geological Society of London*, v. 164, p. 709–730, doi:10.1144/0016-76492006-171.

Brown, M., 2008, Chapter 6: Granites, migmatites and residual granulites: Relationships and processes, *In* Sawyer, E.W., and Brown, M., (eds.), *Working with Migmatites*: Mineralogical Association of Canada, Short Course Series 38, p. 97–144.

Brown, M., 2010, The spatial and temporal patterning of the deep crust and implications for the process of melt extraction: *Philosophical Transactions of the Royal Society*, ser. A, v. 368, p. 11–51, doi:10.1098/rsta.2009.0200.

Brown, M., 2013, Granite: From genesis to emplacement. *Geological Society of America Bulletin*, v. 125 no.7/8, p. 1079–1113.

Brown, M., & Korhonen, F.J., 2009, Some remarks on melting and extreme metamorphism of crustal rocks, *In* Dasgupta, S., (ed.), *Physics and Chemistry of the Earth*: New York, Published for the Indian National Science Academy by Springer, p. 67–87.

Brown, M., & Pressley, R.A., 1999, Crustal melting in nature: Prosecuting source processes: *Physics and Chemistry of the Earth*, v. 24, p. 305–316, doi:10.1016/S1464-1895(99)00034-4.

Brown, M., & Solar, G.S., 1998a, Shear zone systems and melts: Feedback relations and self-organization in orogenic belts: *Journal of Structural Geology*, v. 20, p. 211–227, doi:10.1016/S0191-8141(97)00068-0.

Brown, M., & Solar, G.S., 1998b, Granite ascent and emplacement during contractional deformation in convergent orogens: *Journal of Structural Geology*, v. 20, p. 1365–1393.

Brown, M., & Solar, G.S., 1999, The mechanism of ascent and emplacement of granite magma during transpression: A syntectonic granite paradigm: *Tectonophysics*, v. 312, p. 1–33, doi:10.1016/S0040-1951(99)00169-9.

Brown, M., Averkin, Y.A., McLellan, E.L., & Sawyer, E.W., 1995, Melt segregation in migmatites: *Journal of Geophysical Research*, v. 100, p. 15,655–15,679, doi:10.1029/95JB00517.

Brown, M., Korhonen, F.J., & Siddoway, C.S., 2011, Organizing melt flow through the crust: *Elements*, v. 7, p. 261–266, doi:10.2113/gselements.7.4.261.

Cady, W. M., 1956, Bedrock geology of the Montpelier quadrangle: U.S. Geological Society Geologic Quadrangle Map GQ-79, scale 1:62,500.

Castonguay, S., Ruffet, G., & Tremblay, A., 2007, Dating polyphase deformation across low-grade metamorphic belts: An example based on $^{40}\text{Ar}/^{39}\text{Ar}$ muscovite age constraints from the southern Quebec Appalachians, Canada: *Geological Society of America Bulletin*, v. 119, no. 7–8, p. 978–992.

Castonguay, S., Kim, J., Thompson, P. J., Gale, M. H., Joyce, N., Laird, J., & Doolan, B. L., 2011, Timing of tectonometamorphism across the Green Mountain anticlinorium, northern Vermont Appalachians: $^{40}\text{Ar}/^{39}\text{Ar}$ data and correlations with southern Quebec: *Geological Society of America Bulletin*, v. 124 no. 3–4 p. 352–367.

Cawood, P.A., McCausland, P.J.A., & Dunning, G.R. 2001, Opening Iapetus: Constraints from the Laurentian margin in Newfoundland: *Geological Society of America Bulletin*, v. 113, n. 4, p. 443–453. doi:10.1130/0016-7606(2001)113<0443:OICFTL>2.0. CO;2.

Chan, Y. C., Crespi, J. M., & Hodges, K. V., 2000, Dating cleavage formation in slates and phyllites with the $^{40}\text{Ar}/^{39}\text{Ar}$ laser microprobe: An example from the western New England Appalachians, USA: *Terra Nova*, v. 12, no. 6, p. 264–271.

Clark, C., Fitzsimons, I.C.W., Healy, D., & Harley, S.L., 2011, How does the continental crust get really hot?: *Elements*, v. 7, p. 235–240, doi:10.2113/gselements.7.4.235.

Clemens, J.D., 1998, Observations on the origins and ascent mechanisms of granitic magmas: *Journal of the Geological Society of London*, v. 155, p. 843–851, doi:10.1144/gsjgs.155.5.0843.

Clemens, J.D., 2006, Melting of the continental crust: Fluid regimes, melting reactions, and source-rock fertility, *in* Brown, M., and Rushmer, T., eds., *Evolution and Differentiation of the Continental Crust*: Cambridge, UK, Cambridge University Press, p. 297–331.

Clemens, J.D., & Benn, K., 2010, Anatomy, emplacement and evolution of a shallow-level, post-tectonic laccolith: The Mt. Disappointment pluton, SE Australia: *Journal of the Geological Society of London*, v. 167, p. 915–941, doi:10.1144/0016-76492009-120.

Clemens, J.D., & Mawer, C.K., 1992, Granitic magma transport by fracture propagation: *Tectonophysics*, v. 204, p. 339–360, doi:10.1016/0040-1951(92)90316-X.

Coish, R. A., 2010, Magmatism in the Vermont Appalachians: *Geological Society of America Memoir*, v. 206, p. 91–110.

Coish, R.A., Fleming, F.S., Larsen, M., Poyner, R., & Seibert, J., 1985, Early rift history of the proto-Atlantic ocean: Geochemical evidence from metavolcanic rocks in Vermont: *American Journal of Science*, v. 285, n. 4, p. 351–378, DOI:10.2475/ajs.285.4.351.

Coish, R.A., Perry, D.A., Anderson, C.D., & Bailey, D., 1986, Metavolcanic rocks from the Stowe Formation, Vermont: Remnants of ridge and intraplate volcanism in the Iapetus Ocean: *American Journal of Science*, v. 286, n. 1, p. 1–28.
doi:10.2475/ajs.286.1.1.

Coish, R. A., Bramley, A., Gavigan, T., & Masinter, R.A., 1991, Progressive changes in volcanism during Iapetan rifting; comparisons with the East African Rift – Red Sea system: *Geology*, v. 19, n. 10, p. 1021–1024. doi:10.1130/0091-7613(1991)019<1021:PCIVDL>2.3. CO;2.

Coish, R., Kim, J., Morris, N., & Johnson, D., 2011, Late stage rifting of the Laurentian continent: evidence from the geochemistry of greenstone and amphibolite in the central Vermont Appalachians: *Canadian Journal of Earth Sciences*, v. 49, p. 43–58.
DOI:10.1139/E11-013.

Coleman, D.S., Gray, W., & Glazner, A.F., 2004, Rethinking the emplacement and evolution of zoned plutons: Geochronologic evidence for incremental assembly of the Tuolumne Intrusive Suite, California: *Geology*, v. 32, p. 433–436,
doi:10.1130/G20220.1.

Connolly, J. A. D., 2010, The mechanics of metamorphic fluid expulsion: *Elements*, v. 6, p. 165–172, doi:10.2113/gselements.6.3.165.

Connolly, J.A.D., & Podladchikov, Y.Y., 1998, Compaction driven fluid flow in viscoelastic rock: *Geodinamica Acta*, v. 11, p. 55–84, doi:10.1016/S0985-3111(98)80006-5.

Connolly, J.A.D., & Podladchikov, Y.Y., 2007, Decompaction weakening and channeling instability in ductile porous media: Implications for asthenospheric melt segregation: *Journal of Geophysical Research*, v. 112, B10205,
doi:10.1029/2005JB004213.

Connolly, J.A.D., & Podladchikov, Y.Y., 2012, A hydromechanical model for lower crustal fluid flow, *in* Harlov, D.E., and Austrheim, H., (eds.), *Metasomatism and the Chemical Transformation of Rock*, Lecture Notes in Earth System Sciences: Berlin, Heidelberg, Springer-Verlag, p. 599–658, doi:10.1007/978-3-642-28394-9.

Costa, F., Chakraborty, S., & Dohmen, R., 2003, Diffusion coupling between trace and major elements and a model for calculation of magma residence times using plagioclase: *Geochimica et Cosmochimica Acta*, v. 67, p. 2189–2200.

Cruden, A.R., 1998, On the emplacement of tabular granites: *Journal of the Geological Society of London*, v. 155, p. 853–862, doi:10.1144/gsjgs.155.5.0853.

Cruden, A.R., 2006, Emplacement and growth of plutons: Implications for rates of melting and mass transfer in continental crust, *In* Brown, M., and Rushmer, T., (eds.), *Evolution and Differentiation of the Continental Crust*: Cambridge, UK, Cambridge University Press, p. 455–519.

Cruden, A.R., & McCaffrey, K.J.W., 2001, Growth of plutons by floor subsidence: Implications for rates of emplacement, intrusion spacing and melt-extraction mechanisms: *Physics and Chemistry of the Earth, Part A: Solid Earth and Geodesy*, v. 26, p. 303–315, doi:10.1016/S1464-1895(01)00060-6.

Cruden, A.R., & McCaffrey, K.J.W., 2002, Different scaling laws for sills, laccoliths and plutons: Mechanical thresholds on roof lifting and floor depression, *In* Breitzkreuz, C., Mock, A., and Petford, N., (eds.), *First International Workshop: Physical Geology of Subvolcanic Systems—Laccoliths, Sills and Dikes (LASI)*: Freiberg, Germany, *Wissenschaftliche Mitteilung Institute für Geologie Technische Universität Bergakademie Freiberg*, 20/2002, p. 15–17.

Currier, L. W., & Jahns, R. H., 1941, Ordovician stratigraphy of central Vermont: *Geological Society of America Bulletin*, v. 52, p. 1487–1512.

Dell'Angelo, L.N., & Tullis, J., 1988, Experimental deformation of partially melted granitic aggregates: *Journal of Metamorphic Geology*, v. 6, p. 495–515, doi:10.1111/j.1525-1314.1988.tb00436.x.

Dennis, J. G., 1956, *The Geology of the Lyndonville area, Vermont*: Vermont Geological Survey Bulletin no. 8, p. 1-98.

Deniel, C., Vidal, P., Fernandez, A., LeFort, P., & Peucat, J.J., 1987, Isotopic study of the Manaslu granite (Himalaya, Nepal)—Inferences on the age and source of Himalayan leucogranites: *Contributions to Mineralogy and Petrology*, v. 96, p. 78–92, doi:10.1007/BF00375529.

Dietsch, C., 2015, Bedrock geology of the core and cover rocks of the Collinsville, Bristol, and Waterbury Domes, western Connecticut, *in* *Guidebook for Field Trips in Southeastern New England*. p. C-5, 1–19.

Dietsch, C. W., & Sutter, J. F., 1987, $^{40}\text{Ar}/^{39}\text{Ar}$ age spectrum data bearing on the polyphase thermal and tectonic evolution of the Connecticut Valley synclinorium, SW New England, U.S.A.: *In* *Evolution of metamorphic belts, metamorphic studies group, joint meeting with IGCP project 235*: Dublin, Ireland, University College, p. 6.

- Dohmen, R., & Chakraborty, S., 2003, Mechanism and kinetics of element and isotopic exchange mediated by a fluid phase: *American Mineralogist*, v. 88, p. 1251–1270.
- Doll, C. G., 1951, Geology of the Memphremagog quadrangle and the southeastern portion of the Irashurg quadrangle, Vermont: *Vermont Geological Society Bulletin* n. 3, 113 p.
- Doll, C. G., 1984, Fossils from the metamorphic rocks of the Silurian-Devonian Magog belt in northern Vermont: *Vermont Geology*, v. 3, p. 16.
- Doll, C. G., Cady, W. M., Thompson, J. B., Jr., & Billings, M. P., 1961, Centennial geologic map of Vermont: Montpelier, Vt., Vermont Geological Survey, 1 sheet, scale 1:250,000.
- D’Lemos, R.S., Brown, M., & Strachan, R.A., 1992, Granite magma generation, ascent and emplacement within a transpressional orogeny: *Journal of the Geological Society of London*, v. 149, p. 487–490, doi:10.1144/gsjgs.149.4.0487.
- Fisher, D. W., Isachsen, Y. W., & Rickard, L. V., 1970, Geologic Map of New York State, consisting of 5 sheets: Niagara, Finger Lakes, Hudson-Mohawk, Adirondack, and Lower Hudson: New York State Museum and Science Service, Map and Chart Series No. 15, scale 1:250,000.
- Fisher, G. W., & Karabinos, P., 1980, Stratigraphic sequence of the Gile Mountain and Waits River Formations near Royalton, Vermont: *Geological Society of America Bulletin*, v. 91, no. 5, p. 282–286.
- Hall, L. M., 1958, The geology of the St. Johnsbury quadrangle, Vermont and New Hampshire: Montpelier, Vermont Geological Survey Bulletin 13, 105 p.
- Handy, M.R., Mulch, A., Rosenau, N., & Rosenberg, C.L., 2001, The role of fault zones and melts as agents of weakening, hardening and differentiation of the continental crust: A synthesis: *In* Holdsworth, R.E., Magloughlin, J., Knipe, R.J., Strachan, R.A., and Searle, R.C., (eds.), *The Nature and Tectonic Significance of Fault Zone Weakening*: Geological Society of London Special Publication 186, p. 305–332.
- Hannula, K. A., Onasch, E., Wertheim, J., Lackey, J. S., Mattox, E., & McGrath, G., 1999, Syntectonic pluton intrusion during contractional deformation: Microstructural evidence from the aureole of the Acadian Victory Pluton, north-eastern Vermont, USA: *Journal of Metamorphic Geology*, v. 17, p. 271–286.
- Harris, N.B.W., Vance, D., & Ayers, M., 2000, From sediment to granite: Time scales of anatexis in the upper crust: *Chemical Geology*, v. 162, p. 155–167, doi: 10.1016/S0009-2541(99)00121-7.

Hatch, N. L., Jr., 1982, The Taconian Line in western New England and its implication to the Paleozoic tectonic history; *In* P. St-Julien and J., Béland (eds.), Major Structural Zones and Faults of the Northern Appalachians, Geological Association of Canada, special paper 24, p. 67–85.

Hatch, N. L., Jr., Moench, R. H., & Stanley, R. S., 1988, Stratigraphy of the Connecticut Valley Belt: *In* The bedrock geology of Massachusetts: United States Geological Survey paper P 1366 A–D, p. B1–B34.

Hatch, N. L., Jr., & Stanley, R. S., 1988, Post-Taconian structural geology of the Rowe-Hawley zone and the Connecticut-Valley belt west of the Mesozoic Basins: *In* Hatch, N. L., (ed.), The Bedrock Geology of Massachusetts, United States Geological Survey professional paper, p. C1–C33.

Hatch, N. L., Jr., Moench, R. H., & Stanley, R. S., 1988, Stratigraphy of the Connecticut Valley Belt: *In* The bedrock geology of Massachusetts: United States Geological Survey professional paper, p. B1–B34.

Hermann, J., & Rubatto, D., 2003, Relating zircon and monazite domains to garnet growth zones: age and duration of granulite facies metamorphism in the Val Malenco lower crust: *Journal of Metamorphic Geology*, v. 21, no. 9, p. 833–852.

Hermes, O. D., Gromet, L. P., & Murray, D. P., 1994, Bedrock Geologic Map of Rhode Island: Rhode Island Map Series No. 1, University of Rhode Island, Kingston, scale 1:100,000.

Hobbs, B.E., & Ord, A., 2010, The mechanics of granitoid systems and maximum entropy production rates: *Philosophical Transactions of The Royal Society, ser. A*, v. 368, p. 53–93, doi:10.1098/rsta.2009.0202.

Hogan, J.P., & Sinha, A.K., 1991, The effect of accessory minerals on the redistribution of lead isotopes during crustal anatexis: A model: *Geochimica et Cosmochimica Acta*, v. 55, p. 335–348, doi:10.1016/0016-7037(91)90422-2.

Heuber, F. M., Bothner, W. A., Hatch, N. L., Jr., Finney, S. C., & Aleinikoff, J. N., 1990, Devonian plants from southern Québec and northern New Hampshire and the age of the Connecticut Valley trough: *American Journal of Science*, v. 290, no. 4, p. 360–395.

Hutton, D.H.W., & Reavy, R.J., 1992, Strike-slip tectonics and granite petrogenesis: *Tectonics*, v. 11, p. 960–967, doi:10.1029/92TC00336.

Jackson, M.P.A., & Vendeville, B.C., 1994, Regional extension as a geologic trigger for diapirism: *Geological Society of America Bulletin*, v. 106, p. 57–73, doi: 10.1130/0016-7606(1994)106<0057:REAAGT>2.3.CO;2.

Karabinos, P., 1998, Tectonic and stratigraphic development of the Connecticut Valley Trough in New England Appalachians: *Geologic Society of America Abstracts with Programs*, v. 30, n. 7, p. 191.

Karabinos, P., Samson, S. D., Hepburn, J. C., & Stoll, H. M., 1998, Taconian orogeny in the New England Appalachians; collision between Laurentia and the Shelburne Falls Arc: *Geology*, v. 26, p. 215–218

Keppie, J. D., (compiler), 2000, Geological Map of the Province of Nova Scotia, Nova Scotia Department of Natural Resources (NSDNR) Published Map, scale 1: 500,000.

Keppie, J. D., & Dostal, J., 1994, Late Silurian-Early Devonian transpressive rift origin of the Québec Reentrant, Northern Appalachians: constraints from geochemistry of volcanic rocks. *Tectonics*. v. 13, p. 1183-1189.

Kim, J., Gale, M., Springston, G., Koteas, C., Defelice, C., & Saitta, N., 2015, Bedrock Geologic Map of the Southern Two-Thirds of the Woodbury Quadrangle, Vermont, Washington County, Vermont: Vermont Geological Survey Open File Report VG2015-2. 1 Plate, scale 1:24,000.

Kim, J. J., & Rukznis, A., 2011, Bedrock Geologic Map of the Plainfield Quadrangle, Washington County, Vermont: Vermont Geological Survey Open File Map VG113, 2 plates, scale 1:24,000.

Kim, J., Gale, M., McMillan, M., Zoltos, S., & Springston, G., 2010, Bedrock Geologic Map of the Town of Craftsbury, Vermont, Vermont Geological Survey Open File Map VG10-4, 3 Plates, scale 1:24,000.

Kim, J., & Klepeis, K. A., 2015, The along-strike context of the Richardson Memorial Contact (RMC) in the town of Craftsbury, north-central Vermont: *Geological Society of America, Abstracts with Programs*, v. 47, no. 3, p. 100.

Konig, R. H., 1961, Geology of the Plainfield Quadrangle, Vermont, Montpelier, Vermont Geological Survey Bulletin, n. 16, 86 p.

Korhonen, F.J., Brown, M., Grove, M., Siddoway, C.S., Baxter, E.F., & Inglis, J.D., 2012, Placing constraints on the timing of melting and melt loss events during polymetamorphism in the Fosdick migmatite-granite complex, West Antarctica: *Journal of Metamorphic Geology*, v. 30, p. 165–192, doi:10.1111/j.1525-1314.2011.00961.x.

Koukouvelas, I.K., Pe-Piper, G., & Piper, D.J.W., 2006, The relationship between length and width of plutons within the crustal-scale Cobequid shear zone, Northern Appalachians, Canada: *International Journal of Earth Sciences*, v. 95, p. 963–976, doi:10.1007/s00531-006-0077-7.

Lagarde, J.L., Brun, J.P., & Gapais, D., 1990, Formation of epizonal granitic plutons by in situ assemblage of laterally expanding magma: *Comptes Rendus de l'Academies des Sciences, Serie II*, v. 310, p. 109–114.

Laird, J., & Albee, A. L., 1981, High-pressure metamorphism in mafic schist from northern Vermont: *American Journal of Science*, v. 281, p. 97–126.

Laird, J., Lanphere, M. A., & Albee, A. L., 1984, Distribution of Ordovician and Devonian Metamorphism in mafic and pelitic schists from northern Vermont: *American Journal of Science*, v. 284, p. 376–413.

Lavoie, D., & Asselin, E., 2004, A new stratigraphic framework for the Gaspé Belt in southern Québec; Implications for the pre-Acadian Appalachians of eastern Canada: *Canadian Journal of Earth Sciences*, v. 41, n. 5, p. 507–525.

Lyons, J. B., Wothner, W. A., Moench, R. H., & Thompson, J. B., 1997, Bedrock geologic map of New Hampshire: U.S. Geological Survey, Reston, VA, State Geological Map, 2 sheets, scales 1:250,000 and 1:500,000.

Lucas, S.B., & St. Onge, M.R., 1995, Syn-tectonic magmatism and the development of compositional layering, Ungava orogen (northern Quebec, Canada): *Journal of Structural Geology*, v. 17, p. 475–491, doi:10.1016/0191-8141(94)00076-C.

Mahan, K.H., Bartley, J.M., Coleman, D.S., Glazner, A.F., & Carl, B.S., 2003, Sheeted intrusion of the synkinematic McDoogle pluton, Sierra Nevada, California: *Geological Society of America Bulletin*, v. 115, p. 1570–1582, doi:10.1130/B22083.1.

Marcotte, S.B., Klepeis, K.A., Clarke, G.L., Gehrels, G., & Hollis, J.A., 2005, Intra-arc transpression in the lower crust and its relationship to magmatism in a Mesozoic magmatic arc: *Tectonophysics*, v. 407, p. 135–163, doi:10.1016/j.tecto.2005.07.007.

Matzel, J.E.P., Mundil, R., Paterson, S., Renne, P., & Nomade, S., 2005, Evaluating pluton growth models using high resolution geochronology: Tuolumne intrusive suite, Sierra Nevada, CA: *Geological Society of America Abstracts with Programs*, v. 37, no. 6, p. 131.

Matzel, J.E.P., Bowring, S.A., & Miller, R.B., 2006, Time scales of pluton construction at differing crustal levels: Examples from the Mount Stuart and Tenpeak intrusions, North Cascades, Washington: *Geological Society of America Bulletin*, v. 118, p. 1412–1430.

McLelland, J., Chiarenzelli, J., Whitney, P., & Isachen, Y., U-Pb zircon geochronology of the Adirondack Mountains and implications for their geologic evolution: *Geology*, v. 16, p. 920–924. doi: 10.1130/0091-7613(1988)016<0920:UPZGOT>2.3.CO;2.

McWilliams, C. K., Walsh, G. J., & Wintsch, R. P., 2010, Silurian-Devonian age and tectonic setting of the Connecticut Valley-Gaspé Trough in Vermont based on U-Pb SHRIMP analyses of detrital zircons: *American Journal of Science*, v. 310, p. 325-363.

McWilliams, C. K., Kunk, M. J., Wintsch, R. P., & Bish, D. L., 2013. Determining ages of multiple muscovite-bearing foliations in phyllonites using the $^{40}\text{Ar}/^{39}\text{Ar}$ step heating method: Applications to the Alleghanian orogeny in central New England: *American Journal of Science*, v. 313, p. 996–1016.

Mersereau, K. J., Richard, D. M., & Rennick, M. P., 2008, Bedrock geology of New Brunswick: New Brunswick Department of Natural Resources, Minerals Policy and Planning Division, Map NR-1, scale 1:500,000.

Moench, R. H., & Aleinikoff, J. N., 2002, Stratigraphy, geochronology, and accretionary terrane settings of two Bronson Hill arc sequences, northern New England. *Physics and Chemistry of the Earth*. v. 27, p. 47–95.

Moecher, D. P., Cosca, M. A., & Hanson, G. N., 1997, Petrologic and $^{40}\text{Ar}/^{39}\text{Ar}$ geochronological constraints on the middle to late Paleozoic thermotectonic history of the southern Connecticut Valley zone, New England Appalachians: *Geological Society of America Bulletin*, v. 109, no. 2, p. 164–175.

Miller, J.S., 2008, Assembling a pluton...one increment at a time: *Geology*, v. 36, p. 511–512, doi:10.1130/focus062008.1.

Miller, J.S., Matzel, J.E.P., Miller, C.F., Burgess, S.D., & Miller, R.B., 2007, Zircon growth and recycling during the assembly of large, composite arc plutons: *Journal of Volcanology and Geothermal Research*, v. 167, p. 282–299, doi:10.1016/j.jvolgeores.2007.04.019.

Miller, R.B., & Paterson, S.R., 2001, Construction of mid-crustal sheeted plutons: Examples from the North Cascades, Washington: *Geological Society of America Bulletin*, v. 113, p. 1423–1442.

Montel, J.M., 1993, A model for monazite/melt equilibrium and application to the generation of granitic magmas: *Chemical Geology*, v. 110, p. 127–146, doi: 10.1016/0009-2541(93)90250-M.

Murthy, V. R., 1957, Bed rock geology of the East Barre area, Vermont: Vermont Geological Survey Bulletin n. 10, 121 p.

Murthy, V. R., 1958, A revision of the lower Paleozoic stratigraphy in eastern Vermont: *Journal of Geology*, v. 66, p 276–286.

Nance, R.D., Murphy, J.B., & Keppie, J.D., 2002, A Cordilleran model for the evolution of Avalonia: *Tectonophysics*, v. 352, p. 11–31, doi: 10.1016/S0040-1951(02)00187-7.

Naylor, R. S., 1971. Acadian Orogeny: An Abrupt and Brief Event: *Science* v. 172, p. 558-560.

Osberg, P. H., Hussey, A. M., II, & Boone, G. M. (editors), 1985, Bedrock geologic map of Maine: Maine Geological Survey, 1 plate, correlation chart, tectonic inset map, metamorphic inset map, color geologic map, cross sections, scale 1:500,000.

Paterson, S. R., Vernon, R. H., & Fowler, T. K., Jr., 1991, Aureole Tectonics. *In* Kerrick, D. M. (ed.), *Contact Metamorphism*, Mineralogical Society of America, *Reviews in Mineralogy*, v. 26, p. 673–722.

Patiño Douce, A.E., & Harris, N., 1998, Experimental constraints on Himalayan anatexis: *Journal of Petrology*, v. 39, p. 689–710, doi:10.1093/petroj/39.4.689.

Petford, N., & Koenders, M.A., 1998, Self-organization and fracture connectivity in rapidly heated continental crust: *Journal of Structural Geology*, v. 20, p. 1425–1434, doi:10.1016/S0191-8141(98)00081-9.

Petford, N., Kerr, R.C., & Lister, J.R., 1993, Dike transport of granitoid magmas: *Geology*, v. 21, p. 845–848, doi:10.1130/0091-7613(1993)021<0845:DTOGM>2.3.CO;2.

Petford, N., Cruden, A.R., McCaffrey, K.J.W., & Vigneresse, J.L., 2000, Granite magma formation, transport and emplacement in the Earth's crust: *Nature*, v. 408, p. 669–673, doi:10.1038/35047000.

Pe-Piper, G., & Piper, D. J. W., 2002, A synopsis of the geology of the Cobequid Highlands, Nova Scotia: *Atlantic Geology*, v. 38, p. 145–160.

Pinet, N., & Tremblay, A., 1995, Tectonic evolution of the Quebec-Maine Appalachians: From oceanic spreading to obduction and collision in the northern Appalachians: *American Journal of Science*, v. 295, p. 173–200.

Pressley, R.A., & Brown, M., 1999, The Phillips pluton, Maine, USA: Evidence of heterogeneous crustal sources, and implications for granite ascent and emplacement mechanisms in convergent orogens: *Lithos*, v. 46, p. 335–366, doi:10.1016/S0024-4937(98)00073-5.

Rabinowicz, M., & Vigneresse, J.L., 2004, Melt segregation under compaction and shear channeling: Application to granitic magma segregation in a continental crust: *Journal of Geophysical Research*, v. 109, p. B04407, doi:10.1029/2002JB002372.

- Rankin, D. W., Coish, R. A., Tucker, R. D., Peng, Z. X., Wilson, S. A., & Rouff, A. A., 2007, Silurian extension in the upper Connecticut Valley in the United States and the origin of Middle Paleozoic basins in the Québec embayment: *American Journal of Science*, v. 307, p. 216–264.
- Ratcliffe, N. M., Aleinikoff, J. N., Burton, W. C., & Karabinos, P., 1991 Trondhjemitic 1.35–1.31 Ga gneisses of the Mount Holly Complex of Vermont: evidence for an Elzevirian event in the Grenville Basement of the United States Appalachians: *Canadian Journal of Earth Sciences*, v. 28, p. 77–93.
- Ratcliffe, N.M., Stanley, R.S, Gale, M.H., Thompson, P.J., & Walsh, G.J., 2011, Bedrock Geologic Map of Vermont: [U.S. Geological Survey Scientific Investigations Map 3184](#), 3 sheets, scale 1:100,000.
- Reichardt, H., & Weinberg, R.F., 2012a, The dike swarm of the Karakoram shear zone, Ladakh, NW India: Linking granite source to batholith: *Geological Society of America Bulletin*, v. 124, p. 89–103, doi:10.1130/B30394.1.
- Reichardt, H., & Weinberg, R.F., 2012b, Hornblende chemistry in meta- and diatexites and its retention in the source of leucogranites: An example from the Karakoram shear zone, NW India: *Journal of Petrology*, v. 53, p. 1287–1318, doi:10.1093/petrology/egs017.
- Reno, B.L., Brown, M., Kobayashi, O.T., Nakamura, E., Piccoli, P.M., & Trouw, R.A.J., 2009, Eclogite–high pressure granulite metamorphism records early collision in West Gondwana: New data from the southern Brasília belt, Brazil: *Journal of the Geological Society of London*, v. 166, p. 1013–1032, doi:10.1144/0016-76492008-140.
- Reno, B.L., Piccoli, P.M., Brown, M., & Trouw, R., 2012, In situ chemical dating of monazite from the southern Brasília belt, Brazil: *Journal of Metamorphic Geology*, v. 30, p. 81–112, doi:10.1111/j.1525-1314.2011.00957.x.
- Richter, D. A., 1987, Barre granite quarries, Barre, Vermont, *In* Roy, D. C., (ed.), *Centennial Field Guide Volume 5: Boulder, CO*, Geological Society of America, p. 239–242.
- Richter, D. A., Murray, D., & Simmons, G., 1997, Economic geology of the dimension stone industry, eastern Vermont granite belt, *In* Grover, T. W., Mango, H. N., and Hasenohr, E. J., (eds.), *Guidebook to Field Trips in Vermont and Adjacent New Hampshire and New York*, New England Intercollegiate Geological Conference, p. B4 1–14.
- Robinson, P., Thompson, P. J., & Elbert, D. C., 1991, The nappe theory in the Connecticut Valley region: Thirty-five years since Jim Thompson’s first proposal: *American Mineralogist*, v. 76, p. 689–712.

- Robinson, P., Tucker, T. D., Bradley, D., Berry, H. N. IV, & Osberg, P. H., 1998, Paleozoic orogens in New England, USA: Transactions of the Geological Society of Stockholm. *GFF*. v. 120, p. 119–148.
- Rodgers, J., (compiler), 1985, Bedrock Geological Map of Connecticut: Connecticut Geological and Natural History Survey, Hartford, Connecticut, 2 sheets, scale 1:125,000.
- Rosenberg, C.L., 2004, Shear zones and magma ascent: A model based on a review of the Tertiary magmatism in the Alps: *Tectonics*, v. 23, TC3002, doi:10.1029/2003TC001526.
- Rosenberg, C.L., & Handy, M.R., 2005, Experimental deformation of partially melted granite revisited: Implications for the continental crust: *Journal of Metamorphic Geology*, v. 23, p. 19–28, doi:10.1111/j.1525-1314.2005.00555.x.
- Rutter, E.H., & Mecklenburgh, J., 2006, The extraction of melt from crustal protoliths and the flow behavior of partially molten crustal rocks: An experimental perspective, *in* Brown, M., and Rushmer, T., eds., *Evolution and Differentiation of the Continental Crust*: Cambridge, UK, Cambridge University Press, p. 386–429.
- Sawyer, E.W., 1991, Disequilibrium melting and the rate of melt residuum separation during migmatization of mafic rocks from the Grenville Front, Quebec: *Journal of Petrology*, v. 32, p. 701–738, doi:10.1093/petrology/32.4.701.
- Sawyer, E.W., 1994, Melt segregation in the continental crust: *Geology*, v. 22, p. 1019–1022, doi:10.1130/0091-7613(1994)022<1019:MSITCC>2.3.CO;2.
- Sawyer, E.W., 1998, Formation and evolution of granite magmas during crustal reworking: The significance of diatexites: *Journal of Petrology*, v. 39, p. 1147–1167.
- Sawyer, E.W., 2001, Melt segregation in the continental crust: Distribution and movement of melt in anatectic rocks: *Journal of Metamorphic Geology*, v. 19, p. 291–309, doi:10.1046/j.0263-4929.2000.00312.x.
- Sawyer, E.W., 2010, Migmatites formed by water-fluxed partial melting of a leucogranodiorite protolith: Microstructures in the residual rocks and source of the fluid: *Lithos*, v. 116, p. 273–286, doi:10.1016/j.lithos.2009.07.003.
- Schaltegger, U., Brack, P., Ovtcharova, M., Peytcheva, I., Schoene, B., Stracke, A., Marocchi, M., & Bargossi, G.M., 2009, Zircon and titanite recording 1.5 million years of magma accretion, crystallization and initial cooling in a composite pluton (southern Adamello batholith, northern Italy): *Earth and Planetary Science Letters*, v. 286, p. 208–218, doi:10.1016/j.epsl.2009.06.028.

Simonetti, A., & Doig, R., 1990, U-Pb and Rb-Sr geochronology of Acadian plutonism in the Dunnage zone of southeastern Québec Appalachians: *Canadian Journal of Earth Sciences*, v. 27, p. 881–892.

Solar, G.S., & Brown, M., 2001, Deformation partitioning during transpression in response to Early Devonian oblique convergence, Northern Appalachian orogeny, USA: *Journal of Structural Geology*, v. 23, p. 1043–1065.

Solar, G. S., Pressley, R. A., Brown, M., & Tucker, R. D., 1998. Granite ascent in convergent orogenic belts: testing a model. *Geology*. v. 26, p. 711-714.

Spear, F. S., & Harrison, T. M., 1989, Geochronologic studies in central New England I: evidence for pre-Acadian metamorphism in eastern Vermont. *Geology*. v. 17, p. 181-184.

Stanley, R. S., & Ratcliffe, N. M., 1985, Tectonic synthesis of the Taconian orogeny in western New England: *Geological Society of America Bulletin*, v. 96, p. 1227–1250.

Strong, D.F., & Hanmer, S.K., 1981, Peraluminous granites: *Canadian Mineralogist*, v. 19, p. 163–176.

Sumita, I., & Ota, Y., 2011, Experiments on buoyancy driven crack around the brittle-ductile transition: *Earth and Planetary Science Letters*, v. 304, p. 337–346, doi:10.1016/j.epsl.2011.01.032.

Sutter, J. F., Ratcliffe, N. M., & Musaka, S. B., 1985, $^{40}\text{Ar}/^{39}\text{Ar}$ and K/Ar data bearing on the metamorphic and tectonic history of western New England. *Geological Society of America Bulletin*. v. 96, p. 123–136.

Thériault, R., (compiler), Beauséjour, S., & Tremblay, A., 2012, *Géologie du Québec*: Ministère des Ressources naturelles, Direction générale de Géologie Québec, scale 1:2,000,000.

Thompson, A.B., & Connolly, J., 1995, Melting of the continental crust: Some thermal and petrological constraints on anatexis in continental collision zones and other tectonic settings: *Journal of Geophysical Research*, v. 100, no. B8, p. 15,565–15,579, doi:10.1029/95JB00191.

Thompson, J. B., Rosenfeld, J. L., Hepburn, J. C., & Trzcienski, W. E., 1997, How does New Hampshire connect to Vermont?: *In* *Guidebook to Field Trips in Vermont and Adjacent New Hampshire and New York*, Grover, T. W., Mango, H. N., & Hasenohr, E. J. (eds.), p. C1-1–C1-17.

Tremblay, A., Ruffet, G., & Castonguay, S., 2000. Acadian metamorphism in the Dunnage zone of southern Québec, northern Appalachians: $^{40}\text{Ar}/^{39}\text{Ar}$ evidence for collision diachronism: *Geological Society of America Bulletin*, v. 112, n. 1, p. 136-146.

Tremblay, A., & Pinet, N., 2005, Diachronous supracrustal extension in an intraplate setting and the origin of the Connecticut Valley-Gaspé and Merrimack troughs, northern Appalachians: *Geology Magazine*, v. 142, p. 7–22.

van Staal, C. R., & de Roo, J. A., 1995, Mid-Paleozoic tectonic evolution of the Appalachian Central Mobile Belt in northern New Brunswick, Canada: collision, extensional collapse, and dextral transpression. *In Current Perspectives in the Appalachian-Caledonian Orogen*, Hibbard, J. P., van Staal, C. R., and Cawood, P. A., (eds.), p. 367-389. Geological Association of Canada, Special Paper no. 41.

van Staal, C. R., Whalen, J. B., Valverde-Vaquero, P., Zagorevski, A., & Rogers, N., 2009, Pre-Carboniferous, episodic accretion-related, orogenesis along the Laurentian margin of the northern Appalachians: Geological Society of London, Special Publications, v. 327, p. 271–316, DOI10.1144/SP327.13.

van Staal, C. R., & Barr, S. M., 2012, Lithospheric architecture and tectonic evolution of the Canadian Appalachians and associated Atlantic margin: *In Tectonic Styles in Canada: the LITHOPROBE Perspective*. Edited by J.A. Percival, F.A. Cook, and R.M. Clowes. Geological Association of Canada, Special Paper n. 49, p. 1–55.

Vernon, R.H., & Paterson, S.R., 2001, Axial-surface leucosomes in anatexitic migmatites: *Tectonophysics*, v. 335, p. 183–192, doi:10.1016/S0040-1951(01)00049-X.

Vigneresse, J.-L., 1988, Shape and volume of granitic intrusions: *Bulletin de la Société Géologique de France*, v. 4, p. 897–906.

Vigneresse, J.-L., 1995, Crustal regime of deformation and ascent of granitic magma: *Tectonophysics*, v. 249, p. 187–202, doi:10.1016/0040-1951(95)00005-8.

Vigneresse, J.-L., 2004, Rheology of a two-phase material with applications to partially molten rocks, plastic deformation and saturated soils, *in* Alsop, G.I., Holdsworth, R.E., McCaffrey, K.J.W., and Hand, M., eds., *Flow Processes in Faults and Shear Zones*: Geological Society of London Special Publication 224, p. 79–94.

Vigneresse, J.-L., Tikoff, B., & Ameglio, L., 1999, Modification of the regional stress field by magma intrusion and formation of tabular granitic plutons: *Tectonophysics*, v. 302, p. 203–224, doi:10.1016/S0040-1951(98)00285-6.

Wagner, R., Rosenberg, C., Handy, M.R., Möbus, C., & Albertz, M., 2006, Fracture-driven intrusion and upwelling of a mid-crustal pluton fed from a transpressive shear zone—The Rieserferner pluton (Eastern Alps): *Geological Society of America Bulletin*, v. 118, p. 219–237, doi:10.1130/B25842.1.

Walsh, G. J., Kim, J., & Gale, M. H., 2009, Bedrock geology of the Montpelier area, central Vermont: *In* New England Intercollegiate Geological Conference: Guidebook for Field Trips in Vermont and adjacent New Hampshire. p. C4: 1–18.

Walsh, G.J., Kim, Jonathan, Gale, M.H., & King, S.M., 2010, Bedrock geologic map of the Montpelier and Barre West quadrangles, Washington and Orange Counties, Vermont: U.S. Geological Survey Scientific Investigations, Map 3111, 1 sheet, scale 1:24,000, p. 1–36, text.

Watson, E.B., & Harrison, T.M., 1983, Zircon saturation revisited—Temperature and composition effects in a variety of crustal magma types: *Earth and Planetary Science Letters*, v. 64, p. 295–304, doi:10.1016/0012-821X(83)90211-X.

Weinberg, R.F., 1999, Mesoscale pervasive felsic magma migration: Alternatives to diking: *Lithos*, v. 46, p. 393–410, doi:10.1016/S0024-4937(98)00075-9.

Weinberg, R.F., & Mark, G., 2008, Magma migration, folding, and disaggregation of migmatites in the Karakoram shear zone, Ladakh, NW India: *Geological Society of America Bulletin*, v. 120, p. 994–1009, doi:10.1130/B26227.1.

Weinberg, R.F., & Regenauer-Lieb, K., 2010, Ductile fractures and magma migration from source: *Geology*, v. 38, p. 363–366, doi:10.1130/G30482.1.

Weinberg, R.F., Mark, G., and Reichardt, H., 2009, Magma ponding in the Karakoram shear zone, Ladakh, NW India: *Geological Society of America Bulletin*, v. 121, p. 278–285.

Weinberg, R.F., Hasalová, P., Ward, L., & Fanning, C.M., 2013, Interaction between deformation and magma extraction in migmatites: Examples from Kangaroo Island, South Australia: *Geological Society of America Bulletin*, v. 124, p. 000–000, doi:10.1130/B30781.1.

Westerman, D. S., 1987, Structures in the Dog River fault zone between Northfield and Montpelier, Vermont: *in* New England Intercollegiate Geological Conference: Guidebook for Field Trips in Vermont, 79th Annual Meeting, v. 2, p. 109–132.

Westerman, D., & Coish, R., 2009, Geochemistry and emplacement style in Acadian plutons between Woodbury and Northfield, Vermont: *in* Guidebook for Field Trips in the Northeast Kingdom of Vermont and Adjacent Regions (eds. Westerman, D. S., & Lathrop, A. S.). P. C-5: 261–274.

Wheeler, J. O., Hoffman, P. F., Card, K. D., Davidson, A., Sanford, B. V., Okulitch, A. V., & Roest, W. R., 1996, Geological map of Canada / Carte géologique du Canada: Geological Survey of Canada, "A" Series Map 1860A, scale 1: 5,000,000.

White, W. S., 1949, Cleavage in east-central Vermont: Transactions American Geophysical Union, v. 30, p. 587-594.

Whitehead, J., Reynolds, P. H., & Spray, J. G., 1996, $^{40}\text{Ar}/^{39}\text{Ar}$ age constraints on Taconian and Acadian events in the Quebec Appalachians: *Geology*, v. 24, p. 359-362. doi:10.1130/00917613(1996)024<0359:AAACOT>2.3.CO;2.

Wickham, S.M., 1987, The segregation and emplacement of granitic magma: *Journal of the Geological Society of London*, v. 144, p. 281–297, doi:10.1144/gsjgs.144.2.0281.

Zen, E., Goldsmith, R., Ratcliffe, N. M., Robinson, P., Stanley, R. S., Hatch, N. L., Shride, A. F., Weed, E. G. A., & Wones, D. R., 1983, Bedrock geologic map of Massachusetts: U.S. Geological Survey, scale 1:250,000.

CHAPTER 2: ARTICLE FOR SUBMISSION

Abstract

The Silurian–Devonian metasedimentary rocks of the Connecticut Valley–Gaspé trough (CVGT) were subjected to multiple deformational and metamorphic events during the Acadian orogeny in the Middle–Late Devonian. Plutons intruding the Devonian Waits River and Gile Mountain Formations have been considered post-tectonic, but microstructural studies of the intrusions and their metamorphic aureoles indicate some of these plutons intruded syntectonically. This study investigates the relationship between Acadian deformation and intrusion of the Knox Mountain pluton (KMP) of central Vermont. Structural and geochronological data were collected along a c. 15 km transect from the western limit of the CVGT, where the unconformable Richardson Memorial Contact coincides with the Dog River Fault Zone, into the margin of the KMP in the east. Field and microstructural observations indicate the KMP intruded syntectonically. Evidence for Acadian deformation post-dating intrusion includes folded and boudinaged granitic dikes at the margin of the KMP, and microstructures such as flame perthite, myrmekite, deformation twins, and textures associated with grain-boundary migration recrystallization in the granite. In the metamorphic aureole, biotite porphyroblasts overgrow S_3 , the earliest Acadian secondary foliation, and were deformed during S_4 crenulation cleavage development. The KMP intruded at 377 ± 5.2 Ma based on a U–Th–total Pb monazite crystallization age, which is concordant with the published age of the nearby Barre granite. The timing of S_4 foliation development in the CVGT is constrained locally by $^{40}\text{Ar}/^{39}\text{Ar}$ geochronology at ~ 365 Ma, consistent with the microstructurally-inferred relative-age relationships. Plateau/weighted mean $^{40}\text{Ar}/^{39}\text{Ar}$ ages from across the transect and minimum ages from argon-loss profiles show a general trend of younging towards the east, suggesting these rocks have been affected by Alleghanian and Mesozoic deformation and exhumation.

Keywords:

Acadian, syntectonic, granite, metamorphism, $^{40}\text{Ar}/^{39}\text{Ar}$, U/Pb, monazite, Vermont, CVS

CHAPTER 2: ARTICLE FOR SUBMISSION

1. Introduction

The relative timing and relationship between deformation and magmatic intrusion during orogenesis is often controversial, especially in polyphase orogens (Castonguay *et al.*, 2011). Polyphase deformation structures are pervasive in the metamorphic cores of orogenies affected by multiple generations of folding and fabric development. Structural and metamorphic studies have been correlated with $^{40}\text{Ar}/^{39}\text{Ar}$ geochronologic data to understand the evolution of deformation during the Acadian orogeny (e.g. Castonguay *et al.*, 2007; 2011; McWilliams *et al.*, 2013), but limited work has been done to correlate the timing of deformation with respect to the intrusion of Acadian plutons (e.g. Hannula *et al.*, 1999).

Determining the nature, absolute timing, and duration of both deformation and intrusion are essential for understanding the dynamics of Acadian orogenic events in Vermont. Solar *et al.* (1998; and references therein) have proposed that granite extraction, ascent and emplacement can be determined to be synchronous with metamorphism and deformation with precise determination of crystallization ages from a pluton and cooling ages from its metamorphic aureole. This study aims to define the relationship between Acadian magmatism and deformation along a transect from the margin of the Knox Mountain Pluton in central Vermont, through its metamorphic aureole, to the western limit of the Connecticut Valley Trough (see Figures 1 and 2). The relationship between these tectonically driven processes will be analyzed via: 1) field and microstructural analyses; 2) $^{40}\text{Ar}/^{39}\text{Ar}$ thermochronology of deformed metasediments;

and 3) both U-Th total Pb dating of monazite and $^{40}\text{Ar}/^{39}\text{Ar}$ thermochronology of the Knox Mountain pluton.

2. Geologic Background

2.1. Geologic Setting of the Connecticut Valley-Gaspé Trough

2.1.1. Regional Geology

The rocks of New England preserve a record of the Paleozoic accretionary history of the margin of Laurentia (Figure 1). The Paleozoic geology of central Vermont records the closure of the Iapetus Ocean during collision and accretion of arcs and terranes with the Laurentian margin (Pinet and Tremblay, 1995). The Middle to Late Ordovician Taconic orogeny is associated with east-dipping subduction of the Laurentian margin and eventual closure of the Neo-Iapetus ocean due to collision with the Shelburne Falls island arc (Karabinos *et al.*, 1998). The termination of Taconic orogenesis is marked by the development of a west-dipping subduction zone east of and beneath the Bronson Hill arc to the east of Laurentia within the Iapetus Ocean. During the Silurian, post-Taconian convergence occurred in conjunction with extension due to slab break-off of the west-dipping subducting Gondwanan crust. Rising asthenosphere in the Québec embayment resulted in continuous extension that yielded Paleozoic basins, including the Connecticut Valley-Gaspé trough (CVGT) and Central Maine trough (Karabinos *et al.*, 1998; Rankin *et al.*, 2007).

During the Silurian and Early Devonian, the Taconic orogen was eroded significantly, and the resulting shales, limestones, and sandstones were deposited in the elongate series of marginal basins to the east of the mountains (namely, the CVGT), extending from southern New England to the Gaspé Peninsula (Tremblay and Pinet,

2005). The west-directed contractional events of the ensuing Acadian orogeny folded most of the sediments in the trough into recumbent, isoclinal kilometer-scale nappes that locally verge towards the southwest. Metamorphism due to burial, regional deformation, and contact heat from magmatic intrusion metamorphosed them to schists, phyllites, marbles and quartzites (Hannula *et al.*, 1999; Robinson *et al.*, 1991).

In the Northern Appalachian Belt, up to 50% of the surface exposure consists of the Silurian and Devonian metasedimentary and igneous rocks described above (Figure 1; Tremblay and Pinet, 2005). Contrasting interpretations of these sedimentary basins has yielded the proposal of several possible tectonic scenarios for how Avalonia terranes accreted onto the Laurentian margin (Nance *et al.*, 2002). Robinson *et al.* (1998) suggested these rocks formed from backarc extension in foreland basins with lithosphere delamination along a SE-dipping subduction zone, while other authors believe the delamination occurred along a NW-dipping subduction zone (e.g. van Staal and de Roo, 1995; Moench and Aleinikoff, 2002). Bradley (1983) suggested foreland basins were overlying two subduction zones plunging opposite directions. Finally, multiple authors have proposed these rocks formed in transpressive or transtensional rift basins (e.g. Keppie and Dostal, 1994; Bourque, *et al.*, 1995). Rankin *et al.* (2007) state that delamination of the lithosphere in an east-dipping subduction zone caused asthenospheric upwelling. This upwelling led to basement uplift, partial melting of the crust, and inter-plate magmatism, all of which contributed to the regional extension that resulted in the formation of the CVGT.

In Vermont, the Connecticut Valley-Gaspé trough is bound unconformably to the west by the “Richardson Memorial contact” (RMC), which locally coincides with the

Dog River Fault Zone (DRFZ), and to the east by faults of the Bronson Hill anticlinorium (Westerman, 1987; McWilliams *et al.*, 2010). The debate surrounding the tectonic versus stratigraphic origin of the RMC has historically been controversial, and the contact has been interpreted as a fault related to Acadian deformation (e.g. Hatch *et al.*, 1988), a Silurian erosional unconformity (e.g. Hatch, 1982), or a syn-depositional fault and unconformity (Karabinos, 1998). Although Westerman (1987) suggested that the RMC corresponds to the DRFZ in central Vermont, Walsh *et al.* (2010) note that in central Vermont, the RMC and DRFZ are not always coincident. Because RMC most appropriately refers to a stratigraphic contact, the faulted boundary at the westernmost limit of the CVGT shall be referred to as the DRFZ herein. The DRFZ has been correlated to two décollements based on regional folds, stratigraphic position, and surface trace: the Surface of Acadian Structural Disharmony to the south in Massachusetts, and the La Guadeloupe fault to the north in Québec (Hatch and Stanley, 1988; Kim and Klepeis, 2015).

The metasedimentary rocks of the CVGT include, from oldest to youngest, the Silurian Shaw Mountain Formation, the Silurian and Devonian Northfield Formation, the Silurian and Devonian Waits River Formation, and the Devonian Gile Mountain Formation (Figure 2; Walsh *et al.*, 2010). The Shaw Mountain Formation was first described by Currier and Jahns (1941), and is a predominantly a graded quartz-pebble conglomerate that unconformably overlies the RMC (and all pre-Silurian rocks in the valley). Work by several authors (e.g. Boucot and Thompson, 1963; Doll, 1984; Westerman, 1987) says that the bryozoans, brachiopod, coral and echinoderm fossil content of the Shaw Mountain Formation indicate a Middle Silurian age. The Northfield

Formation is predominantly a dark grey phyllite with thin (<20 cm) layers of micaceous quartzite, matrix-supported conglomerate, and impure limestone, formally named by Doll *et al.* (1961), but also recognized by Currier and Jahns (1941) and Cady (1956) as the Northfield slate. To the east, the Northfield Formation grades into the Waits River Formation (Walsh *et al.*, 2010).

The Waits River Formation was first described by Currier and Jahns (1941) as all rocks stratigraphically above the Northfield Slate, and stratigraphically below the Gile Mountain Formation. The Waits River Formation consists of interbedded phyllites and impure marbles of varying thicknesses, often referred to as crystalline limestones “because of their poor commercial qualities compared to the marbles of western Vermont,” (Cady, 1956). Regional fossil evidence from Hueber *et al.*, (1990) and Lavoie and Asselin (2004), combined with regional structural studies (e.g. Fisher and Karabinos, 1980; Hatch, 1988) suggest the Waits River and Northfield formations both lie stratigraphically beneath the Gile Mountain Formation. The Gile Mountain Formation is dominated by interbedded phyllite and quartzite, with minor calcareous phyllite and impure limestone (Walsh *et al.*, 2010). The segment of Gile Mountain Formation exposed to the west of the Knox Mountain pluton was initially interpreted to be a distinct unit named the Westmore Formation (e.g. Murthy, 1957), but alternate interpretations and revisions to the structure and stratigraphy of eastern Vermont indicate that the Westmore and Gile Mountain formations are one in the same, and are repeated due to the occurrence of the Brownington syncline (whose significance will be discussed below; Konig, 1961). The Gile Mountain and Waits River formations are cut by numerous granitic dikes and plutons associated with the Devonian New Hampshire plutonic suite,

some of which (including the Knox Mountain pluton) have exposed areas of greater than 400 m² (Billings, 1956; Hannula *et al.*, 1999; Westerman and Coish, 2009). Both sedimentary units have experienced significant metamorphism associated with both the orogenic events of the Acadian, as well as the intrusion of this plutonic series.

The Acadian orogeny has been divided into two separate metamorphic realms, the eastern and western belts, based on distinct styles of metamorphism (Armstrong *et al.*, 1992). The western Acadian belt was subjected to Barrovian-type metamorphism and is characterized by high-temperature and high-pressure conditions, and in central Vermont, the metamorphic grade generally increases towards the east (Armstrong *et al.*, 1992; Tremblay *et al.*, 2000; Walsh *et al.*, 2010). McWilliams *et al.* (2013) suggests the rocks of the CVGT were deformed at greenschist-facies conditions in southeastern Vermont. Greenschist-facies conditions in the range of 230–480 °C, ≤0.4 GPa have been cited in northern Vermont east of the Green-Mountain anticlinorium (Laird and Albee, 1981; Castonguay *et al.*, 2007). In terms of index mineralogical zones in central Vermont, the DRFZ is located in the biotite-grade zone, and the biotite–garnet isograd occurs roughly two kilometers east of Montpelier and maintains the same strike as the metasedimentary units in the region (see Figure 2). The garnet–staurolite isograd commences roughly five kilometers west of the Knox Mountain pluton near Plainfield, Vermont, and locally envelopes the Knox Mountain and the Barre plutons, suggesting magmatic intrusion post-dates the peak of regional metamorphism (Richter, 1987).

2.1.2. Magmatism in the CVGT

Significant intrusive magmatism occurred in conjunction with the transpressive orogenic events of the Acadian, yielding 14 distinct plutons within the CVGT as part of

the New Hampshire plutonic series (Arth and Ayuso, 1997; Westerman and Coish, 2009). Many of the plutonic bodies often referred to as “granite” technically have the composition of adamellite, and are most appropriately classified as granodiorites (Konig, 1961). Solar *et al.* (1998) have suggested that there is a general feedback relationship between contractional deformation and crustal anatexis that helps focus granite extraction and ascent through the crust during orogenies that explains how magma emplacement occurs in conjunction with compression. Westerman and Coish (2009) note that plutons in the CVGT with high aspect ratios (length divided by width) typically have a high alignment with regional foliations in the host country rock. Konig (1961) found flow structures in mica-rich sections of the Knox Mountain pluton near its eastern margin that are subparallel to the pluton margin itself. The map-view structures and corresponding shapes of metamorphic aureoles have been cited to suggest that of many Acadian intrusive bodies intruded after peak Acadian deformation and metamorphism (Richter *et al.*, 1997).

Hannula *et al.* (1999) demonstrated that it is possible to correlate microstructures found in an intrusive body with microstructures in a pluton’s metamorphic aureole. Their microstructural analysis of the Acadian Victory pluton in northeast Vermont correlated microstructures from the intrusion with the Monroe Fault and the pluton’s metamorphic aureole to demonstrate syntectonic intrusion, with an intrusion depth of 14–20 kilometers. Numerous lines of evidence have been cited to indicate that the Knox Mountain pluton was injected forcefully, perhaps with the aid of mechanical stoping. Evidence includes unaltered and (mostly) unrotated xenoliths of country rock within the pluton, drag folds and fractures in the country rock migrating away from the Knox

Mountain pluton, and country rock that conforms to the shape of the pluton (i.e. the strike of the country rock changes and remains parallel with the pluton margin near West Dover, Vermont; Hall, 1959; Konig, 1961).

2.1.3. Structural Geology

Five generations of folding from ductile deformation with associated structures are recognized in the field area (See Table 1). The five generations are designated from oldest to youngest D_1 – D_5 , where D_1 and D_2 fabrics are interpreted to be a product of the Taconian orogeny, and D_3 , D_4 , and D_5 are interpreted to be a product of the Acadian orogeny. Locally, Taconian deformation yielded tight to isoclinal folds with penetrative, coplanar fabrics in the pre-Silurian rocks stratigraphically below the RMC. S_1 is a relict layer-parallel foliation in the Cambrian/Ordovician Moretown and Cramhill Formations. S_2 sometimes appears as the dominant schistosity in the Moretown Formation as a pinstripe texture, though it is often a relict texture where overprinted by S_3 . D_3 – D_5 are the three youngest events in the CVGT, and associated fabrics from these three deforming events are present on both sides of the DRFZ. Locally, the third generation foliation (S_3) strikes northeast, dips steeply to the northwest, and is the most penetrative and dominant deformational fabric in the CVGT, especially in close proximity to and on both sides of the DRFZ (Walsh *et al.*, 2010; Westerman, 1987).

D_3 is the first event associated with the Acadian orogeny, and it resulted in the folding of the Silurian–Devonian Northfield, Waits River, and Gile Mountain Formations into a major regional syncline, where F_3 folds plunge 10° – 25° to the north, strike to the north-north-east, and dip 40° – 75° to the west. The field area of interest falls on the western limb of this major synclinal structure. The axial region of the fold consists of

Gile Mountain Formation, and the Waits River Formation is found on both limbs (Konig, 1961; Figure 2; Figure 3). Richardson (1906) first recognized the Brownington syncline in the St. Johnsbury quadrangle. It was officially named by Doll (1951), and then traced southward into the Lynodnville quadrangle by Denis (1956), and eventually the Plainfield quadrangle by Konig (1961), where its axial trace runs parallel to the contact between the Waits River and Gile Mountain formations, and subparallel to the pluton margin (Figure 2). In the western end of the Plainfield quadrangle, Konig (1961) also recognized bedding-cleavage relationships and drag-fold relationships, and proposed the existence of the Woodbury syncline in the western limits of the CVGT, with the Nichols anticline between the two synclinal structures (Figure 2).

D₄ resulted in minor folds that are left-stepping in the west and right-stepping in the east, with strikes to the northwest and dips 30°–35° to the northeast (Walsh *et al.*, 2010). In addition to the development of these minor folds, this deformational event essentially resulted in the tightened the pre-existing F₃ folds. S₄ foliations often display box-fold geometries with crenulation lineations in the eastern segment of the Connecticut Valley Sequence in Vermont (Walsh *et al.*, 2010). Crenulation fabrics are generally visible in the local metapelitic rocks, but are often absent in the massive impure limestone beds (i.e. the thicker calcareous units of the Waits River Formation). S₅ is weakly developed and only locally pervasive in this section of the CVGT, although further south, in the Strafford and Barre East quadrangles, D₅ is responsible for the dome structures, such as the Strafford Dome, from which F₃ folds plunge gently away (Murthy, 1957). The tightness of F₄ minor folds also tend to decrease away from F₅ domes

(Murthy, 1957). Bean (1953) suggested there may be a low-density granitic intrusion beneath the domal structures, citing residual negative gravity anomalies as evidence.

Work by Hannula *et al.* (1990) on the Victory Pluton in the northeastern Vermont segment of the CVGT determined that pluton was emplaced 14–20 kilometers deep after the development of the dominant foliation (S_3), but probably in some conjunction with S_4 or S_5 development, citing brittle and ductile structures within the pluton as evidence.

Anderson and Coish (1999) used hornblende geobarometry to determine that three of the plutons in northeastern Vermont and the CVGT intruded at depths ranging from 8–14 km.

2.2. Constraints on the Timing of Tectonic Events

This section summarizes previous geochronologic investigations within the Connecticut Valley-Gaspé trough, and summarizes a suite of articles that span the regional extent of the trough. Much of the known timing of Acadian deformation has been observed as an overprint on age on Neoproterozoic to Middle Ordovician Taconian structures (west of the CVGT). Therefore, cooling ages attributed to both Taconic and Acadian orogenic events will be presented herein. Because of the extent of work that has been done throughout the region affected by Acadian deformation, this analysis introduces the formation of the Grenvillian basement rocks of Vermont, provides tectonic models for the Taconic and Acadian orogenies, and includes a final note on the timing of intrusion of some members of the New Hampshire Plutonic series within the CVGT.

2.2.1. Formation of Grenvillian Basement

Doolan (2007) suggests the rocks exposed at the surface of the Earth today in Vermont were deposited upon or transported onto an ancient “basement” of rocks, which themselves were accreted onto the Laurentian margin during the Grenville orogeny. Today, rocks of Grenvillian age are exposed in the Adirondack Mountains of New York, and McLelland *et al.* (1988) reported several U-Pb zircon studies from the magmatic Adirondack highlands with ages ranging from 1321 ± 60 Ma– 1009 ± 10 Ma, with errors at 2σ . Exposures of allochthonous Grenvillian basement in southern Vermont yield similar ages, and the trondhjemitic gneisses of the Mount Holly Complex yield ages of volcanism and plutonism that range from 1.35–1.31 Ga (Ratcliffe *et al.*, 1991)

2.2.2. Tectonic Model for the Taconic Orogeny

The Taconic orogenic cycle was a complex orogeny that lasted from Late Cambrian and Late Ordovician time (~500–450 Ma; Stanley and Ratcliffe, 1985; van Staal and Barr, 2012). The orogeny was due to the closure of the Neo-Iapetus Ocean, a basin that originally opened due to rifting of the Rodinian continent and Laurentian continental margin during the Latest Proterozoic to Early Cambrian. Cawood *et al.* (2001) has suggested that rifting may have occurred over multiple episodes between 570–543 Ma.

In western Vermont, only two Taconic tectonic events are recognized, and there remains some difficulty correlating these two events with three events recognized in Canada (Castonguay *et al.*, 2011). Stanley and Ratcliffe (1985) used stratigraphic and structural correlations to determine a relative chronological sequence of events that depict

the evolution of the Taconic orogeny. They conclude that the metasedimentary rocks of the Champlain Valley Sequence and Taconic Allochthons were deposited in the westernmost Neo-Iapetus Ocean on either Grenvillian basement or the aforementioned rift-transitional-rift rocks during the Cambrian and Early Ordovician (~541 Ma–470 Ma). Coarse-grained clastic rocks like the Cheshire and Monkton formations were the product of weathering the Himalaya-scale Grenvillian Mountains, and were deposited in a near-shore environment on the Laurentian margin. These and other sedimentary units were accreted on the Laurentian margin as the Neo-Iapetus closed during the Taconic orogeny in the Middle to Late Ordovician. Stanley and Ratcliffe (1985) suggest that nearly 1,000 km of shortening was accommodated by secondary cleavage development and low-angle thrust faulting. In northern Vermont, a trend in younging is observed from west to east towards the hinterland of the orogeny, where significant folding, refolding, and fault activation occurred. It is also worth noting that the Taconic rocks of New England have been significantly more affected by Acadian deformation in the form of minor folds compared to the rocks of the Canadian Appalachians (Stanley and Ratcliffe, 1985; van Staal and Barr, 2012).

2.2.3. Tectonic Model for the Acadian Orogeny

Tremblay and Pinet (2005) suggested east-dipping slab break-off ca. 435 Ma was responsible for asthenospheric upwelling that lead to the opening of the CVGT. Westward-migrating extension followed upwelling ca. 420–415 Ma, and Rankin *et al.* (2007) demonstrated that magmatism ca. 428–416 Ma was coeval with the extension that formed the CVGT based on $^{207}\text{Pb}/^{206}\text{Pb}$ dating of mafic dikes in northern Vermont. The Acadian orogeny is thought to be a product of closing both the Iapetus ocean between

Laurentia and Avalonia, and a narrow Acadian Seaway that separated Avalonia from the Ganderia terrane further east via northwest-dipping subduction zones (present-day coordinates; van Staal and Barr, 2012). The suturing of Avalonia and Ganderia occurred during the Silurian in association with the closure of the Acadian Seaway from 442–421 Ma, and was followed by subsequent collision between Laurentia and Avalonia from 421–390 Ma (van Staal and Barr, 2012, and references therein).

Dextral-oblique collision between the Meguma terrane and composite Laurentia occurred from ca. 395–340 Ma (van Staal, 2007; van Staal *et al.*, 2009). This oblique, protracted collision was mainly accommodated by the Cobequid-Chedabucto fault system on land in Nova Scotia, and included a component of northwest-directed thrusting (Piper and Piper, 2002; van Staal and Barr, 2012). Orogen-normal structures from Acadian crustal shortening include upright and steeply inclined folds, and high-angle reverse faults, and dextral shear zones are the main orogen-parallel structures (e.g. van Staal and de Roo, 1995).

2.2.4. Acadian Overprinting of Taconic Rocks

Laird *et al.* (1984) were interested in determining the timing of Acadian deformation in rocks east of the Green Mountain anticlinorium (Green Mountain/Rowe-Hawley Slices). The $^{40}\text{Ar}/^{39}\text{Ar}$ data they generated from biotite, muscovite, actinolite, hornblende, and glaucophane indicate high-to-medium-pressure metamorphism during the Taconic orogeny from ca. 471–439 Ma is overprinted by a medium pressure retrograde Acadian metamorphism from ca. 386–355 Ma. They found that Cambrian and Ordovician metamorphism occurred at ca. 460 ± 10 Ma in northeastern Vermont, with a

Devonian overprint around ca. 360 ± 5 Ma just east of the Green Mountain anticlinorium (1σ errors). Whitehead *et al.* (1996) performed $^{40}\text{Ar}/^{39}\text{Ar}$ dating on muscovite and orthoclase from southeastern Québec and observed a clear Taconic age around 460 Ma, with one sample displaying the Acadian overprint at 377 Ma (2σ errors). $^{40}\text{Ar}/^{39}\text{Ar}$ age spectra from within the footwall of La Guadeloupe fault, a fault that correlates to the DRFZ, are in agreement with these Acadian overprint ages (Tremblay *et al.* 2000; Walsh *et al.*, 2010). They report a peak in deformation and metamorphism around 380 Ma, a D_2 recrystallization around 375 Ma, and a D_3 thermal event ca 365 Ma (2σ errors), based on $^{40}\text{Ar}/^{39}\text{Ar}$ dating of biotite and muscovite in southern Québec.

Chan *et al.* (2000) were working in the Taconic Allochthon of southwestern Vermont, and report that Acadian S_1 and S_2 overprinting and foliation development occurred respectively at 370.7 ± 1.0 Ma and 345.5 ± 1.7 Ma (2σ errors) based on $^{40}\text{Ar}/^{39}\text{Ar}$ dating of cleavage domains. Also working in southwestern Vermont, Spear and Harrison (1989) used $^{40}\text{Ar}/^{39}\text{Ar}$ dating to constrain the timing of the Acadian metamorphic overprint in the Green Mountain anticlinorium and CVGT. They concluded that the Acadian overprint is not remarkably pervasive in some sections of southern Vermont, and it is sometimes easiest to observe within the axis of domes exposing Grenvillian basement in the CVGT. Sutter *et al.* (1985) were interested in constraining the Acadian overprint and Taconic peak in the Green Mountain anticlinorium as well, and by doing K/Ar dating on whole rock samples they found that peak metamorphic conditions were reached around 465 ± 5 Ma with the retrograde Acadian event occurring at 376 ± 5 Ma in southwestern Vermont (1σ errors).

2.2.5. Deposition and Deformation of Devonian Rocks in the CVGT

McWilliams *et al.* (2010) determined via U-Pb detrital zircon studies that the deposition of the Waits River formation lasted from ~423 Ma–415 ± 2 Ma, and the age of deposition of the Gile Formation is at 411 ± 1 Ma (1σ errors). Thompson *et al.* (1997) dated a dike crosscutting amphibolites from the Standing Pond Volcanics member of the Waits River Formation to ca. 423 ± 4 Ma (1σ error), providing a minimum age constraint on the eruption age. Spear and Harrison (1989) performed ⁴⁰Ar/³⁹Ar dating on metamorphic hornblendes from the Standing Pond Volcanics, yielding ages ranging from 397 ± 10 Ma–350 ± 7 Ma (1σ errors).

In southeastern Vermont on the eastern margin of the CVGT, McWilliams *et al.* (2013) dated the timing of deformation along the Westminster West Fault zone via ⁴⁰Ar/³⁹Ar step heating. They found that the Waits River formation records cooling ages that correspond to a peak of Acadian deformation at 365 Ma, and have evidence this region was subjected to deformation during the Alleghanian orogeny (c. 300 Ma). Though this late Paleozoic deformation has not been reported in Vermont before, Moecher *et al.* (1997) have reported evidence of static reheating without deformation with a similar age (300–295 Ma) further south in the CVGT within the Waterbury dome. Dietsch (2015) was able to constrain the timing of crystallization of a felsic orthogneiss of the Waterbury gneiss in the Waterbury dome via SHRIMP U-Pb ages of zoned zircons, yielding two populations with ages of 437 ± 4 Ma and 387 ± 5 Ma (2σ errors). Moecher *et al.* (1997) attempted to constrain the cooling ages of the Waterbury dome and CVGT in southern Connecticut via ⁴⁰Ar/³⁹Ar total fusion and ⁴⁰Ar/³⁹Ar step heating of

hornblende and muscovite. They note that ages get notably younger progressively further south, with their southernmost samples yielding cooling ages 50–100 Myr younger than their samples from the Waterbury dome. Their calculated ages range from 374 ± 3 Ma in close proximity to the dome, to 254 ± 1 Ma tens of kilometers south of the dome (2σ errors). This is strong evidence this section of the CVGT was affected by an Alleghanian thermal event.

2.2.6. Timing of Magmatism in the CVGT

Simonetti and Doig (1990) dated several granitic plutons along the La Guadeloupe fault in southern Québec with $^{87}\text{Rb}/^{86}\text{Sr}$ whole-rock and U/Pb zircon dating, yielding a range of ages from 384 ± 3 Ma– 374 ± 1 Ma (2σ errors). Naylor (1971) used Rb/Sr dating techniques to constrain the cooling ages of a number of New Hampshire Plutonic series granitic plutons in the CVGT in northeast and east-central Vermont. Observed ages generated from individual mica grains ranged from 380–316 Ma, but they feared a few of their samples were subjected to some kind of isotopic disturbance. Arth and Ayuso (1997) also performed Rb-Sr dating on multiple plutons from northeast Vermont, yielding the ages of 390 ± 14 Ma, 376 ± 9 Ma, and 370 ± 17 Ma for the Nulhegan, Willoughby, and Derby plutons, respectively. Aleinikoff *et al.* (2011) dated a few Vermont/New Hampshire granite bodies, but they opted to date zircon and monazite grains via the U-Pb method. They claim these bodies intruded at a temperature lower than zircon's closure temperature, so their calculated age dates represent an age of crystallization. They found a granite body in Gassetts, NH crystallized at 392 ± 6 Ma, the Barre granite crystallized at 368 ± 4 Ma, and the Guilford Dome crystallized as late as

366 ± 1 Ma (2σ errors). As noted earlier, work by Hannula *et al.* (1990) in the north eastern Vermont segment of the CVGT has helped constrain the timing of intrusion relative to regional fabric development for the Victory Pluton, stating it was emplaced after the development of the dominant foliation (S₄), but probably in some conjunction with S₅ development.

3. Methods

Field work was conducted along a 15 km-long transect from the RMC in Montpelier, Vermont, towards the Knox Mountain pluton east of Marshfield, Vermont, to document schistosity, mineral lineations, large and small scale folds, and the bedding orientations of the sedimentary units of the CVGT (Figure 2). Field work from this study yielded structural data from 27 field sites across the transect and a number of oriented hand samples, 10 of which have been prepared in oriented thin sections (two orthogonal sections each), and three of which have been prepared in non-oriented thin sections (all available in Appendix A). A wealth of other structural data for the region is available thanks to 7.5-minute and 15-minute quadrangle-study efforts from the United States Geological Survey (e.g. Murthy, 1957; Konig, 1961; Walsh *et al.*, 2009). Petrographic analysis of thin sections was used to determine target minerals for geochronologic investigations. The location of the transect allowed for adaptation and modification of the published cross section (C-C') of Ratcliffe *et al.* (2011; Figure 3a).

3.1. Microstructural Analysis

Microstructural analyses of phyllitic samples were conducted on orthogonally-oriented thin sections that were cut perpendicular to the dominant foliation and both parallel and normal to either mineral lineations (or to dip direction in the absence of mineral lineations). Thin section observations were made on a Nikon Multizoom AZ100 petrographic microscope. Thin sections have been described in terms of modal mineralogy and trace mineralogy and samples have also been analyzed via X-Ray diffractometry (XRD) to verify the modal mineralogy described in thin section. Observations in thin sections of granitic and phyllitic samples have yielded target minerals for geochronologic investigations.

Foliations and lineations observed in thin section are described in terms of generation and have been associated with observations made in the field based on relative timing of development. Deformation observed in samples is characterized by the textures described in Passchier and Trouw (2005) and references therein. Quartz-bearing samples were analyzed to determine if deformation occurred via dissolution-precipitation reactions or dislocation/diffusion creep, and whether grain recrystallization occurred statically or in response to deformation. Porphyroblast-bearing samples have been analyzed to determine the timing of porphyroblast development relative to foliation development, with notes on whether or not porphyroblasts have experienced rotation. One sample containing shear boudins and mica fish has been analyzed to determine the sense of shear of a local shear zone near the west pluton margin. Annotated photomicrographs of key thin sections are available in Figure 4.

3.2. Ca and K Mapping of Biotite Grains under a Scanning Electron Microscope

Elemental maps made to investigate possible zoning in muscovite biotite grains were obtained on a FEI Quanta 450 Environmental Scanning Electron Microscope (SEM) at St. Lawrence University. Images were generated by rastering an electron beam over gold sputter-coated polished thin sections. INCA software was used to generate EDS (Energy Dispersive X-ray Spectroscopy Analysis) X-Rays analysis maps by placing a dot where characteristic X-Rays of any particular element are detected. The elements Fe, Mg, Na, K, and Ca atoms were selected to test for zoning in mica grains. The raster images of individual elements detected were mixed and set to display as false-colors to observe elemental zoning within individual crystals.

3.3. $^{40}\text{Ar}/^{39}\text{Ar}$ Dating of Biotite, Muscovite, and Potassium Feldspar

After petrographic analysis, select potassium-bearing minerals were targeted for $^{40}\text{Ar}/^{39}\text{Ar}$ dating. $^{40}\text{Ar}/^{39}\text{Ar}$ analyses were performed at the University of Vermont Noble Gas Geochronology Laboratory. Inclusion-free biotite, muscovite, and potassium feldspar mineral grains were handpicked from the 125–500 μm fractions of the crushed rock samples under a Leica S6E bioptic microscope after having been washed, sonified, and dried to remove any adhering particulate matter. Grains from each sample were loaded into aluminum foil packets, arranged in suprasil vial, and placed in an aluminum canister (25 mm x 140 mm) for irradiation. Samples have been irradiated with multigrain aliquots of Fish Canyon Tuff Sanidine (FCT-SAN) to act as an apparent flux monitor (age = 28.03 Ma; Renne *et al.*, 1998) to monitor the neutron dose, and CaF_2 and KSO_4 were also irradiated to determine corrections for interfering nuclear reactions. Samples

were irradiated for 8 hours at the Cadmium-Lined In-Core Irradiation Tube (CLICIT) reactor of Oregon State University, Corvallis, Oregon, USA.

Laser step heating for $^{40}\text{Ar}/^{39}\text{Ar}$ dating was conducted at University of Vermont with a Santa Cruz Laser Microfurnace 75 W diode laser system. Biotite samples were loaded directly into 1.5mm wells in a copper planchet. Muscovite and potassium feldspar grains were loaded into degassed Nb foil packets before being loaded in the wells in the planchet.

Argon isotopes were analyzed on a Nu Instruments Noblesse magnetic sector noble gas mass spectrometer during step-heating analyses of single grains, when possible, or multigrain aliquots. Data from samples and flux monitors were corrected for blanks, mass discrimination, atmospheric argon, neutron-induced interfering isotopes, and the decay of ^{37}Ar and ^{39}Ar . Mass discrimination was calculated by analyzing known aliquots of atmospheric argon for which $^{40}\text{Ar}/^{36}\text{Ar}$ measured in the range of 295.9 – 309.6, with an error range of 0.3% – 1.3%, and an assumed atmospheric value of 298.56 (Lee *et al.*, 2006). Interfering nuclear reactions were corrected for by analyzing argon extracted from irradiated and fused optical grade CaF_2 and KSO_4 . Correction factors used to account for interfering nuclear reactions for the irradiated samples are: $(^{40}\text{Ar}/^{39}\text{Ar})_{\text{K}} = 3.39 \times 10^{-02} \pm 3.04 \times 10^{-2}$, $(^{36}\text{Ar}/^{37}\text{Ar})_{\text{Ca}} = 3.07 \times 10^{-04} \pm 4.82 \times 10^{-5}$, $(^{39}\text{Ar}/^{37}\text{Ar})_{\text{Ca}} = 6.20 \times 10^{-04} \pm 6.17 \times 10^{-5}$. A linear interpolation was used to calculate J factors for samples based on sample position between flux monitor packets in the irradiation tube. All ages were calculated using the isotope decay constants recommended by Steiger and Jäger (1977). The age calculations for inverse isochron and apparent age data were achieved using both an in-house data reduction program and Isoplot 3.0 (Ludwig, 2003).

Weighted mean ages are reported, and plateau ages are reported if sufficient criteria were met (see McDougall and Harrison, 1999). Errors on plateaus and weighted mean ages are quoted at the 1σ level and include precision associated with measurement of the irradiation parameter, J , for flux monitors.

3.4.U-Th Total Pb Monazite Dating

A U-Th total Pb age was calculated for a monazite grain from thin section 13SL21A. Monazite geochronology was performed in situ using the Cameca SX-100 “ultrachron microprobe” at the University of Massachusetts, Amherst, following the procedures outlined by Williams *et al.* (2006) and Dumond *et al.* (2008). Five spectrometers were used for measuring U, Th, Pb, S, Ca, K, Sr, Si, Y, and P, and rare earth elements (REEs; see Appendix B). Lead was measured using two very large PET crystals (VLPET) simultaneously, and counts were aggregated to increase count resolution. Background measurements were performed once for each compositional domain. Then, successive peak measurements were made until errors stabilized at an acceptable level.

Measurements were excluded when compositions were significantly outside the mean for the particular compositional domain, and when the values suggest overlap with adjacent domains. Background values for U, Th, and Pb were determined using the multipoint method (e.g. Allaz *et al.*, 2013), whereby 8–10 background intensities are measured at known points of no spectral interference both above and below peak values. The multipoint data are regressed using an exponential fit (Jercinovic *et al.*, 2008; Allaz *et al.*, 2013), and the background intensity at the peak position is calculated. Typically,

between four and eight peak measurements were made per monazite compositional domain. A single date is calculated for each domain based on one background intensity and the 4–8 peak analyses (a set of analyses yield a single “age”). Errors are calculated in several ways (Williams *et al.* 2006). Typically, a single weighted mean and error is calculated for each chemical component and then a single “date” is calculated for each domain. This allows the compositional homogeneity of each domain to be evaluated independent of dates. Individual errors are propagated through the age equation to yield a single error for the calculated date.

Calibration for monazite analysis was performed on natural and synthetic standards. PbPO₄ (pyromorphite) was used for Pb, ThPO₄ (barbanite) was used for Th, and UO₂ was used for U. An “in house” consistency standard (Moacyr) was analyzed prior to, and throughout, analytical sessions (506 ± 1 Ma; see discussion in Williams *et al.*, 2006; Dumond *et al.*, 2008). Calibration was performed prior to every analytical session, and for long sessions the calibration was checked and updated during the session. Peak positions were routinely updated for P, Ce, La, and Nd using synthetic phosphates prior to each analytical session.

4. Results

Observations from the field, petrographic microscope, and, when appropriate, the scanning electron microscope are discussed here for each sample of interest collected in this study. Thin section names ending in “X” have been cut perpendicular to the dominant foliation, and parallel to the trend of a mineral or intersection lineation when present, and parallel to the direction of dip when absent. Thin sections ending in “Y”

have been cut perpendicular to the foliation and respective lineation when present, and parallel to strike when absent. Sample locations are shown in Figure 2, and Table 2 presents a summary of the $^{40}\text{Ar}/^{39}\text{Ar}$ geochronology results, where errors are reported at the (1σ) level, except when otherwise noted. Modal mineralogy for all samples is available in Table 3. Additional photomicrographs and SEM images can be found in Appendix A, and the most important samples in terms of petrography have been annotated in Figure 4. Tabulated data from $^{40}\text{Ar}/^{39}\text{Ar}$ step-heating analyses for individual samples are available in Appendix B.

4.1. 13SL02A

Sample 13SL02A is a quartz-rich black phyllite of the Cram Hill Formation, an Ordovician unit, and the only pre-Silurian sample in this study (Walsh *et al.*, 2010). It was collected in Hubbard Park of Montpelier, Vermont, some tens of meters west of the DRFZ (see west end of transect, Figure 2). Walsh *et al.* (2010) state that this region has been affected by Taconian and Acadian deformation, but S_3 is dominant penetrative fabric on both sides of the DRFZ (Westerman, 1987). In outcrop and hand sample, multiple foliations are visible, and an L_3 stretching lineation is defined by elongate fine-grained poly-crystalline augen-shaped clusters of garnets within quartz-rich layers. In thin section, muscovite was very fine-grained and sparse (<0.2 mm). Muscovite was observed to have crystallized in the hinge of an F_3 fold in thin section 13SL02AX and is therefore interpreted to have grown during Acadian deformation. Biotite is also fine-grained in thin section (~ 0.2 mm), and is believed to have grown prior to or in conjunction with D_3 , as it occurs in seams in the dominant foliation (S_3) that wraps around garnet-rich augens (Appendix A).

4.1.1. $^{40}\text{Ar}/^{39}\text{Ar}$ Dating

Both biotite and muscovite were recovered from the finest size fraction of sieved material deemed suitable for picking (i.e. to avoid problems with ^{39}Ar). Age spectra from a single biotite crystal yielded a well-defined plateau age of 365.1 ± 2.1 Ma, with a minimum age of 307.5 ± 1.4 Ma. Roughly ten muscovite crystals yielded an apparent age spectrum was a well-defined plateau age of 365.7 ± 2 Ma, with a minimum age of 266.4 ± 4.1 Ma (Figure 5a; Table 2).

4.2. 13SL05A

13SL05A is a quartz-rich phyllite of the Waits River Formation, roughly 5 km west of the pluton margin (see eastern-central part of transect, Figure 2). In outcrop large biotite grains were visible (2 mm), and in thin section biotite porphyroblasts have overgrown S_3 . The S_3 foliation is defined by fine-grained, elongate quartz, biotite, and sparse muscovite (all ~ 0.1 mm), and medium grained ilmenite (Figure 4a). The biotite porphyroblasts often contain these minerals as inclusions, and are clearly deformed by the S_4 crenulation cleavage. EDS compositional mapping via SEM, did not indicate any compositional zoning within the porphyroblasts.

4.2.1. $^{40}\text{Ar}/^{39}\text{Ar}$ Dating

Fine grained (≤ 200 μm), inclusion-free biotite was targeted during mineral separation, and a single crystal yielded a weighted mean age of 320.4 ± 2.2 Ma (defined by four steps; Figure 5b; Table 2). With the exception of an anomalously-young step in the middle of the experiment, the apparent age spectrum shape is dominated by serially increasing ages, with a minimum age of 225.8 ± 2 Ma and a maximum age of 373.2 ± 2.7 Ma. Fifteen muscovite crystals yielded flatter apparent age spectrum with a weighted

mean age of 346.4 ± 2.2 Ma for a plateau-like segment and a minimum age of 337.7 ± 1.8 (Figure 5b; Table 2).

4.3. 13SL05B

13SL05B was taken within a few meters of sample 13SL05A, and is also a quartz-rich phyllite of the Waits River Formation (see eastern-central part of transect, Figure 2). In thin section, compositional banding was readily apparent, and biotite porphyroblasts reach up to 2 mm in biotite-rich layers, and up to 1 mm in quartz-rich layers. Quartz matrix grains can reach up to 0.3 mm, but tend to be much finer, with most grains sizes between 0.05–0.1 mm (Appendix A). Quartz grains are often interlocking, and in some cases show signs of grain boundary area reduction (GBAR). White mica was fine grained (50–75 μm) and typically occurs within quartz-rich bands and are elongate along S_3 . Biotite porphyroblasts were inclusion-rich and overgrow S_3 . Fine-grained and inclusion-free biotite was targeted during separation to avoid complications during degassing and analysis.

4.3.1. $^{40}\text{Ar}/^{39}\text{Ar}$ Dating

Fine grained biotite and muscovite were obtained during mineral separation. A single biotite crystal yielded a plateau age of 352.9 ± 1.9 Ma, and a minimum age of 276.1 ± 2.1 Ma (Figure 5b; Table 2). Twenty-five muscovite grains from this sample yielded a plateau age of 346.3 ± 1.8 Ma, with a minimum age of 142.9 ± 8.9 Ma (Figure 5b; Table 2).

4.4. 13SL19A

13SL19A is a quartz-rich black phyllite of the Waits River Formation, obtained within meters of an exposure of the Adamant granite, a $\sim 1 \text{ km}^2$ granodioritic body also

classified as Devonian Granite by Ratcliffe *et al.* (2011), located roughly 10 meters west of the Knox Mountain pluton's northwestern margin (see western end of transect, Figure 2). In outcrop, mm-scale books of biotite were visible, and a shallowly-plunging intersection lineation of unknown generation was subtle but notable on foliation planes. In thin section, coarse ilmenite grains (0.5–1.2 mm) are surrounded by reaction rims of heavily chloritized biotite (~0.5 mm). It has been difficult to determine exactly which Acadian foliations are present within this sample, but in thin section 13SL19AX, S_n (the dominant foliation in outcrop) appears to wrap around the porphyroblasts and reaction rims. In thin section 13SL19AY, S_{n+1} appears to be a subtle crenulation cleavage. While some ilmenite grains are oriented parallel to the S_n foliation, many grains appear to be rotated to varied orientations (Appendix A).

4.4.1. $^{40}\text{Ar}/^{39}\text{Ar}$ Dating

Inclusion-free biotite was targeted during mineral separation, and the twenty-five fine grains analyzed yielded a well-defined plateau age of 343.1 ± 2.1 Ma, with a minimum age of 263.2 ± 2.4 Ma (Figure 5f; Table 2).

4.5. 14SL03A

Samples 14SL03A and 14SL03B are coarse-grained phyllites of the Gile Mountain Formation acquired at the Mitchell Quarry north of Barre, Vermont, roughly 4 km west of the pluton margin (see eastern-central part of transect, Figure 2). Large biotite porphyroblasts (~1 mm) were visible in hand sample. Only 14SL03A was prepared in thin section, where large garnet porphyroblasts (up to 1 mm) are visible as well, and both garnet and biotite preserve an internal S_3 foliation defined by inclusions of

quartz (Figure 4b). Outside of the porphyroblasts, S_3 is defined by fine grained quartz and biotite (~ 0.02 mm), and is deformed by a S_4 crenulation cleavage (Appendix A).

4.5.1. $^{40}\text{Ar}/^{39}\text{Ar}$ Dating

Apparent age spectra were generated from fine biotites obtained from two samples at site 14SL03. In both cases, individual crystals yielded well-defined plateau ages. 14SL03A had a weighted mean age of 330.1 ± 2.5 Ma, with a minimum age 312.9 ± 2.7 Ma. Sample 14SL03B yielded a plateau age of 339.7 ± 2.6 Ma, with a minimum age of 331.9 ± 3.6 (Figure 5c; Table 2).

4.6. 13SL12A

Sample 13SL12A is a quartz-rich phyllite of the Waits River Formation, and it was obtained roughly 12 km west of the pluton margin (see western-central part of transect, Figure 2). Compositional banding in original bedding was visible locally within c. 10 m of the sample locality (i.e. across a two-lane road), with phyllitic and calcareous layers easily distinguishable from one another at the cm–m scale. Where bedding was apparent, S_3 was the dominant secondary foliation and coplanar. Across the road from the outcrop from which sample 13SL12AX was taken (c. 10 m), moderately-plunging L_4 intersection lineations were visible in some phyllitic layers. Outcrop-scale fold hinges with S_5 crenulation lineations were observed on the outcrop from which the sample was taken. In thin section 13SL12AX (cut parallel to the L_x trend), cleavage domains of fine grained muscovite (< 200 μm), and sparse biotite (~ 200 μm) define S_4 and occur up to many millimeters in thickness. The more competent, fine-grained quartz (up to 0.1 mm) microlithons preserve a crenulated S_3 (Figure 4c; Appendix A). In thin section 13SL12AY (cut parallel to strike and perpendicular to the lineation trend), S_5 is visible as

a crenulation cleavage. Elongate ilmenite porphyroblasts (up to 0.5 mm) are locally preserved in microlithons helping to define S₄ cleavage domains, and show signs of rotation into S₅ (Figure 4e; Appendix A).

4.6.1. ⁴⁰Ar/³⁹Ar Dating

A single biotite crystal yielded a well-defined plateau age of 369.2 ± 3.8 Ma, with a minimum age of 356.9 ± 2.5 Ma (Figure 5d; Table 2). No ⁴⁰Ar/³⁹Ar data was collected from muscovite in this sample due to the extremely fine grain size and expected issues with ³⁹Ar recoil (McDougall and Harrison, 1999).

4.7. 14SL02A

14SL02A is another quartz-rich black phyllite of the Waits River Formation, obtained less than a kilometer from the pluton margin (see eastern end of transect, Figure 2). Asymmetric boudinage of quartz veins with a dextral sense of shear were recognized in the field, in addition to compositional bands of phyllite, sandy marble, and veins/boudins of quartz. In thin section 14SL02AY, the dextral sense of shear defined by the asymmetry of boudins is readily apparent, and coarse calcite, biotite, and ilmenite have recrystallized in the low-strain zones of the boudin necks. GBAR also appears to have affected the coarse-grained quartz veins (Appendix A).

4.8. 13SL20B

Sample 13SL20B is a quartz-rich schist member of the Waits River Formation obtained at the northwest margin of the pluton at the Bickford Quarry in Marshfield (see eastern end of transect, Figure 2). In thin section, original bedding is inferred to be defined by compositional banding (several cm's in scale) and is subparallel to S₃, defined by platy biotite (0.5 mm) and flattened quartz grains (~0.1 mm). Biotite porphyroblasts

(1.3 mm) have grown oblique to those two fabrics in both quartz-rich and mica-rich sections and define S_4 . Muscovite from this sample is often much finer grained than biotite, but some elongate crystals reach up to 0.7 mm. In thin section 13SL20BY, muscovite appears to have been deformed by the S_4 crenulation cleavage along which biotite porphyroblasts have grown (Figure 4f; Appendix A).

4.8.1. $^{40}\text{Ar}/^{39}\text{Ar}$ Dating

A single biotite crystal from this sample yielded a weighted mean age of 360.1 ± 2.3 Ma, and a minimum age of 270.2 ± 1.7 Ma (2σ errors; Figure 5e; Table 2). A single muscovite crystal yielded a well-defined plateau age of 350.2 ± 1.5 Ma, with a minimum age of 342.2 ± 5.3 Ma (Figure 5e; Table 2).

4.9. 13SL20C

Sample 13SL20C is a fairly coarse-grained granodiorite sample of the Knox Mountain pluton, obtained at the northwest margin of the pluton at the Bickford Quarry in Marshfield (see eastern end of transect, Figure 2). Westerman and Coish (2009) have noted that numerous aplitic and pegmatitic dikes cut the main granitoid body at this location. In thin section, there is ample evidence for solid-state deformation of most or all phases. Large potassium feldspar (4 mm) grains are often inclusion-rich and surrounded by grains of myrmekite (up to 0.5 mm). Additionally, flame perthite and deformation twins were observed in plagioclase feldspar grains (2 mm). Biotite grains are largely inclusion-free and reach up to 1 mm (though they are usually 0.3–0.8 mm). Muscovite tends to be fine grained (~0.2 mm). Finally, grain boundaries in this coarse-grained sample can be described as convoluted (Figure 6c; Appendix A).

4.9.1. $^{40}\text{Ar}/^{39}\text{Ar}$ Dating

A single biotite crystal from this sample yielded a plateau age of 343.6 ± 2.0 , with a minimum age 295.2 ± 1.4 Ma (Figure 5g; Table 2). An individual muscovite crystal from this sample yielded a plateau age of 325.1 ± 3.2 Ma, and a minimum age of 316.2 ± 5.2 Ma (Figure 5g; Table 2). A single potassium feldspar grain yielded a loss profile that climbs from a minimum age of 212.5 ± 1.3 to a plateau-like segment yielding a weighted mean age of 285.2 ± 1.5 Ma (Figure 5g; Table 2).

4.10. 13SL20D

13SL20D is another granitoid sample from the Bickford quarry on the northwest margin of the pluton (see eastern end of transect, Figure 2). It had many features in common with 13SL20C, including deformation twins, intergrowth textures, and convoluted grain boundaries, that provide evidence for solid-state deformation at the thin section scale. Potassium feldspar in this sample is slightly finer than other granite samples, reaching up to 1.5 mm in coarsest grains. Myrmekite is much less prevalent in this sample, though it was still noted. Biotite (~1 mm) and muscovite (~0.5 mm) tend to be coarse euhedral to subhedral grains that are largely inclusion-free (Appendix A).

4.10.1. $^{40}\text{Ar}/^{39}\text{Ar}$ Dating

The individual biotite grain analyzed from this sample yielded a well-defined plateau age of 362.3 ± 1.4 Ma, and a minimum age of 351.4 ± 1 Ma (Figure 5g; Table 2). Roughly twenty fine-grained muscovite crystals yielded a well-defined plateau age of 357.9 ± 1.7 Ma and a minimum age of 144.1 ± 9.2 Ma (Figure 5h; Table 2). An individual potassium feldspar crystal from this sample yielded a loss profile with a

maximum age of 338.5 ± 1.7 Ma, a minimum age of 177.9 ± 3.6 Ma, and a weighted mean age of 325.1 ± 7.9 Ma (2σ errors; Figure 5h; Table 2).

4.11. 13SL21A

Sample 13SL21A is a granodiorite sample of the Knox Mountain pluton obtained from cliffs near the summit of Marshfield Mountain in Marshfield near the northeastern pluton margin (see eastern end of transect, Figure 2). In thin section, this sample displays some features similar to those observed in samples 13SL20C and 13SL20D, with some notable differences. Evidence for solid-state deformation is less prevalent in this sample, though it is still present. Myrmekite grains (up to 0.8 mm) are less abundant, and flame perthite is lacking in potassium feldspar, and deformation twins are not a prevalent in plagioclase (1.5 mm) compared to sample 13SL20C. Micas tend to be coarser grained, with elongate muscovite up to 1 mm in length, and elongate biotite up to 2 mm. Monazite ($50 \mu\text{m}$) was observed after running a samarium scan over the carbon-coated thin section in an ion microprobe (Appendix A). Zircon ($\leq 40 \mu\text{m}$) was deemed too small for mechanical separation and not suitable for geochronologic investigation.

4.11.1. $^{40}\text{Ar}/^{39}\text{Ar}$ Dating

A single biotite crystal yielded a plateau age of 336.6 ± 2.6 Ma, and a minimum age of 138.8 ± 1.7 Ma (Figure 5i; Table 2). An individual coarse muscovite grain from this sample yielded a well-defined plateau age of 344.3 ± 2.5 Ma, with a minimum age of 341.9 ± 1.3 (Figure 5i; Table 2). A potassium feldspar crystal yielded a loss profile with a weighted mean age of 285.7 ± 2.2 Ma, and a minimum age of 235.64 ± 1.4 Ma (Figure 5i; Table 2).

4.11.2. U/Th Total Pb Dating

Monazite and zircon were notably lacking in samples of the Knox Mountain pluton granodiorite, and the two minerals were observed only in one of three samples prepared in thin section. Zircon was determined to be too fine grained for mechanical separation (the largest grains were ~40 μm along the longest axis), and monazite was targeted for U-Th total Pb geochronology because it can be dated in-situ (Williams and Jercinovic, 2002). Four grains of monazite were located and mapped in thin section 13SL21A, and some grains display core–rim zonation (high-[Th] cores and high-[Y] rims; Appendix A). Weighted mean ages of monazite domains are reported (instead of ages from individual analyses) because the mean of sets of analyses are used as the basis to calculate a single date for a monazite domain (Williams and Jercinovic, 2002). A final weighted mean for the sample was calculated to be 377 ± 5.2 Ma (MSWD = 2.9; 95% c.l.; Figure 7).

5. Discussion

Our ability to understand the assembly and evolution of orogenic belts is directly linked to our ability to precisely date deformational and/or thermal events. In order to successfully date deformation via $^{40}\text{Ar}/^{39}\text{Ar}$ dating of biotite and muscovite (both referred to generally as “mica” below), it is necessary to determine whether the timing of mineral crystallization (i.e. a deformation age), or the timing of passing below a mineral’s closure temperature for argon retention has been dated (i.e. a cooling age; Dunlap, 1997). To successfully determine this, one must recognize if mica minerals experienced full, partial, or no recrystallization during foliation development, and whether or not radiogenic argon

was lost due to sustained residence time at elevated temperatures (Dunlap *et al.*, 1991). The retention and loss of radiogenically-produced ^{40}Ar is controlled by thermally-activated diffusion (Dodson, 1973; Reiners and Brandon, 2006). Therefore, peak temperature attained during deformation must be taken into consideration in order to interpret an age.

When deformation occurs well above the temperature of argon retention within a crystal lattice, ages are indicative of the time elapsed since cooling below the closure temperature for argon (Dodson, 1973; Dunlap *et al.*, 1991). When deformation occurs well below the temperature of argon retention, three possible scenarios ensue: 1) If new mica growth or complete recrystallization of mica occurs, preexisting radiogenic argon is completely lost and ages represent the timing of deformation. 2) If partial recrystallization of mica occurs, calculated ages represent a “mixed population” (due to the partial loss of radiogenic argon), and timing of deformation may only be inferred from selected steps in the spectra. 3) If mica does not recrystallize, calculated ages will not be affected by deformation and therefore represent a cooling age (Dunlap *et al.*, 1991; Dunlap, 1997). Careful interpretations of $^{40}\text{Ar}/^{39}\text{Ar}$ spectra can be combined with petrographic fabric-characterizations to determine whether calculated ages represent an age of cooling below the argon closure temperature of mica, the timing of deformation, or a mixed population of both. However, interpretations are complicated further due to the existence of a partial retention zone, a temperature range where decay products (e.g. ^{40}Ar) are thermally activated enough to partially diffuse out of a crystal lattice (Reiners and Brandon, 2006). Utilizing the step heating method allows for the characterization of multiple age populations from $^{40}\text{Ar}/^{39}\text{Ar}$ spectra (McWilliams *et al.*, 2013).

In the shallow to upper crust, under greenschist-facies conditions, micas often represent a heterogeneous system where individual grains within a population can grow over a range of time and temperature (Dunlap, 1997). The diffusivity of argon within an individual mica lattice is controlled mainly by the interlayer bond length, which itself is controlled by many factors, including (but not limited to) bulk chemistry, crystal defects, vacancies, and major and minor element concentrations. Experiments by Hames and Bowring (1994) show that ^{40}Ar concentrations decrease outwards from grain centers to boundaries, indicating that the closer a radiogenic argon atom is to a grain boundary, the higher its potential to diffuse out of the grain. Therefore, grain size plays an important role in determining the diffusion domains for argon gas (and therefore closure temperature) within individual crystals. McDougall and Harrison (1999) suggest that the size of Ar diffusion domains in potassium feldspar range from 1 to 100 μm , and are equivalent to the physical size of dated grains for micas. Given an average crustal cooling rate of $10\text{ }^{\circ}\text{C}\cdot\text{Myr}^{-1}$, biotite and muscovite have respective closure temperatures in the ranges of $350 \pm 30\text{ }^{\circ}\text{C}$ and $380 \pm 30\text{ }^{\circ}\text{C}$ (Reiners and Brandon, 2006). Reiners and Brandon (2006) state that a calculated cooling age likely represents a rock's final passage through the partial retention zone of the dated mineral.

When multiple populations of a mineral phase are present (i.e. mica that defines multiple cleavages), step-heating will degas different proportions of both age populations, and the resulting apparent age will be a weighted average of those populations (McWilliams *et al.*, 2013). Samples from the pluton's metamorphic aureole all have multiple mica populations. However, because the region was deformed under greenschist-facies conditions, mica from outside the pluton's metamorphic aureole is

believed to have recrystallized below its closure temperature, suggesting grain size will not affect argon diffusivity and therefore should not impact the conclusions reached (McWilliams *et al.*, 2013). Given the fact that multiple schistosity within these rocks may have developed below the closure temperatures of muscovite and biotite, and given the impossible task of separating fabrics during mineral separation, multiple age populations must be considered for all phyllitic samples (McWilliams *et al.*, 2013). In contrast, ages generated from grains of biotite, muscovite, and potassium feldspar from the granitoid samples may be interpreted as cooling ages.

5.1. Timing of Intrusion of the Knox Mountain Pluton

A primary goal of this study is to say definitively whether the Knox Mountain pluton intruded in conjunction with, or after the three foliation-forming deformational events of the Acadian orogeny (S_3 , S_4 , and S_5). As noted above, observations including folded and boudinaged dikes of granite in the field (interpreted to be F_4), microstructures in the metamorphic aureole, and solid-state deformation structures observed in granitoid thin sections have been paired with the isotopic ages obtained in this study to suggest the Knox Mountain granite has been subjected to Acadian deformation (Figure 6; Appendix A).

The weighted mean age of 377 ± 5.2 Ma, calculated from six U/Th total Pb analyses of a monazite grain from sample 13SL21A is interpreted as the age of crystallization of the Knox Mountain pluton. An additional (perhaps multi-transect) study would be required to determine a more precise intrusion and crystallization history for the pluton, as field evidence (and general knowledge about pluton construction (Brown, 2013, and references therein) indicates that it was constructed over the course of

multiple diking events (Westerman and Coish, 2009). However, the biotite, white mica, and potassium feldspar $^{40}\text{Ar}/^{39}\text{Ar}$ age spectra from a single sample can be analyzed in conjunction with U/Th total Pb data from the same locality, and a cooling history for the granite at that location can be constructed (see Figure 8).

Sample site 13SL21A's white mica and biotite plateau ages and potassium feldspar weighted mean age are 344.3 ± 2.5 Ma, 336.6 ± 2.6 Ma, and 285.7 ± 2.2 Ma, respectively. These ages indicate the Knox Mountain pluton initially experienced a relatively rapid cooling following crystallization, with a cooling rate >10 °C·Myr⁻¹ for ~70 Myr following intrusion and crystallization. The stepped spectra observed in potassium feldspar and biotite suggest the monotonic cooling phase was disrupted sometime around 300 Ma, roughly coincident with the timing of the Alleghanian Orogeny (Robinson et al., 1998; McWilliams *et al.*, 2013). Many respective minimum ages from these samples are 300 Ma or younger, suggesting this region may have experienced the thermal and/or deformational effects from events postdating the Acadian orogeny (Figure 8).

While no U-bearing minerals were found in samples 13SL20C and 13SL20D, the $^{40}\text{Ar}/^{39}\text{Ar}$ data from these granitic samples are also indicative of the pluton's cooling history along its western margin. 13SL20C had respective biotite and white mica plateau ages and a potassium feldspar weighted mean age of 343.6 ± 2.0 Ma, 325.1 ± 3.2 Ma, and 285.2 ± 1.5 Ma. Sample 13SL20D had respective biotite and white mica plateau ages and a potassium feldspar weighted mean age of 362.3 ± 1.4 Ma, 357.9 ± 1.7 Ma, and 325.1 ± 7.9 Ma.

The ages yielded from these two samples suggests the pluton's cooling rate may have slowed to the range of $2.5\text{--}5\text{ }^{\circ}\text{C}\cdot\text{Ma}^{-1}$ sometime between 360–320 Ma. Samples 20C and 20D were obtained within meters of one another and yielded a spread of ages from mostly individual grains, suggesting a non-uniform thermal history within the granite, and highlighting the complexity of the data and regional history. The available data suggests the Knox Mountain pluton crystallized at ca. 375 Ma, followed initially by a period of rapid cooling, then by a slower and more irregular cooling and/or reheating during subsequent tectonic events, and exhumation was episodic.

5.2. Timing of Cooling for the Knox Mountain Pluton's Metamorphic Aureole

The interbedded phyllite and sandy marble units of the Waits River and Gile Mountain formations within the metamorphic aureole of the pluton have experienced a complex thermal history. They were deposited nearly 420 Mya in a marginal/marine basin as interbedded sandstones, limestones, and mudstones derived from the Taconic mountains, and were subjected to greenschist-facies metamorphism, deformed multiple times (by D_3 and D_4 , sometimes D_5), and subsequently intruded during the Acadian orogeny (Tremblay and Pinet, 2005; Walsh *et al.*, 2009; McWilliams *et al.*, 2010). The relationship between porphyroblastic minerals that grew during pluton intrusion and fabrics that developed during Acadian deformation make it possible to deduce the relative timing of events and further interpret $^{40}\text{Ar}/^{39}\text{Ar}$ spectra.

Samples 13SL19A and 13SL20B are worthy of comparison because they are both Waits River phyllites taken from within meters of a contact between local country rock and granite intrusion. Sample 13SL19A was obtained within a few meters of an exposure of the Adamant granite, a small ($\sim 1\text{ km}^2$) intrusive body located at the western end of the

field area, roughly 2 km from the western limit of the CVGT. In thin section, metamorphic ilmenite grains can be seen to be surrounded by reaction rims of (often) heavily-chloritized biotite. These metamorphic porphyroblasts are enveloped by a penetrative schistosity, inferred here to be the S_4 foliation, and are crenulated by an S_5 crenulation cleavage (Appendix A). 13SL19A's plateau age of 343 Ma was generated from more than 20 grains, and is likely the product of mixing an older population with a younger one. Thus 343 Ma provides a minimum age constraint for S_4 and a maximum age constraint for S_5 . 263 Ma is the sample's minimum age from its argon loss profile, and this age could represent the minimum age for the younger population of grains.

Sample 13SL20B is a schistose Waits River sample from the Knox Mountain pluton margin that yielded respective white mica plateau age and biotite weighted mean ages of 350 and 360 Ma. Because biotite was elongate along both S_3 and S_4 (see Figure 4f), this age likely represents a mixed population, making it difficult to say precisely whether this age dates cooling through a closure temperature or a specific stage of deformation. It is worth noting that biotite in this sample has an Alleghanian minimum age of 270 Ma.

Sites 13SL05 and 14SL03 are both within 5 km of the pluton margin, and samples from these localities contained large porphyroblasts of biotite (and in the latter case, garnet) that are interpreted to have grown during contact metamorphism. In both cases, these porphyroblasts overgrow the S_3 fabric and are affected by an S_4 crenulation cleavage, suggesting the porphyroblasts grew in inter-tectonically with respect to the development of these foliations (see Figure 4a,b). Because fine muscovite grains help define the S_3 and S_4 foliations, and multiple grains were dated in the allanite, the

muscovite ages reported here need to be considered as potentially mixed ages. Biotites and white micas from site 13SL05 have a spread of plateau and weighted mean ages, from ca. 320–365 Ma. Because samples 13SL05A and 13SL05B were obtained within meters of each other, we interpret that any differences in their thermal history metamorphism related to deformation, and not their location within a contact aureole. Minimum ages of these samples are also spread and diverse, and include dates at ca. 143 Ma, 226 Ma, 276 Ma, and 337 Ma. White mica from samples 05A and 05B both fall at 346 Ma, and this age could be interpreted either as a minimum age for the local development of S₄, or as a cooling age (compare to the cooling ages of granite sample 13SL21A). The biotites from site 13SL03 had weighted mean and plateau ages that range from 330–340 Ma, and respective minimum ages at 313–331 Ma. The spread in these ages also illustrates the complexity and variability of the region’s cooling history due to polyphase orogenic events, exhumation, and cooling in the metamorphic aureole.

5.3. Timing of Foliation Development in the CVGT

The oldest recorded ⁴⁰Ar/³⁹Ar ages are from samples in the westernmost part of the field area. The oldest age is from Waits River phyllite sample 13SL12A, which yielded biotite minimum and plateau ages of 357 Ma and 369 Ma, respectively. The S₄ compositional banding (with recrystallized biotite and white mica in mica-rich microlithons) observed in thin section suggests these ages bracket a minimum age for development of the S₄ fabric for that particular belt and latitude of the CVGT (Figure 3b). The local development of S₄ occurred sometime around ca. 370 Ma (Figure 3b). The timing of local development of S₅ has not been fully constrained in this study, though the

sheer number of samples with ages around 345 Ma suggests S_5 fabric development may have occurred at that time (discussed below).

The Ordovician Cram Hill Formation is the only unit west of the DRFZ sampled in this study. Walsh *et al.* (2010) note that while Taconic-derived S_2 is the dominant planar fabric in pre-Silurian rocks, Acadian-derived S_3 locally overprints the older Taconian foliations, and is the dominant fabric in close proximity to the DRFZ. Sample 13SL02A was obtained several meters west of the DRFZ, and yielded biotite and muscovite plateau ages of 365 Ma. This age is interpreted to represent either the minimum age for the local development of S_3 , or movement along the fault planes of the DRFZ. Significantly more work must be conducted across the DRFZ in order to properly understand the context of these age dates.

5.4. Observations Across the Transect and Region

Plateau, weighted mean, and minimum ages from across the transect show a general trend of younging towards the east (Figures 3b, 3c). The fact that the timing of fabric development in the western end of the transect coincides with the timing of intrusion of the Knox Mountain pluton in the eastern end of the transect means this trend of younging cannot be attributed to the intrusion of the Knox Mountain pluton. While Alleghanian deformation is well documented south of New England, the effects of post-Acadian deformation have limited recognition in Vermont (e.g. McWilliams *et al.*, 2013). The minimum ages in argon-loss profiles from various samples suggests these rocks have been affected by Alleghanian and/or Mesozoic deformation and exhumation, and significantly more work must be done to characterize the effect of post-Acadian deformation in New England.

The findings of this study pair nicely with other recent regional geochronologic investigations. Building off the work of Hannula *et al.* (1999), we have documented that the Knox Mountain pluton is indeed a syntectonic intrusion with regards to the foliation-forming events of the Acadian, and propose similar investigations may be conducted on other intrusive bodies of various scales in the New Hampshire plutonic series. It is also known that metamorphic grade generally increases, and age generally decreases from north-to-south along strike within the CVGT. Tremblay *et al.* (2000) have reported that the peak of Acadian metamorphism and deformation occurred from roughly 375–380 Ma in southern Québec. We conclude that the development of S₃ predates pluton emplacement, and the absolute minimum age of S₃ development is 371.8 Ma (the lower error bounds of the monazite crystallization age presented here).

Chan *et al.* (2000) reported that S₃ and S₄ fabric development occurred respectively at 370.7 ± 1.0 Ma and 345.5 ± 1.7 Ma in the Taconic Allochthon of southwestern Vermont. Eight samples from this study yielded plateau or weighted mean ages in the range of 345 ± 10 Ma, suggesting foliation development in the CVGT was coincident with foliation development in certain allochthonous blocks further west. The number of samples presented in this study with ages clustered around 345 Ma that also display S₅ foliations suggests the S₅ fabric may have developed at that time (Figure 3b; making S₅ in this field area correlative with S₄ of Chan *et al.* (2000)). Finally, McWilliams *et al.* (2013) were the first to report on Alleghanian deformation observed in Vermont. The number of samples from this study with minimum ages falling around the time of Alleghanian deformation (~300 Ma) confirms that post-Acadian deformation is more pervasive in New England than what has been recognized previously.

After working in the Plainfield quadrangle, Konig (1961) suggested that granite emplacement caused regional doming (F_5) after the regional development of the Woodbury syncline, Nichols anticline, and Brownington syncline. He also noted that the axial trace of the Woodbury syncline is sub-parallel to the Knox Mountain pluton's margin, and that shear sense in drag folds suggested rocks in the east of the quadrangle had risen with respect to those in the west. When considering the relationship between these major regional folds and the geometry of the Knox Mountain pluton's margin, we suggest the pluton forcefully intruded into an antiformal structure many kilometers in amplitude that once existed east of the Brownington syncline. Structural data from the Bickford Quarry compared with structural data from across the region suggests the Knox Mountain pluton (at least partially) was injected in an orientation similar to regionally folded structures during its intrusion history (Figure 9). Outlier data in stereonet may be related to local-scale deformation that occurred during injection, resulting in the dome-and-basin structures observed at the walls of the Bickford Quarry.

5.5. Future Investigations

The dextral shear zone or zones recognized near the Knox Mountain pluton's eastern margin at sites 13SL20 and 14SL02 present an opportunity for further investigation. Though fieldwork was conducted along the trend of shearing recognized in sample 14SL02A, no other shearing was recognized along that trend. Limited bedrock exposure makes it difficult to determine if the outcrop at this locality is in place or if it is perhaps a loose block that only appears to be intact because of soil cover. Hall (1959) recognized boudinaged neck lines with a dextral sense of shear both perpendicular and parallel to minor, northwest dipping fold axes in the St. Johnsbury quadrangle, though the

information provided in that report makes it difficult to say if the boudins there could be correlated with the ones recognized in this study. Dextral shearing is well-recognized elsewhere in the Acadian orogenic belt; in Nova Scotia the Cobequid-Chedabucto fault system records dextral shearing and northwest-directed thrusting (Pe-Piper and Piper, 2002; van Staal and Barr, 2012). West and Hubbard (1997) found that dextral transpression occurred along the Norumbega fault in coastal Maine, with mylonitization occurring there at ~290 Ma. Additionally, Short (2010) recognized a Devonian-aged, northeast-trending dextral shear zone in central Maine that continuously evolved from a contractional to transpressive environment. Contrastingly, McWilliams *et al.* (2013) suggest that the sinistral transpression observed along the eastern margin of the CVGT at the Westminster West fault zone may have helped to accommodate some of that same Alleghanian strain. A more thorough investigation along the trend of shearing recognized at the two sheared sites from this study may be able to resolve the significance of the shear zone (or zones) at the northwestern margin of the Knox Mountain pluton.

6. Conclusions

This study demonstrates that the Knox Mountain pluton intruded at 371 Ma, in between or during progressive regional D₃ and D₄ deformational events associated with the Acadian orogeny. Evidence from the field for syntectonic intrusion includes folded and boudinaged granitic dikes at the margin of the pluton. The granite also appears deformed in thin section; deformation twins in feldspar, flame perthite and myrmekite in potassium feldspar, and grain-boundary migration recrystallization of quartz have all

been documented at that scale). Five kilometers west of the intrusion, in the pluton's metamorphic aureole, coarse porphyroblasts have overgrown the S₃ fabric, but are crenulated by the S₄ fabric. This suggests that intrusion occurred after the regional development of S₃, but prior to the development of S₄. The monazite crystallization age for the pluton constrains c. 372 Ma as the minimum age for local development of S₃.

In the western end of the transect, the timing of development of S₄ has been constrained to ~369 Ma based on observations and analytical data obtained from sample 13SL12A, where the development of S₄ cleavage domains locally transposed S₃. The number of samples with plateau and weighted mean ages clustering around ~345 Ma suggests S₅ fabric development likely occurred around ~345 Ma across the transect. It is possible this age is slightly younger than the true age of fabric development, because these samples may have been partially reset due to a later reheating event(s).

A general trend of younging is observed in plateau, weighted mean, and minimum ages from across the transect from west to east (Figure 3b, 3c). Nine different samples, including phyllites west of the DRFZ, from the center of the transect, and at the pluton margin, had minimum ages in the range of 300 ± 30 Ma. This provides strong evidence that the region was affected by Alleghanian orogeny deformation and/or metamorphism. Five samples from the eastern end of the transect, including micas from the metamorphic aureole and mica and potassium feldspar from the granite, have a spread in minimum ages from 142–235 Ma. These ages suggest the region was also affected by Mesozoic tectonic activity, such as the rifting of Pangea (~200 Ma) or local passage of the New England hot spot (~110 Ma; Figure 8).

This study highlights certain complexities of radiometrically dating rocks that have been subjected to multiple deformation events. Due to limits in a mineral's ability to retain radiometrically-produced gas in its crystal lattice at elevated temperatures, it can be difficult to precisely determine the timing of deformation in certain cases. However, careful analysis of $^{40}\text{Ar}/^{39}\text{Ar}$ spectra, paired with diligent field work and integration of regional data sets can reveal much about a region's complex history. It is evident that some of the largest intrusive bodies in the CVGT segment of the New Hampshire plutonic series are syntectonic plutons. Similar investigations on other Devonian-aged plutons will continue to provide a better understanding on the evolution of the Acadian Orogeny and the relationship between deformation and magmatism in orogenic belts.

FIGURES

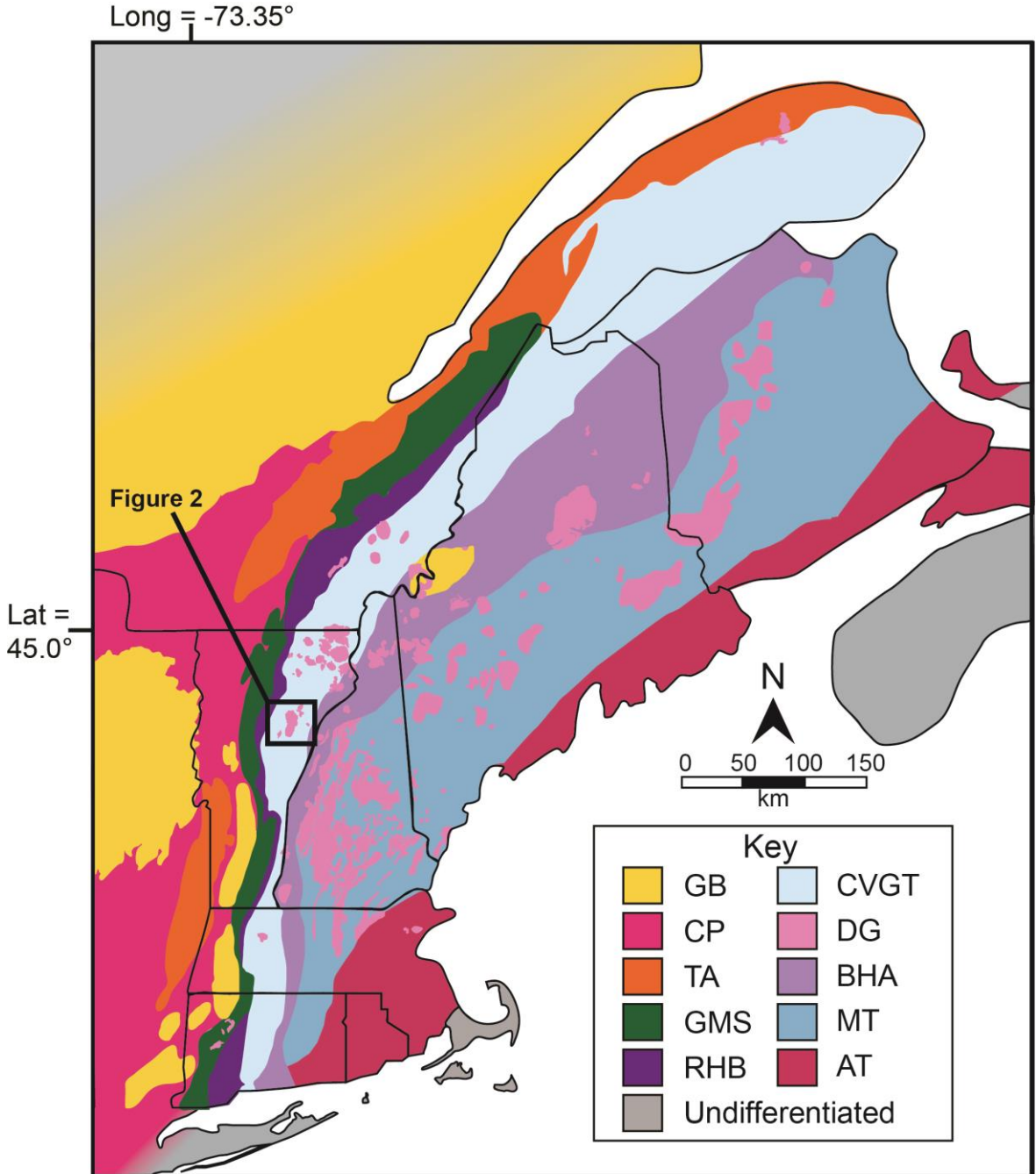


Figure 1: The geologic provinces of New England and maritime Canada record the Paleozoic accretionary history of North America. The following abbreviations have been assigned to the region's tectonic elements: GB- Grenvillian Basement; CP- Carbonate Platform; TA- Taconic Allochthon; GMS- Green Mountain Slice; RHB- Rowe-Hawley Belt; CVGT- Connecticut Valley Gaspé Trough; BHA: Bronson Hill Anticlinorium; MT- Merrimack Trough; AT- Avalon Terrane. Devonian-aged granitic plutons associated

with the Acadian orogeny have been highlighted in pink, and the field area shown in Figure 2 is highlighted in the thick black box. The following state and provincial bedrock maps were used in compilation of this figure: Canada: Weeler *et al.* (1996); Québec: Thériault *et al.* (2012); New Brunswick: Mersereau *et al.* (2008); Nova Scotia: Keppie *et al.* (2000); Maine: Osberg *et al.* (1985); New Hampshire: Lyons *et al.* (1997); Massachusetts: Zen *et al.* (1983); Rhode Island: Hermes *et al.* (1994); Connecticut: Rodgers, (1985); New York: Fisher *et al.* (1970); Vermont: Ratcliffe *et al.* (2011).

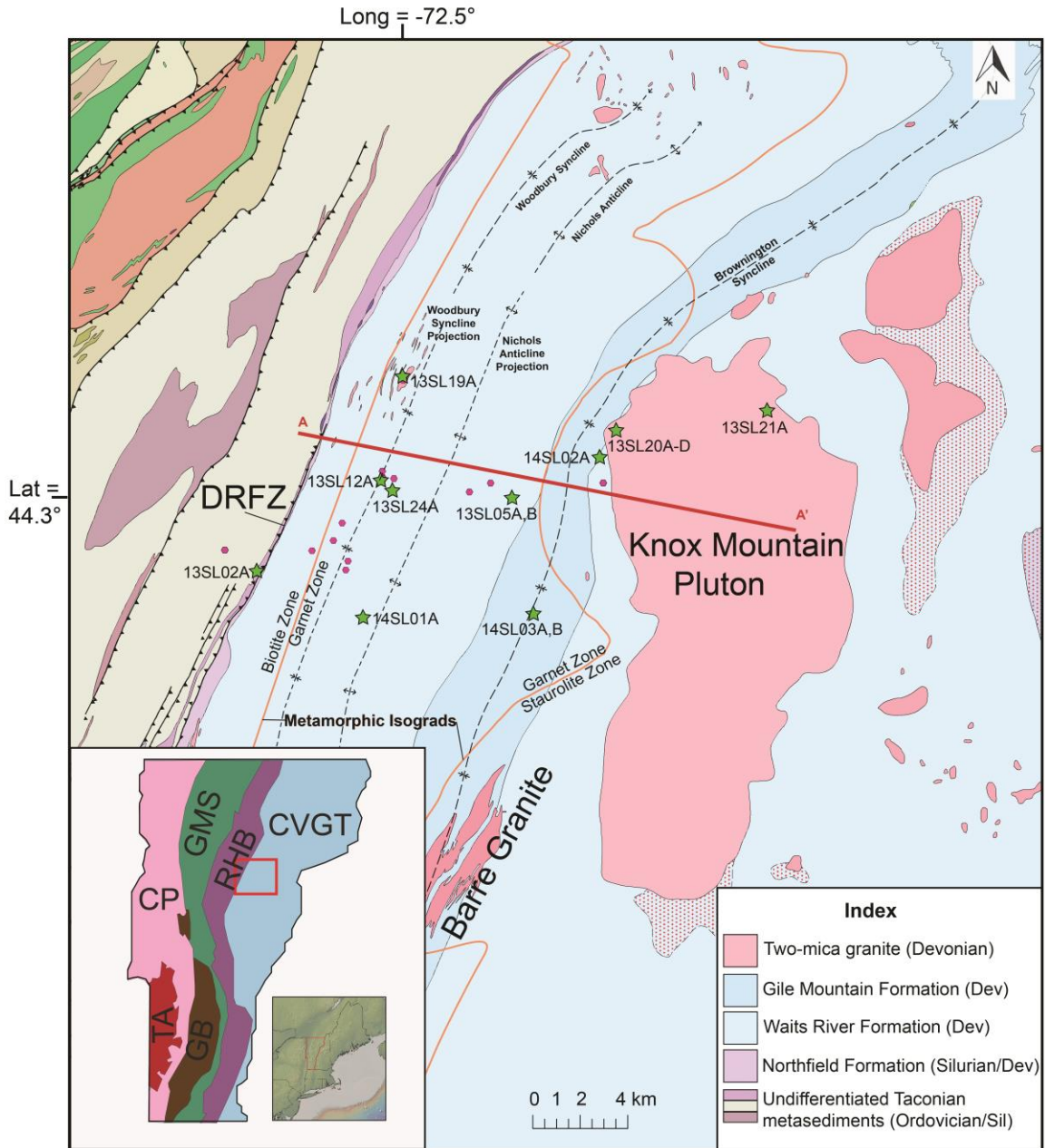


Figure 2: Geologic bedrock map of field locality, modified from the USGS Vermont state bedrock map by Ratcliffe *et al.* (2011). The red line A–A' designates the transect of interest (shown in cross section in Figure 3), extending from the Dog River fault zone (DRFZ) in the west to the margins of the Knox Mountain Pluton in the east. Oriented hand samples have been obtained from localities designated with a green star. Additional structural data was collected at localities marked with a pink hexagon (may appear as a dot). The red stipple pattern is defined by Ratcliffe *et al.* (2011) as a granite overprint. Inset shows map area within the geologic provinces of Vermont.

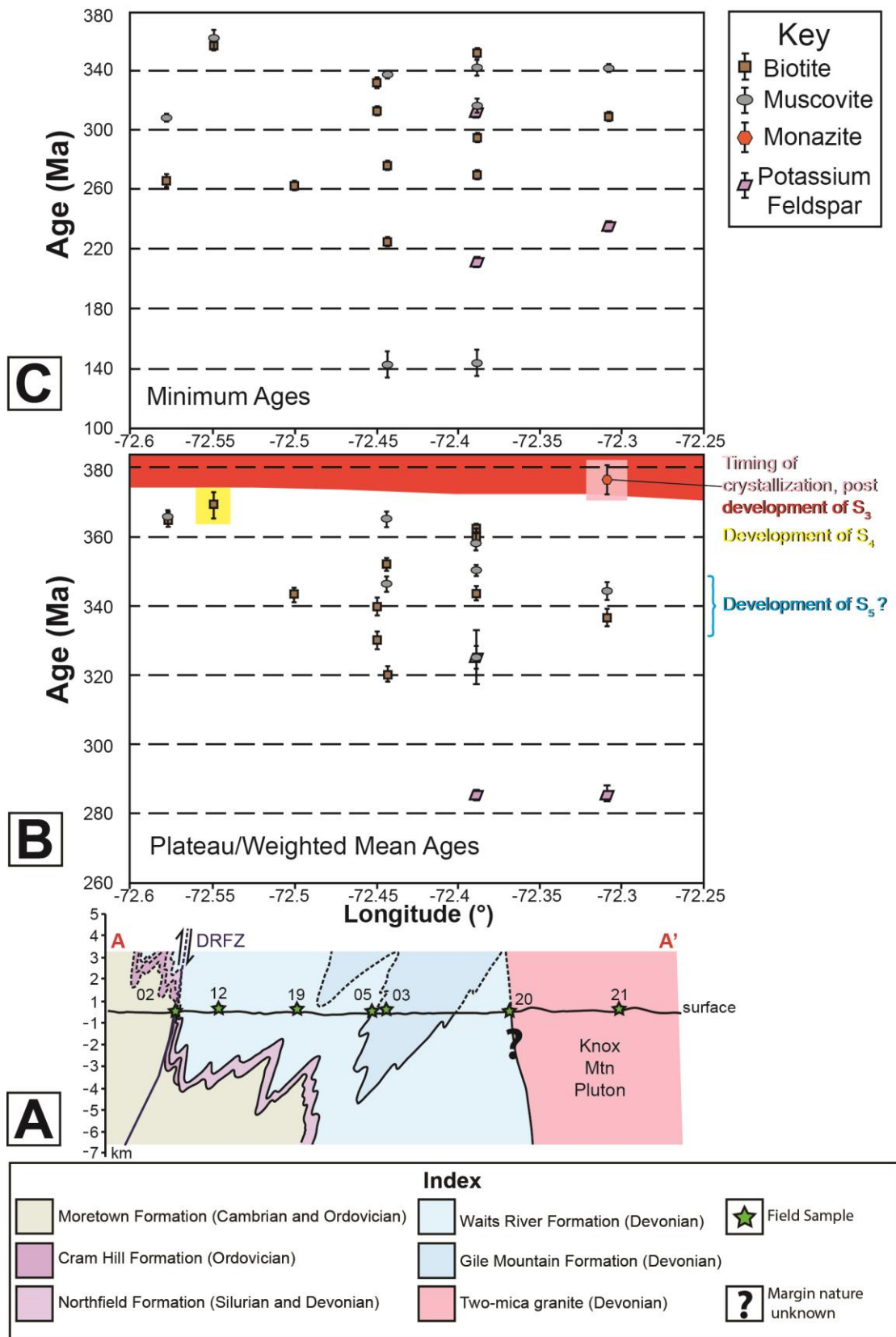


Figure 3: (a) Cross section of the transect of interest, modified after Ratcliffe *et al.* (2011). Cross section A–A' (highlighted as a red line in Figure 3) shows the steeply-dipping reverse faulting that has occurred along the RMC, the margins of the Knox Mountain pluton, and the locations of field samples within the km-scale southeast-verging Acadian folds. Sample locations, denoted with green stars, can be used to better understand the trends highlighted in parts B and C of this figure. (b) Plot of respective plateau or weighted mean ages of samples versus their projected location along transect A–A'. Certain relationships observed in thin section (see Figure 4) allow the relative timing of events to be deduced. Biotite and garnet porphyroblasts in the pluton's metamorphic aureole (see Figure 4A, B) suggest intrusion occurred after the development of S₃ and prior to the development of S₄. The nature of samples 13SL12A and 13SL20B (see Figure 4C, E, F) suggests the development of S₄ was not coeval across the region. The timing of development of S₅ in the region was not successfully deduced in this study. (c) Plot of samples minimum ages versus their projected location along transect A–A'. Note the number of samples with minimum ages around or below 300 Ma, evidence to suggest the region has experienced reheating and/or deformation during Alleghanian and Mesozoic events.

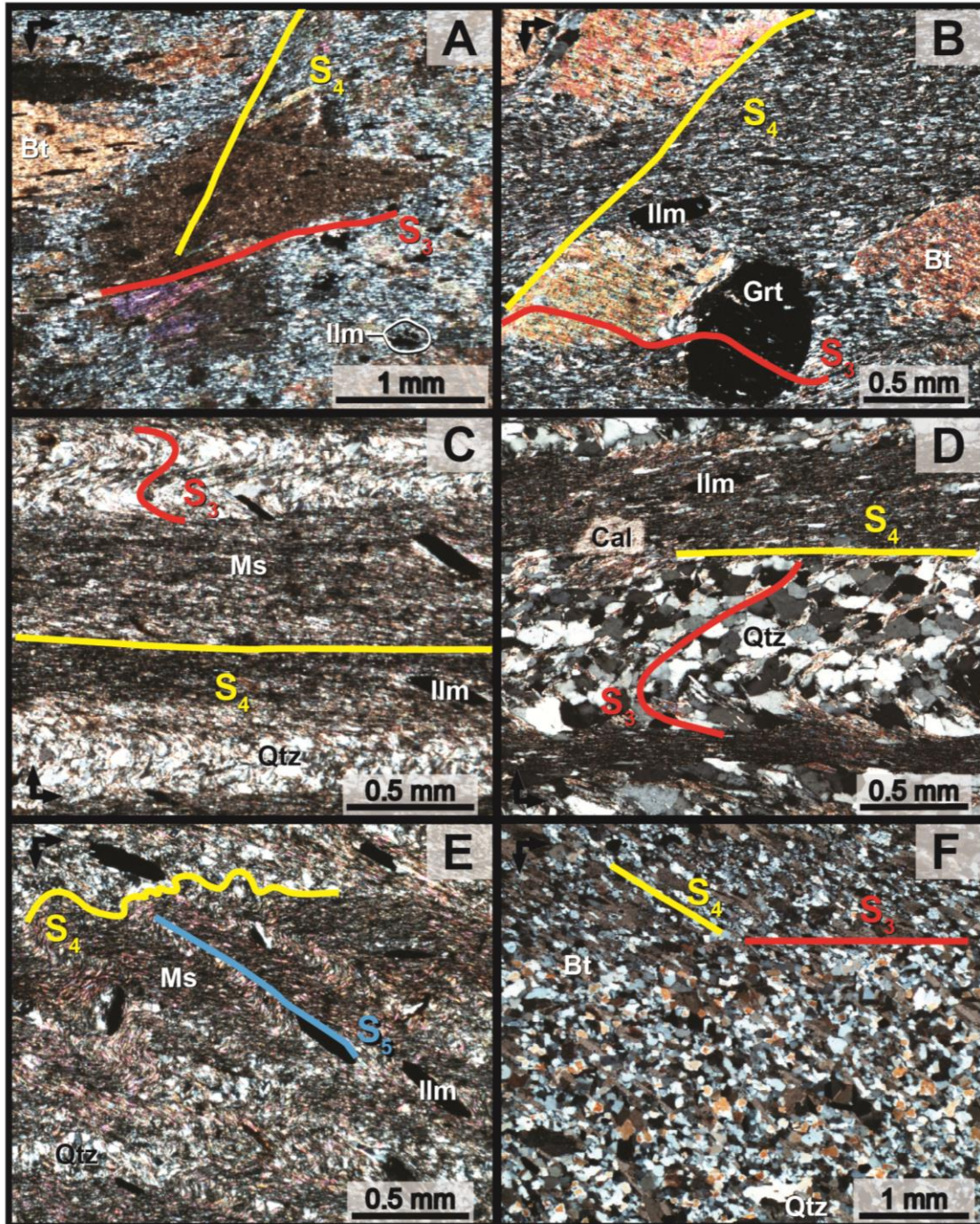
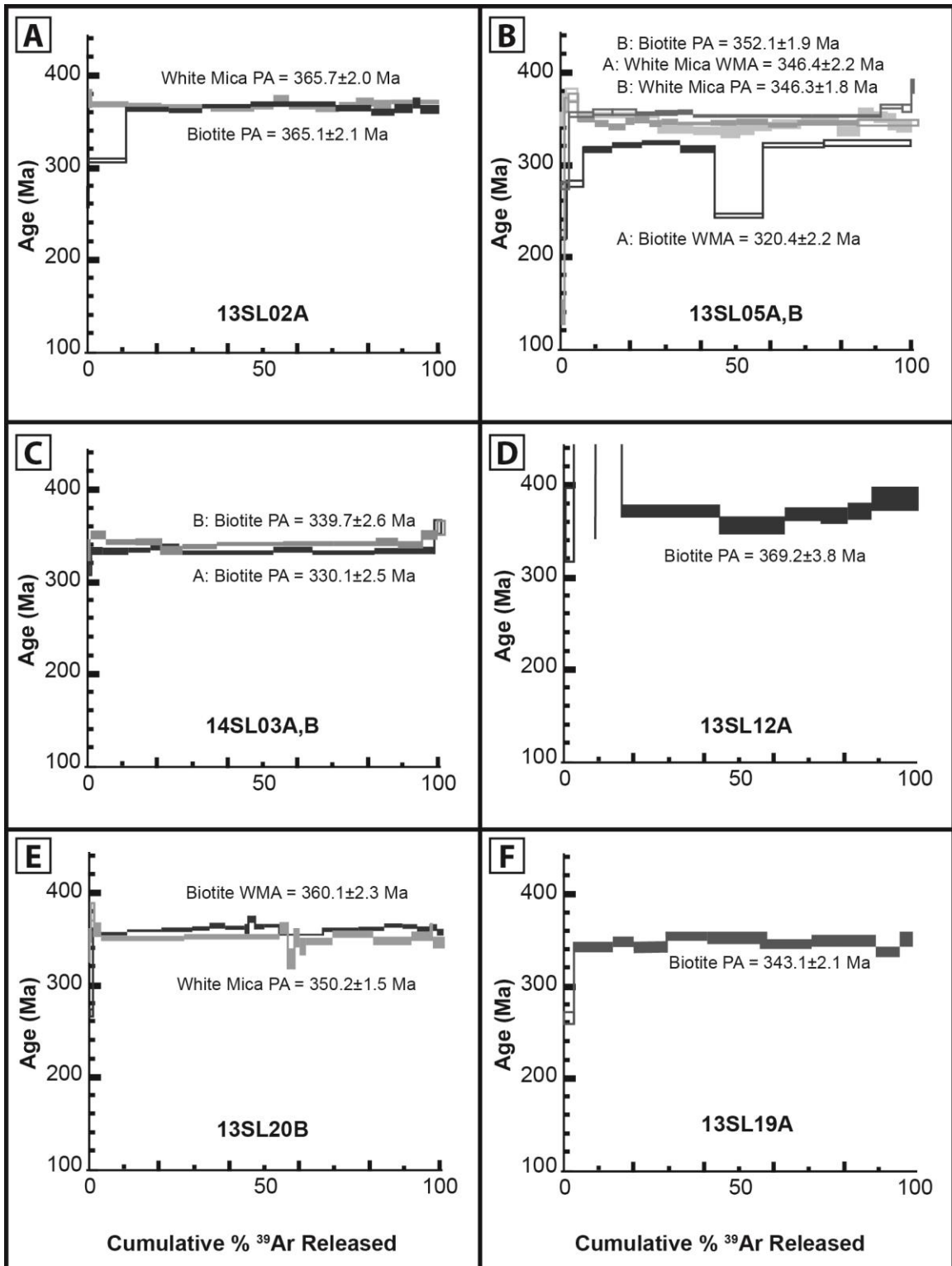


Figure 4: Select photomicrographs from oriented thin sections in cross polarized light. Mineral abbreviations from Siivola and Schmid (2007), where Bt = biotite, Cal = calcite, Grt = garnet, Ilm = ilmenite and Qtz = quartz. (a) 13SL05AY: Large biotite porphyroblasts have overgrown S_3 (red) and are deformed by S_4 crenulation cleavage (yellow). Elongate opaque grains and microlithons of fine-grained quartz are also visible and define the S_3 foliation. (b) 14SL03AX: S_3 is preserved in large biotite and garnet

porphyroblasts, and are deformed by S_4 crenulation cleavage. Elongate opaque grains and microlithons of fine-grained quartz are also visible and define the S_3 foliation. **(c)** 13SL12AX: Crenulated S_3 is preserved in quartz-rich S_4 microlithons, and is defined by fine-grained muscovite within those cleavage domains. S_4 is the dominant cleavage domain, and is defined by compositional banding of quartz and mica. **(d)** 14SL01AX: S_3 is preserved in quartz-rich microlithons, and is defined by fine-grained muscovite within those cleavage domains. S_4 defines the cleavage domains. **(e)** 13SL12AY (oriented perpendicular to 13SL12AX, above): S_3 is not readily visible in this orientation. S_4 is defined by the quartz-rich and mica-rich cleavage domains. S_5 is a crenulation cleavage (blue) that has developed locally. **(f)** 13SL20BY: S_3 is subparallel to original bedding (S_0) and is defined by grain size variation and abundance of quartz. S_4 is defined by elongate biotite porphyroblasts that have developed in both the quartz-rich and quartz-poor sections of the slide. For photomicrographs of all samples prepared in thin section, refer to Appendix A.



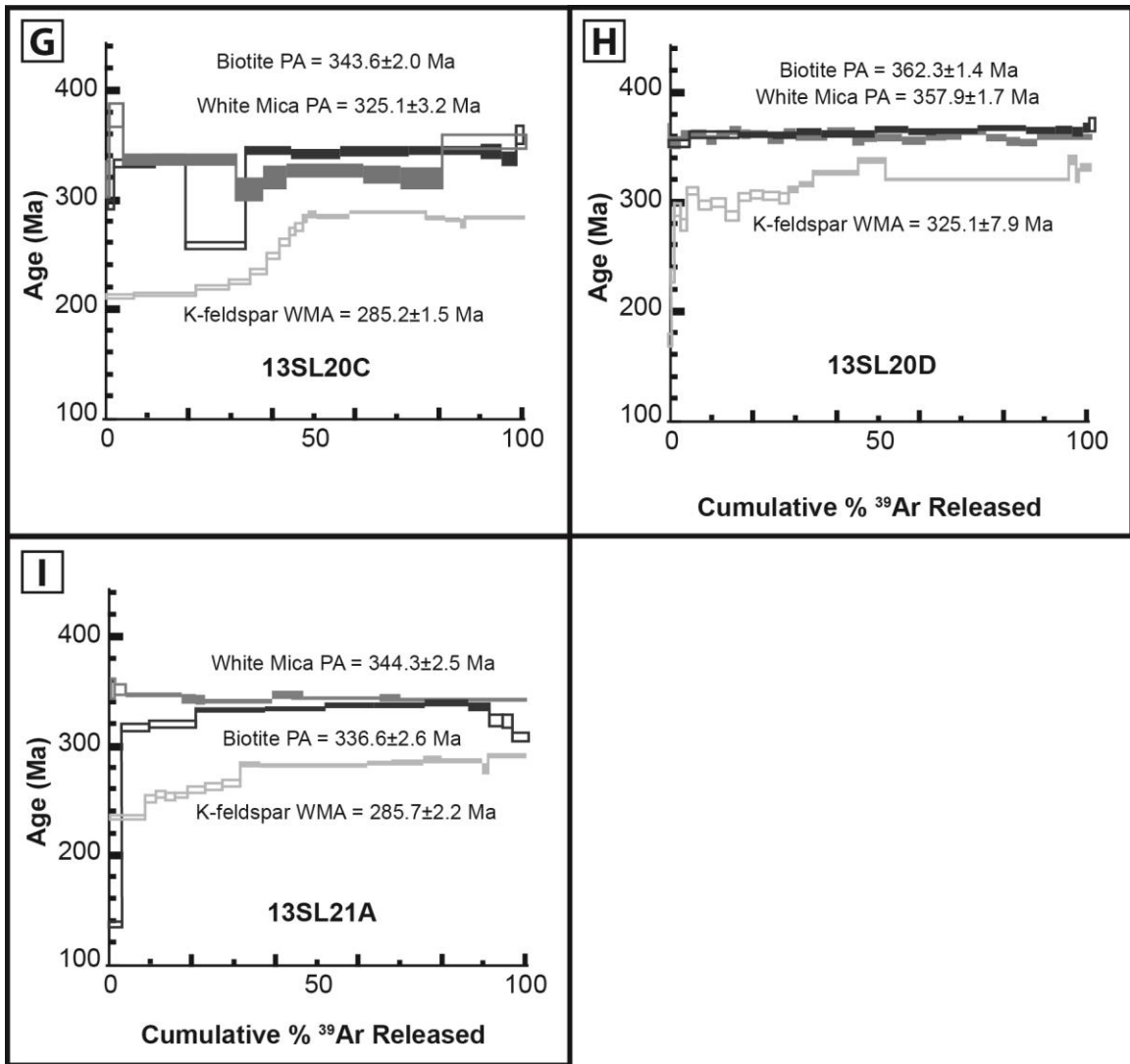


Figure 5: Compiled apparent $^{40}\text{Ar}/^{39}\text{Ar}$ age spectra from phyllitic (a–f) and KMP granite (g–i) samples. Box heights and quoted errors are at the 1σ level, except for samples 13SL20B Biotite (e) and 13SL20D K-feldspar (g), which are reported at 2σ . Filled-in boxes have been used in plateau age (PA) and weighted mean age (WMA) calculations; outlined boxes with no fill have been excluded from calculations. For each sample, the darkest grey spectra are biotite, spectra that are medium dark grey are white mica, and the lightest greys spectra are potassium feldspar.

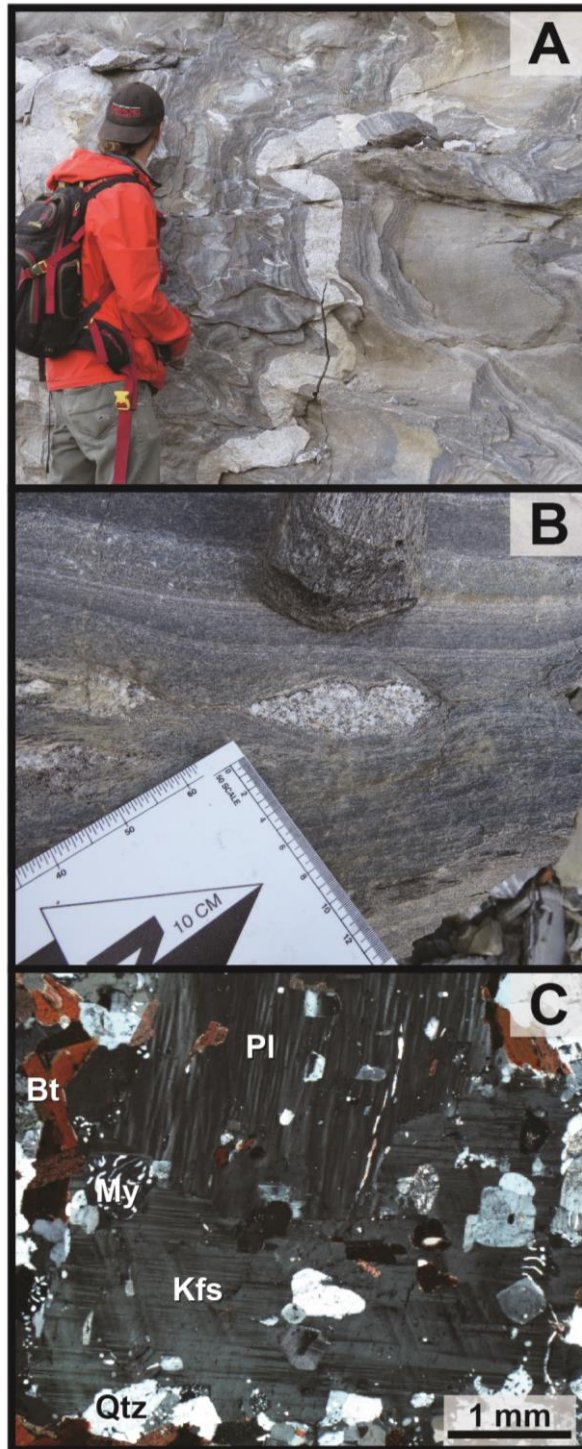


Figure 6: Evidence for solid-state deformation granite in thin section and outcrop from field site 13SL20 (the Bickford Quarry), at the northwest margin of the Knox Mountain pluton. (a) A xenolith-bearing granitic dike displays similar folds to the Waits River

Formation country rock into which it intruded. **(b)** Boudins of granitic material within coarse-grained Waits River Formation indicate that local deformation continued after the solidification of some granitic material. **(c)** Photomicrograph of thin section 13SL20C in cross polarized light, with mineral abbreviations from Siivola and Schmid (2007). Evidence for deformation at the thin section scale includes the development of myrmekite (My) grains at the expense of potassium feldspar (Kfs), the convoluted nature of grain boundaries in this coarse grained plutonic rock, and deformation twins and flame perthite in plagioclase feldspar (Pl).

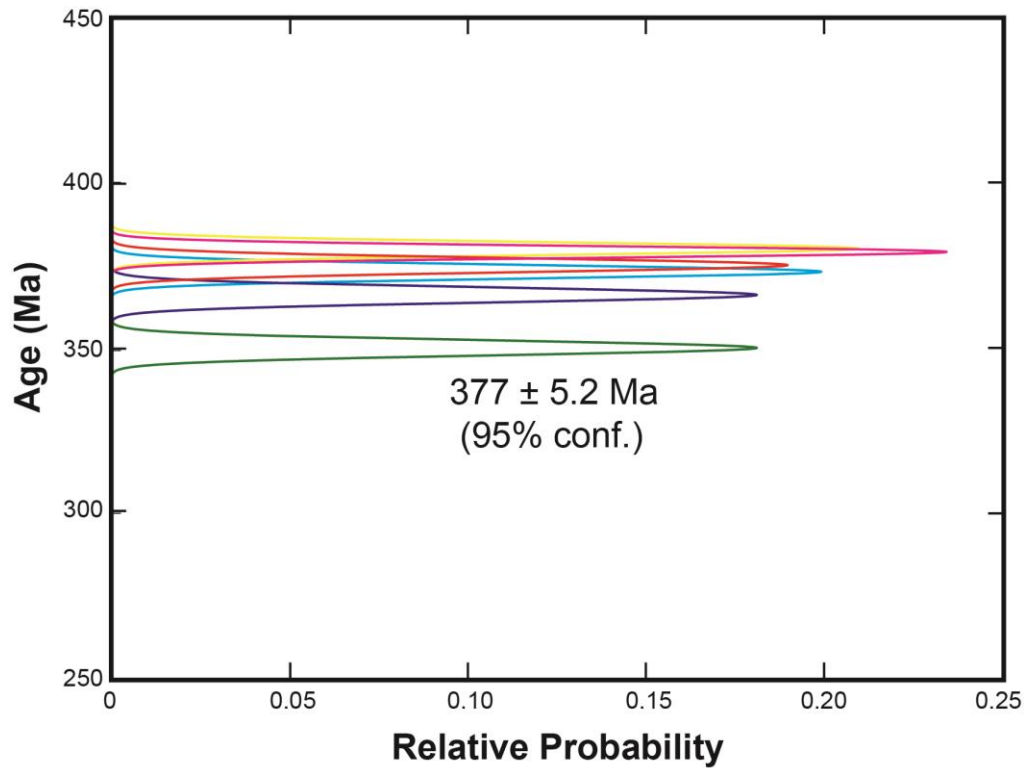


Figure 7: Gaussian histogram, displaying ages calculated from the series of analyses within distinct compositional domains in a single monazite grain from sample 13SL21A, which have been combined to produce a single weighted mean age of 377 ± 5.2 Ma with an MSWD of 2.9.

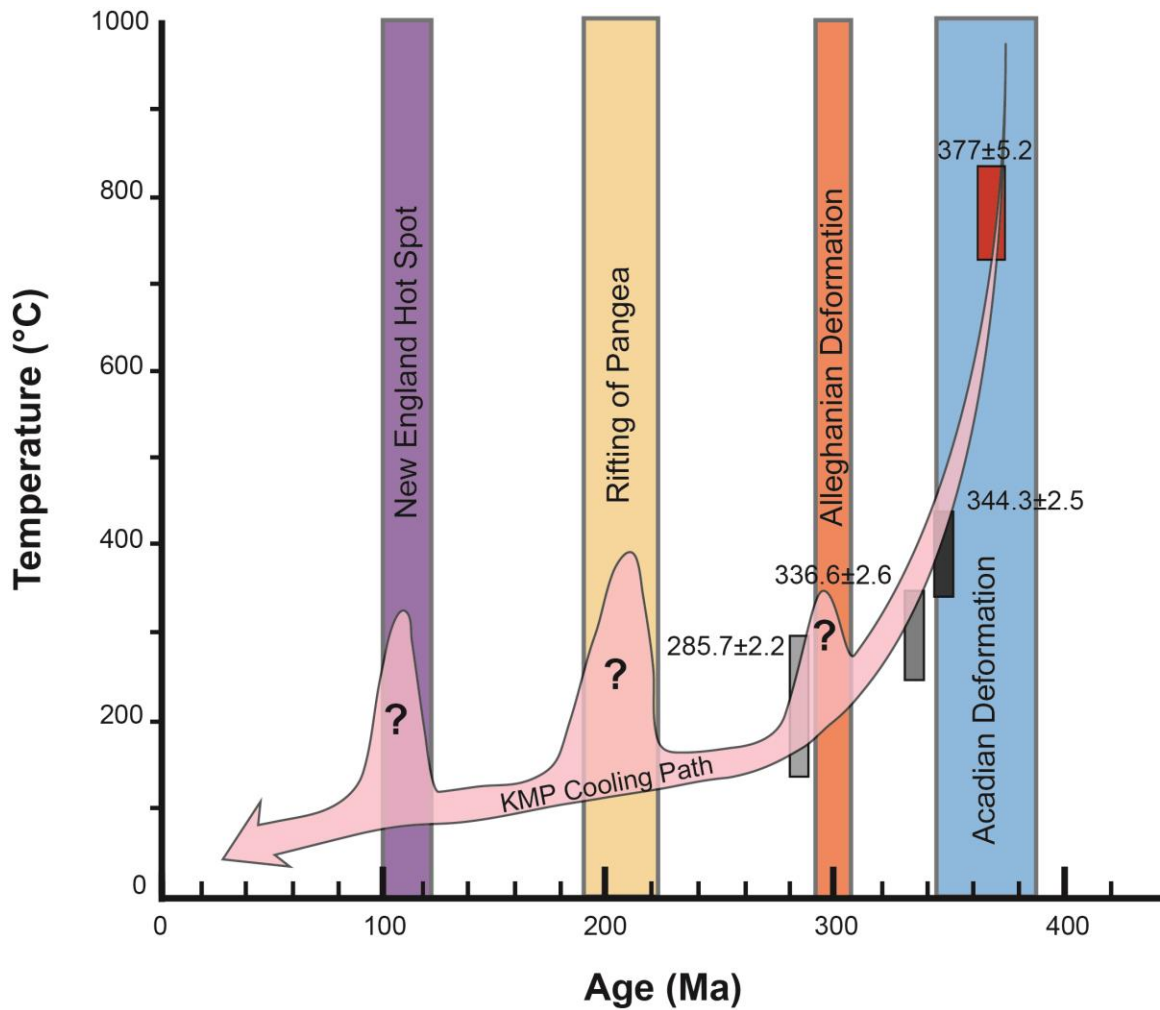


Figure 8: Deformational and thermal tectonic events that have affected the modern east coast of North America, compared to the apparent cooling history for the Knox Mountain pluton constructed with the $^{40}\text{Ar}/^{39}\text{Ar}$ and U-Th total Pb data produced by granitic sample 13SL21A. The monazite weighted mean age of 377 ± 5.2 Ma is shown in red. The biotite, white mica, and potassium feldspar $^{40}\text{Ar}/^{39}\text{Ar}$ plateau and weighted mean ages are respectively shown in progressively lighter shades of grey. The inferred cooling path of the Knox Mountain pluton is shown in pink. Box widths and reported errors are 1σ .

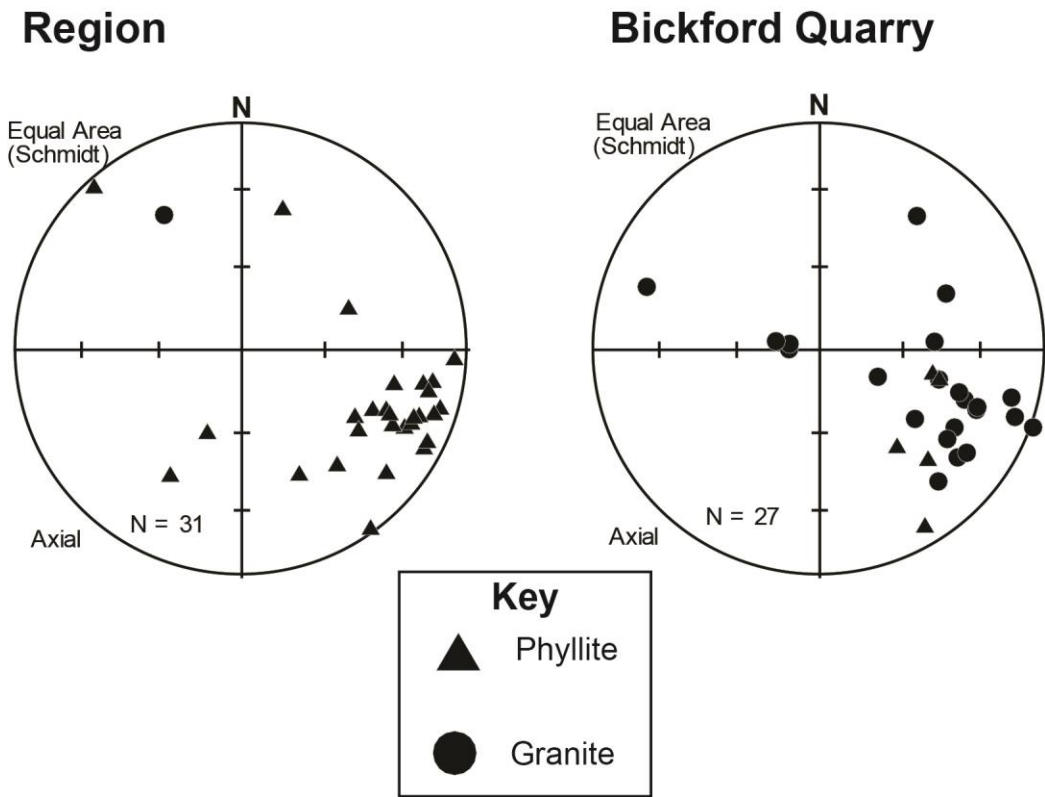


Figure 9: Comparison of structural data collected at the Bickford Quarry (site 13SL20) and the rest of the field area, displayed on equal area Schmidt lower hemisphere projections. The available data suggests the Knox Mountain pluton may have intruded into the fold hinges of large, kilometer-scale regional folds. The data points from the Bickford that are orthogonal to this regional folding are likely due to local deformation that occurred during intrusion, producing the dome-and-basin style folds observed at quarry walls. The granite in the regional stereonet is that of the Adamant granite.

TABLES

Table 1: Regional Taconian and Acadian deformation fabrics.

Deformation		Foliation	Found in this study
D ₅	Weak dome-stage cleavage	S ₅ (Acadian S ₃)	Local crenulation cleavage
D ₄	Northeast-striking/northwest-dipping and lesser northwest-striking/ northeast-dipping cleavage and folds	S ₄ (Acadian S ₂)	Can be dominant schistosity in close proximity to the Woodbury syncline
D ₃	Dominant schistosity with tight-isoclinal folding in Devonian and Silurian rocks. Cleavage to fault-related fabric along Dog River fault zone	S ₃ (Acadian S ₁)	Often subparallel to original bedding. Relict foliation where overprinted by S ₄
D ₂	Dominant schistosity and “pinstripe” in Moretown Formation (west of DRFZ). Relict foliation where overprinted by S ₃	Taconian S ₂	
D ₁	Relict layer-parallel foliation in Moretown and Cram Hill Formations (west of DRFZ)	Composite Taconian S ₀ /S ₁	

Table 2: $^{40}\text{Ar}/^{39}\text{Ar}$ results. Samples with a higher longitude value occur further west along transect. Errors reported are at the 1σ level unless noted.

Sample	Lat (°N)	Long (°E)	Description	Phase Dated (N) ^U	Textural Context	Grain Size	Min Age (Ma)	Plateau Age (Ma)	% ^{39}Ar	MSWD
13SL02A	44.2667	72.5781	Cram Hill Black Phyllite	Bt (1 xtl)	In seams that wrap around augens of garnet	<200 μm	307.5 \pm 1.4	365.1 \pm 2.1	89.1	1.16
				Wm (10 xtls)	In Acadian S ₃ fold hinges	~200 μm	266.4 \pm 4.1	365.7 \pm 2.0	99.81	0.7
13SL05A	44.2949	72.4437	Waits River Grey Phyllite	Bt (1 xtl)	Fine grains define S ₃ ; Porphyroblasts overgrow S ₃	200 μm^*	225.8 \pm 2	320.4 \pm 2.2 ^Q	37.3	1.6
				Wm (15 xtls)	Define S ₃ foliation	~100 μm	337.7 \pm 1.8	346.4 \pm 2.2 ^Q	95.2	2
13SL05B	44.2949	72.4437	Waits River Grey Phyllite	Bt (1 xtl)	Fine grains define S ₃ ; Porphyroblasts overgrow S ₃	~200 μm^*	276.1 \pm 2.1	352.1 \pm 1.9	69.2	0.77
				Wm (~25 xtls)	Define S ₃ foliation	50–75 μm	142.9 \pm 8.9	365.1 \pm 2.1	95.9	0.45
13SL12A	44.2748	72.5496	Waits River Grey Phyllite	Bt (1 xtl)	Define S ₄ foliation	200 μm	356.9 \pm 2.5	369.2 \pm 3.8	83.6	0.73
				Wm (~20 xtls)	Define S ₄ foliation	200 μm	361.6 \pm 5.4	No plateau		
13SL19A	44.3409	72.5004	Waits River Black Phyllite	Bt (~25 xtls)	Occurs as reaction rims around ilmenite	~0.5 mm	263.2 \pm 2.4	343.1 \pm 2.1	97.2	0.83
13SL20B	44.3202	72.3887	Waits River Grey Schist	Bt (1 xtl)	Defines both S ₃ and S ₄	2.5 mm	270.2 \pm 1.7	360.1 \pm 2.3 ^{Qx}	99.22	2.8
				Wm (1 xtl)	Deformed by S ₄	0.3 mm	342.2 \pm 5.3	350.2 \pm 1.5	98.9	1.01
13SL20C	44.3203	72.3887	Knox Mountain Granodiorite	Bt (1 xtl)	Euhedral and subhedral grains	1 mm	295.2 \pm 1.4	343.6 \pm 2.0	64.9	0.28
				Wm (1 xtl)	Euhedral and subhedral grains	0.2 mm	316.2 \pm 5.2	325.1 \pm 3.2	75.7	1.4
				Ksp (1 xtl)	Anhedral, often altered to myrmekite	5 mm	212.5 \pm 1.3	285.2 \pm 1.5 ^Q	53	1.4

Table 2 continued.

Sample	Lat (°N)	Long (°E)	Description	Phase Dated (N) [⊖]	Textural Context	Grain Size	Min Age (Ma)	Plateau Age (Ma)	% ³⁹ Ar	MSWD
13SL20D	44.3203	72.3887	Knox Mountain Granodiorite	Bt (1 xtl)	Euhedral and subhedral grains	1 mm	351.4±1	362.3±1.4	82.5	0.48
				Wm (~20 xtls)	Some euhedral, some anhedral, some occur as inclusions in ksp	0.5 mm	144.1±9.2	357.9±1.7	99.92	0.73
				Ksp (1 xtl)	Anhedral	1.5 mm	312.3±1.6	325.1±7.9 ^{⊖λ}	71.4	8.5
13SL21A	44.3279	72.3086	Knox Mountain Granodiorite	Bt (1 xtl)	Euhedral and subhedral grains	1 mm	309.2±1.7	336.6±2.6	70.2	0.71
				Wm (1 xtl)	Euhedral and subhedral grains	1.2 mm	341.9±1.3	344.3±2.5	96.2	0.8
				Ksp (1 xtl)	Anhedral, full of inclusions, sometimes rimmed by myrmekite	1.5 mm	235.6 ±1.4	285.7±2.2 [⊖]	68.6	1.6
14SL03A	44.2494	72.4498	Waits River Grey Phyllite	Bt (1 xtl)	Fine grains define S ₃ ; Porphyroblasts overgrow S ₃	0.02–1 mm	312.9 ± 2.7	330.1±2.5 [⊖]	96.9	0.45
14SL03B	44.2494	72.4498	Waits River Grey Phyllite	Bt (1 xtl)	Fine grains define S ₃ ; Porphyroblasts overgrow S ₃	0.02–1 mm	331.9±3.6	339.7±2.6	97.7	0.94

[⊖] Number of mineral grains in aliquot

[⊖] Weighted Mean Age

^λ 2σ errors reported

* Grainsize targeted during mineral separation

Table 3: Modal mineralogy based on petrographic observations of samples prepared in thin section.

Sample Number	Quartz	Biotite	Muscovite	Calcite	Potassium Feldspar	Plagioclase	Opakes	Chlorite	Other	Comments
13SL02A	40%	8%	5%	5%			<5%	7%	Garnet 25% Epidote 5%	Two species of garnet present in augens. Possibly a shear fabric modifying crenulation cleavage
13SL05A	40%	40%	10%	<2%			3%			Two generations of biotite
13SL05B	70%	20%	<1%				5%	5%		Coarse-grained poikiloblastic biotite confined to single layer
13SL12A	35%	trace	55%				5%			Two generation of muscovite. All very fine grained
13SL19A	30%	15%	5%				25%	25%		Opaque poikiloblasts have reaction rims of amphibole
13SL20B	50%	40%					trace	10%		Two generations of biotite
13SL20C	20%	10%			30%	25%			Myrmekite 5%	Extensive myrmekite development. Deformation twins and flame perthite in plagioclase
13SL20D	35%	15%			30%	20%				
13SL21A	20%	7%	8%		35%	25%			Zircon (trace) Monazite (trace) Apatite (trace) Myrmekite <5%	Only sample with U-bearing minerals

Table 3 continued.

Sample Number	Quartz	Biotite	Muscovite	Calcite	Potassium Feldspar	Plagioclase	Opaques	Chlorite	Other	Comments
13SL24A	75%	5%	10%				10%			Quartz is angular/anedral and is not recrystallized
14SL01A	45%		35%	5%			10%			Qtz has GBAR and fluid inclusions. Evidence of ductile deformation in msc and bt via basal slip
14SL02A	55%	10%		30%			5%			Dexteral C'-S fabric with recrystallized calcite at sheared boudin margins
14SL03A	40%	20%	13%				10%		Garnet 17%	Large subeuhedral garnets with inclusion trails

COMPREHENSIVE BIBLIOGRAPHY

Ablay, G.J., Clemens, J.D., & Petford, N., 2008, Large-scale mechanics of fracture-mediated felsic magma intrusion driven by hydraulic inflation and buoyancy pumping, *in* Thompson, K., and Petford, N., eds., *Structure and Emplacement of High-Level Magmatic Systems: Geological Society of London Special Publication 302*, p. 3–29.

Acosta-Vigil, A., Buick, I., Cesare, B., London, D., & Morgan VI, G.B., 2012, The extent of equilibration between melt and residuum during regional anatexis and its implications for differentiation of the continental crust: A study of partially melted metapelitic enclaves: *Journal of Petrology*, v. 53, p. 1319–1356, doi: 10.1093/petrology/egs018.

Aleinikoff, J. N., Ratcliffe, N. M., & Walsh, G. J., 2011, Provisional zircon and monazite Uranium-Lead geochronology for selected rocks from Vermont: U.S. Geological Survey Open-File Report 2011–1309, p. 1–46, available only online at <http://pubs.usgs.gov/of/2011/1309/>.

Allaz, J., Selleck, B., Williams, M. L., & Jercinovic, M. J., 2013, Microprobe analysis and dating of monazite from the Potsdam Formation, New York: A progressive record of chemical reaction and fluid interaction: *in* *Versatile Monazite: Resolving geological records and solving challenges in materials science*, *American Mineralogist*, v. 98, p. 1106–1119.

Anderson, M. T., & Coish, R. A., 1999, Depth constraints on the origin of Northeast Kingdom granites: *Geological Society of America, Abstracts with Programs*, v. 31, no. 2, p. A-1.

Armstrong, T. R., Tracy, R. J. & Hames, W. E., 1992. Contrasting styles of Taconian, eastern Acadian, and Western Acadian metamorphism, central and western New England. *In* *Journal of Metamorphic Geology*. v. 10, p. 415–426.

Arth, J. G., & Ayuso, R. A., 1997, The Northeast Kingdom batholiths, Vermont: Geochronology and Nd, O, Pb, and Sr isotopic constraints on the origin of Acadian granitic rocks: *In* *The Nature of Magmatism in the Appalachian Orogen*, *Geological Society of America Memoir 191*. p. 1–18.

Ayres, M., & Harris, N., 1997, REE fractionation and Nd isotope disequilibrium during crustal anatexis: Constraints from Himalayan leucogranites: *Lithos*, v. 139, p. 249–269.

Bartley, J.M., Coleman, D.S., & Glazner, A.F., 2008, Incremental pluton emplacement by magmatic crack-seal: *Transactions of the Royal Society of Edinburgh–Earth Sciences*, v. 97, p. 383–396.

Bean, R. J., 1953, Relation of Gravity anomalies to the geology of Central Vermont and New Hampshire: *Geological Society of America Bulletin*, v. 64, p. 509–538.

Benn, K., Horne, R.J., Kontak, D.J., Pignotta, G.S., & Evans, N.G., 1997, Syn-Acadian emplacement model for the South Mountain batholith, Meguma terrane, Nova Scotia: Magnetic fabric and structural analyses: *Geological Society of America Bulletin*, v. 109, p. 1279–1293, doi:10.1130/0016-7606(1997)109<1279:SAEMFT>2.3.CO;2.

Billings, M. P., 1956, *The geology of New Hampshire, Part II, Bedrock geology*, Concord, New Hampshire. State Planning and Development Commission: Mineral Resources Survey, p. 203.

Bons, P.D., & Elburg, M.A., 2001, Fractal size distribution of plutons: An example from the Lachlan fold belt, Australia, *in* Chappell, B.W., and Fleming, P.D., eds., *S-Type Granites and Related Rocks*: Australian Geological Survey Organisation Record 2001/2, p. 21–22.

Bons, P.D., & van Milligen, B.P., 2001, New experiment to model self-organized critical transport and accumulation of melt and hydrocarbons from their source rocks: *Geology*, v. 29, p. 919–922, doi:10.1130/0091-7613(2001)029<0919:NETMSO>2.0.CO;2.

Bons, P.D., Dougherty-Page, J., & Elburg, M.A., 2001, Stepwise accumulation and ascent of magmas: *Journal of Metamorphic Geology*, v. 19, p. 627–633, doi:10.1046/j.0263-4929.2001.00334.x.

Bons, P.D., Arnold, J., Elburg, M.A., Kalda, J., Soesoo, A., & van Milligen, B.P., 2004, Melt extraction and accumulation from partially molten rocks: *Lithos*, v. 78, p. 25–42, doi:10.1016/j.lithos.2004.04.041.

Bourque, P.-A., Brisebois, D., & Malo, M., 1995, Gaspé Belt, *In* Williams, H., (ed.), *Geology of the Appalachian-Caledonian Orogen in Canada and Greenland*: Geological Survey of Canada, *Geology of Canada*, v. 6, p. 316–351.

Bradley, D. C., 1983, Tectonics of the Acadian orogeny in New England and adjacent Canada. *Journal of Geology*. v. 91, p. 381–400.

Brown, M., 1994, The generation, segregation, ascent and emplacement of granite magma: The migmatite-to crustally- derived granite connection in thickened orogens: *Earth-Science Reviews*, v. 36, p. 83–130, doi: 10.1016/0012-8252(94)90009-4.

Brown, M., 2001a, Crustal melting and granite magmatism: Key issues: *Physics and Chemistry of the Earth*, v. 26, p. 201–212, doi:10.1016/S1464-1895(01)00047-3.

Brown, M., 2001b, Orogeny, migmatites and leucogranites: A review: *Proceedings of the Indiana Academy of Sciences*, v. 110, p. 313–336.

- Brown, M., 2004, Melt extraction from lower continental crust: Transactions of the Royal Society of Edinburgh–Earth Sciences, v. 95, p. 35–48, doi:10.1017/S0263593300000900.
- Brown, M., 2005, Synergistic effects of melting and deformation: An example from the Variscan belt, western France, *In* Gapais, D., Brun, J.-P., and Cobbold, P.R., (eds.), Deformation Mechanism, Rheology and Tectonics: From Minerals to the Lithosphere: Geological Society of London Special Publication 243, p. 205–226.
- Brown, M., 2006, Melt extraction from the lower continental crust of orogens: The field evidence, *In* Brown, M., and Rushmer, T., (eds.), Evolution and Differentiation of the Continental Crust: Cambridge, UK, Cambridge University Press, p. 332–384.
- Brown, M., 2007, Crustal melting and melt extraction, ascent and emplacement in orogens: Mechanisms and consequences: Journal of the Geological Society of London, v. 164, p. 709–730, doi:10.1144/0016-76492006-171.
- Brown, M., 2008, Chapter 6: Granites, migmatites and residual granulites: Relationships and processes, *In* Sawyer, E.W., and Brown, M., (eds.), Working with Migmatites: Mineralogical Association of Canada, Short Course Series 38, p. 97–144.
- Brown, M., 2010, The spatial and temporal patterning of the deep crust and implications for the process of melt extraction: Philosophical Transactions of the Royal Society, ser. A, v. 368, p. 11–51, doi:10.1098/rsta.2009.0200.
- Brown, M., 2013, Granite: From genesis to emplacement. Geological Society of America Bulletin, v. 125 no.7/8, p. 1079–1113.
- Brown, M., & Korhonen, F.J., 2009, Some remarks on melting and extreme metamorphism of crustal rocks, *In* Dasgupta, S., (ed.), Physics and Chemistry of the Earth: New York, Published for the Indian National Science Academy by Springer, p. 67–87.
- Brown, M., & Pressley, R.A., 1999, Crustal melting in nature: Prosecuting source processes: Physics and Chemistry of the Earth, v. 24, p. 305–316, doi:10.1016/S1464-1895(99)00034-4.
- Brown, M., & Solar, G.S., 1998a, Shear zone systems and melts: Feedback relations and self-organization in orogenic belts: Journal of Structural Geology, v. 20, p. 211–227, doi:10.1016/S0191-8141(97)00068-0.
- Brown, M., & Solar, G.S., 1998b, Granite ascent and emplacement during contractional deformation in convergent orogens: Journal of Structural Geology, v. 20, p. 1365–1393.

- Brown, M., & Solar, G.S., 1999, The mechanism of ascent and emplacement of granite magma during transpression: A syntectonic granite paradigm: *Tectonophysics*, v. 312, p. 1–33, doi:10.1016/S0040-1951(99)00169-9.
- Brown, M., Averkin, Y.A., McLellan, E.L., & Sawyer, E.W., 1995, Melt segregation in migmatites: *Journal of Geophysical Research*, v. 100, p. 15,655–15,679, doi:10.1029/95JB00517.
- Brown, M., Korhonen, F.J., & Siddoway, C.S., 2011, Organizing melt flow through the crust: *Elements*, v. 7, p. 261–266, doi:10.2113/gselements.7.4.261.
- Cady, W. M., 1956, Bedrock geology of the Montpelier quadrangle: U.S. Geological Society Geologic Quadrangle Map GQ-79, scale 1:62,500.
- Castonguay, S., Ruffet, G., & Tremblay, A., 2007, Dating polyphase deformation across low-grade metamorphic belts: An example based on $^{40}\text{Ar}/^{39}\text{Ar}$ muscovite age constraints from the southern Quebec Appalachians, Canada: *Geological Society of America Bulletin*, v. 119, no. 7–8, p. 978–992.
- Castonguay, S., Kim, J., Thompson, P. J., Gale, M. H., Joyce, N., Laird, J., & Doolan, B. L., 2011, Timing of tectonometamorphism across the Green Mountain anticlinorium, northern Vermont Appalachians: $^{40}\text{Ar}/^{39}\text{Ar}$ data and correlations with southern Quebec: *Geological Society of America Bulletin*, v. 124 no. 3–4 p. 352–367.
- Cawood, P.A., McCausland, P.J.A., & Dunning, G.R. 2001, Opening Iapetus: Constraints from the Laurentian margin in Newfoundland: *Geological Society of America Bulletin*, v. 113, n. 4, p. 443–453. doi:10.1130/0016-7606(2001)113<0443:OICFTL>2.0. CO;2.
- Chan, Y. C., Crespi, J. M., & Hodges, K. V., 2000, Dating cleavage formation in slates and phyllites with the $^{40}\text{Ar}/^{39}\text{Ar}$ laser microprobe: An example from the western New England Appalachians, USA: *Terra Nova*, v. 12, no. 6, p. 264–271.
- Clark, C., Fitzsimons, I.C.W., Healy, D., & Harley, S.L., 2011, How does the continental crust get really hot?: *Elements*, v. 7, p. 235–240, doi:10.2113/gselements.7.4.235.
- Clemens, J.D., 1998, Observations on the origins and ascent mechanisms of granitic magmas: *Journal of the Geological Society of London*, v. 155, p. 843–851, doi:10.1144/gsjgs.155.5.0843.
- Clemens, J.D., 2006, Melting of the continental crust: Fluid regimes, melting reactions, and source-rock fertility, *in* Brown, M., and Rushmer, T., eds., *Evolution and Differentiation of the Continental Crust*: Cambridge, UK, Cambridge University Press, p. 297–331.

Clemens, J.D., & Benn, K., 2010, Anatomy, emplacement and evolution of a shallow-level, post-tectonic laccolith: The Mt. Disappointment pluton, SE Australia: *Journal of the Geological Society of London*, v. 167, p. 915–941, doi:10.1144/0016-76492009-120.

Clemens, J.D., & Mawer, C.K., 1992, Granitic magma transport by fracture propagation: *Tectonophysics*, v. 204, p. 339–360, doi:10.1016/0040-1951(92)90316-X.

Coish, R. A., 2010, Magmatism in the Vermont Appalachians: *Geological Society of America Memoir*, v. 206, p. 91–110.

Coish, R.A., Fleming, F.S., Larsen, M., Poyner, R., & Seibert, J., 1985, Early rift history of the proto-Atlantic ocean: Geochemical evidence from metavolcanic rocks in Vermont: *American Journal of Science*, v. 285, n. 4, p. 351–378, DOI:10.2475/ajs.285.4.351.

Coish, R.A., Perry, D.A., Anderson, C.D., & Bailey, D., 1986, Metavolcanic rocks from the Stowe Formation, Vermont: Remnants of ridge and intraplate volcanism in the Iapetus Ocean: *American Journal of Science*, v. 286, n. 1, p. 1–28. doi:10.2475/ajs.286.1.1.

Coish, R. A., Bramley, A., Gavigan, T., & Masinter, R.A., 1991, Progressive changes in volcanism during Iapetan rifting; comparisons with the East African Rift – Red Sea system: *Geology*, v. 19, n. 10, p. 1021–1024. doi:10.1130/0091-7613(1991)019<1021:PCIVDL>2.3.CO;2.

Coish, R., Kim, J., Morris, N., & Johnson, D., 2011, Late stage rifting of the Laurentian continent: evidence from the geochemistry of greenstone and amphibolite in the central Vermont Appalachians: *Canadian Journal of Earth Sciences*, v. 49, p. 43–58. DOI:10.1139/E11-013.

Coleman, D.S., Gray, W., & Glazner, A.F., 2004, Rethinking the emplacement and evolution of zoned plutons: Geochronologic evidence for incremental assembly of the Tuolumne Intrusive Suite, California: *Geology*, v. 32, p. 433–436, doi:10.1130/G20220.1.

Connolly, J.A.D., 2010, The mechanics of metamorphic fluid expulsion: *Elements*, v. 6, p. 165–172, doi:10.2113/gselements.6.3.165.

Connolly, J.A.D., & Podladchikov, Y.Y., 1998, Compaction driven fluid flow in viscoelastic rock: *Geodinamica Acta*, v. 11, p. 55–84, doi:10.1016/S0985-3111(98)80006-5.

Connolly, J.A.D., & Podladchikov, Y.Y., 2007, Decompaction weakening and channeling instability in ductile porous media: Implications for asthenospheric melt segregation: *Journal of Geophysical Research*, v. 112, B10205, doi:10.1029/2005JB004213.

Connolly, J.A.D., & Podladchikov, Y.Y., 2012, A hydromechanical model for lower crustal fluid flow, *in* Harlov, D.E., and Austrheim, H., (eds.), *Metasomatism and the Chemical Transformation of Rock*, Lecture Notes in Earth System Sciences: Berlin, Heidelberg, Springer-Verlag, p. 599–658, doi:10.1007/978-3-642-28394-9.

Costa, F., Chakraborty, S., & Dohmen, R., 2003, Diffusion coupling between trace and major elements and a model for calculation of magma residence times using plagioclase: *Geochimica et Cosmochimica Acta*, v. 67, p. 2189–2200.

Cruden, A.R., 1998, On the emplacement of tabular granites: *Journal of the Geological Society of London*, v. 155, p. 853–862, doi:10.1144/gsjgs.155.5.0853.

Cruden, A.R., 2006, Emplacement and growth of plutons: Implications for rates of melting and mass transfer in continental crust, *In* Brown, M., and Rushmer, T., (eds.), *Evolution and Differentiation of the Continental Crust*: Cambridge, UK, Cambridge University Press, p. 455–519.

Cruden, A.R., & McCaffrey, K.J.W., 2001, Growth of plutons by floor subsidence: Implications for rates of emplacement, intrusion spacing and melt-extraction mechanisms: *Physics and Chemistry of the Earth, Part A: Solid Earth and Geodesy*, v. 26, p. 303–315, doi:10.1016/S1464-1895(01)00060-6.

Cruden, A.R., & McCaffrey, K.J.W., 2002, Different scaling laws for sills, laccoliths and plutons: Mechanical thresholds on roof lifting and floor depression, *In* Breitzkreuz, C., Mock, A., and Petford, N., (eds.), *First International Workshop: Physical Geology of Subvolcanic Systems—Laccoliths, Sills and Dikes (LASI)*: Freiberg, Germany, Wissenschaftliche Mitteilung Institute für Geologie Technische Universität Bergakademie Freiberg, 20/2002, p. 15–17.

Currier, L. W., & Jahns, R. H., 1941, Ordovician stratigraphy of central Vermont: *Geological Society of America Bulletin*, v. 52, p. 1487–1512.

Dietsch, C. W., & Sutter, J. F., 1987, $^{40}\text{Ar}/^{39}\text{Ar}$ age spectrum data bearing on the polyphase thermal and tectonic evolution of the Connecticut Valley synclinorium, SW New England, U.S.A.: *In* *Evolution of metamorphic belts, metamorphic studies group, joint meeting with IGCP project 235*: Dublin, Ireland, University College, p. 6.

Dell'Angelo, L.N., & Tullis, J., 1988, Experimental deformation of partially melted granitic aggregates: *Journal of Metamorphic Geology*, v. 6, p. 495–515, doi:10.1111/j.1525-1314.1988.tb00436.x.

Deniel, C., Vidal, P., Fernandez, A., LeFort, P., & Peucat, J.J., 1987, Isotopic study of the Manaslu granite (Himalaya, Nepal)—Inferences on the age and source of Himalayan leucogranites: *Contributions to Mineralogy and Petrology*, v. 96, p. 78–92, doi:10.1007

/BF00375529.

Dennis, J. G., 1956, The Geology of the Lyndonville are, Vermont: Vermont Geological Survey Bulletin no. 8, p. 1-98.

Dietsch, C., 2015, Bedrock geology of the core and cover rocks of the Collinsville, Bristol, and Waterbury Domes, western Connecticut, *in* Guidebook for Field Trips in Southeastern New England. p. C-5, 1–19.

Dodson, M. H., 1973, Closure temperature in cooling geochronological and petrological systems: Contributions to Mineralogy and Petrology. v. 40, no. 3, p. 259–274.

Dohmen, R., & Chakraborty, S., 2003, Mechanism and kinetics of element and isotopic exchange mediated by a fluid phase: American Mineralogist, v. 88, p. 1251–1270.

Doll, C. G., 1951, Geology of the Memphremagog quadrangle and the southeastern portion of the Irashurg quadrangle, Vermont: Vermont Geological Society Bulletin n. 3, 113 p.

Doll, C. G., 1984, Fossils from the metamorphic rocks of the Silurian-Devonian Magog belt in northern Vermont: Vermont Geology, v. 3, p. 16.

Doll, C. G., Cady, W. M., Thompson, J. B., Jr., & Billings, M. P., 1961, Centennial geologic map of Vermont: Montpelier, Vt., Vermont Geological Survey, 1 sheet, scale 1:250,000.

Dumond, G., McLean, N., Williams, M.L., Jercinovic, M.J., & Bowring, S.A., 2008, High resolution dating of granite petrogenesis and deformation in a lower crustal shear zone: Athabasca granulite terrane, western Canadian Shield: Chemical Geology, v. 16, no. 4, p. 175–196. doi:10.1016/j.chemgeo.2008.04.014.

Dunlap, W.J., 1997, Neocrystallization or cooling? $^{40}\text{Ar}/^{39}\text{Ar}$ ages of white micas from low grade mylonites: Chemical Geology, v. 143, p. 181–203, doi: 10.1016/S0009-2541(97)00113-7.

Dunlap, W. J., Teyssier, C., McDougall, I., & Baldwin, S., 1991, Ages of deformation from K/Ar and $^{40}\text{Ar}/^{39}\text{Ar}$ dating of white micas: Geology, v. 19, p. 1213-1216.

D'Lemos, R.S., Brown, M., & Strachan, R.A., 1992, Granite magma generation, ascent and emplacement within a transpressional orogeny: Journal of the Geological Society of London, v. 149, p. 487–490, doi:10.1144/gsjgs.149.4.0487.

Fisher, D. W., Isachsen, Y. W., & Rickard, L. V., 1970, Geologic Map of New York State, consisting of 5 sheets: Niagara, Finger Lakes, Hudson-Mohawk, Adirondack, and Lower Hudson: New York State Museum and Science Service, Map and Chart Series No. 15, scale 1:250,000.

Fisher, G. W., & Karabinos, P., 1980, Stratigraphic sequence of the Gile Mountain and Waits River Formations near Royalton, Vermont: Geological Society of America Bulletin, v. 91, no. 5, p. 282–286.

Hall, L. M., 1958, The geology of the St. Johnsbury quadrangle, Vermont and New Hampshire: Montpelier, Vermont Geological Survey Bulletin 13, 105 p.

Hames, W. E., & Bowring, S. A., 1994, An empirical evaluation of the argon diffusion geometry in muscovite: Earth and Planetary Science Letters, v. 124, p. 161–167.

Handy, M.R., Mulch, A., Rosenau, N., & Rosenberg, C.L., 2001, The role of fault zones and melts as agents of weakening, hardening and differentiation of the continental crust: A synthesis: *In* Holdsworth, R.E., Magloughlin, J., Knipe, R.J., Strachan, R.A., and Searle, R.C., (eds.), The Nature and Tectonic Significance of Fault Zone Weakening: Geological Society of London Special Publication 186, p. 305–332.

Hannula, K. A., Onasch, E., Wertheim, J., Lackey, J. S., Mattox, E., & McGrath, G., 1999, Syntectonic pluton intrusion during contractional deformation: Microstructural evidence from the aureole of the Acadian Victory Pluton, north-eastern Vermont, USA: Journal of Metamorphic Geology, v. 17, p. 271–286.

Harris, N.B.W., Vance, D., & Ayers, M., 2000, From sediment to granite: Time scales of anatexis in the upper crust: Chemical Geology, v. 162, p. 155–167, doi: 10.1016/S0009-2541(99)00121-7.

Hatch, N. L., Jr., 1982, The Taconian Line in western New England and its implication to the Paleozoic tectonic history; *In* P. St-Julien and J., Béland (eds.), Major Structural Zones and Faults of the Northern Appalachians, Geological Association of Canada, special paper 24, p. 67–85.

Hatch, N. L., Jr., & Stanley, R. S., 1988, Post-Taconian structural geology of the Rowe-Hawley zone and the Connecticut-Valley belt west of the Mesozoic Basins: *In* Hatch, N. L., (ed.), The Bedrock Geology of Massachusetts, United States Geological Survey professional paper, p. C1–C33.

Hatch, N. L., Jr., Moench, R. H., & Stanley, R. S., 1988, Stratigraphy of the Connecticut Valley Belt: *In* The bedrock geology of Massachusetts: United States Geological Survey professional paper, p. B1–B34.

Hermann, J., & Rubatto, D., 2003, Relating zircon and monazite domains to garnet growth zones: age and duration of granulite facies metamorphism in the Val Malenco lower crust: Journal of Metamorphic Geology, v. 21, no. 9, p. 833–852.

Hobbs, B.E., & Ord, A., 2010, The mechanics of granitoid systems and maximum entropy production rates: Philosophical Transactions of The Royal Society, ser. A, v. 368, p. 53–93, doi:10.1098/rsta.2009.0202.

- Hermes, O. D., Gromet, L. P., & Murray, D. P., 1994, Bedrock Geologic Map of Rhode Island: Rhode Island Map Series No. 1, University of Rhode Island, Kingston, scale 1:100,000.
- Hogan, J.P., & Sinha, A.K., 1991, The effect of accessory minerals on the redistribution of lead isotopes during crustal anatexis: A model: *Geochimica et Cosmochimica Acta*, v. 55, p. 335–348, doi:10.1016/0016-7037(91)90422-2.
- Heuber, F. M., Bothner, W. A., Hatch, N. L., Jr., Finney, S. C., & Aleinikoff, J. N., 1990, Devonian plants from southern Québec and northern New Hampshire and the age of the Connecticut Valley trough: *American Journal of Science*, v. 290, no. 4, p. 360–395.
- Hutton, D.H.W., & Reavy, R.J., 1992, Strike-slip tectonics and granite petrogenesis: *Tectonics*, v. 11, p. 960–967, doi:10.1029/92TC00336.
- Jackson, M.P.A., & Vendeville, B.C., 1994, Regional extension as a geologic trigger for diapirism: *Geological Society of America Bulletin*, v. 106, p. 57–73, doi: 10.1130/0016-7606(1994)106<0057:REAAGT>2.3.CO;2.
- Jercinovic, M.J., Williams, M.L., & Lane, E.D. 2008, In-situ trace element analysis of monazite and other fine-grained accessory minerals by EPMA: *Chemical Geology*, v. 254, p. 197–215. doi:10.1016/j.chemgeo.2008.05.016.
- Karabinos, P., 1998, Tectonic and stratigraphic development of the Connecticut Valley Trough in New England Appalachians: *Geologic Society of America Abstracts with Programs*, v. 30, n. 7, p. 191.
- Karabinos, P., Samson, S. D., Hepburn, J. C., & Stoll, H. M., 1998, Taconian orogeny in the New England Appalachians; collision between Laurentia and the Shelburne Falls Arc: *Geology*, v. 26, p. 215–218.
- Keppie, J. D., (compiler), 2000, Geological Map of the Province of Nova Scotia, Nova Scotia Department of Natural Resources (NSDNR) Published Map, scale 1: 500,000.
- Keppie, J. D., & Dostal, J., 1994, Late Silurian-Early Devonian transpressive rift origin of the Québec Reentrant, Northern Appalachians: constraints from geochemistry of volcanic rocks. *Tectonics*. v. 13, p. 1183-1189.
- Kim, J., & Klepeis, K. A., 2015, The along-strike context of the Richardson Memorial Contact (RMC) in the town of Craftsbury, north-central Vermont: *Geological Society of America, Abstracts with Programs*, v. 47, no. 3, p. 100.
- Kim, J., Gale, M., Springston, G., Koteas, C., Defelice, C., & Saitta, N., 2015, Bedrock Geologic Map of the Southern Two-Thirds of the Woodbury Quadrangle, Vermont,

Washington County, Vermont: Vermont Geological Survey Open File Report VG2015-2. 1 Plate, scale 1:24,000.

Kim, J. J., & Rukznis, A., 2011, Bedrock Geologic Map of the Plainfield Quadrangle, Washington County, Vermont: Vermont Geological Survey Open File Map VG113, 2 plates, scale 1:24,000.

Kim, J., Gale, M., McMillan, M., Zoltos, S., & Springston, G., 2010, Bedrock Geologic Map of the Town of Craftsbury, Vermont, Vermont Geological Survey Open File Map VG10-4, 3 Plates, scale 1:24,000.

Konig, R. H., 1961, Geology of the Plainfield Quadrangle, Vermont, Montpelier, Vermont Geological Survey Bulletin, n. 16, 86 p.

Korhonen, F.J., Brown, M., Grove, M., Siddoway, C.S., Baxter, E.F., & Inglis, J.D., 2012, Placing constraints on the timing of melting and melt loss events during polymetamorphism in the Fosdick migmatite-granite complex, West Antarctica: *Journal of Metamorphic Geology*, v. 30, p. 165–192, doi:10.1111/j.1525-1314.2011.00961.x.

Koukouvelas, I.K., Pe-Piper, G., & Piper, D.J.W., 2006, The relationship between length and width of plutons within the crustal-scale Cobequid shear zone, Northern Appalachians, Canada: *International Journal of Earth Sciences*, v. 95, p. 963–976, doi:10.1007/s00531-006-0077-7.

Lagarde, J.L., Brun, J.P., & Gapais, D., 1990, Formation of epizonal granitic plutons by in situ assemblage of laterally expanding magma: *Comptes Rendus de l'Academie des Sciences, Serie II*, v. 310, p. 109–114.

Laird, J., & Albee, A. L., 1981, High-pressure metamorphism in mafic schist from northern Vermont: *American Journal of Science*, v. 281, p. 97–126.

Laird, J., Lanphere, M. A., & Albee, A. L., 1984, Distribution of Ordovician and Devonian Metamorphism in mafic and pelitic schists from northern Vermont: *American Journal of Science*, v. 284, p. 376–413.

Lavoie, D., & Asselin, E., 2004, A new stratigraphic framework for the Gaspé Belt in southern Québec; Implications for the pre-Acadian Appalachians of eastern Canada: *Canadian Journal of Earth Sciences*, v. 41, n. 5, p. 507–525.

Lee, J. Y., Marti, K., Severinghaus, J. P., Kawamura, K., Yoo, H. S., Lee, J. B., & Kim, J. S., 2006, A redetermination of the isotopic abundances of atmospheric Ar: *Ceochimica et Cosmochimica Acta*, v. 70, p. 4507–4512.

Lucas, S.B., & St. Onge, M.R., 1995, Syn-tectonic magmatism and the development of compositional layering, Ungava orogen (northern Quebec, Canada): *Journal of Structural Geology*, v. 17, p. 475–491, doi:10.1016/0191-8141(94)00076-C.

Ludwig, K.R., 2003. Isoplot/EX, rev. 3.00, a Geochronological Toolkit for Microsoft Excel: Berkeley Geochronology Center Special Publication, v. 4, 71 pp.

Lyons, J. B., Wothner, W. A., Moench, R. H., & Thompson, J. B., 1997, Bedrock geologic map of New Hampshire: U.S. Geological Survey, Reston, VA, State Geological Map, 2 sheets, scales 1:250,000 and 1:500,000.

Mahan, K.H., Bartley, J.M., Coleman, D.S., Glazner, A.F., & Carl, B.S., 2003, Sheeted intrusion of the synkinematic McDoogle pluton, Sierra Nevada, California: *Geological Society of America Bulletin*, v. 115, p. 1570–1582, doi:10.1130/B22083.1.

Marcotte, S.B., Klepeis, K.A., Clarke, G.L., Gehrels, G., & Hollis, J.A., 2005, Intra-arc transpression in the lower crust and its relationship to magmatism in a Mesozoic magmatic arc: *Tectonophysics*, v. 407, p. 135–163, doi:10.1016/j.tecto.2005.07.007.

Matzel, J.E.P., Mundil, R., Paterson, S., Renne, P., & Nomade, S., 2005, Evaluating pluton growth models using high resolution geochronology: Tuolumne intrusive suite, Sierra Nevada, CA: *Geological Society of America Abstracts with Programs*, v. 37, no. 6, p. 131.

Matzel, J.E.P., Bowring, S.A., & Miller, R.B., 2006, Time scales of pluton construction at differing crustal levels: Examples from the Mount Stuart and Tenpeak intrusions, North Cascades, Washington: *Geological Society of America Bulletin*, v. 118, p. 1412–1430.

McDougall, I., & Harrison, T. M., 1999, *Geochronology and Thermochronology by the $^{40}\text{Ar}/^{39}\text{Ar}$ Method*. Oxford University Press, Oxford. 269 pp.

McLelland, J., Chiarenzelli, J., Whitney, P., & Isachen, Y., U-Pb zircon geochronology of the Adirondack Mountains and implications for their geologic evolution: *Geology*, v. 16, p. 920–924. doi: 10.1130/0091-7613(1988)016<0920:UPZGOT>2.3.CO;2.

McWilliams, C. K., Walsh, G. J., & Wintsch, R. P., 2010, Silurian-Devonian age and tectonic setting of the Connecticut Valley-Gaspé Trough in Vermont based on U-Pb SHRIMP analyses of detrital zircons: *American Journal of Science*, v. 310, p. 325–363.

McWilliams, C. K., Kunk, M. J., Wintsch, R. P., & Bish, D. L., 2013. Determining ages of multiple muscovite-bearing foliations in phyllonites using the $^{40}\text{Ar}/^{39}\text{Ar}$ step heating method: Applications to the Alleghanian orogeny in central New England: *American Journal of Science*, v. 313, p. 996–1016.

Mersereau, K. J., Richard, D. M., & Rennick, M. P., 2008, Bedrock geology of New Brunswick: New Brunswick Department of Natural Resources, Minerals Policy and Planning Division, Map NR-1, scale 1:500,000.

Moench, R. H., & Aleinikoff, J. N., 2002, Stratigraphy, geochronology, and accretionary terrane settings of two Bronson Hill arc sequences, northern New England. *Physics and Chemistry of the Earth*. v. 27, p. 47–95.

Moecher, D. P., Cosca, M. A., & Hanson, G. N., 1997, Petrologic and $^{40}\text{Ar}/^{39}\text{Ar}$ geochronological constraints on the middle to late Paleozoic thermotectonic history of the southern Connecticut Valley zone, New England Appalachians: *Geological Society of America Bulletin*, v. 109, no. 2, p. 164–175.

Miller, J.S., 2008, Assembling a pluton...one increment at a time: *Geology*, v. 36, p. 511–512, doi:10.1130/focus062008.1.

Miller, J.S., Matzel, J.E.P., Miller, C.F., Burgess, S.D., & Miller, R.B., 2007, Zircon growth and recycling during the assembly of large, composite arc plutons: *Journal of Volcanology and Geothermal Research*, v. 167, p. 282–299, doi:10.1016/j.jvolgeores.2007.04.019.

Miller, R.B., & Paterson, S.R., 2001, Construction of mid-crustal sheeted plutons: Examples from the North Cascades, Washington: *Geological Society of America Bulletin*, v. 113, p. 1423–1442.

Montel, J.M., 1993, A model for monazite/melt equilibrium and application to the generation of granitic magmas: *Chemical Geology*, v. 110, p. 127–146, doi: 10.1016/0009-2541(93)90250-M.

Murthy, V. R., 1957, Bed rock geology of the East Barre area, Vermont: Vermont Geological Survey Bulletin n. 10, 121 p.

Murthy, V. R., 1958, A revision of the lower Paleozoic stratigraphy in eastern Vermont: *Journal of Geology*, v. 66, p 276–286.

Nance, R.D., Murphy, J.B., & Keppie, J.D., 2002, A Cordilleran model for the evolution of Avalonia: *Tectonophysics*, v. 352, p. 11–31, doi: 10.1016/S0040-1951(02)00187-7.

Naylor, R. S., 1971. Acadian Orogeny: An Abrupt and Brief Event: *Science* v. 172, p. 558-560.

Osberg, P. H., Hussey, A. M., II, & Boone, G. M. (editors), 1985, Bedrock geologic map of Maine: Maine Geological Survey, 1 plate, correlation chart, tectonic inset map, metamorphic inset map, color geologic map, cross sections, scale 1:500,000.

Passchier, C. W., & Trouw, R. A. J., 2005, *Microtectonics*. Springer-Verlag, Berlin. 366 pp.

Paterson, S. R., Vernon, R. H., & Fowler, T. K., Jr., 1991, Aureole Tectonics. *In* Kerrick, D. M. (ed.), *Contact Metamorphism*, Mineralogical Society of America, *Reviews in Mineralogy*, v. 26, p. 673–722.

Patiño Douce, A.E., & Harris, N., 1998, Experimental constraints on Himalayan anatexis: *Journal of Petrology*, v. 39, p. 689–710, doi:10.1093/petroj/39.4.689.

Pe-Piper, G., & Piper, D. J. W., 2002, A synopsis of the geology of the Cobequid Highlands, Nova Scotia: *Atlantic Geology*, v. 38, p. 145–160.

Petford, N., & Koenders, M.A., 1998, Self-organization and fracture connectivity in rapidly heated continental crust: *Journal of Structural Geology*, v. 20, p. 1425–1434, doi:10.1016/S0191-8141(98)00081-9.

Petford, N., Kerr, R.C., & Lister, J.R., 1993, Dike transport of granitoid magmas: *Geology*, v. 21, p. 845–848, doi:10.1130/0091-7613(1993)021<0845:DTOGM>2.3.CO;2.

Petford, N., Cruden, A.R., McCaffrey, K.J.W., & Vigneresse, J.L., 2000, Granite magma formation, transport and emplacement in the Earth's crust: *Nature*, v. 408, p. 669–673, doi:10.1038/35047000.

Pinet, N., & Tremblay, A., 1995, Tectonic evolution of the Quebec-Maine Appalachians: From oceanic spreading to obduction and collision in the northern Appalachians: *American Journal of Science*, v. 295, p. 173–200.

Pressley, R.A., & Brown, M., 1999, The Phillips pluton, Maine, USA: Evidence of heterogeneous crustal sources, and implications for granite ascent and emplacement mechanisms in convergent orogens: *Lithos*, v. 46, p. 335–366, doi:10.1016/S0024-4937(98)00073-5.

Rabinowicz, M., & Vigneresse, J.L., 2004, Melt segregation under compaction and shear channeling: Application to granitic magma segregation in a continental crust: *Journal of Geophysical Research*, v. 109, p. B04407, doi:10.1029/2002JB002372.

Rankin, D. W., Coish, R. A., Tucker, R. D., Peng, Z. X., Wilson, S. A., & Rouff, A. A., 2007, Silurian extension in the upper Connecticut Valley in the United States and the origin of Middle Paleozoic basins in the Québec embayment: *American Journal of Science*, v. 307, p. 216–264.

Ratcliffe, N. M., Aleinikoff, J. N., Burton, W. C., & Karabinos, P., 1991 Trondhjemitic 1.35 – 1.31 Ga gneisses of the Mount Holly Complex of Vermont: evidence for an

Elzevirian event in the Grenville Basement of the United States Appalachians: *Canadian Journal of Earth Sciences*, v. 28, p. 77–93.

Ratcliffe, N.M., Stanley, R.S., Gale, M.H., Thompson, P.J., & Walsh, G.J., 2011, *Bedrock Geologic Map of Vermont*: [U.S. Geological Survey Scientific Investigations Map 3184](#), 3 sheets, scale 1:100,000.

Reiners, P. W., & Brandon, M. T., 2006, Using thermochronology to understand orogenic erosion. *Annual Reviews in Earth and Planetary Science* v. 34, p. 419–466.

Renne, P. R., Swisher, C. C., Deino, A. L., Karner, D. B., Owens, T. L., & DePaolo, D. J., 1998, Intercalibration of standards, absolute ages and uncertainties in $^{40}\text{Ar}/^{39}\text{Ar}$ dating: *Chemical Geology*, v. 145, p. 117–152.

Reichardt, H., & Weinberg, R.F., 2012a, The dike swarm of the Karakoram shear zone, Ladakh, NW India: Linking granite source to batholith: *Geological Society of America Bulletin*, v. 124, p. 89–103, doi:10.1130/B30394.1.

Reichardt, H., & Weinberg, R.F., 2012b, Hornblende chemistry in meta- and diatexites and its retention in the source of leucogranites: An example from the Karakoram shear zone, NW India: *Journal of Petrology*, v. 53, p. 1287–1318, doi:10.1093/petrology/egs017.

Reno, B.L., Brown, M., Kobayashi, O.T., Nakamura, E., Piccoli, P.M., & Trouw, R.A.J., 2009, Eclogite–high pressure granulite metamorphism records early collision in West Gondwana: New data from the southern Brasília belt, Brazil: *Journal of the Geological Society of London*, v. 166, p. 1013–1032, doi:10.1144/0016-76492008-140.

Reno, B.L., Piccoli, P.M., Brown, M., & Trouw, R., 2012, In situ chemical dating of monazite from the southern Brasília belt, Brazil: *Journal of Metamorphic Geology*, v. 30, p. 81–112, doi:10.1111/j.1525-1314.2011.00957.x.

Richter, D. A., 1987, Barre granite quarries, Barre, Vermont, *In* Roy, D. C., (ed.), *Centennial Field Guide Volume 5*: Boulder, CO, Geological Society of America, p. 239–242.

Richter, D. A., Murray, D., & Simmons, G., 1997, Economic geology of the dimension stone industry, eastern Vermont granite belt, *In* Grover, T. W., Mango, H. N., and Hasenohr, E. J., (eds.), *Guidebook to Field Trips in Vermont and Adjacent New Hampshire and New York*, New England Intercollegiate Geological Conference, p. B4 1–B14.

Robinson, P., Thompson, P. J., & Elbert, D. C., 1991, The nappe theory in the Connecticut Valley region: Thirty-five years since Jim Thompson's first proposal: *American Mineralogist*, v. 76, p. 689–712.

Robinson, P., Tucker, T. D., Bradley, D., Berry, H. N. IV, & Osberg, P. H., 1998, Paleozoic orogens in New England, USA: Transactions of the Geological Society of Stockholm. *GFF*, v. 120, p. 119–148.

Rodgers, J., (compiler), 1985, Bedrock Geological Map of Connecticut: Connecticut Geological and Natural History Survey, Hartford, Connecticut, 2 sheets, scale 1:125,000.

Rosenberg, C.L., 2004, Shear zones and magma ascent: A model based on a review of the Tertiary magmatism in the Alps: *Tectonics*, v. 23, TC3002, doi:10.1029/2003TC001526.

Rosenberg, C.L., & Handy, M.R., 2005, Experimental deformation of partially melted granite revisited: Implications for the continental crust: *Journal of Metamorphic Geology*, v. 23, p. 19–28, doi:10.1111/j.1525-1314.2005.00555.x.

Rutter, E.H., & Mecklenburgh, J., 2006, The extraction of melt from crustal protoliths and the flow behavior of partially molten crustal rocks: An experimental perspective, *in* Brown, M., and Rushmer, T., eds., *Evolution and Differentiation of the Continental Crust*: Cambridge, UK, Cambridge University Press, p. 386–429.

Sawyer, E.W., 1991, Disequilibrium melting and the rate of melt residuum separation during migmatization of mafic rocks from the Grenville Front, Quebec: *Journal of Petrology*, v. 32, p. 701–738, doi:10.1093/petrology/32.4.701.

Sawyer, E.W., 1994, Melt segregation in the continental crust: *Geology*, v. 22, p. 1019–1022, doi:10.1130/0091-7613(1994)022<1019:MSITCC>2.3.CO;2.

Sawyer, E.W., 1998, Formation and evolution of granite magmas during crustal reworking: The significance of diatexites: *Journal of Petrology*, v. 39, p. 1147–1167.

Sawyer, E.W., 2001, Melt segregation in the continental crust: Distribution and movement of melt in anatectic rocks: *Journal of Metamorphic Geology*, v. 19, p. 291–309, doi:10.1046/j.0263-4929.2000.00312.x.

Sawyer, E.W., 2010, Migmatites formed by water-fluxed partial melting of a leucogranodiorite protolith: Microstructures in the residual rocks and source of the fluid: *Lithos*, v. 116, p. 273–286, doi:10.1016/j.lithos.2009.07.003.

Schaltegger, U., Brack, P., Ovtcharova, M., Peytcheva, I., Schoene, B., Stracke, A., Marocchi, M., & Bargossi, G.M., 2009, Zircon and titanite recording 1.5 million years of magma accretion, crystallization and initial cooling in a composite pluton (southern Adamello batholith, northern Italy): *Earth and Planetary Science Letters*, v. 286, p. 208–218, doi:10.1016/j.epsl.2009.06.028.

- Short, H. A., Timing and significance of dextral transpression in Central Maine: Its early and important: Geological Society of America, Abstracts with Programs, v. 42, no. 1, p. 127.
- Siivola, J., & Schmid, R., 2007 List of Mineral Abbreviations: Recommendations by the IUGS subcommission on the systematic of metamorphic rocks: web version 01.02.07, 14 p.
- Simonetti, A., & Doig, R., 1990, U-Pb and Rb-Sr geochronology of Acadian plutonism in the Dunnage zone of southeastern Québec Appalachians: Canadian Journal of Earth Sciences, v. 27, p. 881–892.
- Solar, G.S., & Brown, M., 2001, Deformation partitioning during transpression in response to Early Devonian oblique convergence, Northern Appalachian orogeny, USA: Journal of Structural Geology, v. 23, p. 1043–1065.
- Solar, G. S., Pressley, R. A., Brown, M., & Tucker, R. D., 1998. Granite ascent in convergent orogenic belts: testing a model. *Geology*. v. 26, p. 711-714.
- Spear, F. S., & Harrison, T. M., 1989, Geochronologic studies in central New England I: evidence for pre-Acadian metamorphism in eastern Vermont. *Geology*. v. 17, p. 181-184.
- Stanley, R. S., & Ratcliffe, N. M., 1985, Tectonic synthesis of the Taconian orogeny in western New England: Geological Society of America Bulletin, v. 96, p. 1227–1250.
- Steiger, R. H., & Jäger, E., 1977, Subcommittee on geochronology: convention on the use of decay constants in geo- and cosmochronology: *Earth and Planetary Science Letters* v. 36, p. 359–362.
- Strong, D.F., & Hanmer, S.K., 1981, Peraluminous granites: *Canadian Mineralogist*, v. 19, p. 163–176.
- Sumita, I., & Ota, Y., 2011, Experiments on buoyancy driven crack around the brittle-ductile transition: *Earth and Planetary Science Letters*, v. 304, p. 337–346, doi:10.1016/j.epsl.2011.01.032.
- Sutter, J. F., Ratcliffe, N. M., & Musaka, S. B., 1985, $^{40}\text{Ar}/^{39}\text{Ar}$ and K/Ar data bearing on the metamorphic and tectonic history of western New England. *Geological Society of America Bulletin*. v. 96, p. 123–136.
- Thériault, R., (compiler), Beauséjour, S., & Tremblay, A., 2012, *Géologie du Québec*: Ministère des Ressources naturelles, Direction générale de Géologie Québec, scale 1:2,000,000.

- Thompson, A.B., & Connolly, J., 1995, Melting of the continental crust: Some thermal and petrological constraints on anatexis in continental collision zones and other tectonic settings: *Journal of Geophysical Research*, v. 100, no. B8, p. 15,565–15,579, doi:10.1029/95JB00191.
- Thompson, J. B., Rosenfeld, J. L., Hepburn, J. C., & Trzcienski, W. E., 1997, How does New Hampshire connect to Vermont?: *In* Guidebook to Field Trips in Vermont and Adjacent New Hampshire and New York, Grover, T. W., Mango, H. N., & Hasenohr, E. J. (eds.), p. C1-1–C1-17.
- Tremblay, A., Ruffet, G., & Castonguay, S., 2000. Acadian metamorphism in the Dunnage zone of southern Québec, northern Appalachians: $^{40}\text{Ar}/^{39}\text{Ar}$ evidence for collision diachronism: *Geological Society of America Bulletin*, v. 112, n. 1, p. 136-146.
- Tremblay, A., & Pinet, N., 2005, Diachronous supracrustal extension in an intraplate setting and the origin of the Connecticut Valley-Gaspé and Merrimack troughs, northern Appalachians: *Geology Magazine*, v. 142, p. 7–22.
- van Staal, C. R., & de Roo, J. A., 1995, Mid-Paleozoic tectonic evolution of the Appalachian Central Mobile Belt in northern New Brunswick, Canada: collision, extensional collapse, and dextral transpression. *In* Hibbard, J. P., van Staal, C. R., and Cawood, P. A., (eds.), *Current Perspectives in the Appalachian-Caledonian Orogen*, p. 367-389. Geological Association of Canada, Special Paper no. 41.
- van Staal, C. R., Whalen, J. B., Valverde-Vaquero, P., Zagorevski, A., & Rogers, N., 2009, Pre-Carboniferous, episodic accretion-related, orogenesis along the Laurentian margin of the northern Appalachians: *Geological Society of London, Special Publications*, v. 327, p. 271–316, DOI10.1144/SP327.13.
- van Staal, C. R., & Barr, S. M., 2012, Lithospheric architecture and tectonic evolution of the Canadian Appalachians and associated Atlantic margin: *In* *Tectonic Styles in Canada: the LITHOPROBE Perspective*. Edited by J.A. Percival, F.A. Cook, and R.M. Clowes. Geological Association of Canada, Special Paper n. 49, p. 1–55.
- Vernon, R.H., & Paterson, S.R., 2001, Axial-surface leucosomes in anatectic migmatites: *Tectonophysics*, v. 335, p. 183–192, doi:10.1016/S0040-1951(01)00049-X.
- Vigneressse, J.-L., 1988, Shape and volume of granitic intrusions: *Bulletin de la Société Géologique de France*, v. 4, p. 897–906.
- Vigneressse, J.-L., 1995, Crustal regime of deformation and ascent of granitic magma: *Tectonophysics*, v. 249, p. 187–202, doi:10.1016/0040-1951(95)00005-8.
- Vigneressse, J.-L., 2004, Rheology of a two-phase material with applications to partially molten rocks, plastic deformation and saturated soils, *in* Alsop, G.I., Holdsworth, R.E.,

McCaffrey, K.J.W., and Hand, M., eds., *Flow Processes in Faults and Shear Zones: Geological Society of London Special Publication 224*, p. 79–94.

Vigneresse, J.-L., Tikoff, B., & Ameglio, L., 1999, Modification of the regional stress field by magma intrusion and formation of tabular granitic plutons: *Tectonophysics*, v. 302, p. 203–224, doi:10.1016/S0040-1951(98)00285-6.

Wagner, R., Rosenberg, C., Handy, M.R., Möbus, C., & Albertz, M., 2006, Fracture-driven intrusion and upwelling of a mid-crustal pluton fed from a transpressive shear zone—The Rieserferner pluton (Eastern Alps): *Geological Society of America Bulletin*, v. 118, p. 219–237, doi:10.1130/B25842.1.

Walsh, G. J., Kim, J., & Gale, M. H., 2009, Bedrock geology of the Montpelier area, central Vermont: *In New England Intercollegiate Geological Conference: Guidebook for Field Trips in Vermont and adjacent New Hampshire*. p. C4: 1–18.

Walsh, G.J., Kim, Jonathan, Gale, M.H., & King, S.M., 2010, Bedrock geologic map of the Montpelier and Barre West quadrangles, Washington and Orange Counties, Vermont: U.S. Geological Survey Scientific Investigations, Map 3111, 1 sheet, scale 1:24,000, p. 1–36, text.

Watson, E.B., & Harrison, T.M., 1983, Zircon saturation revisited—Temperature and composition effects in a variety of crustal magma types: *Earth and Planetary Science Letters*, v. 64, p. 295–304, doi:10.1016/0012-821X(83)90211-X.

Weinberg, R.F., 1999, Mesoscale pervasive felsic magma migration: Alternatives to diking: *Lithos*, v. 46, p. 393–410, doi:10.1016/S0024-4937(98)00075-9.

Weinberg, R.F., & Mark, G., 2008, Magma migration, folding, and disaggregation of migmatites in the Karakoram shear zone, Ladakh, NW India: *Geological Society of America Bulletin*, v. 120, p. 994–1009, doi:10.1130/B26227.1.

Weinberg, R.F., & Regenauer-Lieb, K., 2010, Ductile fractures and magma migration from source: *Geology*, v. 38, p. 363–366, doi:10.1130/G30482.1.

Weinberg, R.F., Mark, G., & Reichardt, H., 2009, Magma ponding in the Karakoram shear zone, Ladakh, NW India: *Geological Society of America Bulletin*, v. 121, p. 278–285.

Weinberg, R.F., Hasalová, P., Ward, L., & Fanning, C.M., 2013, Interaction between deformation and magma extraction in migmatites: Examples from Kangaroo Island, South Australia: *Geological Society of America Bulletin*, v. 124, p. 000–000, doi:10.1130/B30781.1.

West, D., & Hubbard, M. S., 1997, Structural geology of the dextral Norumbega Fault Zone, Maine; *Tectonophysics*, v. 273, n. 3–4, p. 185–201.

Westerman, D. S., 1987, Structures in the Dog River fault zone between Northfield and Montpelier, Vermont: *in* New England Intercollegiate Geological Conference: Guidebook for Field Trips in Vermont, 79th Annual Meeting, v. 2, p. 109–132.

Westerman, D., & Coish, R., 2009, Geochemistry and emplacement style in Acadian plutons between Woodbury and Northfield, Vermont: *In* Westerman, D. S., & Lathrop, A. S. (eds.), Guidebook for Field Trips in the Northeast Kingdom of Vermont and Adjacent Regions, p. C-5: 261–274.

Wheeler, J. O., Hoffman, P. F., Card, K. D., Davidson, A., Sanford, B. V., Okulitch, A. V., & Roest, W. R., 1996, Geological map of Canada / Carte géologique du Canada: Geological Survey of Canada, "A" Series Map 1860A, scale 1: 5,000,000.

White, W. S., 1949, Cleavage in east-central Vermont: *Transactions American Geophysical Union*, v. 30, p. 587-594.

Whitehead, J., Reynolds, P. H., & Spray, J. G., 1996, $^{40}\text{Ar}/^{39}\text{Ar}$ age constraints on Taconian and Acadian events in the Quebec Appalachians: *Geology*, v. 24, p. 359-362. doi:10.1130/00917613(1996)024<0359:AAACOT>2.3.CO;2.

Wickham, S.M., 1987, The segregation and emplacement of granitic magma: *Journal of the Geological Society of London*, v. 144, p. 281–297, doi:10.1144/gsjgs.144.2.0281.

Williams, M. L., & Jercinovic, M. J., 2002, Microprobe monazite geochronology: putting absolute time into microstructural analysis: *Journal of Structural Geology*, v. 24, p. 1013–1028. doi:10.1016/S0191-8141(01)00088-8.

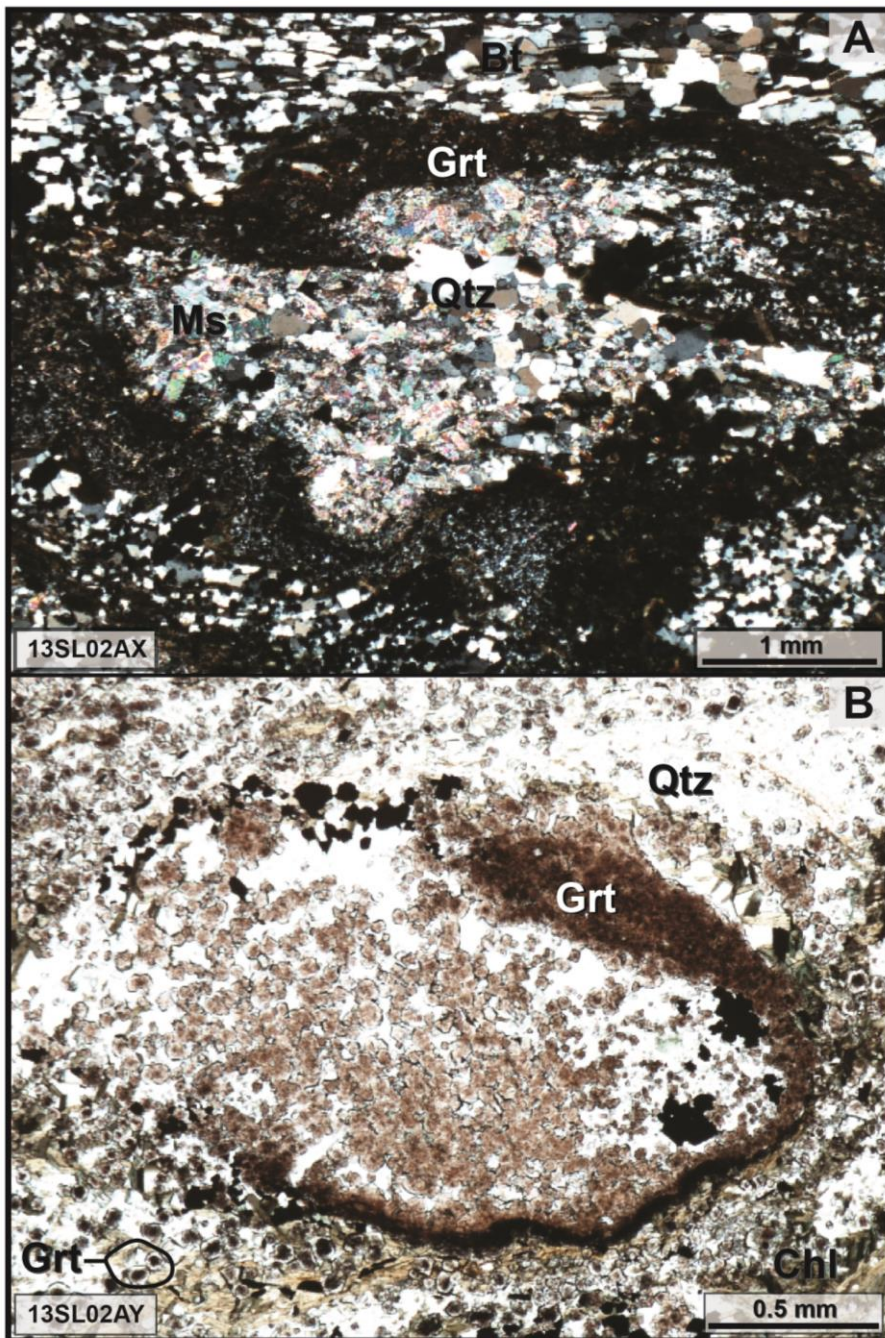
Williams, M. L., Jercinovic, M. J., Goncalves, P., & Mahan, K., 2006, Format and philosophy for collecting, compiling, and reporting microprobe monazite ages: *Chemical Geology*, v. 225 no. 1–2, p. 1–15. doi:10.1016/j.chemgeo.2005.07.024.

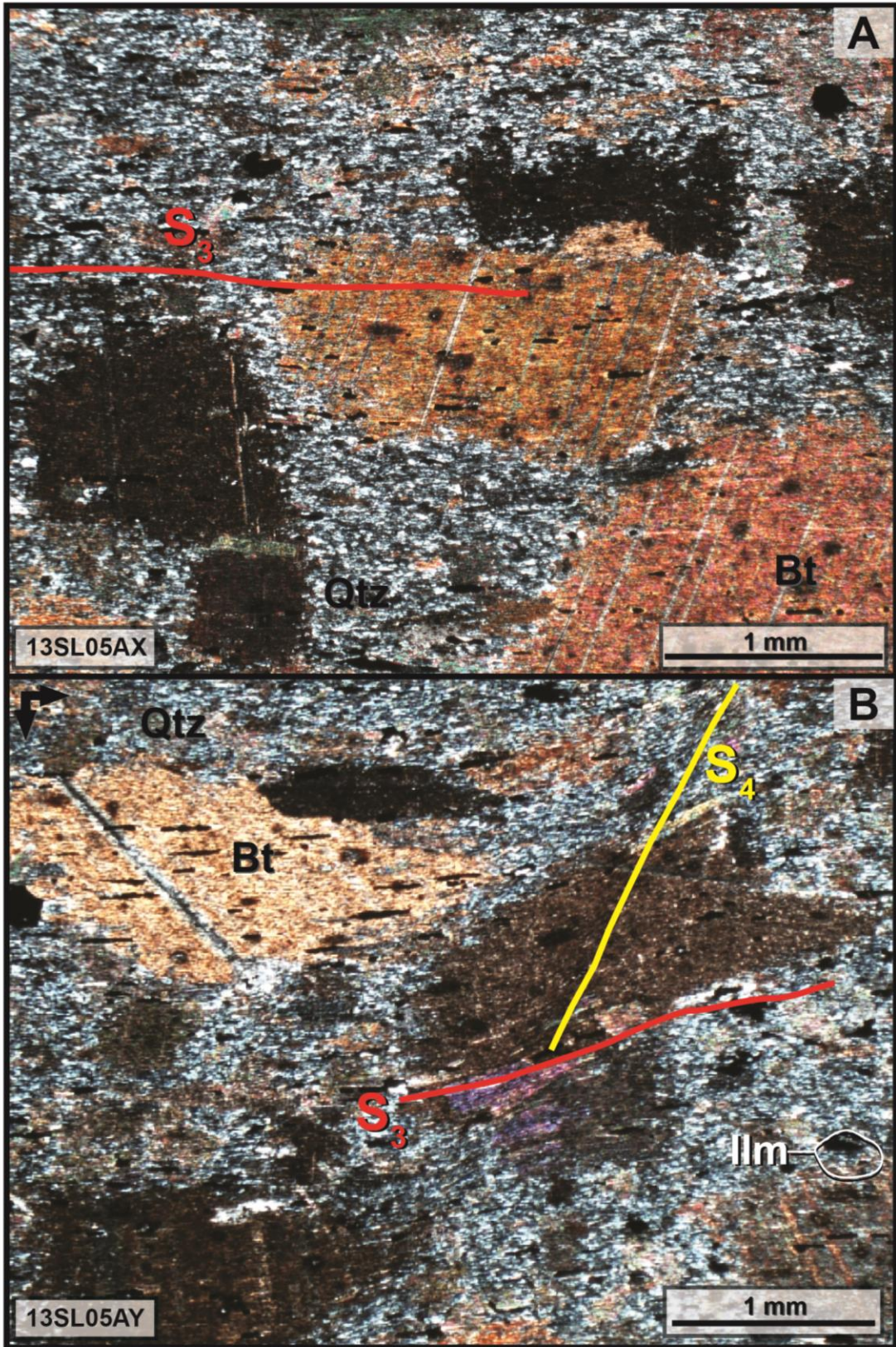
Zen, E., Goldsmith, R., Ratcliffe, N. M., Robinson, P., Stanley, R. S., Hatch, N. L., Shride, A. F., Weed, E. G. A., & Wones, D. R., 1983, Bedrock geologic map of Massachusetts: U.S. Geological Survey, scale 1:250,000.

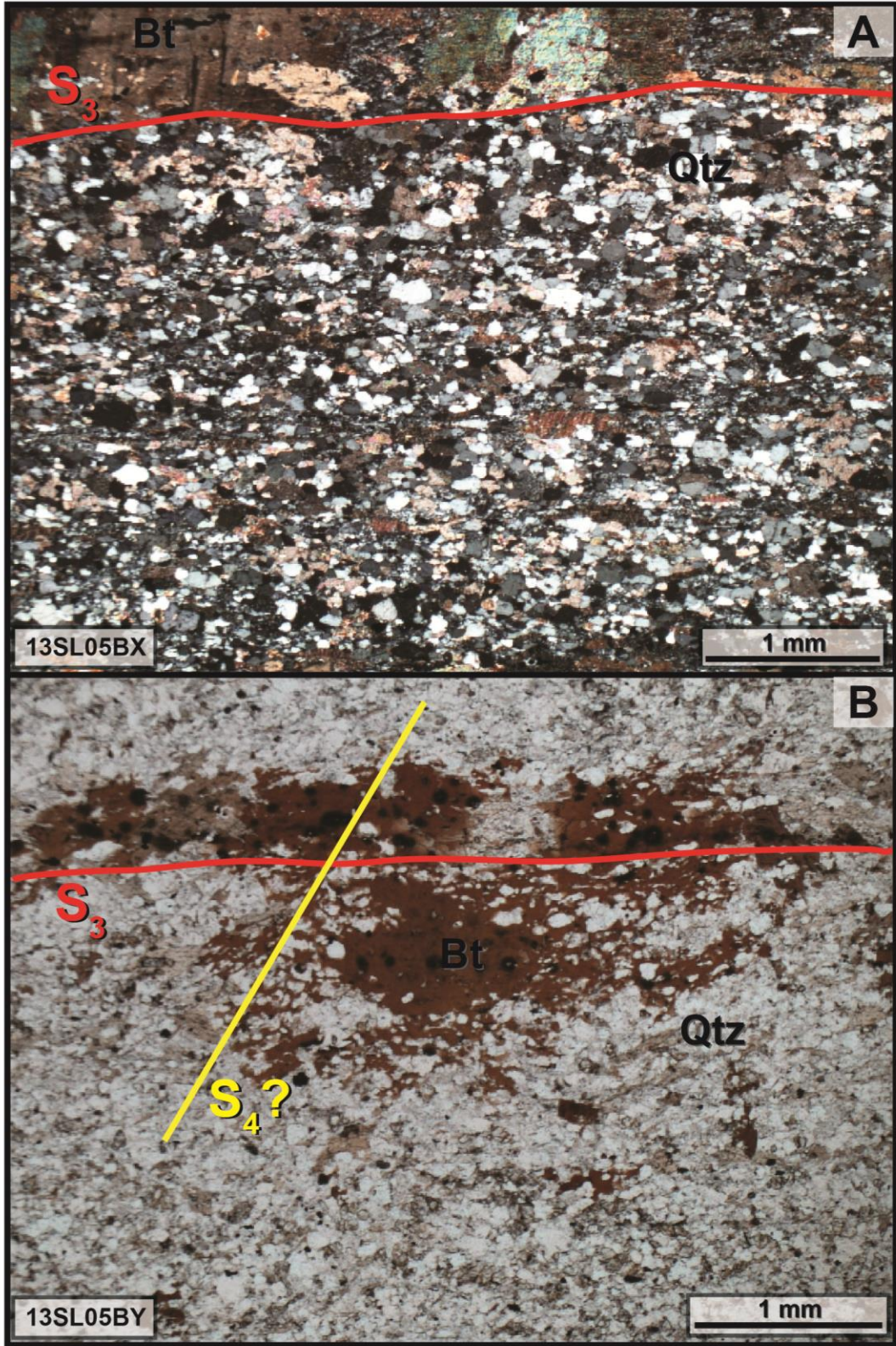
APPENDICES

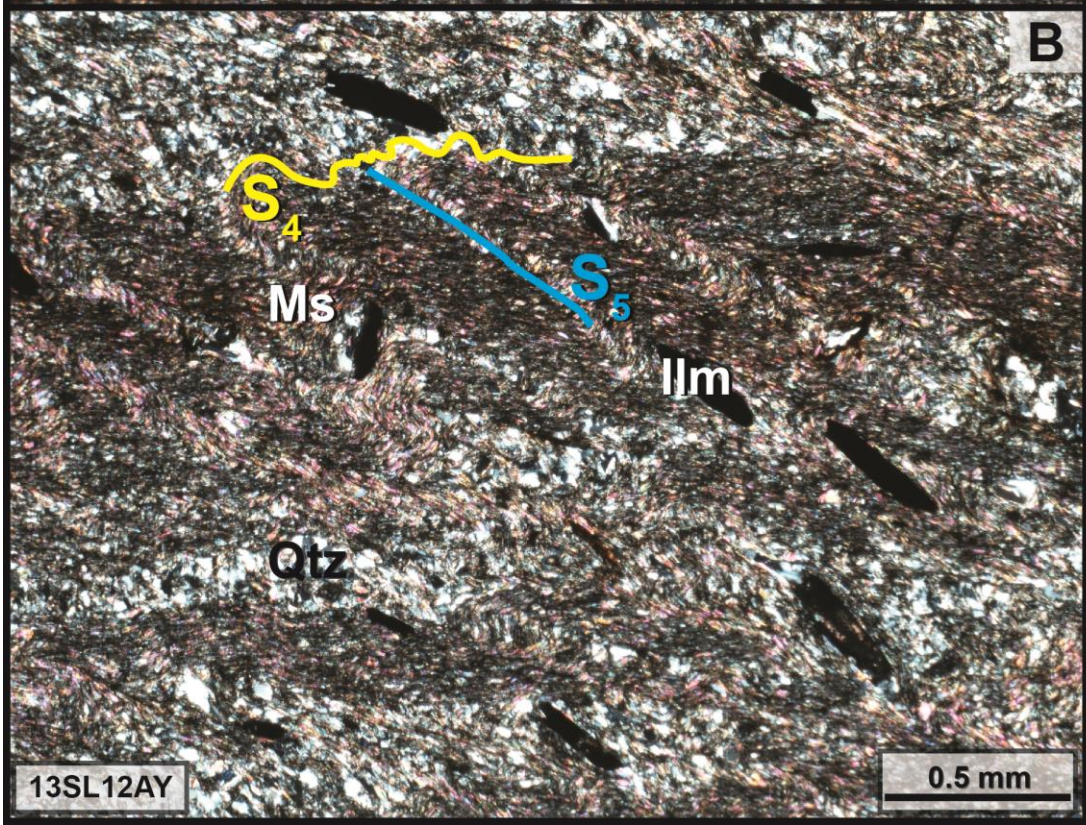
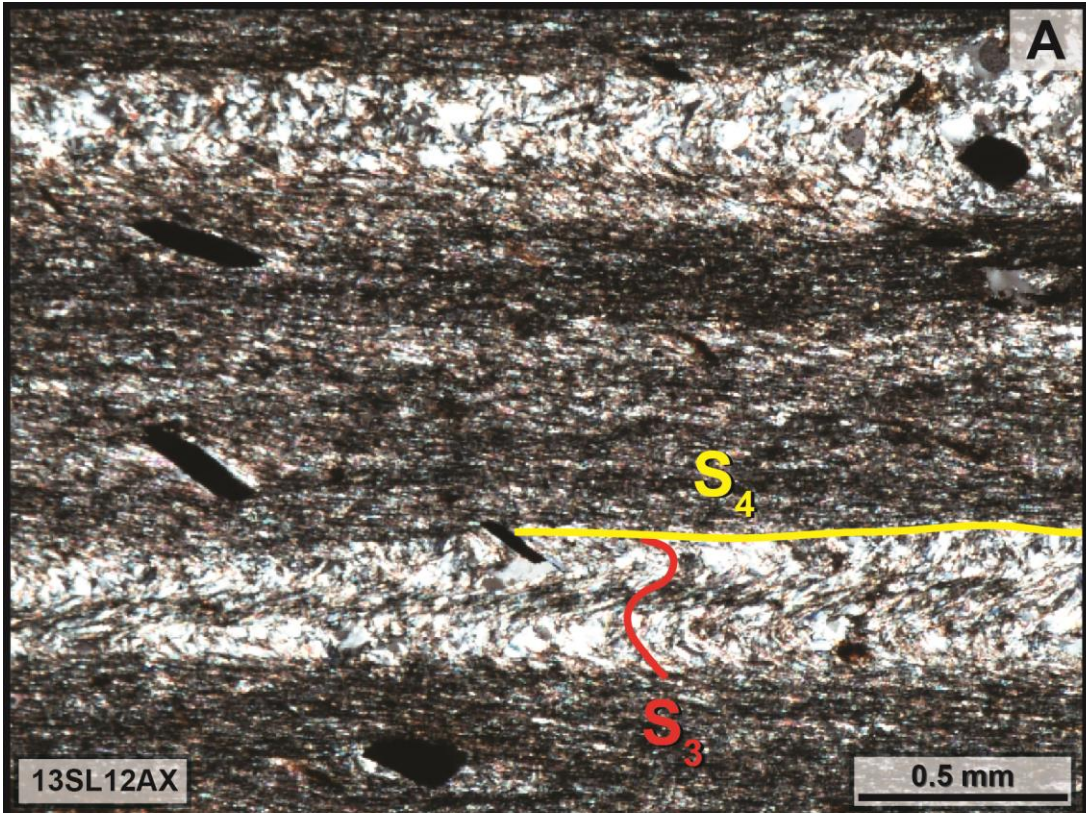
Appendix A — Photomicrographs

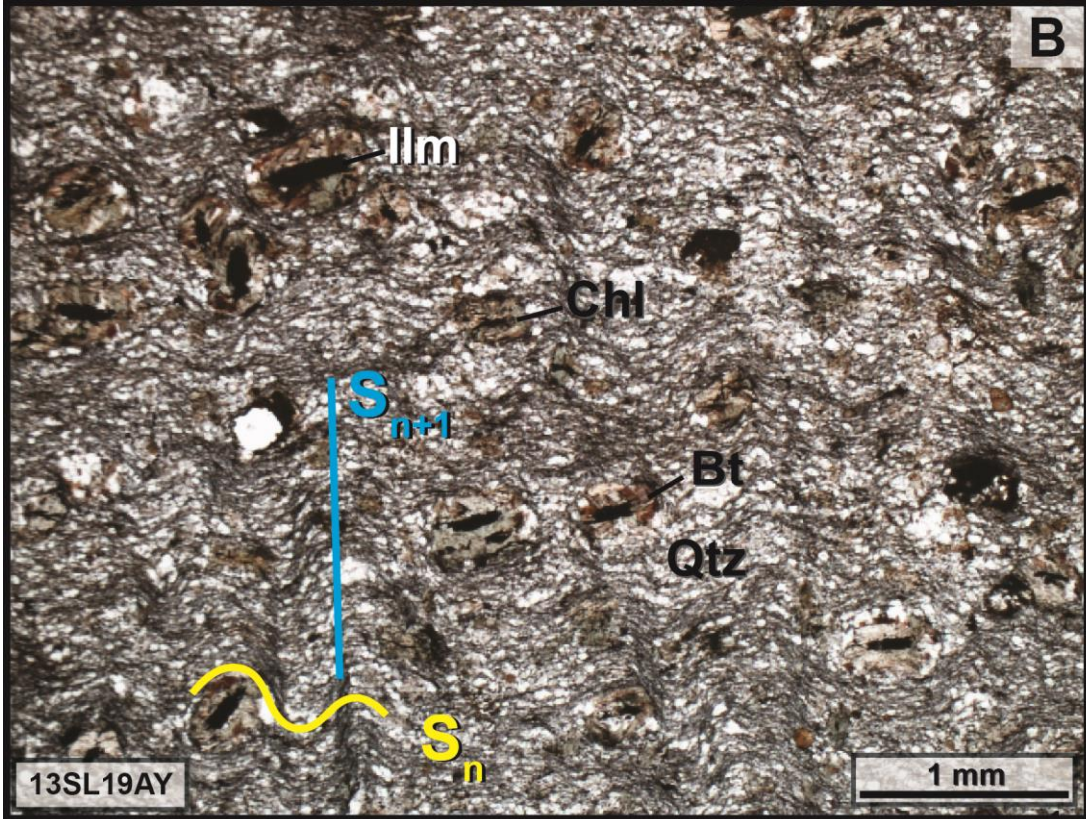
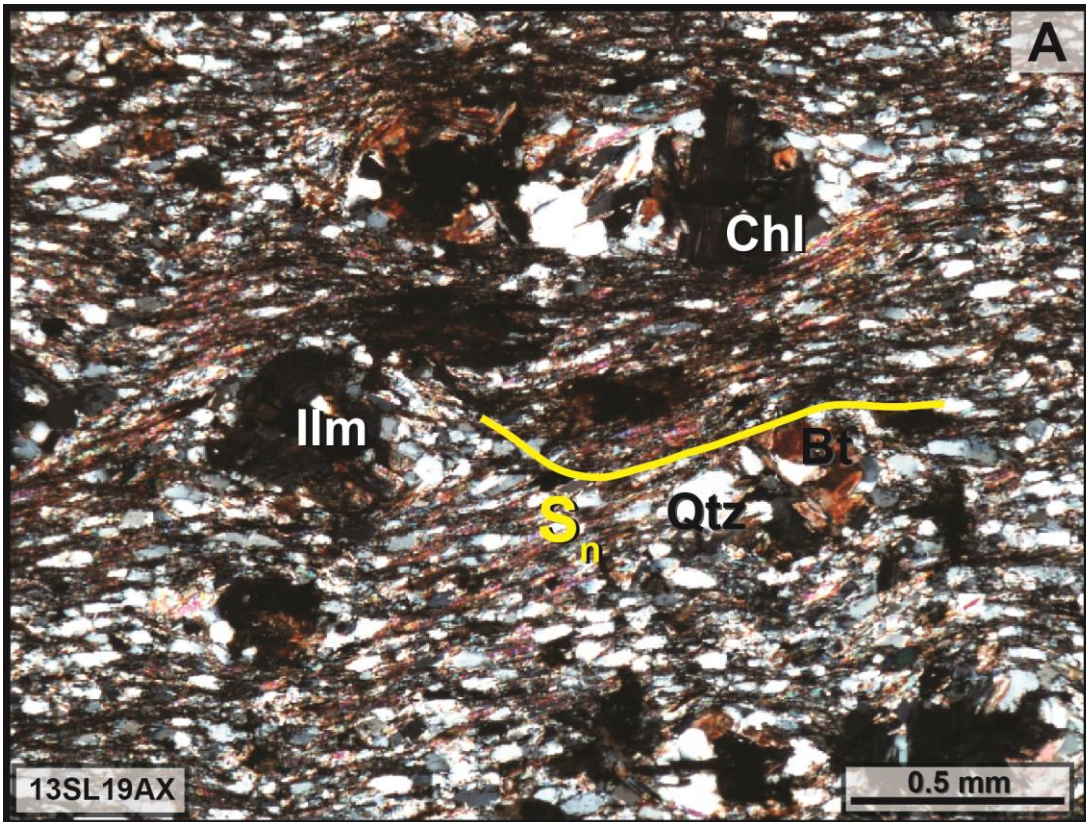
Photomicrographs follow a standard presentation style with one image from each orthogonal section, and utilize the mineral abbreviations of Siivola and Schmid, (2007).

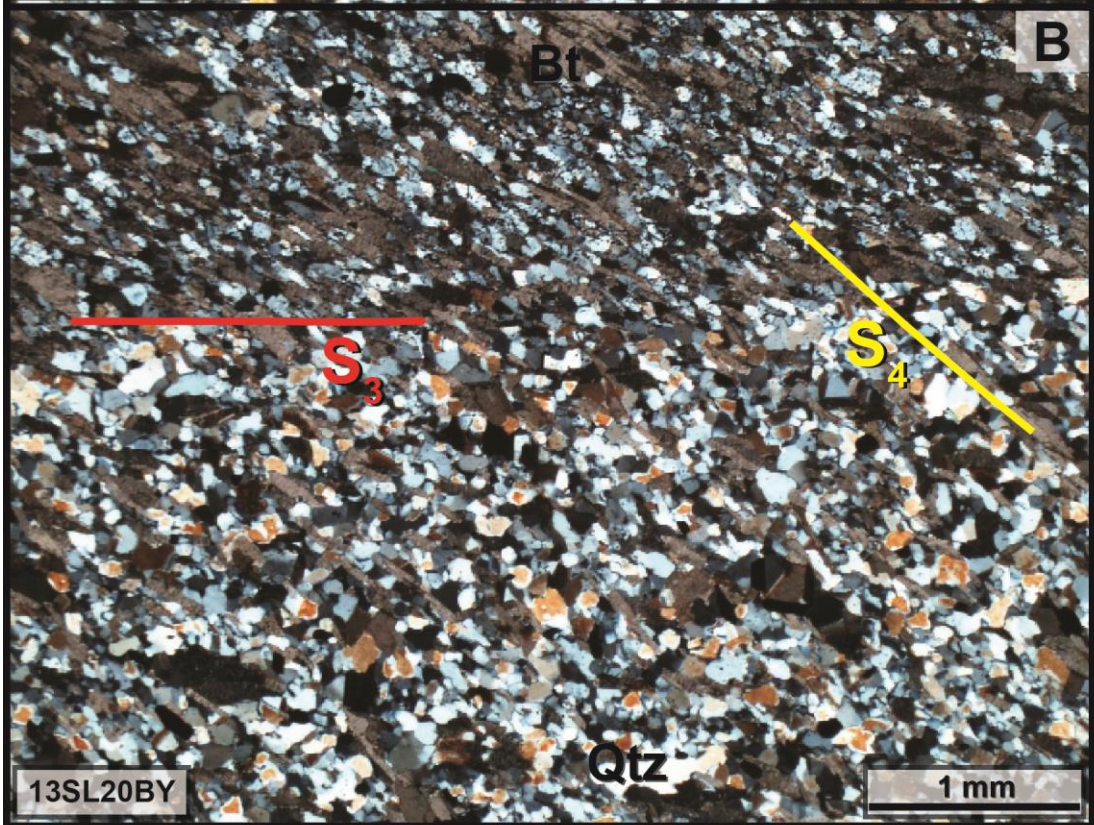
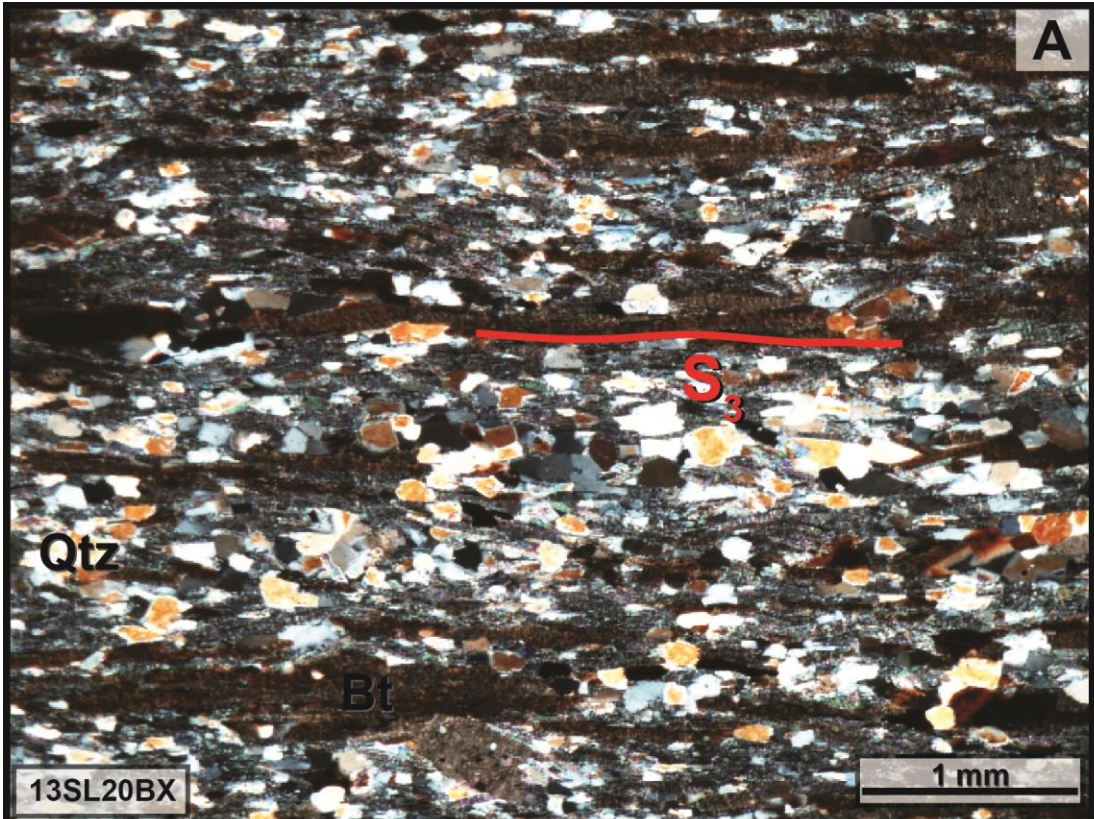


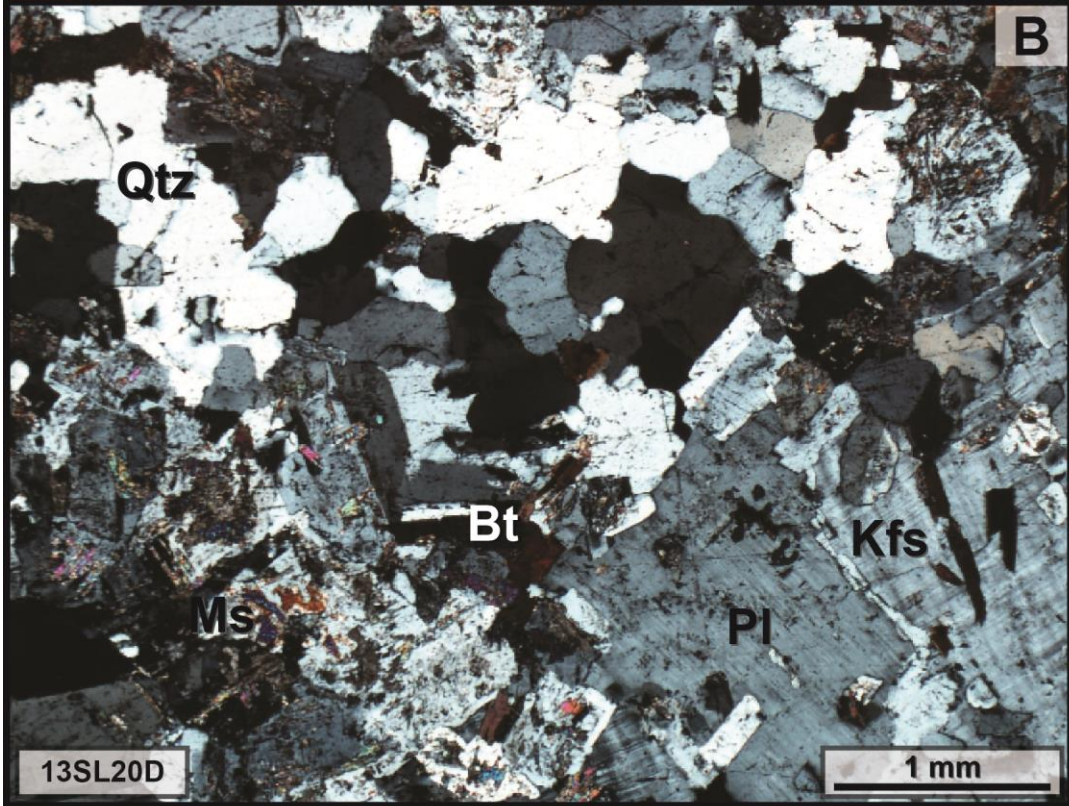
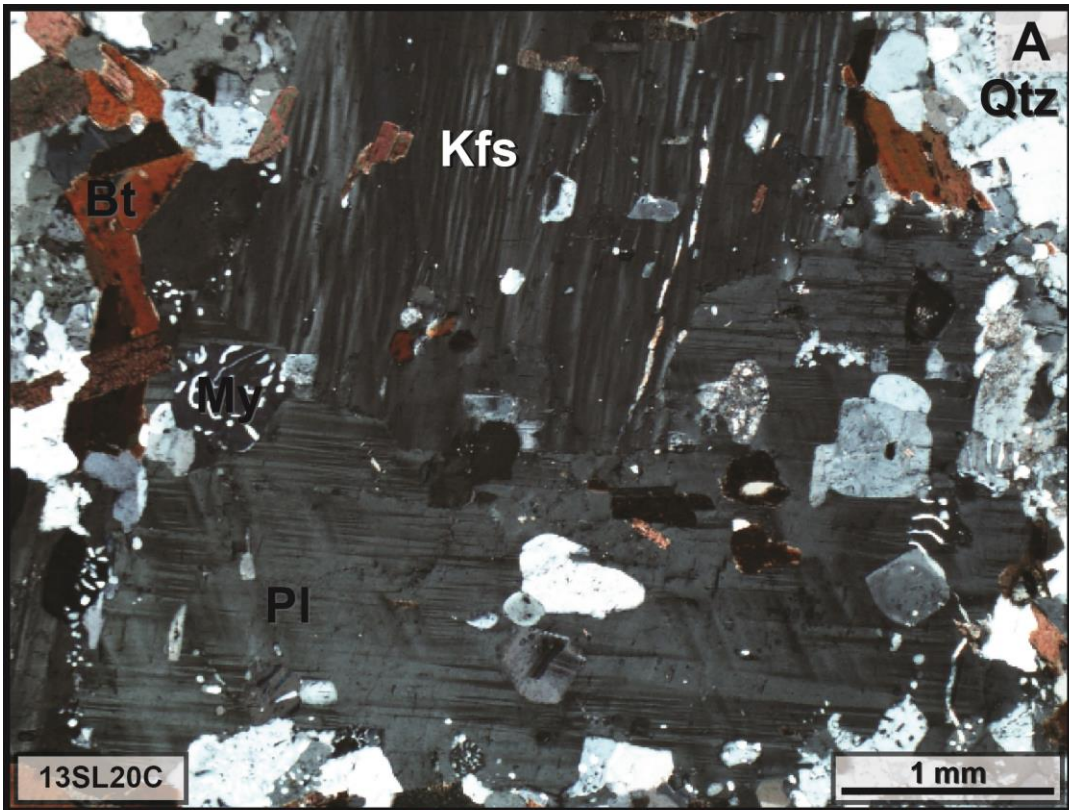


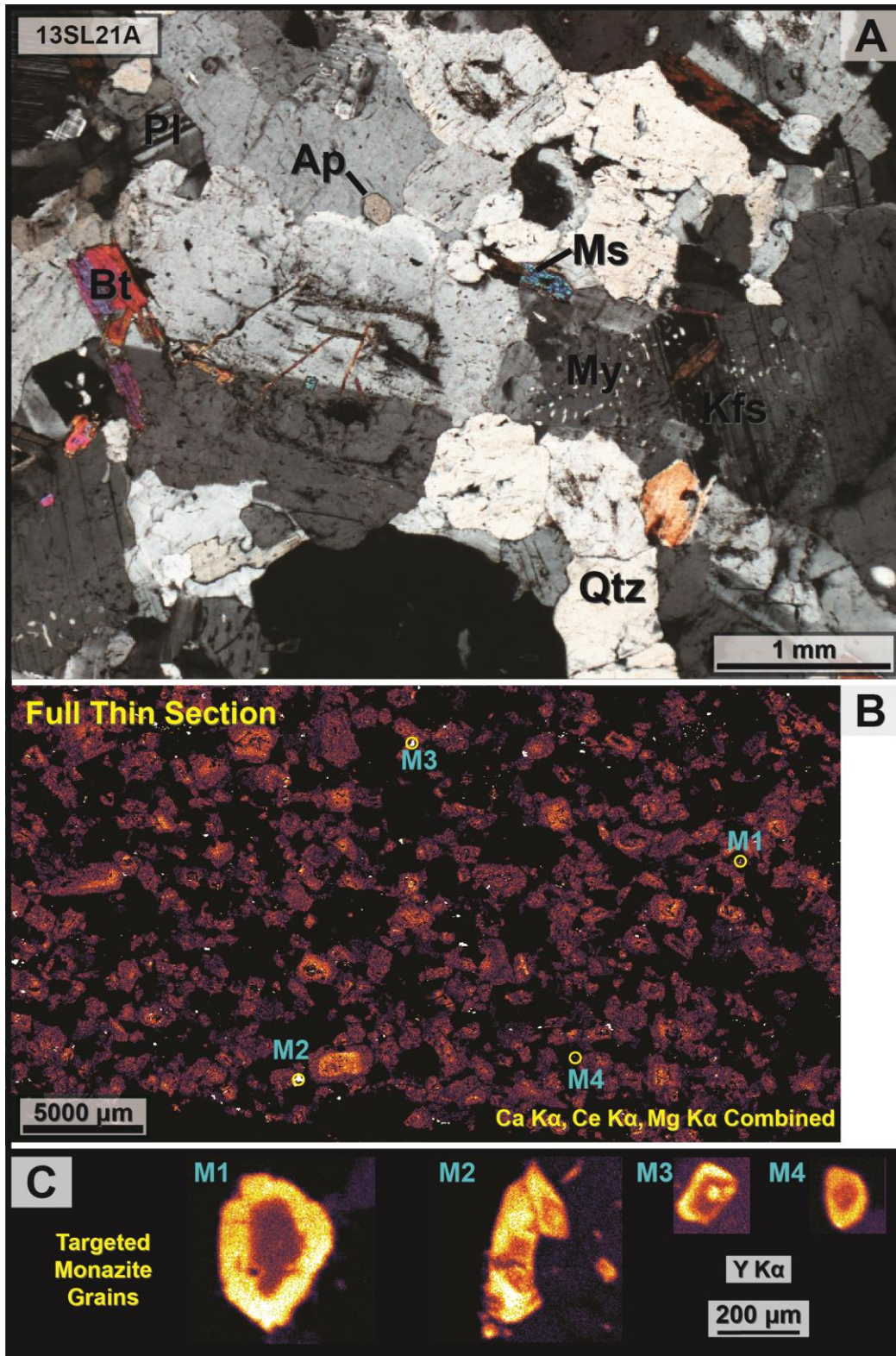




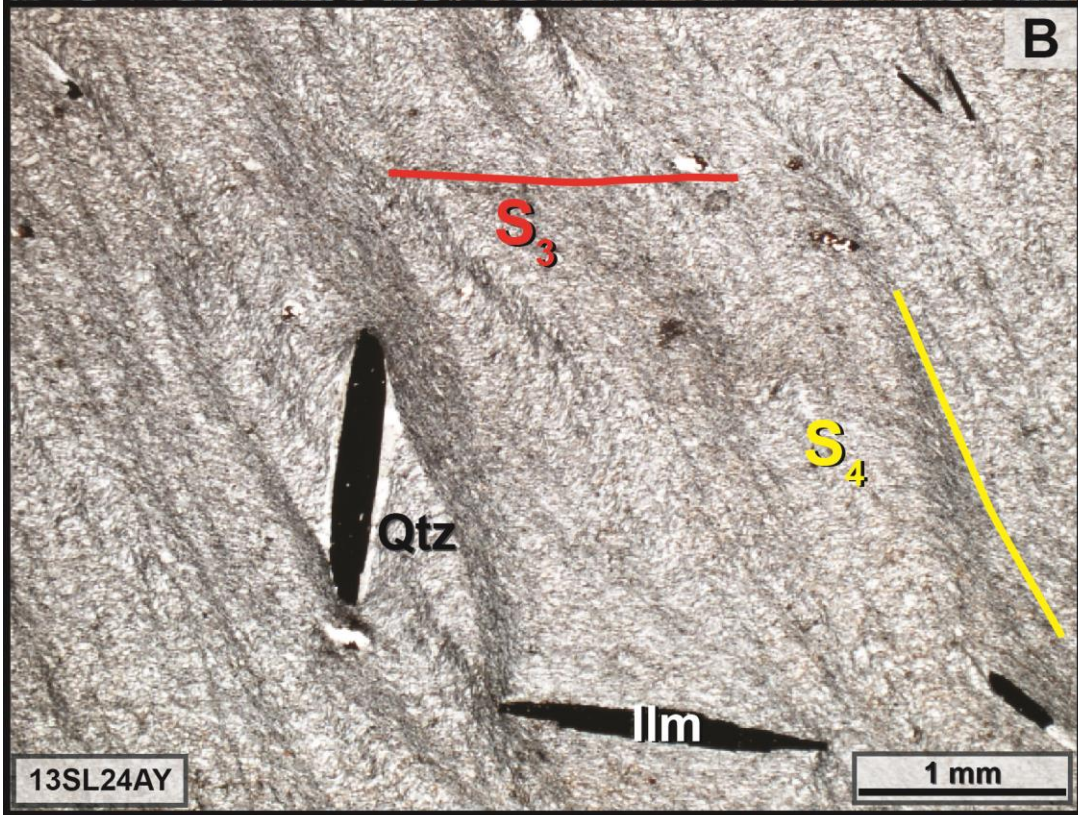
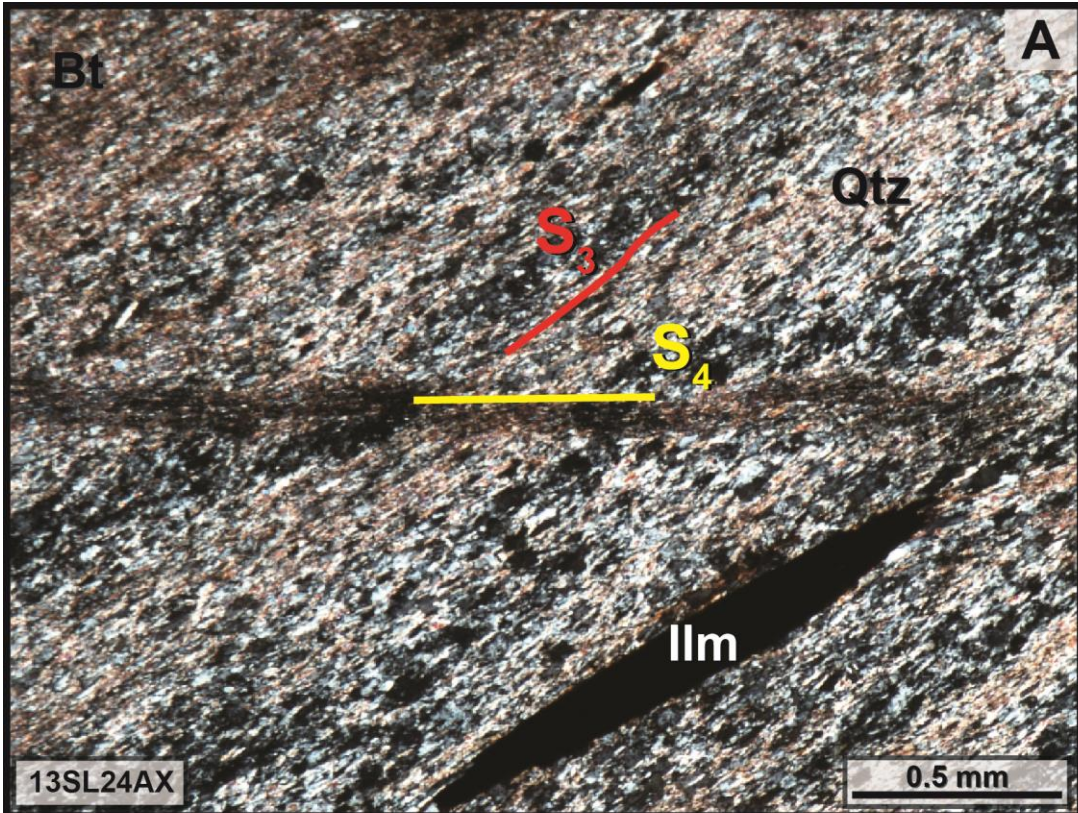


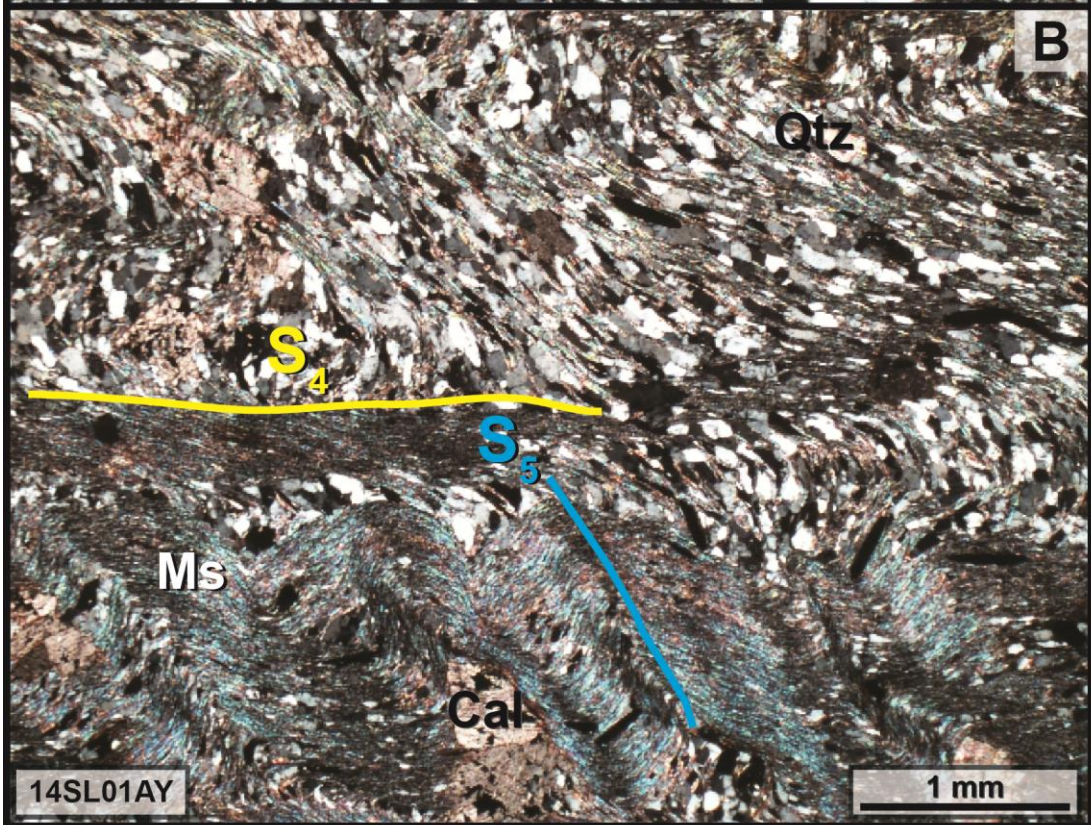
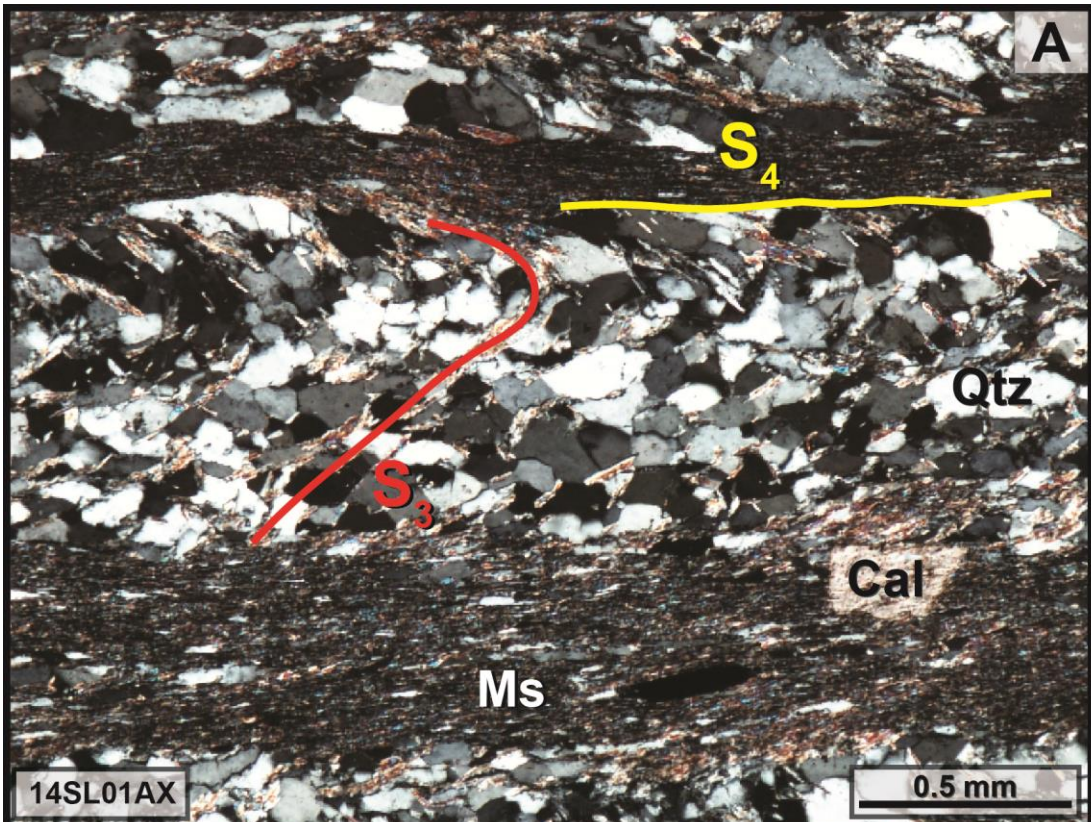


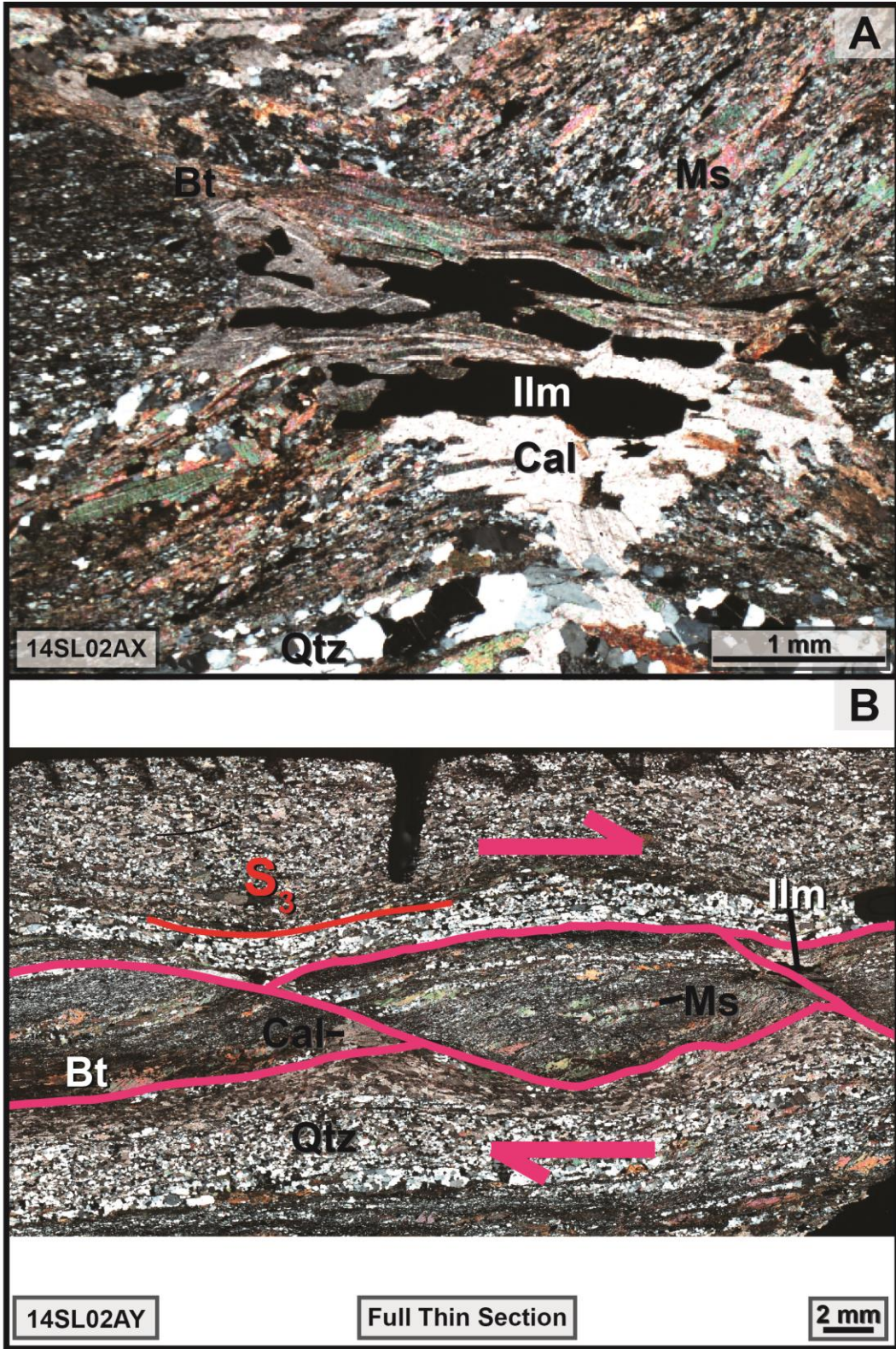




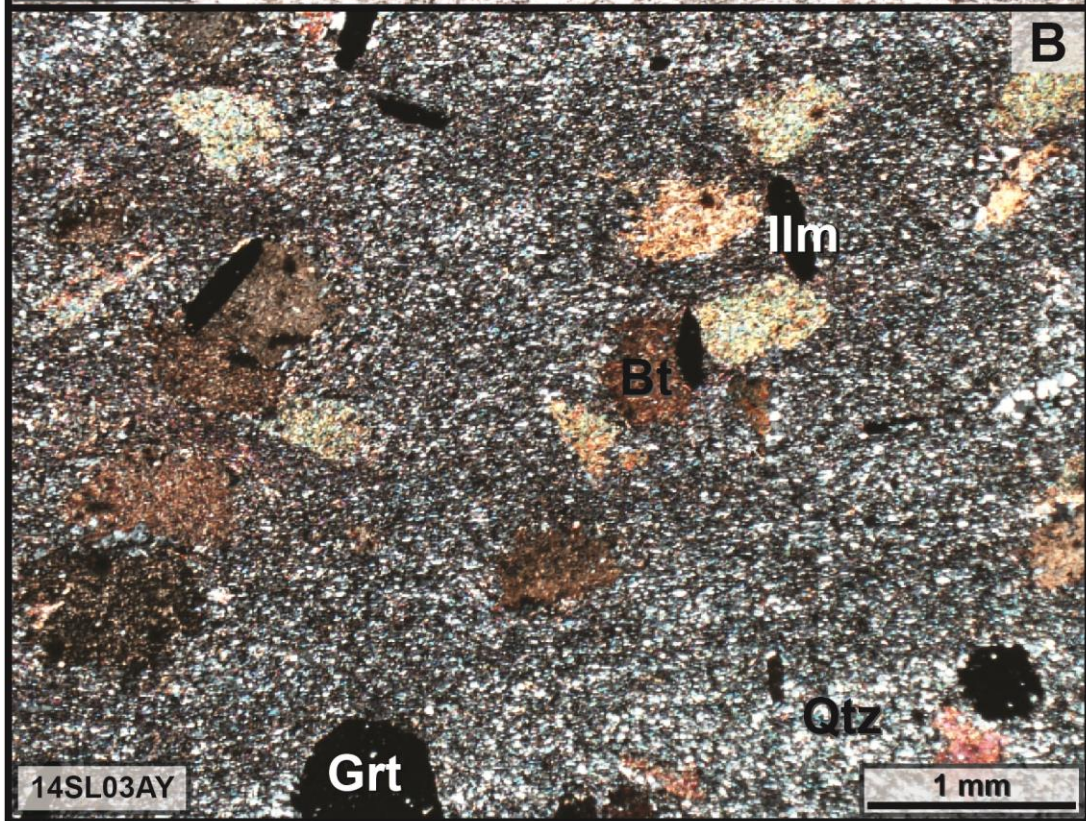
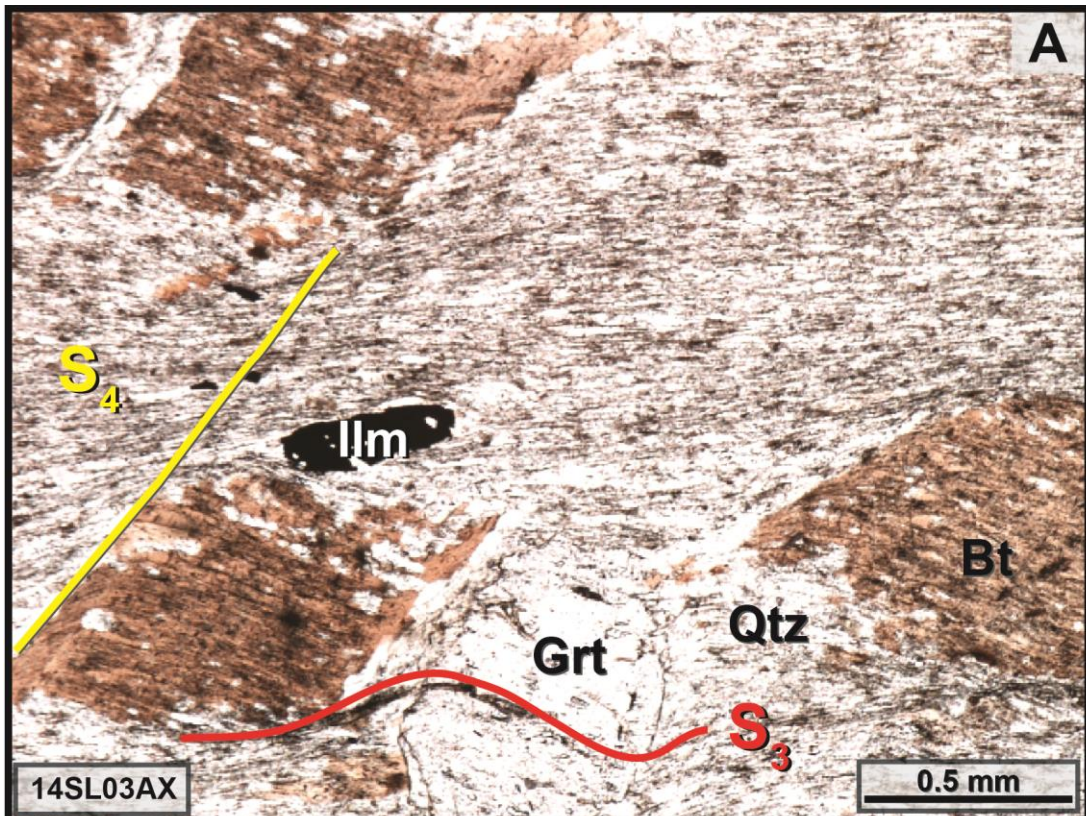
Parts (B) and (C) of this figure show the four monazite grains targeted for geochronology







14SL02AY: Pink lines highlight shear boudins and dextral sense of shear.



APPENDIX B: $^{40}\text{Ar}/^{39}\text{Ar}$ Analytical Results

Table 02/01. $^{40}\text{Ar}/^{39}\text{Ar}$ analytical results for sample 13SL02A, biotite (n=1 xtl; J= 2.11146E-03 ± 0.50%)

Laser Wattage	Dwell Time (min)	$^{37}\text{Ar}/^{39}\text{Ar}$	$^{37}\text{Ar}/^{39}\text{Ar}$ Error	$^{36}\text{Ar}/^{39}\text{Ar}$	$^{36}\text{Ar}/^{39}\text{Ar}$ Error	^{39}Ar (cps)	^{39}Ar (cps) Err	Cumulative % ^{39}Ar Released	% $^{40}\text{Ar}^*$	$^{39}\text{Ar}/^{40}\text{Ar}$	$^{39}\text{Ar}/^{40}\text{Ar}$ Error	Age (Ma)	1 σ % Error (Ma)
3.8	1	0.01495	0.00736	0.01177	0.00043	3279.5	23.2	10.89	96.16	0.01093	0.00008	307.53	0.76
3.875	1	0.02515	0.00661	0.00416	0.00036	3649.9	25.5	23.02	98.84	0.00937	0.00007	363.05	0.72
3.95	1	0.01759	0.00769	0.00361	0.00050	2841.5	20.0	32.46	98.98	0.00944	0.00007	361.12	0.72
4.1	1	0.01210	0.00545	0.00456	0.00032	4148.7	25.3	46.24	98.74	0.00926	0.00006	366.39	0.64
4.25	1	0.01573	0.00599	0.00300	0.00033	4032.4	26.9	59.64	99.17	0.00924	0.00006	368.77	0.69
4.4	1	0.02698	0.00666	0.00350	0.00040	3283.1	22.3	70.54	99.03	0.00923	0.00007	368.72	0.71
4.6	1	0.01393	0.00791	0.00382	0.00046	3053.9	24.8	80.69	98.93	0.00935	0.00008	364.14	0.83
4.85	1	-0.00201	-0.01283	0.00469	0.00070	1997.9	20.0	87.32	98.68	0.00944	0.00010	359.86	1.03
5.2	1	0.00369	0.01573	0.00655	0.00083	1583.1	18.7	92.58	98.19	0.00928	0.00011	364.03	1.22
5.6	1	-0.02094	-0.04289	0.00763	0.00206	615.9	9.3	94.63	97.93	0.00908	0.00014	370.46	1.57
fuse	1	0.07514	0.02394	0.04487	0.00188	1616.6	17.8	100	88.73	0.00842	0.00009	362.87	1.26

Table 02/02. $^{40}\text{Ar}/^{39}\text{Ar}$ analytical results for sample 13SL02A, muscovite (n=10 xtls; $J = 2.11154\text{E-}03 \pm 0.47\%$)

Laser Wattage	Dwell Time (min)	$^{37}\text{Ar}/^{39}\text{Ar}$	$^{37}\text{Ar}/^{39}\text{Ar}$ Error	$^{36}\text{Ar}/^{39}\text{Ar}$	$^{36}\text{Ar}/^{39}\text{Ar}$ Error	^{39}Ar (cps)	^{39}Ar (cps) Err	Cumulative % ^{39}Ar Released	% $^{40}\text{Ar}^*$	$^{39}\text{Ar}/^{40}\text{Ar}$	$^{39}\text{Ar}/^{40}\text{Ar}$ Error	Age (Ma)	1 σ % Error (Ma)
3.8	1	-3.50857	-0.60029	0.05081	0.01891	46.4	1.1	0.19	83.33	0.01099	0.00038	266.42	4.13
4	1	-0.55089	-0.10200	0.00673	0.00297	281.0	7.4	1.34	98.18	0.00903	0.00024	372.82	2.75
4.2	1	-0.03315	-0.01087	0.00636	0.00035	2539.5	22.4	11.72	98.25	0.00921	0.00008	366.85	0.91
4.3	1	0.03095	0.01672	0.00418	0.00039	2287.9	20.3	21.06	98.84	0.00931	0.00008	364.92	0.91
4.4	1	0.00706	0.00831	0.00357	0.00026	3415.7	23.4	35.02	99.00	0.00935	0.00007	364.19	0.71
4.425	1	0.00563	0.00886	0.00207	0.00029	3019.1	24.8	47.36	99.41	0.00947	0.00008	361.54	0.84
4.45	1	0.02585	0.01834	0.00286	0.00062	1365.0	14.7	52.94	99.20	0.00933	0.00010	365.63	1.11
4.5	1	-0.00171	-0.02346	0.00236	0.00085	1103.3	14.5	57.45	99.35	0.00918	0.00012	371.45	1.34
4.6	1	0.02967	0.01466	0.00341	0.00052	1826.7	17.0	64.91	99.05	0.00935	0.00009	364.33	0.96
4.7	1	0.03911	0.01614	0.00124	0.00049	1622.0	15.8	71.54	99.65	0.00949	0.00010	361.51	1.01
4.85	1	0.05178	0.02274	0.00125	0.00077	1151.2	14.5	76.24	99.65	0.00939	0.00012	364.92	1.30
5.2	1	0.05318	0.01993	0.00375	0.00066	1273.9	16.5	81.45	98.97	0.00922	0.00012	368.80	1.33
6	1	0.05235	0.02241	0.00518	0.00070	1244.3	15.5	86.53	98.57	0.00926	0.00012	366.14	1.29
fuse	1	0.03475	0.00820	0.00130	0.00041	3295.9	19.7	100	99.64	0.00927	0.00006	369.25	0.63

Table 02/03. $^{40}\text{Ar}/^{39}\text{Ar}$ analytical results for sample 13SL05A, biotite (n=1 xtl; J = 2.11161E-03 ± 0.50%)

Laser Wattage	Dwell Time (min)	$^{37}\text{Ar}/^{39}\text{Ar}$	$^{37}\text{Ar}/^{39}\text{Ar}$ Error	$^{36}\text{Ar}/^{39}\text{Ar}$	$^{36}\text{Ar}/^{39}\text{Ar}$ Error	^{39}Ar (cps)	^{39}Ar (cps) Err	Cumulative % ^{39}Ar Released	% ^{40}Ar *	$^{39}\text{Ar}/^{40}\text{Ar}$	$^{39}\text{Ar}/^{40}\text{Ar}$ Error	Age (Ma)	1 σ % Error (Ma)
3.8	1	1.35656	0.10112	0.02011	0.00589	471.3	8.0	1.71	91.29	0.01450	0.00025	225.83	1.92
3.9	1	0.25119	0.02581	-0.00079	-0.00157	1293.9	15.2	6.40	100.30	0.01263	0.00015	279.94	1.20
4.05	1	0.07002	0.01470	0.00094	0.00089	2282.4	21.1	14.67	99.69	0.01097	0.00010	316.91	0.95
4.2	1	0.04360	0.01410	0.00085	0.00088	2325.2	24.4	23.09	99.73	0.01078	0.00012	322.14	1.08
4.35	1	0.04117	0.00594	0.00173	0.00043	3054.6	26.4	34.16	99.45	0.01065	0.00009	324.92	0.88
4.5	1	0.03560	0.00711	0.00195	0.00049	2643.4	25.5	43.74	99.37	0.01091	0.00011	317.48	0.99
4.65	1	0.02297	0.00553	0.00783	0.00066	3770.9	31.6	57.41	96.74	0.01397	0.00012	246.24	0.89
4.8	1	0.02869	0.00364	0.00135	0.00029	4821.2	38.9	74.88	99.57	0.01076	0.00009	322.21	0.83
4.95	1	0.06862	0.00553	0.00219	0.00032	6819.8	49.0	99.60	99.30	0.01066	0.00008	324.03	0.74
5.1	1	1.72905	0.23061	-0.00262	-0.01412	90.8	2.0	99.93	100.73	0.00928	0.00025	373.22	2.67
5.5	1	21.35866	1.49240	0.36600	0.11424	19.0	0.9	99.96	57.72	0.00387	0.00022	506.01	9.78
fuse	1	270.13481	216.78637	1.34800	1.55251	1.2	1.0	100	93.46	0.00016	0.00013	4963.36	85.27

Table 02/04. $^{40}\text{Ar}/^{39}\text{Ar}$ analytical results for sample 13SL05A, muscovite (n=15 xtls; J = 2.15654E-03 ± 0.43%)

Laser Wattage	Dwell time (min)	$^{37}\text{Ar}/^{39}\text{Ar}$	$^{37}\text{Ar}/^{39}\text{Ar}$ error	$^{36}\text{Ar}/^{39}\text{Ar}$	$^{36}\text{Ar}/^{39}\text{Ar}$ error	^{39}Ar (cps)	^{39}Ar (cps) Err	Cumulative % ^{39}Ar released	% $^{40}\text{Ar}^*$	$^{39}\text{Ar}/^{40}\text{Ar}$	$^{39}\text{Ar}/^{40}\text{Ar}$ Error	Age (Ma)	1 σ % error (Ma)
3.8	1	0.47229	0.70315	0.04988	0.01689	52.0	1.1	0.51	87.39	0.00847	0.00025	356.06	3.38
3.9	1	0.44421	0.35332	0.01404	0.00885	94.3	2.2	1.43	96.23	0.00900	0.00024	367.90	2.74
4.1	1	0.05072	0.10300	0.01659	0.00276	344.1	5.9	4.79	95.69	0.00869	0.00015	377.33	1.82
4.3	1	0.01040	0.01455	0.00643	0.00041	2361.8	20.7	27.87	98.17	0.00954	0.00008	355.01	0.91
4.375	1	0.04985	0.03632	0.00250	0.00088	1007.5	14.0	37.71	99.25	0.01012	0.00014	339.87	1.42
4.45	1	-0.01907	-0.04526	0.00095	0.00118	787.2	10.6	45.41	99.71	0.01021	0.00014	338.48	1.36
4.55	1	0.02450	0.05232	0.00281	0.00141	576.6	11.4	51.04	99.15	0.01019	0.00020	337.21	2.02
4.7	1	0.05143	0.07438	0.00693	0.00210	421.6	7.5	55.16	97.93	0.00999	0.00018	339.66	1.85
4.9	1	0.08008	0.06236	0.00519	0.00167	503.2	7.8	60.08	98.46	0.00994	0.00016	342.85	1.62
5.1	1	0.06433	0.03848	0.00471	0.00101	847.3	10.3	68.36	98.61	0.00990	0.00012	344.79	1.25
5.25	1	0.07333	0.03013	0.00227	0.00081	1082.6	11.3	78.93	99.34	0.00977	0.00010	351.02	1.07
5.35	1	0.00389	0.05590	0.00264	0.00147	625.2	9.2	85.04	99.20	0.01018	0.00015	337.65	1.51
5.5	1	0.07942	0.08024	-0.00739	-0.00320	405.8	6.9	89.01	102.18	0.00988	0.00017	356.52	1.69
5.8	1	0.00158	0.08618	0.00307	0.00221	405.8	7.0	92.97	99.11	0.00970	0.00017	352.79	1.77
6.3	1	-0.12344	-0.13161	0.00635	0.00345	256.6	6.5	95.48	98.15	0.00973	0.00025	348.53	2.62
fuse	1	-0.05852	-0.06561	0.03309	0.00213	462.6	8.6	100	90.94	0.00917	0.00017	343.39	2.07

Table 02/05. $^{40}\text{Ar}/^{39}\text{Ar}$ analytical results for sample 13SL05B, biotite (n=1 xtl; J = 2.11178E-0 ± 0.49%)

Laser Wattage	Dwell Time (min)	$^{37}\text{Ar}/^{39}\text{Ar}$	$^{37}\text{Ar}/^{39}\text{Ar}$ Error	$^{36}\text{Ar}/^{39}\text{Ar}$	$^{36}\text{Ar}/^{39}\text{Ar}$ Error	^{39}Ar (cps)	^{39}Ar (cps) Err	Cumulative % ^{39}Ar Released	% $^{40}\text{Ar}^*$	$^{39}\text{Ar}/^{40}\text{Ar}$	$^{39}\text{Ar}/^{40}\text{Ar}$ Error	Age (Ma)	1 σ % Error (Ma)
3.8	1	0.67031	0.02965	0.01340	0.00188	1031.8	12.4	2.05	95.13	0.01217	0.00015	276.05	1.29
3.9	1	0.16550	0.00822	0.00313	0.00059	3413.2	25.2	8.84	99.10	0.00969	0.00007	352.96	0.76
3.95	1	0.07317	0.00918	0.00008	0.00069	2771.6	21.7	14.34	99.98	0.00969	0.00008	355.69	0.80
4	1	0.07691	0.00866	0.00022	0.00056	3402.3	24.3	21.11	99.94	0.00969	0.00007	355.76	0.73
4.05	1	0.10156	0.01076	0.00016	0.00071	2660.3	18.8	26.39	99.95	0.00976	0.00007	353.56	0.73
4.1	1	0.06761	0.00791	0.00210	0.00040	3206.8	22.2	32.77	99.40	0.00964	0.00007	355.54	0.72
4.15	1	0.07400	0.01094	0.00215	0.00055	2242.7	19.3	37.23	99.38	0.00964	0.00008	355.40	0.88
4.25	1	0.05969	0.00759	0.00177	0.00036	3570.5	26.3	44.32	99.49	0.00977	0.00007	351.67	0.76
4.35	1	0.05984	0.00927	0.00138	0.00027	4521.2	27.6	53.31	99.60	0.00978	0.00006	351.52	0.63
4.45	1	0.02428	0.00319	0.00115	0.00013	8779.3	39.1	70.76	99.66	0.00982	0.00005	350.55	0.47
4.5	1	0.02076	0.00282	0.00103	0.00011	9846.3	46.5	90.33	99.70	0.00981	0.00005	350.94	0.49
4.77	1	0.07688	0.00899	0.00165	0.00035	3098.8	21.2	96.49	99.53	0.00946	0.00007	362.05	0.71
4.85	1	0.20740	0.02127	0.00476	0.00146	1275.9	12.6	99.03	98.65	0.00947	0.00010	359.16	1.03
5.1	1	2.44429	0.12876	0.00656	0.00284	396.7	6.8	99.81	98.27	0.00881	0.00016	383.10	1.81
5.6	1	7.45449	0.58111	0.00999	0.02096	50.8	0.9	99.91	98.19	0.00608	0.00016	533.71	2.64
fuse	1	5.81290	0.65717	0.26752	0.04369	43.1	0.9	100	65.70	0.00429	0.00011	508.63	3.80

Table 02/06. $^{40}\text{Ar}/^{39}\text{Ar}$ analytical results for sample 13SL05B, muscovite (n=25 xtls; $J = 2.11259\text{E-}03 \pm 0.48\%$)

Laser Wattage	Dwell Time (min)	$^{37}\text{Ar}/^{39}\text{Ar}$	$^{37}\text{Ar}/^{39}\text{Ar}$ Error	$^{36}\text{Ar}/^{39}\text{Ar}$	$^{36}\text{Ar}/^{39}\text{Ar}$ Error	^{39}Ar (cps)	^{39}Ar (cps) Err	Cumulative % ^{39}Ar Released	% $^{40}\text{Ar}^*$	$^{39}\text{Ar}/^{40}\text{Ar}$	$^{39}\text{Ar}/^{40}\text{Ar}$ Error	Age (Ma)	1 σ % Error (Ma)
3.8	1	0.95243	0.58580	0.19505	0.03103	50.43	1.59	0.09	40.02	0.01030	0.00037	142.91	8.85
4	1	0.35943	0.17462	0.05744	0.00893	174.50	3.09	0.42	84.57	0.00900	0.00017	327.24	2.18
4.2	1	1.76250	0.06632	0.02551	0.00263	584.62	10.40	1.52	93.28	0.00882	0.00016	364.87	1.92
4.35	1	1.27160	0.04743	0.01384	0.00112	1383.10	16.15	4.13	96.33	0.00888	0.00011	373.03	1.23
4.4	1	0.06450	0.01182	0.00837	0.00065	2428.18	24.53	8.70	97.59	0.00964	0.00010	349.85	1.06
4.425	1	0.03169	0.01216	0.00393	0.00077	2133.45	21.70	12.72	98.84	0.00992	0.00010	344.91	1.06
4.45	1	0.01124	0.01084	0.00277	0.00064	2483.99	24.79	17.40	99.17	0.01006	0.00010	341.56	1.04
4.475	1	0.03360	0.01775	0.00455	0.00111	1461.80	16.47	20.16	98.67	0.00980	0.00011	348.03	1.18
4.525	1	0.04375	0.01231	0.00558	0.00076	2191.56	21.96	24.28	98.38	0.00971	0.00010	350.12	1.05
4.575	1	0.06298	0.01579	0.00487	0.00091	1774.24	18.58	27.63	98.56	0.00987	0.00011	345.55	1.10
4.65	1	0.00153	0.01208	0.00177	0.00038	2528.84	25.74	32.39	99.48	0.00990	0.00010	347.34	1.06
4.8	1	0.01100	0.00645	0.00185	0.00019	4876.78	34.79	41.58	99.45	0.00996	0.00007	345.51	0.73
4.95	1	0.01208	0.00784	0.00176	0.00024	3900.97	29.04	48.92	99.48	0.00994	0.00007	346.13	0.76
5.2	1	0.00663	0.00701	0.00399	0.00022	4623.22	34.32	57.63	98.83	0.00983	0.00007	347.67	0.76
5.5	1	0.01955	0.00645	0.00205	0.00022	4476.88	33.86	66.07	99.39	0.01002	0.00008	343.45	0.77
5.8	1	-0.00265	-0.00693	0.00116	0.00023	4558.98	33.51	74.65	99.66	0.00994	0.00007	346.79	0.75
6.2	1	-0.00002	-0.00641	0.00180	0.00024	4487.85	33.07	83.11	99.47	0.00992	0.00007	346.84	0.75
fuse	1	0.02410	0.00332	0.00272	0.00013	8967.31	67.34	100	99.20	0.00990	0.00007	346.57	0.76

Table 02/07. $^{40}\text{Ar}/^{39}\text{Ar}$ analytical results for sample 13SL12A, biotite (n=1 xtl; J = 2.11399E-03 ± 0.42%)

Laser Wattage	Dwell Time (min)	$^{37}\text{Ar}/^{39}\text{Ar}$	$^{37}\text{Ar}/^{39}\text{Ar}$ Error	$^{36}\text{Ar}/^{39}\text{Ar}$	$^{36}\text{Ar}/^{39}\text{Ar}$ Error	^{39}Ar (cps)	^{39}Ar (cps) Err	Cumulative % ^{39}Ar Released	% $^{40}\text{Ar}^*$	$^{39}\text{Ar}/^{40}\text{Ar}$	$^{39}\text{Ar}/^{40}\text{Ar}$ Error	Age (Ma)	1 σ % Error (Ma)
3.8	1	2.27675	0.94384	0.68378	0.06035	42.6	1.5	2.89	33.54	0.00326	0.00012	357.34	11.09
3.9	1	0.08617	0.28899	1.00445	0.04474	90.6	2.1	9.04	36.87	0.00211	0.00005	569.40	6.40
4	1	-0.05828	-0.25072	0.00764	0.01694	108.0	2.4	16.37	98.34	0.00726	0.00018	454.39	2.48
4.2	1	0.06176	0.06624	-0.00150	-0.00440	408.9	7.3	44.12	100.42	0.00927	0.00017	372.06	1.84
4.4	1	0.08789	0.10046	0.01847	0.00989	269.8	6.3	62.43	94.94	0.00918	0.00022	356.86	2.54
4.7	1	0.12639	0.20023	0.02001	0.00741	147.9	2.6	72.47	94.72	0.00884	0.00017	368.69	2.08
5.1	1	0.14949	0.24445	0.01744	0.00974	114.7	2.2	80.25	95.35	0.00893	0.00020	367.51	2.30
5.8	1	0.09700	0.30286	0.01404	0.01149	97.8	2.1	86.89	96.27	0.00890	0.00021	371.89	2.50
fuse	1	0.17235	0.14132	0.03543	0.00607	193.2	5.8	100	91.40	0.00813	0.00025	385.11	3.37

Table 02/08. $^{40}\text{Ar}/^{39}\text{Ar}$ analytical results for sample 13SL19A, biotite (n~25 xtls; J = 2.11586E-03 ± 0.35%)

Laser Wattage	Dwell Time (min)	$^{37}\text{Ar}/^{39}\text{Ar}$	$^{37}\text{Ar}/^{39}\text{Ar}$ Error	$^{36}\text{Ar}/^{39}\text{Ar}$	$^{36}\text{Ar}/^{39}\text{Ar}$ Error	^{39}Ar (cps)	^{39}Ar (cps) Err	Cumulative % ^{39}Ar Released	% ^{40}Ar *	$^{39}\text{Ar}/^{40}\text{Ar}$	$^{39}\text{Ar}/^{40}\text{Ar}$ Error	Age (Ma)	1σ % Error (Ma)
3.8	1	-0.19562	-0.05119	0.01694	0.00171	616.1	13.6	2.81	93.62	0.01261	0.00028	263.22	2.39
3.9	1	-0.08559	-0.01300	0.00411	0.00046	2365.3	34.3	13.62	98.76	0.01014	0.00015	338.26	1.48
3.95	1	-0.20397	-0.02214	0.00120	0.00080	1323.1	21.4	19.66	99.64	0.01004	0.00016	343.89	1.63
4.05	1	-0.14137	-0.01460	0.00228	0.00052	2007.6	30.3	28.84	99.31	0.01019	0.00016	338.19	1.54
4.2	1	-0.13326	-0.01183	0.00177	0.00042	2492.9	35.7	40.22	99.48	0.00984	0.00014	349.68	1.46
4.4	1	-0.00850	-0.00808	0.00165	0.00028	3671.9	51.5	57.00	99.51	0.00990	0.00014	348.09	1.42
4.55	1	-0.03225	-0.01030	0.00228	0.00034	3149.2	45.5	71.38	99.31	0.01007	0.00015	342.01	1.47
4.7	1	-0.05743	-0.01589	0.00160	0.00057	1764.9	27.2	79.45	99.52	0.01002	0.00016	344.38	1.56
5	1	-0.07853	-0.01309	0.00220	0.00044	2216.3	32.6	89.57	99.35	0.00996	0.00015	345.68	1.49
5.5	1	-0.00257	-0.01884	0.00332	0.00065	1462.1	26.7	96.25	98.98	0.01032	0.00019	333.59	1.86
fuse	1	-0.02744	-0.03457	0.06902	0.00315	820.9	15.3	100	82.92	0.00829	0.00016	346.61	2.26

Table 02/09. $^{40}\text{Ar}/^{39}\text{Ar}$ analytical results for sample 13SL20B, biotite (n=1 xtl; J = 2.12457E-03 ± 0.20%)

Laser Wattage	Dwell time (min)	$^{37}\text{Ar}/^{39}\text{Ar}$	$^{37}\text{Ar}/^{39}\text{Ar}$ error	$^{36}\text{Ar}/^{39}\text{Ar}$	$^{36}\text{Ar}/^{39}\text{Ar}$ error	^{39}Ar (cps)	^{39}Ar (cps) Err	Cumulative % ^{39}Ar released	% ^{40}Ar *	$^{39}\text{Ar}/^{40}\text{Ar}$	$^{39}\text{Ar}/^{40}\text{Ar}$ Error	Age (Ma)	1σ % error (Ma)
3.8	1	0.04293	0.03153	0.01235	0.00406	726.5	9.5	0.78	95.37	0.01255	0.00017	270.16	1.44
3.9	1	0.02252	0.00429	0.00084	0.00025	8929.2	41.7	10.37	99.76	0.00975	0.00005	355.16	0.49
3.95	1	0.00877	0.00230	-0.00098	-0.00025	8971.6	42.5	20.01	100.28	0.00971	0.00005	358.02	0.49
3.975	1	0.01566	0.00281	-0.00124	-0.00027	8148.4	41.0	28.77	100.36	0.00967	0.00005	359.56	0.52
4	1	-0.04177	-0.00870	0.00029	0.00047	4628.5	31.3	33.74	99.92	0.00962	0.00007	360.00	0.69
4.025	1	-0.03013	-0.01008	0.00088	0.00055	3993.0	26.9	38.03	99.75	0.00949	0.00007	363.68	0.69
4.05	1	-0.02461	-0.00803	0.00018	0.00043	5165.5	26.1	43.58	99.95	0.00957	0.00005	361.76	0.52
4.075	1	-0.11507	-0.03541	-0.00309	-0.00190	1161.3	16.4	44.83	100.90	0.00970	0.00014	360.37	1.43
4.125	1	0.00517	0.01432	0.00236	0.00067	1753.9	15.0	46.71	99.35	0.00925	0.00008	371.02	0.89
4.2	1	0.00024	0.01133	0.00231	0.00053	2344.9	17.5	49.23	99.35	0.00948	0.00007	362.89	0.78
4.3	1	0.00732	0.00622	0.00184	0.00031	3930.4	24.1	53.46	99.48	0.00947	0.00006	363.56	0.64
4.45	1	0.00695	0.00231	0.00111	0.00011	11494.5	49.7	65.81	99.68	0.00977	0.00004	354.26	0.45
4.55	1	0.00930	0.00267	0.00104	0.00014	9409.8	44.9	75.92	99.70	0.00961	0.00005	359.63	0.50
4.65	1	0.02383	0.00628	0.00122	0.00019	6847.7	35.5	83.27	99.65	0.00956	0.00005	361.08	0.54
4.75	1	-0.01780	-0.00830	0.00196	0.00024	4786.2	27.1	88.41	99.45	0.00945	0.00006	364.30	0.59
4.9	1	-0.00616	-0.01011	0.00185	0.00031	3885.2	22.3	92.59	99.48	0.00947	0.00006	363.52	0.60
5.1	1	-0.00181	-0.01202	0.00235	0.00036	3232.5	24.1	96.06	99.33	0.00956	0.00007	359.90	0.77
5.5	1	0.02676	0.01193	0.00319	0.00056	1901.6	17.0	98.11	99.10	0.00948	0.00009	362.15	0.94
6.2	1	0.02736	0.01286	0.00417	0.00061	1763.7	16.9	100	98.81	0.00960	0.00009	356.91	1.00

Table 02/10. $^{40}\text{Ar}/^{39}\text{Ar}$ analytical results for sample 13SL20B, muscovite (n=1 xtl; J = 2.12652E-03 ± 0.22%)

Laser Wattage	Dwell Time (min)	$^{37}\text{Ar}/^{39}\text{Ar}$	$^{37}\text{Ar}/^{39}\text{Ar}$ Error	$^{36}\text{Ar}/^{39}\text{Ar}$	$^{36}\text{Ar}/^{39}\text{Ar}$ Error	^{39}Ar (cps)	^{39}Ar (cps) Err	Cumulative % ^{39}Ar Released	% $^{40}\text{Ar}^*$	$^{39}\text{Ar}/^{40}\text{Ar}$	$^{39}\text{Ar}/^{40}\text{Ar}$ Error	Age (Ma)	1σ % Error (Ma)
3.8	1	-3.31731	-1.50066	0.05763	0.04888	20.1	0.8	0.14	85.15	0.00863	0.00039	342.19	5.33
4.2	1	-2.71896	-1.80744	0.01648	0.06017	17.8	0.8	0.27	95.52	0.00910	0.00045	362.25	5.19
4.4	1	-0.37408	-0.25960	0.00197	0.00857	112.3	2.5	1.05	99.47	0.00908	0.00022	377.76	2.41
4.6	1	-0.27060	-0.09378	0.01099	0.00314	311.4	6.7	3.23	96.92	0.00938	0.00020	358.52	2.25
4.7	1	0.00549	0.00963	0.00233	0.00029	3318.1	25.7	26.44	99.31	0.00988	0.00008	349.78	0.80
4.71	1	-0.00249	-0.00830	0.00130	0.00024	3853.8	28.5	53.39	99.62	0.00987	0.00007	351.00	0.76
4.72	1	-0.11711	-0.08573	0.00238	0.00264	357.2	6.4	55.89	99.32	0.00956	0.00017	360.19	1.84
4.75	1	-0.08034	-0.13166	0.00750	0.00353	240.5	7.9	57.57	97.66	0.01044	0.00035	327.53	3.41
4.85	1	-0.13310	-0.14562	0.01301	0.00407	210.5	6.1	59.04	96.28	0.00957	0.00028	350.02	3.05
5	1	-0.00238	-0.10091	0.00655	0.00309	284.2	8.1	61.03	98.04	0.01003	0.00029	340.88	2.95
5.5	1	-0.04788	-0.02867	0.00203	0.00090	1034.8	11.8	68.27	99.39	0.01000	0.00012	346.19	1.16
6	1	0.00899	0.01805	0.00109	0.00057	1651.1	16.4	79.82	99.68	0.00979	0.00010	353.80	1.02
6.5	1	0.05133	0.01877	0.00135	0.00065	1534.2	16.3	90.55	99.60	0.00999	0.00011	347.18	1.08
7	1	0.14708	0.03991	0.00414	0.00135	722.5	10.5	95.60	98.79	0.00976	0.00014	351.86	1.48
7.75	1	0.52554	0.19654	0.01162	0.00663	136.8	3.5	96.56	96.73	0.00943	0.00025	356.43	2.74
fuse	1	0.03888	0.05850	0.00445	0.00188	492.4	10.0	100	98.67	0.00997	0.00020	344.72	2.08

Table 02/11. $^{40}\text{Ar}/^{39}\text{Ar}$ analytical results for sample 13SL20C, biotite (n=1 xtl; J = 2.13200E-03 ± 0.20%)

Laser Wattage	Dwell Time (min)	$^{37}\text{Ar}/^{39}\text{Ar}$	$^{37}\text{Ar}/^{39}\text{Ar}$ Error	$^{36}\text{Ar}/^{39}\text{Ar}$	$^{36}\text{Ar}/^{39}\text{Ar}$ Error	^{39}Ar (cps)	^{39}Ar (cps) Err	Cumulative % ^{39}Ar Released	% ^{40}Ar *	$^{39}\text{Ar}/^{40}\text{Ar}$	$^{39}\text{Ar}/^{40}\text{Ar}$ Error	Age (Ma)	1 σ % Error (Ma)
3.8	1	0.02408	0.01001	0.02988	0.00158	172.0	20.9	1.15	90.33	0.01084	0.00013	295.16	1.36
3.9	1	0.00564	0.00121	0.00104	0.00010	1477.9	138.1	10.99	99.67	0.01048	0.00010	333.19	0.95
3.93	1	0.00445	0.00154	0.00117	0.00012	1115.5	105.0	18.43	99.64	0.01033	0.00010	337.59	0.95
4	1	0.00412	0.00837	-0.00001	-0.00039	2198.2	26.1	33.08	100.00	0.01389	0.00017	257.66	1.20
4.115	1	0.00557	0.01202	0.00052	0.00053	1636.9	20.3	43.98	99.84	0.01013	0.00013	344.32	1.26
4.3	1	-0.00073	-0.01146	-0.00023	-0.00049	1774.9	21.2	55.81	100.07	0.01021	0.00012	342.57	1.21
4.5	1	0.00616	0.00751	-0.00028	-0.00035	2454.3	28.5	72.16	100.08	0.01014	0.00012	344.63	1.17
4.75	1	0.03150	0.00787	0.00103	0.00031	2627.5	30.3	89.67	99.69	0.01009	0.00012	345.01	1.17
5	1	0.06446	0.02597	-0.00004	-0.00119	744.8	12.9	94.63	100.01	0.01013	0.00018	344.83	1.75
5.5	1	-0.09260	-0.03561	0.00259	0.00162	508.5	8.9	98.02	99.20	0.01029	0.00018	337.22	1.81
fuse	1	0.24704	0.06336	-0.01281	-0.00482	296.7	6.8	100	103.84	0.01003	0.00023	360.02	2.24

Table 02/12. $^{40}\text{Ar}/^{39}\text{Ar}$ analytical results for sample 13SL20C, potassium feldspar (n=1 xtl; J = 2.15654E-03 ± 0.43%)

Laser Wattage	Dwell time (min)	$^{37}\text{Ar}/^{39}\text{Ar}$	$^{37}\text{Ar}/^{39}\text{Ar}$ error	$^{36}\text{Ar}/^{39}\text{Ar}$	$^{36}\text{Ar}/^{39}\text{Ar}$ error	^{39}Ar (cps)	^{39}Ar (cps) Err	Cumulative % ^{39}Ar released	% $^{40}\text{Ar}^*$	$^{39}\text{Ar}/^{40}\text{Ar}$	$^{39}\text{Ar}/^{40}\text{Ar}$ Error	Age (Ma)	1 σ % error (Ma)
4	1	16.02876	36.67515	1.02737	0.46986	2.1	0.4	0.00	88.45	0.00038	0.00008	3258.99	23.48
4.4	1	-0.15864	-1.70124	0.17724	0.01901	48.7	1.4	0.07	90.75	0.00175	0.00005	1349.34	3.11
4.8	1	0.03336	0.01656	0.00290	0.00022	4563.0	32.3	6.64	98.54	0.01689	0.00012	212.45	0.74
5.2	1	0.07439	0.00765	0.00076	0.00009	10217.0	62.8	21.34	99.61	0.01694	0.00011	214.15	0.64
5.4	1	0.03718	0.01425	0.00020	0.00015	5648.3	37.6	29.47	99.90	0.01647	0.00011	220.49	0.69
5.6	1	0.06276	0.02311	0.00056	0.00024	3370.3	27.7	34.32	99.73	0.01605	0.00013	225.49	0.84
5.9	1	0.02311	0.02809	0.00038	0.00029	2865.9	23.8	38.45	99.82	0.01537	0.00013	235.04	0.85
6.2	1	0.04617	0.03561	0.00155	0.00040	2046.9	19.0	41.39	99.34	0.01436	0.00014	249.32	0.95
6.6	1	0.03363	0.04523	0.00055	0.00052	1612.1	17.1	43.71	99.77	0.01369	0.00015	261.81	1.07
7	1	0.01377	0.06799	0.00205	0.00081	1072.9	12.3	45.26	99.20	0.01308	0.00015	271.65	1.17
7.5	1	0.01767	0.06599	0.00059	0.00080	1181.8	14.3	46.96	99.77	0.01294	0.00016	275.81	1.23
8.5	1	0.03541	0.08704	-0.00029	-0.00102	896.3	12.9	48.25	100.11	0.01262	0.00018	283.35	1.45
10	1	0.05710	0.05442	0.00148	0.00063	1387.0	16.6	50.25	99.45	0.01236	0.00015	286.95	1.21
11	1	0.09099	0.01411	0.00118	0.00017	5462.8	39.1	58.11	99.56	0.01245	0.00009	285.40	0.74
11.5	1	0.02829	0.00652	0.00095	0.00007	12681.8	73.6	76.36	99.65	0.01229	0.00007	289.03	0.60
11.6	1	0.07001	0.02608	0.00167	0.00026	3172.4	27.1	80.92	99.38	0.01250	0.00011	283.77	0.87
12	1	0.09773	0.03097	0.00203	0.00035	2578.8	22.1	84.64	99.24	0.01255	0.00011	282.45	0.88
12.5	1	0.12689	0.09374	0.00144	0.00102	852.5	11.8	85.86	99.45	0.01276	0.00018	278.76	1.42
fuse	1	0.02155	0.00785	0.00462	0.00012	9822.9	60.7	100	98.30	0.01234	0.00008	284.41	0.65

Table 02/13. $^{40}\text{Ar}/^{39}\text{Ar}$ analytical results for sample 13SL20C, muscovite (n=1 xtl; J = 2.13758E-03 ± 0.22%)

Laser Wattage	Dwell Time (min)	$^{37}\text{Ar}/^{39}\text{Ar}$	$^{37}\text{Ar}/^{39}\text{Ar}$ Error	$^{36}\text{Ar}/^{39}\text{Ar}$	$^{36}\text{Ar}/^{39}\text{Ar}$ Error	^{39}Ar (cps)	^{39}Ar (cps) Err	Cumulative % ^{39}Ar Released	% $^{40}\text{Ar}^*$	$^{39}\text{Ar}/^{40}\text{Ar}$	$^{39}\text{Ar}/^{40}\text{Ar}$ Error	Age (Ma)	1 σ % Error (Ma)
3.8	1	-58.03197	142.93479	7.18131	13.87285	-0.3	-0.4	-0.01	275.67	-0.00082	-0.00141	Calc error	-62.55
4	1	-0.25671	-8.27971	0.44926	0.30559	3.4	0.5	0.10	10.07	0.00670	0.00159	57.2568	235.14
4.2	1	1.02488	1.17403	0.04417	0.04178	24.7	0.8	0.91	87.15	0.00975	0.00044	316.2425	5.18
4.4	1	0.36801	0.29602	0.00417	0.01007	97.9	2.4	4.13	98.86	0.00917	0.00025	374.5614	2.76
4.55	1	0.00850	0.03193	0.00592	0.00123	821.1	12.4	31.15	98.18	0.01031	0.00016	334.3626	1.58
4.6	1	0.15782	0.15252	0.03652	0.00859	187.9	5.8	37.33	88.85	0.01023	0.00033	307.5281	3.59
4.7	1	0.06564	0.17273	0.02507	0.00973	165.9	5.0	42.79	92.36	0.01021	0.00032	319.1008	3.38
4.9	1	0.03919	0.05289	0.00966	0.00292	557.9	10.2	61.15	96.97	0.01051	0.00020	325.0155	1.93
5.2	1	-0.09710	-0.10989	0.00664	0.00350	268.2	6.6	69.97	97.87	0.01073	0.00027	321.3345	2.56
5.8	1	-0.09073	-0.09855	0.01024	0.00312	299.2	9.1	79.81	96.71	0.01076	0.00033	317.1610	3.17
fuse	1	0.00142	0.04657	0.06429	0.00218	613.6	9.0	100	83.93	0.00837	0.00013	350.6267	1.78

Table 02/14. $^{40}\text{Ar}/^{39}\text{Ar}$ analytical results for sample 13SL20D, biotite (n=1 xtl; J = 2.15139E-03 ± 0.32%)

Laser Wattage	Dwell time (min)	$^{37}\text{Ar}/^{39}\text{Ar}$	$^{37}\text{Ar}/^{39}\text{Ar}$ error	$^{36}\text{Ar}/^{39}\text{Ar}$	$^{36}\text{Ar}/^{39}\text{Ar}$ error	^{39}Ar (cps)	^{39}Ar (cps) Err	Cumulative % ^{39}Ar released	% ^{40}Ar *	$^{39}\text{Ar}/^{40}\text{Ar}$	$^{39}\text{Ar}/^{40}\text{Ar}$ Error	Age (Ma)	1 σ % error (Ma)
3.8	1	-0.00816	-0.00653	0.01547	0.00090	3019.2	24.8	4.62	95.58	0.00957	0.00008	351.38	0.88
3.875	1	-0.00330	-0.00257	0.00215	0.00018	7665.1	55.4	16.35	99.38	0.00971	0.00007	359.04	0.74
3.9	1	-0.00123	-0.00363	0.00192	0.00025	5255.3	37.9	24.40	99.44	0.00969	0.00007	360.01	0.74
3.925	1	0.00530	0.00523	0.00154	0.00038	3533.7	29.1	29.81	99.55	0.00973	0.00008	358.98	0.84
3.975	1	-0.00179	-0.00487	0.00160	0.00034	3924.3	32.2	35.81	99.54	0.00964	0.00008	361.94	0.84
4.05	1	0.00237	0.00573	0.00196	0.00037	3785.1	30.9	41.61	99.43	0.00969	0.00008	360.08	0.84
4.15	1	-0.00117	-0.00489	0.00184	0.00035	4316.6	35.3	48.21	99.47	0.00968	0.00008	360.46	0.83
4.25	1	0.00298	0.00434	0.00147	0.00029	5140.0	38.5	56.08	99.58	0.00958	0.00007	364.23	0.76
4.35	1	0.00191	0.00519	0.00192	0.00034	4180.8	33.4	62.48	99.45	0.00963	0.00008	362.15	0.81
4.5	1	0.00931	0.00289	0.00155	0.00048	6412.1	44.8	72.30	99.55	0.00963	0.00007	362.38	0.71
4.65	1	0.01046	0.00247	0.00060	0.00032	7489.1	54.0	83.76	99.83	0.00957	0.00007	365.35	0.73
4.75	1	0.02254	0.00442	0.00089	0.00043	4539.7	34.4	90.71	99.74	0.00962	0.00007	363.51	0.77
4.85	1	0.03097	0.00755	0.00101	0.00074	2655.8	24.0	94.77	99.71	0.00960	0.00009	363.86	0.93
5	1	0.06893	0.01401	0.00164	0.00121	1574.0	17.7	97.18	99.53	0.00963	0.00011	362.30	1.16
5.5	1	0.48981	0.03240	-0.00024	-0.00175	1107.9	12.9	98.88	100.07	0.00959	0.00011	365.83	1.19
fuse	1	0.19134	0.02843	-0.00277	-0.00267	733.0	11.9	100	100.79	0.00958	0.00016	368.33	1.64

Table 02/15. $^{40}\text{Ar}/^{39}\text{Ar}$ analytical results for sample 13SL20D, potassium feldspar (n=1 xtl; J = 2.15654E-03 ± 0.43%)

Laser Wattage	Dwell Time (min)	$^{37}\text{Ar}/^{39}\text{Ar}$	$^{37}\text{Ar}/^{39}\text{Ar}$ Error	$^{36}\text{Ar}/^{39}\text{Ar}$	$^{36}\text{Ar}/^{39}\text{Ar}$ Error	^{39}Ar (cps)	^{39}Ar (cps) Err	Cumulative % ^{39}Ar Released	% ^{40}Ar *	$^{39}\text{Ar}/^{40}\text{Ar}$	$^{39}\text{Ar}/^{40}\text{Ar}$ Error	Age (Ma)	1 σ % Error (Ma)
4	1	-	-8.94278	0.34842	0.18623	4.4	0.5	0.01	97.28	0.00026	0.00003	3964.69	10.87
4.2	1	-	-6.93407	-0.08329	-0.16618	5.6	0.5	0.02	104.23	0.00170	0.00016	1511.02	9.05
4.4	1	-	-7.42178	-0.03732	-0.17088	5.2	0.5	0.04	104.33	0.00389	0.00041	812.50	10.12
4.5	1	-7.00550	-2.46584	0.07958	0.06075	14.7	0.5	0.07	87.34	0.00533	0.00023	544.41	4.98
4.6	1	-0.51378	-0.20994	0.00182	0.00493	176.3	2.9	0.48	99.14	0.01586	0.00030	228.74	1.90
4.8	1	3.33421	0.15227	0.04255	0.00357	244.8	6.0	1.04	78.88	0.01662	0.00042	177.92	3.18
4.85	1	2.68164	0.11914	0.03539	0.00288	301.5	6.4	1.74	85.80	0.01344	0.00029	234.79	2.52
4.9	1	1.39102	0.05908	0.01742	0.00154	581.5	9.8	3.09	94.01	0.01151	0.00020	294.41	1.82
5	1	0.00748	0.05304	0.00268	0.00147	642.9	10.5	4.57	98.98	0.01275	0.00021	280.38	1.68
5.2	1	0.01717	0.02630	0.00176	0.00076	1251.8	13.6	7.47	99.40	0.01145	0.00013	310.79	1.11
5.4	1	0.02433	0.02748	0.00158	0.00072	1286.2	16.4	10.44	99.44	0.01198	0.00015	298.25	1.30
5.6	1	0.04707	0.02401	0.00187	0.00065	1421.7	16.6	13.73	99.34	0.01189	0.00014	300.13	1.19
5.8	1	-0.00395	-0.02456	0.00087	0.00068	1342.1	16.5	16.84	99.68	0.01245	0.00015	288.51	1.25
6	1	0.03199	0.02915	-0.00237	-0.00133	1169.4	12.5	19.54	100.84	0.01184	0.00013	305.50	1.07
6.3	1	0.07253	0.02631	0.00084	0.00066	1340.7	14.7	22.64	99.71	0.01161	0.00013	307.79	1.12
6.6	1	0.04909	0.02162	0.00082	0.00056	1578.4	18.8	26.29	99.72	0.01168	0.00014	306.15	1.21
6.9	1	0.01102	0.03626	0.00233	0.00090	1005.6	14.9	28.62	99.19	0.01169	0.00018	304.36	1.52
7.4	1	0.09904	0.03418	0.00197	0.00087	1033.5	12.2	31.01	99.33	0.01138	0.00014	312.30	1.21
8.2	1	0.02837	0.02333	0.00130	0.00062	1464.2	13.2	34.40	99.56	0.01123	0.00010	316.77	0.92
9	1	0.02286	0.00742	0.00092	0.00020	4603.4	31.0	45.04	99.70	0.01085	0.00008	327.37	0.70
9.5	1	0.03303	0.01361	0.00133	0.00033	2774.8	21.9	51.46	99.59	0.01045	0.00008	338.38	0.81
10	1	0.00196	0.00190	0.00063	0.00005	18675.1	99.5	94.66	99.79	0.01109	0.00006	321.12	0.54
10.25	1	0.09326	0.04850	0.00109	0.00122	707.3	10.0	96.29	99.66	0.01046	0.00015	338.47	1.44
10.75	1	0.00213	0.08722	0.00302	0.00244	379.5	7.5	97.17	99.02	0.01087	0.00022	324.70	2.02
fuse	1	0.02337	0.02804	0.00469	0.00074	1223.6	14.4	100	98.52	0.01058	0.00013	331.55	1.21

Table 02/16. $^{40}\text{Ar}/^{39}\text{Ar}$ analytical results for sample 13SL20D, muscovite (n~20 xtls; J = 2.15654E-03 ± 0.43%)

Laser Wattage	Dwell Time (min)	$^{37}\text{Ar}/^{39}\text{Ar}$	$^{37}\text{Ar}/^{39}\text{Ar}$ Error	$^{36}\text{Ar}/^{39}\text{Ar}$	$^{36}\text{Ar}/^{39}\text{Ar}$ Error	^{39}Ar (cps)	^{39}Ar (cps) Err	Cumulative % ^{39}Ar Released	% ^{40}Ar *	$^{39}\text{Ar}/^{40}\text{Ar}$	$^{39}\text{Ar}/^{40}\text{Ar}$ Error	Age (Ma)	1σ % Error (Ma)
3.8	1	-0.00328	-0.00731	0.57406	0.28377	3.2	-0.00328	0.01	-582.71	0.03983	0.04782	-684.23	-20.56
4	1	0.00043	0.00076	0.20682	0.03169	28.5	0.00043	0.08	38.56	0.00995	0.00035	144.10	9.15
4.2	1	0.00003	0.00013	0.03323	0.00504	166.8	0.00003	0.49	91.22	0.00885	0.00019	361.29	2.32
4.4	1	0.00000	0.00002	0.01280	0.00088	1098.1	0.00000	3.17	96.33	0.00961	0.00014	352.25	1.51
4.425	1	0.00004	0.00002	0.00815	0.00091	992.4	0.00004	5.60	97.67	0.00956	0.00012	358.74	1.32
4.45	1	-0.00001	-0.00002	0.01338	0.00072	1420.3	-0.00001	9.08	96.26	0.00935	0.00009	360.96	0.99
4.47	1	-0.00002	-0.00002	0.00673	0.00095	1000.1	-0.00002	11.52	98.05	0.00971	0.00011	354.71	1.12
4.5	1	0.00002	0.00002	0.00755	0.00078	1278.8	0.00002	14.65	97.85	0.00955	0.00010	359.61	1.06
4.525	1	-0.00005	-0.00002	0.01039	0.00089	1122.5	-0.00005	17.40	97.09	0.00937	0.00011	363.32	1.20
4.55	1	0.00008	0.00002	0.00585	0.00098	924.6	0.00008	19.66	98.33	0.00958	0.00011	360.14	1.20
4.575	1	0.00007	0.00001	0.00450	0.00059	1606.3	0.00007	23.59	98.71	0.00961	0.00009	360.32	0.99
4.6	1	0.00004	0.00001	0.00325	0.00056	1526.6	0.00004	27.33	99.05	0.00980	0.00010	355.23	1.03
4.625	1	0.00000	-0.00002	0.00191	0.00081	1159.9	0.00000	30.17	99.45	0.00965	0.00011	361.26	1.14
4.65	1	0.00002	0.00001	0.00430	0.00035	3027.8	0.00002	37.58	98.75	0.00971	0.00008	357.11	0.83
4.675	1	0.00001	0.00001	0.00298	0.00040	2514.7	0.00001	43.73	99.15	0.00959	0.00009	362.51	0.95
4.7	1	0.00005	0.00002	0.00459	0.00091	1108.3	0.00005	46.44	98.66	0.00979	0.00012	354.11	1.28
4.75	1	-0.00003	-0.00002	0.00247	0.00076	1218.8	-0.00003	49.43	99.28	0.00977	0.00011	356.81	1.17
4.825	1	0.00000	-0.00001	0.00316	0.00040	2355.6	0.00000	55.19	99.08	0.00975	0.00008	356.92	0.81
4.9	1	0.00001	0.00001	0.00352	0.00043	2254.0	0.00001	60.71	98.97	0.00982	0.00009	354.09	0.88
4.975	1	0.00001	0.00001	0.00374	0.00052	2001.1	0.00001	65.61	98.92	0.00970	0.00009	357.98	0.92
5.05	1	0.00000	0.00002	0.00285	0.00067	1450.3	0.00000	69.15	99.18	0.00968	0.00011	359.56	1.20
5.2	1	0.00000	0.00001	0.00242	0.00042	2411.5	0.00000	75.06	99.30	0.00962	0.00008	362.02	0.79
5.4	1	0.00001	0.00001	0.00097	0.00049	1906.0	0.00001	79.72	99.71	0.00981	0.00009	356.80	0.95
5.7	1	-0.00002	-0.00002	0.00437	0.00067	1347.4	-0.00002	83.02	98.72	0.00982	0.00010	353.46	1.08
6.5	1	0.00001	0.00002	0.00245	0.00057	1611.1	0.00001	86.96	99.28	0.00990	0.00010	352.49	0.99
fuse	1	0.00002	0.00000	0.00210	0.00017	5328.4	0.00002	100	99.39	0.00975	0.00006	357.83	0.66

Table 02/17. $^{40}\text{Ar}/^{39}\text{Ar}$ analytical results for sample 13SL21A, biotite (n=1 xtl; J = 2.16855E-03 ± 0.67%)

Laser Wattage	Dwell Time (min)	$^{37}\text{Ar}/^{39}\text{Ar}$	$^{37}\text{Ar}/^{39}\text{Ar}$ Error	$^{36}\text{Ar}/^{39}\text{Ar}$	$^{36}\text{Ar}/^{39}\text{Ar}$ Error	^{39}Ar (cps)	^{39}Ar (cps) Err	Cumulative % ^{39}Ar Released	% ^{40}Ar *	$^{39}\text{Ar}/^{40}\text{Ar}$	$^{39}\text{Ar}/^{40}\text{Ar}$ Error	Age (Ma)	1 σ % Error (Ma)
3.8	1	0.06792	0.02046	0.01744	0.00099	919.6	13.2	2.83	87.62	0.02376	0.00035	138.80	1.70
3.9	1	0.04953	0.00921	0.00306	0.00041	2120.2	20.5	9.35	98.98	0.01115	0.00011	317.72	0.99
4	1	0.03321	0.00492	0.00232	0.00024	3696.3	29.2	20.71	99.24	0.01104	0.00009	321.48	0.81
4.1	1	0.01692	0.00345	0.00148	0.00017	5263.9	40.3	36.89	99.53	0.01064	0.00008	333.40	0.78
4.2	1	0.02517	0.00411	0.00118	0.00019	4747.9	36.0	51.49	99.63	0.01059	0.00008	335.06	0.77
4.3	1	0.02099	0.00526	0.00142	0.00020	3826.5	31.1	63.25	99.56	0.01048	0.00009	337.98	0.83
4.425	1	0.01713	0.00483	0.00097	0.00021	3918.3	33.6	75.30	99.70	0.01051	0.00009	337.52	0.87
4.6	1	0.03012	0.00582	0.00149	0.00027	3358.1	29.8	85.62	99.54	0.01041	0.00009	340.16	0.90
4.8	1	0.04978	0.01203	0.00146	0.00045	1731.1	20.8	90.95	99.54	0.01052	0.00013	336.83	1.22
5.2	1	0.07278	0.01837	0.00134	0.00086	993.3	16.2	94.00	99.56	0.01097	0.00018	324.40	1.66
6	1	0.05210	0.02707	0.00747	0.00173	785.7	12.0	96.42	97.59	0.01078	0.00017	323.43	1.61
fuse	1	0.06379	0.01708	0.00598	0.00113	1165.8	13.9	100	97.97	0.01137	0.00014	309.20	1.25

Table 02/18. $^{40}\text{Ar}/^{39}\text{Ar}$ analytical results for sample 13SL21A, potassium feldspar (n=1 xtl; J = 2.17073E-03 ± 0.70%)

Laser Wattage	Dwell time (min)	$^{37}\text{Ar}/^{39}\text{Ar}$	$^{37}\text{Ar}/^{39}\text{Ar}$ error	$^{36}\text{Ar}/^{39}\text{Ar}$	$^{36}\text{Ar}/^{39}\text{Ar}$ error	^{39}Ar (cps)	^{39}Ar (cps) Err	Cumulative % ^{39}Ar released	% ^{40}Ar *	$^{39}\text{Ar}/^{40}\text{Ar}$	$^{39}\text{Ar}/^{40}\text{Ar}$ Error	Age (Ma)	1 σ % error (Ma)
3.8	1	-7.99344	-6.36866	0.11636	0.17505	5.4	0.5	0.01	90.27	0.00280	0.00029	952.70	11.43
3.9	1	-4.67292	12.85780	-2.31557	-0.62651	2.8	0.5	0.02	259.80	0.00231	0.00041	2225.03	6.77
4	1	-3.86344	-7.28345	-0.90618	-0.29331	4.9	0.5	0.03	272.17	0.00636	0.00096	1182.16	5.55
4.1	1	-1.31904	-3.67644	0.08935	0.09660	9.3	0.5	0.05	91.12	0.00333	0.00020	840.94	6.70
4.2	1	-0.31827	-3.23052	0.01021	0.07549	10.9	0.5	0.08	98.16	0.00603	0.00036	546.21	6.16
4.4	1	-1.25978	-0.44380	0.00740	0.01195	72.7	1.8	0.25	98.32	0.00760	0.00020	446.39	2.69
4.6	1	0.01483	0.00924	0.00122	0.00027	3597.4	26.8	8.63	99.44	0.01548	0.00012	235.64	0.77
4.65	1	0.04498	0.03085	0.00104	0.00088	1112.0	14.2	11.23	99.55	0.01441	0.00019	252.28	1.30
4.75	1	0.04302	0.03716	0.00088	0.00101	923.6	11.0	13.38	99.63	0.01418	0.00018	256.24	1.24
4.9	1	0.04116	0.03440	0.00085	0.00096	998.0	13.0	15.71	99.64	0.01429	0.00019	254.36	1.33
5.2	1	-0.02958	-0.02326	0.00017	0.00071	1339.0	14.6	18.83	99.93	0.01422	0.00016	256.23	1.11
5.6	1	-0.03184	-0.02007	0.00177	0.00060	1659.2	18.1	22.70	99.27	0.01387	0.00015	260.56	1.11
6.2	1	0.02303	0.01658	0.00289	0.00080	1908.9	18.6	27.15	98.82	0.01365	0.00014	263.43	1.01
7	1	0.03114	0.01782	0.00344	0.00084	1837.2	18.5	31.43	98.62	0.01343	0.00014	266.95	1.04
8	1	0.02936	0.01573	0.00343	0.00077	2013.9	18.9	36.13	98.71	0.01259	0.00012	283.78	0.97
9.5	1	0.00879	0.00318	0.00216	0.00015	10999.7	67.0	61.77	99.18	0.01269	0.00008	282.86	0.64
9.75	1	0.00530	0.01352	0.00166	0.00037	2520.3	22.8	67.65	99.38	0.01261	0.00012	285.10	0.94
10	1	-0.00880	-0.01068	0.00203	0.00031	3191.9	23.3	75.09	99.24	0.01258	0.00010	285.30	0.76
10.25	1	-0.00419	-0.01567	0.00131	0.00050	1886.8	17.7	79.49	99.51	0.01247	0.00012	288.29	0.96
10.5	1	-0.01297	-0.00836	0.00095	0.00023	4224.2	32.7	89.34	99.64	0.01257	0.00010	286.62	0.81
10.75	1	-0.03643	-0.04972	0.00311	0.00148	595.1	10.4	90.73	98.81	0.01279	0.00023	279.78	1.79
fuse	1	-0.00208	-0.00799	0.00085	0.00024	3977.4	30.3	100	99.69	0.01237	0.00010	291.06	0.78

Table 02/19. $^{40}\text{Ar}/^{39}\text{Ar}$ analytical results for sample 13SL21A, muscovite (n=1 xtl; J = 2.17051E-03 ± 0.70%)

Laser Wattage	Dwell Time (min)	$^{37}\text{Ar}/^{39}\text{Ar}$	$^{37}\text{Ar}/^{39}\text{Ar}$ Error	$^{36}\text{Ar}/^{39}\text{Ar}$	$^{36}\text{Ar}/^{39}\text{Ar}$ Error	^{39}Ar (cps)	^{39}Ar (cps) Err	Cumulative % ^{39}Ar Released	% $^{40}\text{Ar}^*$	$^{39}\text{Ar}/^{40}\text{Ar}$	$^{39}\text{Ar}/^{40}\text{Ar}$ Error	Age (Ma)	1σ % Error (Ma)
3.8	1	9.76754	3.86045	-0.09964	-0.12311	7.1	0.6	0.02	122.42	0.00754	0.00085	550.57	9.12
4	1	4.74025	1.20087	-0.03601	-0.04091	20.9	0.7	0.08	110.32	0.00960	0.00045	404.26	4.27
4.2	1	0.30369	0.08645	0.03386	0.00348	278.9	6.2	0.85	90.77	0.00913	0.00021	353.00	2.50
4.4	1	0.11417	0.02229	0.02112	0.00098	1080.8	12.5	3.83	94.03	0.00947	0.00011	352.35	1.25
4.5	1	0.03579	0.00536	0.00183	0.00020	4823.6	28.0	17.12	99.45	0.01015	0.00006	347.96	0.60
4.8	1	0.03230	0.02300	0.00245	0.00069	1206.1	15.5	20.45	99.25	0.01026	0.00013	344.13	1.31
4.65	1	0.19203	0.05047	0.00195	0.00105	847.2	11.4	22.78	99.40	0.01032	0.00014	342.65	1.38
4.525	1	0.00402	0.00513	0.00101	0.00015	5827.2	31.3	38.84	99.69	0.01037	0.00006	341.91	0.57
4.535	1	0.03856	0.01677	0.00130	0.00053	1652.2	19.7	43.40	99.61	0.01019	0.00012	347.32	1.23
4.575	1	0.02600	0.02646	0.00135	0.00080	1073.8	12.5	46.36	99.59	0.01020	0.00012	346.87	1.20
5.2	1	-0.01666	-0.00595	0.00144	0.00014	6643.6	32.7	64.67	99.56	0.01028	0.00005	344.23	0.51
5.6	1	-0.07309	-0.02137	0.00084	0.00049	1798.3	16.9	69.63	99.74	0.01028	0.00010	344.93	0.96
fuse	1	-0.00543	-0.00344	0.00037	0.00008	11017.4	47.3	100	99.89	0.01036	0.00005	343.01	0.45

Table 02/20. $^{40}\text{Ar}/^{39}\text{Ar}$ analytical results for sample 14SL03A, biotite (n=1 xtl; J = 2.17051E-03 ± 0.70%)

Laser Wattage	Dwell Time (min)	$^{37}\text{Ar}/^{39}\text{Ar}$	$^{37}\text{Ar}/^{39}\text{Ar}$ Error	$^{36}\text{Ar}/^{39}\text{Ar}$	$^{36}\text{Ar}/^{39}\text{Ar}$ Error	^{39}Ar (cps)	^{39}Ar (cps) Err	Cumulative % ^{39}Ar Released	% ^{40}Ar *	$^{39}\text{Ar}/^{40}\text{Ar}$	$^{39}\text{Ar}/^{40}\text{Ar}$ Error	Age (Ma)	1 σ % Error (Ma)
3.8	1	0.51750	0.35043	0.05672	0.01219	72.8	1.7	0.31	86.31	0.00808	0.00021	376.67	3.03
3.9	1	0.34872	0.14882	0.00462	0.00534	166.9	4.3	1.02	98.44	0.01130	0.00030	312.86	2.72
4	1	0.12871	0.03332	0.00419	0.00111	790.0	10.3	4.39	98.67	0.01067	0.00014	330.44	1.36
4.15	1	0.06882	0.01602	0.00157	0.00049	1692.3	17.8	11.60	99.50	0.01075	0.00012	330.65	1.08
4.3	1	0.08840	0.01694	0.00216	0.00060	1466.3	11.9	17.85	99.31	0.01071	0.00009	331.10	0.85
4.45	1	0.02041	0.01376	0.00243	0.00045	1912.6	18.0	26.01	99.23	0.01057	0.00010	334.84	0.97
4.6	1	0.02066	0.00832	0.00178	0.00028	3164.6	22.2	39.50	99.43	0.01082	0.00008	328.24	0.73
4.7	1	0.02719	0.00840	0.00145	0.00027	3039.9	23.9	52.45	99.53	0.01082	0.00009	328.62	0.81
4.8	1	0.02631	0.01045	0.00183	0.00032	2602.3	23.4	63.55	99.42	0.01071	0.00010	331.32	0.93
4.95	1	0.01315	0.00571	0.00130	0.00023	4078.0	28.8	80.93	99.58	0.01085	0.00008	328.12	0.73
5.1	1	0.04255	0.01387	0.00099	0.00032	2660.3	21.6	92.27	99.68	0.01077	0.00009	330.46	0.83
5.3	1	0.05895	0.01870	0.00195	0.00064	1326.2	14.6	97.92	99.37	0.01073	0.00012	330.73	1.14
5.7	1	0.19448	0.05705	0.00318	0.00208	421.3	8.7	99.72	99.06	0.00988	0.00021	355.67	2.12
fuse	1	2.46757	0.61089	0.02267	0.01332	65.8	1.9	100	94.99	0.00740	0.00023	444.85	3.31

Table 02/21. $^{40}\text{Ar}/^{39}\text{Ar}$ analytical results for sample 14SL03B, biotite (n=1 xtl; J = 2.17166E-03 ± 0.70%)

Laser Wattage	Dwell Time (min)	$^{37}\text{Ar}/^{39}\text{Ar}$	$^{37}\text{Ar}/^{39}\text{Ar}$ Error	$^{36}\text{Ar}/^{39}\text{Ar}$	$^{36}\text{Ar}/^{39}\text{Ar}$ Error	^{39}Ar (cps)	^{39}Ar (cps) Err	Cumulative % ^{39}Ar Released	% ^{40}Ar *	$^{39}\text{Ar}/^{40}\text{Ar}$	$^{39}\text{Ar}/^{40}\text{Ar}$ Error	Age (Ma)	1 σ % Error (Ma)
3.8	1	-0.69119	-0.29015	0.00856	0.00564	136.4	4.6	0.79	97.33	0.01046	0.00036	331.88	3.56
3.9	1	-0.15116	-0.05704	0.00082	0.00108	711.6	9.5	4.91	99.75	0.01019	0.00014	347.94	1.37
4	1	-0.04600	-0.02719	0.00184	0.00062	1434.0	14.7	13.20	99.43	0.01039	0.00011	340.86	1.05
4.1	1	-0.06157	-0.03050	0.00239	0.00067	1263.1	13.6	20.51	99.26	0.01037	0.00011	340.96	1.11
4.2	1	0.00865	0.05076	0.00262	0.00079	1026.6	14.4	26.44	99.17	0.01065	0.00015	332.29	1.44
4.35	1	0.01769	0.01522	0.00091	0.00054	1652.0	15.8	36.00	99.71	0.01057	0.00010	336.35	0.99
4.5	1	0.01142	0.00733	0.00093	0.00028	3211.5	22.2	54.58	99.71	0.01048	0.00007	339.09	0.71
4.55	1	0.04102	0.01001	0.00144	0.00038	2432.8	17.6	68.65	99.55	0.01045	0.00008	339.55	0.75
4.6	1	0.05345	0.01232	-0.00050	-0.00068	2043.7	17.2	80.47	100.16	0.01052	0.00009	339.31	0.86
4.65	1	0.02518	0.02433	0.00092	0.00084	1069.9	13.4	86.66	99.71	0.01042	0.00013	340.81	1.30
4.75	1	0.00610	0.02050	0.00224	0.00077	1149.4	13.5	93.31	99.30	0.01047	0.00012	338.09	1.20
5	1	-0.04753	-0.03229	0.00294	0.00116	756.6	10.3	97.68	99.11	0.01011	0.00014	348.27	1.42
5.5	1	0.04629	0.06332	0.00319	0.00239	372.5	7.9	99.84	99.06	0.00987	0.00021	355.85	2.18
fuse	1	-1.10222	-0.86849	0.36077	0.03425	28.2	0.8	100	48.80	0.00475	0.00019	363.02	8.16